

**Model-based Design Framework for
Shape Memory Alloy Wire Actuation Devices**

by

Wonhee Kim

A dissertation submitted in partial fulfillment
of the requirements for the degree of
Doctor of Philosophy
(Mechanical Engineering)
in the University of Michigan
2016

Doctoral Committee:

Professor Diann E. Brei, Co-chair
Associate Research Scientist Jonathan E. Luntz, Co-chair
Paul W. Alexander, General Motors Company
Associate Professor Brent Gillespie
Nilesh D. Mankame, General Motors Company
Professor John A. Shaw

Table of Contents

List of Figures	viii
List of Tables	xv
List of Appendices	xvi
Abstract	xix
Chapter 1. Introduction.....	1
1.1. Shape Memory Alloy actuation device applications.....	1
1.1.1. Material behavior of Shape Memory Alloys.....	2
1.1.1.1. Shape memory effect	3
1.1.1.2. Superelasticity.....	4
1.1.2. Operation concept of a simple SMA actuator	4
1.1.3. SMA actuator benefits and examples.....	6
1.2. SMA actuation device design.....	8
1.2.1. Stakeholders of SMA actuation device development.....	9
1.2.2. SMA actuation device design problem example: latch release device	12
1.2.3. SMA actuation device design methods	14
1.2.3.1. Force-deflection curve design method.....	14
1.2.3.2. Empirical design method	16
1.2.4. SMA actuation device architectures.....	17
1.2.4.1. SMA web architecture design example: Active inner belt seal device.....	19
1.2.4.2. SMA driven ratchet design example: SMART hood lift reset device	20
1.3. Research Issues.....	22
1.3.1. Device grammar	23
1.3.2. Design methods	25
1.3.3. Design process.....	27
1.3.4. Design framework	29
1.4. Goal and objectives.....	31

1.5. Research approach	31
1.5.1. Device grammar	32
1.5.2. Design methods	33
1.5.3. Design process.....	34
1.5.4. Design framework	34
1.6. Contributions and expected outcomes	35
1.7. Refernces	37
Chapter 2. SMA Device Grammar	43
2.1. Generalized device structure	45
2.1.1. Basic element types	46
2.1.1.1. Behavior definition elements	46
2.1.1.1.1. Active element	47
2.1.1.1.2. Reactive element.....	47
2.1.1.2. Modifier element.....	48
2.1.1.3. Coupling element	49
2.1.2. Connectivity rules	50
2.1.3. Macro elements	52
2.2. SMA device hierarchical structure	55
2.2.1. SMA active element	56
2.2.1.1. SMA material	57
2.2.1.2. SMA architectures.....	57
2.2.2. Device modifiers	59
2.2.2.1. Bias.....	60
2.2.2.1.1. Bias device	61
2.2.2.1.2. Bias device interface.....	62
2.2.2.2. Stroke limiters	62
2.2.2.2.1. Mechanical hard stop	63
2.2.2.2.2. Position-based heating current cutoff	64
2.2.2.3. Device leverage.....	64
2.2.2.4. Friction	64
2.2.2.5. Stroke accumulator	65
2.2.3. Target element.....	65
2.3. SMA device architecture examples	66
2.3.1. Latch release device: straight wire example.....	66

2.3.2.	Active inner belt seal device: web actuator example	67
2.3.3.	SMART hood lift reset device: ratchet example	68
2.4.	Conclusions.....	70
2.5.	References.....	72
Chapter 3.	SMA Design Methods	74
3.1.	General modeling approach.....	77
3.1.1.	Behavior definition elements (active and reactive elements).....	77
3.1.2.	Modifier elements.....	78
3.1.3.	Coupling elements	79
3.2.	Model aggregation and performance prediction.....	79
3.2.1.	Solution coupling and model aggregation.....	79
3.2.2.	SMA actuator device performance prediction approaches.....	81
3.2.2.1.	Discrete equilibrium performance prediction approach.....	82
3.2.2.2.	Integrated dynamic performance prediction approach.....	84
3.3.	Visualization of actuation device system behavior	85
3.3.1.	Solution coupling	86
3.3.2.	Behavior flow grouping.....	87
3.3.3.	Performance prediction projection	88
3.4.	SMA device modeling approach	89
3.4.1.	SMA material (active element) models.....	89
3.4.1.1.	Empirical representation	90
3.4.1.2.	Constitutive models.....	91
3.4.2.	Reactive element models.....	92
3.4.2.1.	Empirical representation	93
3.4.2.2.	Analytical model.....	93
3.4.2.3.	CAE model.....	93
3.4.3.	Modifier element models.....	94
3.4.3.1.	SMA architecture (Geometric modifier element)	94
3.4.3.1.1.	Homogeneous geometric modifier element transformation	95
3.4.3.1.2.	Heterogeneous geometric modifier element transformation.....	97
3.4.3.2.	Kinematic modifiers.....	99
3.4.3.2.1.	Stroke limiters	100
3.4.3.2.2.	Mechanical leverage	101

3.4.3.2.3. Friction.....	102
3.4.3.2.4. Interface modifier transformation.....	103
3.4.3.2.5. Stroke accumulator transformation.....	103
3.5.SMA device modeling examples using discrete equilibrium performance prediction	107
3.5.1. Latch release device: straight wire example.....	107
3.5.2. Active inner belt seal device: web actuator example	108
3.5.3. SMART hood lifter reset device: ratchet example.....	109
3.6. Conclusions.....	111
3.7. References.....	112

Chapter 4. SMA Design Process 114

4.1. Initial design decisions	117
4.2. Discrete equilibrium design method.....	121
4.2.1. Kinematic design step	124
4.2.2. Kineto-static design step	128
4.2.3. Thermo-mechanical design step.....	134
4.3. Integrated transient behavior evaluation	139
4.4. Common SMA actuator architecture design examples	140
4.4.1. Latch release device: straight wire example.....	141
4.4.1.1. Initial design decision stage	142
4.4.1.2. Discrete equilibrium design stage	142
4.4.1.2.1. Kinematic design step.....	143
4.4.1.2.2. Kineto-static design step.....	143
4.4.1.2.3. Thermo-mechanical design step	146
4.4.2. Active inner belt seal device: web actuator example	147
4.4.2.1. Initial design decision stage	148
4.4.2.2. Discrete equilibrium design stage	148
4.4.2.2.1. Kinematic design step.....	149
4.4.2.2.2. Kineto-static design step.....	150
4.4.3. SMART hood lifter reset device: ratchet example.....	151
4.4.3.1. Initial design decision stage	152
4.4.3.2. Discrete equilibrium design stage	153
4.4.3.2.1. Kinematic design step.....	155

4.4.3.2.2. Kineto-static design step.....	155
4.5. Conclusions.....	157
4.6. References.....	158
Chapter 5. SMA Design Framework	161
5.1. Model-based design tool modular platform	163
5.2. User interface work flows.....	164
5.2.1. Expert engineer supporting design tool interface.....	165
5.2.1.1. Design problem definition and initial design decisions	166
5.2.1.2. Setting device structure	166
5.2.1.3. Planning state sequence and evaluation	166
5.2.2. Non-expert engineer guiding design tool interface	167
5.2.2.1. Problem definition and initial design decisions	167
5.2.2.2. Kinematic design.....	168
5.2.2.3. Kineto-static design.....	168
5.2.2.4. Thermo-mechanical design	168
5.3. Design decision manager module.....	169
5.4. Evaluation manager module	170
5.5. Actuation device system modular structure	171
5.5.1. Basic element objects	171
5.5.1.1. Active and reactive element objects.....	172
5.5.1.2. Modifier element objects	173
5.5.1.3. Compatibility coupling objects	173
5.5.2. Solution coupling object.....	174
5.6. Design tool use case examples	174
5.6.1. Non-expert engineer use case: classroom design project.....	175
5.6.2. Expert engineer use case: industrial prototype debugging	179
5.7. Conclusions.....	180
5.8. References.....	181
Chapter 6. Conclusions.....	182
6.1. Research summary and contributions.....	183

6.1.1. Device grammar	183
6.1.2. Design methods	185
6.1.3. Design process.....	186
6.1.4. Design framework	187
6.2. Future research.....	189
6.2.1. Additional SMA design methods	189
6.2.2. Comprehensive design process	189
6.2.3. Expand to new smart materials and architectures	190
6.3. Closing	191
Appendices	192

List of Figures

Figure 1.1. Increasing SMA actuation device patents.	2
Figure 1.2. SMA material behavior [7].....	3
Figure 1.3. Schematic of a simple SMA actuator.	4
Figure 1.4. SMA behavior of simple actuation device during actuation.	5
Figure 1.5. SMA actuator examples.	7
Figure 1.6. Actuation device development cycle (modified from [6]).	8
Figure 1.7. Latch release device.	12
Figure 1.8. Multiple stages of SMA actuation device design.....	13
Figure 1.9. Force-deflection curve design method.	14
Figure 1.10. Example of non-proportional performance change: effect of increased SMA wire length on actuation stroke.	15
Figure 1.11. Empirical design method example: SMA wire actuated compliant finger [25].	17
Figure 1.12. Examples of SMA architectures.....	18
Figure 1.13. Active inner belt seal.	19
Figure 1.14. Multi-layer structure of the SMA web actuator.	20
Figure 1.15. SMART hood lift reset device [22].	21
Figure 1.16. SMA wire ratchet mechanism.	21
Figure 1.17. Modular system methods examples.....	24
Figure 1.18. Simple conceptual SMA actuator examples.....	25
Figure 1.19. Performance prediction method examples.	26
Figure 1.20. Bias spring selection plots [18].	27

Figure 1.21. Methodical design procedure for developing SMA-based components [84].	28
Figure 1.22. Polymers/Smart Materials Database (PSMD) [86].	29
Figure 1.23. SMA straight wire design tool [85].	30
Figure 1.24. Computer-Aided Shape Memory Actuator Development Application (CASMADA) [87].	30
Figure 2.1. Actuation device system.	45
Figure 2.2. Active element.	47
Figure 2.3. Reactive element.	47
Figure 2.4. Modifier element.	48
Figure 2.5. Irreversible modifier element.	49
Figure 2.6. Interface modifier element.	49
Figure 2.7. Coupling element. Coupling elements represent the mechanical connection between three or more elements.	50
Figure 2.8. Simple actuator device example.	51
Figure 2.9. Macro behavior definition element example.	52
Figure 2.10. Multi-layer hierarchical structure of automotive powertrain.	53
Figure 2.11. Macro element regrouping using coupling decomposition.	54
Figure 2.12. A reference SMA actuation device system.	55
Figure 2.13. SMA active element.	56
Figure 2.14. Multi-layer structure of the SMA web actuator.	58
Figure 2.15. Device modifier macro element.	59
Figure 2.16. Device behavior definition macro element.	60
Figure 2.17. Bias macro modifier element.	61
Figure 2.18. SMA wire ratchet mechanism.	65
Figure 2.19. Latch release device hierarchical structure.	67
Figure 2.20. Active inner belt seal hierarchical structure.	68

Figure 2.21. SMART hood lift reset device hierarchical structure.....	69
Figure 2.22. Two operation modes of SMART hood lift reset device.	70
Figure 3.1. Relocating solution coupling element.	80
Figure 3.2. Limitation on selecting solution coupling due to irreversible modifier.	81
Figure 3.3. A simple straight SMA wire actuator device example.....	82
Figure 3.4. Discrete equilibrium performance prediction approach.....	83
Figure 3.5. Integrated dynamic performance prediction results of a simple SMA actuation device system.....	85
Figure 3.6. Diverse discrete equilibrium performance prediction visualization.....	86
Figure 3.7. Diverse grouping of behavior flows at a single solution coupling element.	87
Figure 3.8. Projection of performance prediction visualization.	88
Figure 3.9. Empirical stress-strain measurement along with a curve fit.....	90
Figure 3.10. Stress-strain behavior prediction using a modified Brinson type model.....	92
Figure 3.11. Multi-layer homogeneous geometric modifier element transformation: web actuator.	96
Figure 3.12. Hierarchical structure of the SMA web actuator.....	97
Figure 3.13. Heterogeneous geometric modifier element transformation example: spool packaging [6].	98
Figure 3.14. Hierarchical structure of the SMA spooling.....	99
Figure 3.15. Stress-strain distribution over the spool packaged SMA wire [6].....	99
Figure 3.16. Martensite mechanical stroke limiter.	100
Figure 3.17. Position-based heating current cutoff switch.	101
Figure 3.18. Mechanical leverage.....	102
Figure 3.19. Two modes of friction modifier.	103
Figure 3.20. Stroke accumulator transformation example: ratchet actuator.....	104
Figure 3.21. Discrete equilibrium performance prediction of latch release device.	108

Figure 3.22. Discrete equilibrium performance prediction of active inner belt seal.	109
Figure 3.23. Two operation modes of SMA ratchet actuator.	110
Figure 3.24. Ratchet actuator loading / unloading path of a single actuation step.	111
Figure 4.1. Design process of SMA coil spring actuator [11].	115
Figure 4.2. Architecture suggestion map.	119
Figure 4.3. Initial design decision stage flow.	120
Figure 4.4. Effect of longer length of SMA wire.....	121
Figure 4.5. Effect of larger cross sectional area of SMA wire.	122
Figure 4.6. Kinematic design step flow for straight SMA wires.	125
Figure 4.7. Kinematic Actuation Map for mechanical leverage.....	126
Figure 4.8. Kinematic Actuation Map for SMA web actuator.	127
Figure 4.9. Visualization of actuation device system behavior and performance prediction results for discrete equilibrium design method.....	129
Figure 4.10. Adjusting the target element stiffness using bias device to ensure the operation at high ambient temperature.....	131
Figure 4.11. Kineto-static design step flow for straight SMA wires.	133
Figure 4.12. Bias design map example.	134
Figure 4.13. Temperature-stress behavior during the actuation.	135
Figure 4.14. Thermo-mechanical design step flow.....	138
Figure 4.15. Integrated transient behavior evaluation (Simulink) example of an SMA wire- extension spring system.	140
Figure 4.16. Design process for latch release device.....	141
Figure 4.17. Mechanical leverage actuation map example.....	143
Figure 4.18. Latch release device bias design map example.	146
Figure 4.19. Design process for active inner belt seal.	148
Figure 4.20. SMA web actuator design using Kinematic Actuation Map.	149

Figure 4.21. Verification of SMA web actuator design using target element coordinates.....	151
Figure 4.22. Design process for SMART hood lifter reset device.....	152
Figure 4.23. SMA ratchet actuator performance evaluation.....	154
Figure 4.24. SMART hood lifter reset device bias design map.....	156
Figure 4.25. Actuator performance evaluation for hood lift reset device.....	157
Figure 5.1. Model-based Design Tool modular platform.	163
Figure 5.2. Example of expert user supporting design tool interface.	164
Figure 5.3. Concept of non-expert user guiding design tool interface.....	165
Figure 5.4. Concept of Smart Vent [4].	175
Figure 5.5. Operation of SMA helical spring driven ratchet and pawl mechanism [4].....	176
Figure 5.6. Target element behavior characterization setup and the result [4].....	177
Figure 5.7. Smart vent design improvement using design tool [4].	178
Figure 5.8. SMA helical spring driven ratchet mechanism of Smart Vent [4].	179
Figure 5.9. Design tool helped to identify manufacturing issue.	180
Figure A.1. Shallow packaging challenges.....	193
Figure A.2. Operation concept of SMA web architecture.	196
Figure A.3. Experimental setup for model validation.....	203
Figure A.4. SMA material constitutive relation for experimental validation (0.01 inch diameter 70°C Flexinol®) and Internal leveraging of external system.	204
Figure A.5. Experimental validation result.....	205
Figure A.6. SMA Web Actuator Kinematic Actuation Map.	208
Figure A.7. Internal tension amplification (200 MPa maximum allowable stress).....	209
Figure A.8. Actuator output strain amplification.....	214
Figure A.9. Actuator Output Performance Plot.	215
Figure A.10. Kinematic Actuation Map in stroke relative to package width.	217
Figure A.11. Actuator Output Performance Plot in stroke relative to the width.	217

Figure A.12. SMA material constitutive relations for output performance comparison.	218
Figure A.13. Material limits for different SMA material properties (Kinematic Actuation Map).....	219
Figure A.14. Effect of different SMA material properties (Actuator Output Performance Plot).....	220
Figure A.15. Material limits for different external system stiffness (Kinematic Actuation Map).....	222
Figure A.16. Effect of external system stiffness (Actuator Output Performance Plot).	222
Figure B.1. Schematic of SMA wire ratchet actuator.....	231
Figure B.2. SMA ratchet actuation cycle.....	233
Figure B.3. Ratchet actuator loading / unloading path of a single actuation step in SMA wire coordinate system.....	235
Figure B.4. Rack and pawl geometry parameters.....	238
Figure B.5. An example SMA wire ratchet actuator performance prediction in SMA wire view.....	244
Figure B.6. Effect of device bias stiffness on the SMA wire ratchet actuator performance.	247
Figure B.7. Effect of bias free clearance on the SMA wire ratchet actuator performance.....	248
Figure B.8. Effect of SMA wire length on the SMA wire ratchet actuator performance.....	250
Figure C.1. Shakedown of Shape Memory Alloy.....	255
Figure C.2. Negative Effect of Strain Shakedown.....	255
Figure C.3. Traditional stress-strain curve SMA actuator design method and the effect of shakedown.....	257
Figure C.4. Schematic of shakedown Experimental Setup.....	261
Figure C.5. Shakedown Processes With and Without Strain Limiter.....	262
Figure C.6. Strain Limiter Position Effects on Strain Shakedown.	264
Figure C.7. Strain Limiter Position Effects on Stabilized Stroke.	264
Figure C.8. Effect of Stress on Strain Loss, Stabilized Stroke, and Work Density (4 % Strain Limiter).	265

Figure C.9. Reverse Shakedown (80 MPa).....	266
Figure C.10. Optimal Stroke Contour.....	267
Figure C.11. Optimal Work Density Contour.....	268
Figure C.12. Conglomerate Stabilization Design Curve (4 % Strain Limiter Curve).....	270
Figure C.13. A Set of Conglomerate Stabilization Design Curves.	270
Figure C.14. SMA Wire Actuator Design Example with Traditional Design Method.....	272
Figure C.15. Conglomerate Stabilization Curve Design Method.	273
Figure C.16. A Latch Release SMA Actuator.	275
Figure C.17. A Latch Release actuation test result.	276

List of Tables

Table 1.1. Stakeholders of SMA actuation device design	11
Table 2.1. Hierarchical architectures of three device examples	72
Table 4.1. Initial design decisions for latch release device.....	142
Table B.1. Rack and pawl geometric parameters	245
Table C.1. Experimental Parameter Matrix.	260
Table C.2. Convergence Test Results (4000 cycles).	263

List of Appendices

Appendix A. Model-based design process for the shape memory alloy web actuator architecture	192
1. Introduction.....	192
2. Web Architecture.....	195
3. Discrete state quasi-static Force – Deflection Model and Experimental Validation	197
3.1. Discrete state quasi-static Force-deflection Model Derivation	198
3.1.1. Reference strain-free state.....	199
3.1.2. Austenite equilibrium state	200
3.1.3. Martensite equilibrium state.....	201
3.1.4. Stroke evaluation.....	202
3.2. Experimental Validation.....	203
4. Web actuator design Process	206
4.1. Kinematic Design	206
4.2. Kineto-static Design.....	210
4.3. Thermo-mechanical Design	211
5. Design Parameter Tradeoff Study	212
5.1. Architecture geometry: width/gap ratio	213
5.1.1. Effect of width/gap ratio on actuator stroke amplification	213
5.1.2. Effect of width/gap ratio on output force.....	214
5.1.3. Effect of partial use of packaging	216
5.2. Material properties: initial two-way strain	218
5.3. External system characteristics: stiffness	220
5.4. Design insight.....	223
6. Conclusion	224
7. References.....	224

Appendix B. Model-based shape memory alloy wire ratchet actuator design.....	228
1. Introduction.....	229
2. Ratchet mechanism.....	231
3. Ratchet design model.....	236
3.1. Force balance model.....	237
3.2. Rack and pawl interaction kinematic and kinetic model review	237
3.3. Effective stroke evaluation and free clearance update	239
4. Design study	242
4.1. SMA actuation design	243
4.2. Design parameter studies.....	246
4.2.1. Effect of the device bias stiffness	246
4.2.2. Effect of the bias free clearance	248
4.2.3. Effect of the SMA wire length.....	249
5. Conclusions.....	251
6. References.....	251
Appendix C. Conglomerate stabilization curve design method for shape memory alloy wire actuators with cyclic shakedown.....	253
1. Introduction.....	254
2. Empirical study of the effect of strain limiters on shakedown.....	259
2.1. Experimental parameter set	259
2.2. Experimental setup and procedure	260
2.3. Experimental Results.....	261
2.3.1. Effect of strain limiter position	263
2.3.2. Effect of applied stress.....	265
3. Conglomerate stabilization curve design method accounting for shakedown	269
3.1. Conglomerate stabilization design curves.....	269
3.2. Shakedown design example	271
3.3. Experimental validation of design example	274
4. Conclusions.....	276

5. References.....	277
--------------------	-----

Appendix D. Design Tool User Scenario281

1. Initial design decisions	281
1.1. Problem definition.....	281
1.2. Feasibility check and SMA architecture selection	283
1.3. Material usage decision	284
2. Non-expert engineer design process.....	285
2.1. Kinematic design: select design parameters related to actuation stroke	285
2.2. Kineto-static design step: select design parameters related to force	286
2.3. Thermo-mechanical design: select design parameters to actuation time	287
3. Expert engineer design process	288
3.1. Set actuation device system structure.....	288
3.2. Plan actuation state sequence	289
3.3. Design evaluation.....	290
3.4. Design modification	291

Appendix E. SMA Wire Design Tool Tutorial.....292

1. Initial Design with estimated external system.....	295
1.1. Setting External System	295
1.2. Setting Material parameters.....	299
1.3. Select actuator architecture	301
1.4. Diameter / Number of wires selection.....	303
1.5. Set the cold stop position and the wire length.....	305
1.6. Set the free clearance.....	307
2. Design reset element to increase the M_f	309
2.1. Increase the cross-sectional area of the SMA wire.	311
2.2. Find the available reset load increase.....	313
2.3. Find the softest reset spring which can provide the available reset force	317
2.4. Find reset free clearance to provide the available reset force	319
2.5. Repeat the procedure until reach the target M_f	321
3. Verify the design with the empirically measured external system data from the prototype and find the current to actuate in 1 sec.....	329
3.1. Import the experimental data.....	329
3.2. Find the current to actuate the wire in 1 sec.....	339

Abstract

While Shape Memory Alloys (SMAs) have exceptional actuation characteristics such as high energy density, silent operation, flexible packaging, etc., they have not found widespread use in commercial applications because of the significant learning curve required of engineers before they are capable of designing actuation devices using this unique material. An SMA actuation device design framework consisting of grammar, design methods, and design process enables engineers of different backgrounds to make efficient and appropriate design decisions in different stages of the design process. A reference SMA actuation device structure built on a generalized actuation device hierarchical structure using the actuation device grammar works as a reference structure to identify and populate device design options, and to model and analyze the device actuation performance as well as to enlighten non-expert engineers about the essential elements of SMA actuation devices. Design methods consisting of modular modeling, model aggregation and performance prediction, and visualization approaches support design decisions to serve diverse stakeholders of actuation device design by exposing the effects of individual device elements not only for SMA actuation devices, but also for a wide range of actuation devices. A multi-stage design process is formalized to help engineers create a detailed design including a three-step decoupled equilibrium design procedure which prevents potential iteration by decoupling the force and deflection of actuation output behavior, and hides the complexity of material and SMA architectural models from engineers while still exposing the impact of design parameters. The design framework makes SMA design knowledge more accessible to engineers with different levels of expertise and roles in device development by systematically organizing and presenting the device grammar, design methods, and design process. A design tool software platform based on the framework enables the creation of computer-aided design tools to support a variety of design tasks, which were demonstrated in two use case examples. By having the SMA actuation device design framework, the acceptance of the SMA actuation technology into both research and commercial applications can be increased to utilize promising SMA actuation benefits, and the device development cycle leading to these applications can be streamlined.

Chapter 1.

Introduction

While Shape Memory Alloys (SMAs) have exceptional actuation characteristics such as high energy density, silent operation, flexible packaging, etc., they have not found widespread use in commercial applications even though they are now readily available in a low cost wire form with reliable performance. While scientific developments have enabled advancements in material understanding, these advances have not generally been seen in practice because of the significant learning curve required of engineers before they are capable of designing actuation devices using this unique material.

1.1. Shape Memory Alloy actuation device applications

Using their stress-strain-temperature coupled material behavior, Shape Memory Alloys can produce actuation with exceptional characteristics such as high energy density, silent actuation, and compact and simple design. The research effort on Shape Memory Alloy actuation has been increased in the aerospace, automotive, medical and robotics fields [1–6]. Figure 1.1 shows the increasing number of SMA actuation device patents issued in U.S. during the last 20 years. This trend reflects the increasing expectations of utilizing SMA actuation in many application areas to expand the design space beyond that of conventional actuators. However, in spite of the advancements in research labs, these benefits of SMA are not fully exploited in real world applications because few engineers know how to design actuation devices using this sophisticated material.

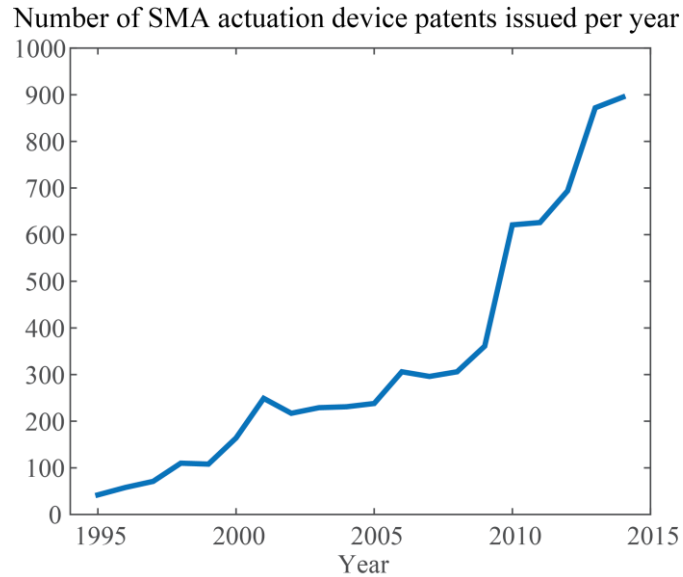


Figure 1.1. Increasing SMA actuation device patents.

The number of patents issued in U.S. has been increased in the last 20 years. The patents are searched within the United States Patent and Trademark Office website using query (“shape memory alloy” OR “SMA” OR “muscle wire” OR “NiTiNOL”) AND (“actuator” OR “actuation device”).

1.1.1. Material behavior of Shape Memory Alloys

Shape Memory Alloys (SMAs) are a type of material which transforms its crystal structure upon temperature and/or applied stress changes. A series of tests consisting of loading/unloading of SMA at two different temperatures and the unloaded transition between these temperatures (Figure 1.2) shows the stress-strain-temperature coupled behavior [7]. These stress and temperature induced transformations are characterized in two prominent properties: superelasticity (pseudoelasticity) and the shape memory effect. Superelasticity is based on a stress induced transformation, exhibiting a large recoverable deflection. The shape memory effect is based on a temperature induced transformation, exhibiting shape recovery upon temperature increase.

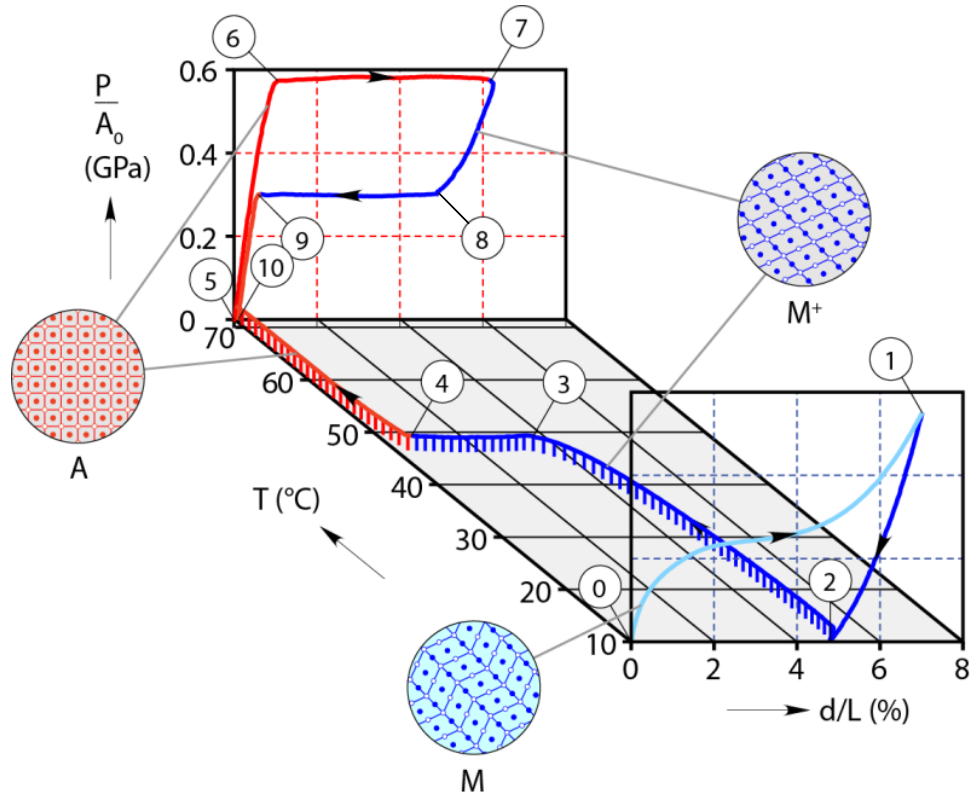


Figure 1.2. SMA material behavior [7].

The stress and temperature induced transformations are characterized in two prominent modes: superelasticity (pseudoelasticity) and shape memory effect. The superelasticity is based on stress induced transformation, exhibiting a large recoverable deflection under a stress level. The shape memory effect is based on temperature induced transformation, exhibiting a shape recovery upon temperature increase.

1.1.1.1. Shape memory effect

SMA is in the twinned martensite phase (⊙ on Figure 1.2) at low temperatures under no applied stress. When the stress in the SMA increases, the SMA transforms into the detwinned martensite phase (⊙→①) allowing large strain deformation up to 8 %. During this deformation and material transformation, if the stress is removed, the SMA only recovers the elastic portion of the deformation, but the deformation due to the transformation remains (①→②). However, when the temperature of the SMA is increased, the SMA transforms to the austenite phase (③→④), recovering its deformation due to the material transformation from twinned martensite to detwinned martensite (⑤). This effect is called the shape memory effect.

1.1.1.2. Superelasticity

The SMA material is in its parent austenite phase (⑤ on Figure 1.2) at high temperatures under no applied stress. When stress is applied, the SMA first behaves like an ordinary material showing a linear elastic deflection (⑤→⑥). However, when it reaches a certain stress level, which varies depending on the temperature of the SMA, the deflection strain increases without an increase in stress showing a plateau on the stress-strain plot (⑥→⑦). During this deflection, the crystal structure of the SMA transforms from the austenite phase to the stress-induced detwinned martensite phase. When the stress is removed from the SMA, the stress-strain curve does not follow its loading path. It shows a linear path from the point where the unloading starts, which is similar to that of conventional metals unloaded from the plastic region (⑦→⑧). The SMA then shows another lower plateau region, where the crystal structure of the SMA returns to the austenite phase (⑧→⑨), until it meets its original linear elastic deflection path (⑨→⑩).

1.1.2. Operation concept of a simple SMA actuator

In the simple SMA actuator example in Figure 1.3, actuation is produced by changing the temperature of the SMA wire while it is subject to a load. SMA actuation is achieved by shifting the force balance between the SMA wire and the load upon the SMA material behavior change due to its temperature change; changing temperature causes the material phase change between hot austenite and cold martensite, and the material behavior change causes the shift of the equilibrium between the SMA wire and the load, creating actuation stroke.

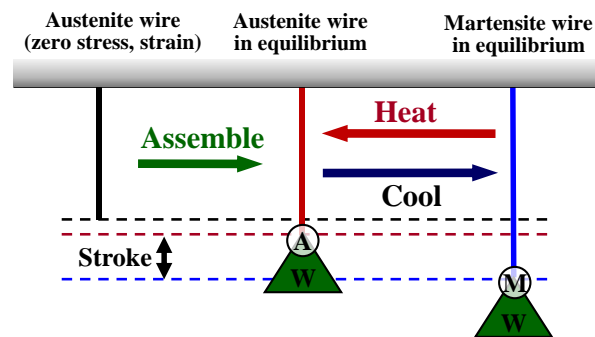


Figure 1.3. Schematic of a simple SMA actuator.

SMA actuation is achieved by shifting the force balance between the SMA wire and the load upon the SMA material behavior change due to its temperature change. The actuation is produced by changing temperatures of SMA wire while it is subject to a load.

When its temperature is below the martensite finish temperature, SMA shows a compliant detwinning behavior as shown in Figure 1.2, and it shows a stiff elastic behavior followed by a superelastic plateau when its temperature is higher than the austenite finish temperature. By changing the temperature of the SMA between a temperature above the austenite finish temperature and a temperature below the martensite finish temperature, the material behavior change produces actuation by shifting the equilibrium with the applied load. In Figure 1.4, the blue stress-strain curve on the left plot represents the cold compliant martensite SMA behavior (⑤→① on Figure 1.2), and the red stress-strain curve represents the hot stiff austenite SMA behavior (⑥→② on Figure 1.2). The green horizontal line represents the applied load in Figure 1.3 example in terms of the applied stress, which is converted using the total cross-sectional area of the SMA wire. The intersection between the red austenite stress-strain curve and the green load line (Ⓐ on Figure 1.4) represents the austenite equilibrium, and the intersection between the blue martensite stress-strain curve and the green load line (Ⓜ on Figure 1.4) represents the martensite equilibrium. The equilibrium shifts between these two equilibria upon the temperature change, and the distance between them is the net actuation strain, which can be converted to an actuation stroke using the length of the SMA wire.

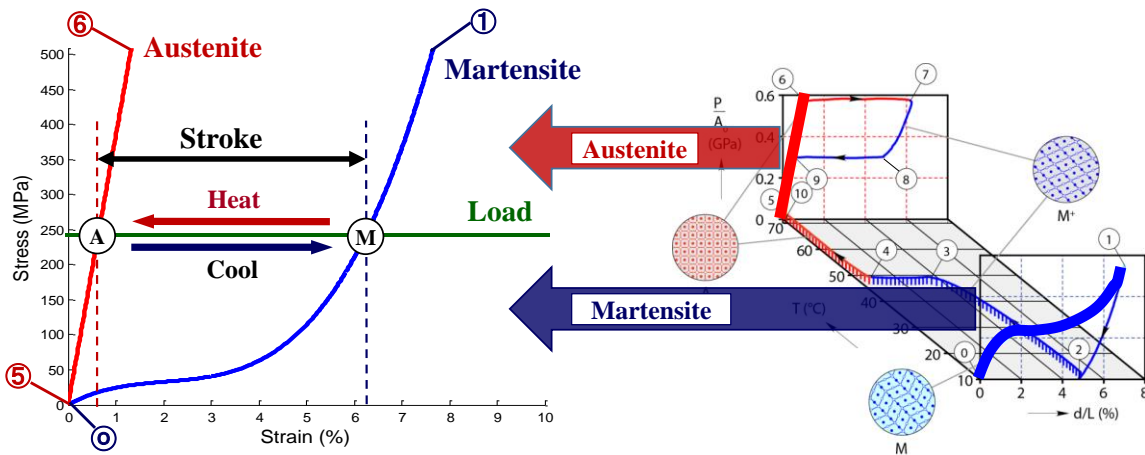


Figure 1.4. SMA behavior of simple actuation device during actuation.

When its temperature is below the martensite finish temperature, SMA shows the compliant detwinning behavior, and it shows the stiff elastic behavior followed by superelastic plateau when its temperature is higher than the austenite finish temperature. By changing the temperature of the SMA between the above austenite finish temperature and the below martensite finish temperature, the material behavior change produces the actuation by shifting the equilibrium with applied load.

As the simple SMA actuator example in Figure 1.3 illustrates an example using a straight wire form of SMA, other forms of SMA actuators follow the same principle to create actuation. SMA actuation utilizes the material behavior change upon a temperature change, and the material behavior change leads to a force balance change with applied load. As shown in Figure 1.2, without applied stress, SMA only transforms its crystal structure ($\text{ⓐ} \leftrightarrow \text{ⓑ}$) upon a temperature change without producing actuation. It is very important to note that SMA actuation relies on a force balance shift because SMA does not create actuation if there is no applied load. *Target Element* will be the term used to indicate the source of the applied load to emphasize that it is part of an actuation device system and it is the subject of actuation.

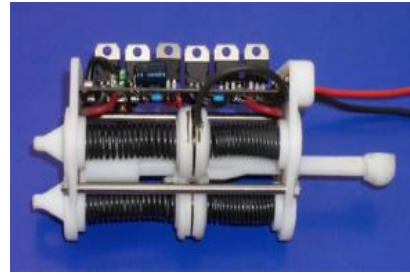
1.1.3. SMA actuator benefits and examples

Compared to conventional electromagnetic or hydraulic/pneumatic actuators, SMA actuators have many benefits such as high energy density, light weight, silent actuation, flexible and compact packaging, biocompatibility, and low cost. Many previous research efforts focused on creating applications to exploit these benefits to enable new types of actuation characteristics such as creating out of plane actuation without additional mechanisms [8,9], or to replace conventional actuators with low cost, flexible packaging, or light weight actuators. Research efforts on SMA actuation have increased in aerospace, automotive, medical, and robotics applications.

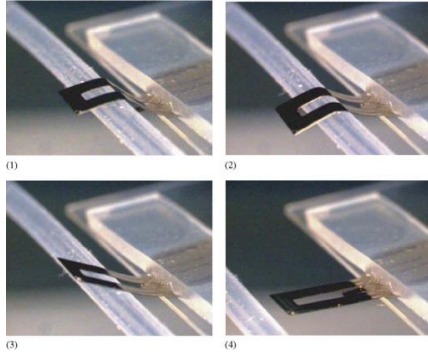
In aerospace applications, the main benefit of using SMA actuation is its light weight and flexible/compact packaging. Boeing demonstrated the possibility of using SMA actuation to control the F-15 tactical aircraft inlet geometry and internal flows to provide a large range increase with improved survivability as part of the DARPA SAMPSON project [4,10]. Diverse forms of SMA actuation devices were investigated for adaptive control of the aircraft surface wing shape to achieve a high lift coefficient in low-speed flight and low drag in high-speed flight [3,11–13]. The SMART (Smart Material-actuated Rotor Technology) project utilized SMA actuation to mitigate vibration and noise of rotorcraft [14,15]. Boeing also demonstrated the Variable Geometry Chevron (Figure 1.5a) using SMA actuation with full scale test flights to reduce the noise of commercial aircraft during take-off and reduce shock cell noise during cruise [8,16].



a) Active Chevron



b) Tumble Flap Actuator



c) Blood Vessel Grabber



d) SMA Robotic Finger

Figure 1.5. SMA actuator examples.

The research effort on Shape Memory Alloy actuation has been increased in aerospace, automotive, medical and robotics applications. a) Boeing demonstrated the Variable Geometry Chevron using SMA actuation with full scale flight test to reduce the noise of commercial aircraft during the take-off and reduce shock cell noise during cruise. b) Bellini et al. developed tumble flap actuator for automotive application. c) Sugawara et al. developed a thin film actuator to hold a fine blood vessel for microsurgery. d) Lan et al. developed a robotic finger using SMA wires embedded inside the structural parts.

In medical applications, the main benefit of SMA is biocompatibility as well as light weight and flexible compact packaging. Utter et al. demonstrated a surgical mechanotransduction device for correcting Short Bowel Syndrome with in-vivo tests for over 2 weeks [17]. Furst et al. developed a dual-joint smart inhaler nozzle actuated by SMA wires to provide targeted drug delivery to a certain location [18]. Sugawara et al. developed a thin film actuator (Figure 1.5c) to hold a fine blood vessel for microsurgery [19].

In automotive applications, light weight actuators enable an increase in fuel efficiency by providing actuation with lower weight than conventional actuators in addition to the compact / flexible packaging and possibly increased safety due to the replacement of the heavy weight and concentrated mass of conventional actuators with light weight distributed SMA actuators. General Motors demonstrated an active air dam and active louver to increase fuel efficiency by

improving the aerodynamics of a vehicle during cruise [20,21]. Barnes et al. developed a pedestrian protection device using SMA actuators [22]. Bellini et al. developed a tumble flap actuator (Figure 1.5b) for internal engine air flow control, and Williams et al. developed a self-contained mirror positioning device [23,24].

In robotics applications, flexible and distributed packaging is the main benefit of SMA. Lan et al. developed a robotic finger (Figure 1.5d) using SMA wires embedded inside the structural components [25]. Lee et al. and Kim et al. developed earth worm like locomotive robots using different types of SMA spring actuators [26,27]. Son et al. developed a quadruped robot with SMA actuators for dynamic walking [28].

While there are many research efforts to develop novel SMA actuated devices in many application areas which have demonstrated the benefits of using SMA over conventional actuators, it is hard to find many applications in practice because there is a limited number of engineers who know how to design actuation devices using this unique material.

1.2. SMA actuation device design

There are multiple stages in the actuation device development cycle [6] as shown in Figure 1.6. In the early stage, the design problem is defined to set the required performance and

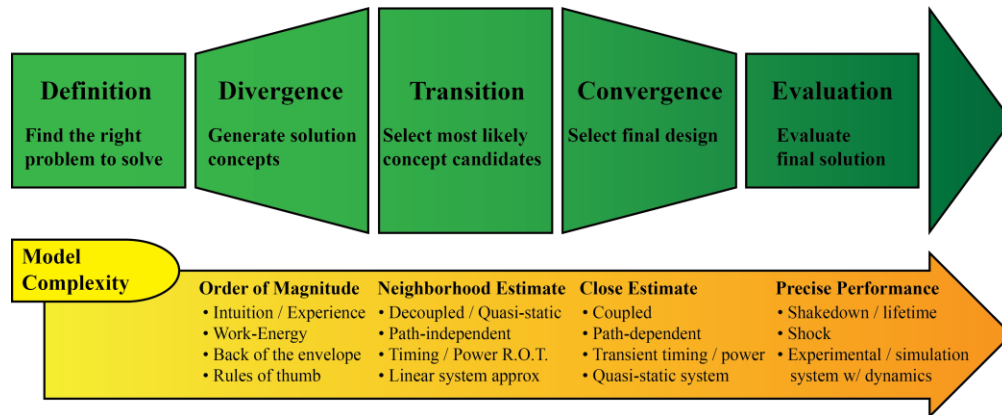


Figure 1.6. Actuation device development cycle (modified from [6]).

There are multiple stages in actuation device development cycle. In the early stage, the design problem is defined to set the required performance and to identify the constraints. Using these problem definition, the next stage is generating diverse solution concepts, and then select most likely concept candidates to develop detailed designs to select a final design. Once a final design is selected in the later design stage, the detailed design is finalized using analysis and/or optimization techniques. The finalized design is evaluated and fine-tuned by building prototypes, and performing in-depth analysis.

to identify the constraints. Using this problem definition, the next stage is to generate diverse solution concepts. The most likely concept candidates are then selected from which detailed designs are developed. Once a final design is selected from these design candidates in the later design stage, the detailed design is finalized using analysis and/or optimization techniques. The finalized design is evaluated and fine-tuned by building prototypes, and performing in-depth analysis.

Well trained engineers can follow through the actuation device development cycle using conventional actuators because there is a body of well developed intuition and community experience as well as diverse design tools to help engineers to apply models with diverse complexity in different stages of the device development cycle (Figure 1.6). However, it is not easy to follow through the development cycle using SMA to design actuation devices because most of the previous research efforts focused solely on the design analysis part of the convergence stage in the actuation device development cycle. While there have been research efforts on SMA actuation device application development, research on design was limited to modeling of SMA material constitutive relations [29–34] and/or particular device mechanisms [25,35–38], and implementation of material models to computer-aided engineering tools [33,39–42]. Moreover, the previous research efforts focused on particular aspects of actuation device development, and there is limited effort to tie these disconnected design research efforts together.

1.2.1. Stakeholders of SMA actuation device development

While the actuation device development cycle illustrates the major activities of SMA actuation device design, developing SMA actuation devices involves a diverse group of stakeholders (Table 1.1) whose activities are not necessarily included in the development cycle. *Material scientists* act as *material developers* developing new materials by changing the composition ratio and/or establishing new treatment processes, and as *material modelers* characterizing and modeling the material behavior. While they do not develop actuation devices by themselves, properties of the new materials affect actuation device design by imposing different material usage constraints, and material models are used in the design and analysis of actuation devices. *System engineers* assign design tasks to design teams and integrate SMA actuation devices into a system. They provide actuation requirements and constraints to SMA device engineers, and consolidate individual actuation devices into a system. *SMA actuation*

device researchers develop new SMA architectures and device structures to make the best use of the SMA material to produce actuation. *SMA device engineers* design a particular actuation device for a specific application. They generate the concepts of actuation device within the constraints, evaluate and downselect the concepts, create a detailed design with the chosen concept, and finalize the device design.

To design actuation devices, SMA device engineers must evaluate the feasibility of using SMA to produce the required force and stroke, choose SMA architecture and device structure / elements, make material usage decisions, set design parameters while exploring the design space, and finalize the detailed design using in-depth analysis. While expert SMA device engineers design SMA actuation devices using known SMA design methods and/or intuition built upon their experiences, they are not necessarily experts in all potential application areas such as aerospace, automotive, medical, robotics, etc. Expert engineers in application areas are usually non-experts in SMA technology, and often apply an ad-hoc design approach without knowing existing SMA technology. However, due to the lack of understanding of the complex material behavior, they commonly fail to create a good SMA actuation device design, and this failure by non-expert SMA engineers hinders the acceptance of SMA technology.

It is important to keep all these stakeholders in mind when we discuss SMA actuation device design. While the main design activities are done by device researchers or device engineers, they have to evaluate the effect of constraints imposed by material scientists and system engineers. Moreover, other stakeholders, i.e. material scientists and system engineers, also need to evaluate the actuation device behavior to perform their tasks. Design methods, which serve not only the device researchers or device engineers but also other stakeholders, can improve SMA actuation device design.

Table 1.1. Stakeholders of SMA actuation device design

Stakeholder Group	Material Developer / Vendor	Material Modeler	Design Researcher	Expert Device Engineer	Non-expert Device Engineer	System Engineer
SMA modeling	Experienced / Limited	Experienced	Limited	Limited	Inexperienced	Inexperienced
SMA device design	Limited	Inexperienced	Experienced	Experienced	Inexperienced	Inexperienced
Engineering design	Limited	Inexperienced	Experienced	Experienced	Experienced	Experienced
Role	<ul style="list-style-type: none"> Develop new materials 	<ul style="list-style-type: none"> Characterize and model material behavior 	<ul style="list-style-type: none"> Develop SMA architecture and device structure 	<ul style="list-style-type: none"> Develop SMA actuation device design for specific application 	<ul style="list-style-type: none"> Integrate SMA actuation devices into system 	
Activities	<ul style="list-style-type: none"> Change the composition ratio Develop treatment process 	<ul style="list-style-type: none"> Material characterization 	<ul style="list-style-type: none"> Evaluate feasibility of using SMA to produce required force and stroke 	<ul style="list-style-type: none"> Set design constraints 	<ul style="list-style-type: none"> Provide actuation requirements Set design constraints Modify the design to integrate into system (most likely interface) 	
Impact	<ul style="list-style-type: none"> Impose (different) material constraints Enable new device design 	<ul style="list-style-type: none"> Provide material model 	<ul style="list-style-type: none"> Choose SMA architecture and device structure / elements Set design parameters Finalize design using in-depth analysis 	<ul style="list-style-type: none"> Provide new SMA architecture 	<ul style="list-style-type: none"> Impose design constraints Change initial interface condition 	

Actuation Devices Design

1.2.2. SMA actuation device design problem example: latch release device

To discuss the design of SMA actuation devices, an example latch release device is introduced. A latch release device (Figure 1.7) is an SMA wire actuation device which uses straight wires to release a trunk latch in an automobile. SMA wires are connected to a latch mechanism through a mechanical lever, and an extension spring provides the additional resetting force to the SMA.



Figure 1.7. Latch release device.

A latch release device is an SMA wire actuation device which uses straight wires to release a trunk latch in an automobile. SMA wires are connected to a latch mechanism through a mechanical lever, and an extension spring provides resetting force for the restoration stage.

To design an SMA actuation device, device engineers go through multiple design stages (Figure 1.8), which have been narrowed down from the full device development cycle (Figure 1.6). Before starting the actual design, engineers evaluate the feasibility of using SMA for a given design task. For feasibility evaluation, *back-of-the-envelope calculation* is commonly used estimating the target element behavior as single force and stroke values to be compared with the usable stress and strain of the SMA.

Once the feasibility of using SMA is established, the geometric design parameters of the SMA actuation device, such as the length, and diameter/number of wires, are set within the packaging and material usage constraints (usable stress and strain). For most SMA actuation device design problems, the available packaging footprint is the main design driver because of the typical 1 ~ 4 % usable actuation strain. However, the usable actuation strain varies depending on the applied stress in the SMA, which is set not only by the device geometric parameters but also by the installation condition, defined by the relative position between the actuation device and the target element. Moreover, producing the required force is often tied

with the actuation time requirement. In many SMA wire actuation devices, resistive heating (Joule heating or ohmic heating) is the most commonly used method to heat the SMA because of its simplicity. The electric current and voltage required to heat the SMA wires to the necessary temperature within the desired actuation time to transform the SMA to the austenite phase are important design parameters. The actuation restoration time is decided by the cooling time of the SMA, which in many cases relies on convective heat transfer. For convective heat transfer, the wire diameter, environmental medium, and ambient temperature are key parameters to decide the cooling time.

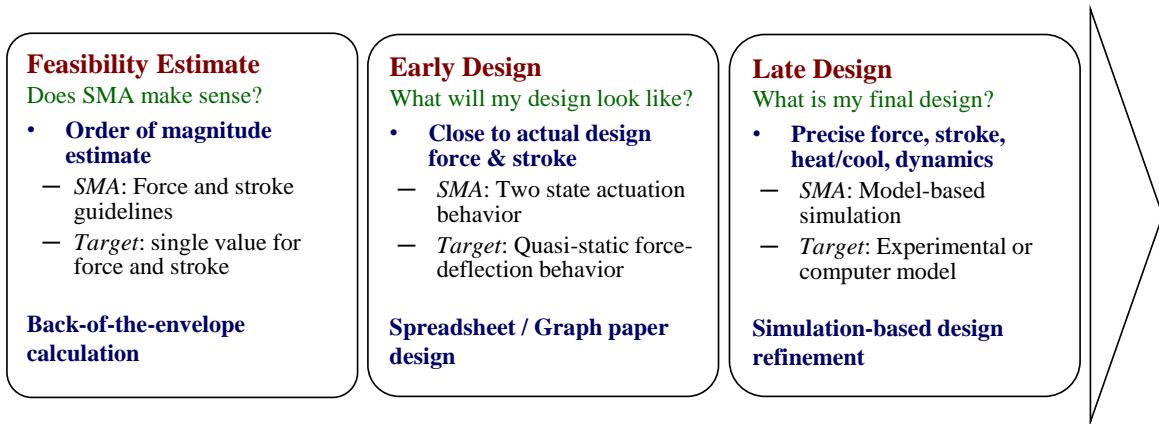


Figure 1.8. Multiple stages of SMA actuation device design.

Design of SMA actuation device goes through multiple design stages. The feasibility of using SMA to produce required force and stroke is first evaluated, and then a detailed design is created in the early design. Finally the design is finalized using in-depth analysis such as dynamic simulations.

In the early stage of detailed design, the SMA is often assumed to be actuated between two states, i.e. austenite and martensite, and the target element behavior is simplified using quasi-static assumptions. The main goal of this early stage design is to create a detailed design to produce a required force and stroke within the available packaging footprint under the usable SMA stress and strain limits. Once a detailed design is set, the design is finalized in the late design stage using an in-depth analysis such as dynamic simulation or FEA. While in-depth analysis requires a higher level of understanding of the SMA material, there have been advancements in both the understanding of the SMA material [31,34,43–45] and the implementation into FEA models [16,39,46]. However, improvements are still needed in the early stage to create a detailed design.

1.2.3. SMA actuation device design methods

There are two types of design methods which are widely used to set the geometric design parameters in the early design stage: force-deflection curve design methods and empirical design methods. Force-deflection curve design methods use a graphical method to predict the actuation stroke by finding the equilibrium shift between the hot austenite phase and the cool martensite phase. Empirical design methods usually generate a surrogate performance model through a set of experiments of a pre-determined actuation device configuration, and use the surrogate model to set design parameters.

1.2.3.1. Force-deflection curve design method

Force-deflection curve design methods [47,48] use the same assumption which was used to illustrate the basic concept of SMA actuation. The SMA material behavior is assumed to be switched between the full austenite phase above the austenite finish temperature and the full martensite phase below the martensite finish temperature. The SMA force-deflection behavior curves at the austenite and martensite phases (red and blue curves on Figure 1.9) and the target element behavior curve (green line on Figure 1.9) are used to predict the motion by finding the

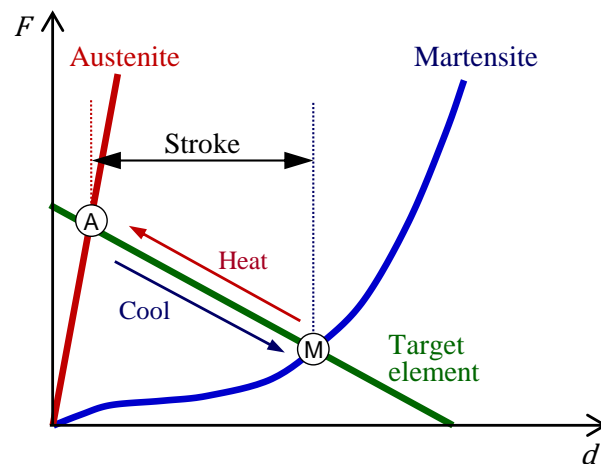


Figure 1.9. Force-deflection curve design method.

The SMA material behavior is assumed to be switched between the fully austenite phase and the fully martensite phase. The SMA force-deflection behavior curves at the austenite and martensite phases (red and blue curves) and the target element behavior curve (green line) are used to predict the motion by finding the intersections between the material curves and the system curve (points **A** and **M**).

intersections between the material curves and the system curve (points \textcircled{A} and \textcircled{M}), thereby, defining the equilibrium at each phase. The difference between the equilibria determines the actuation stroke. The SMA force-deflection curves are created by mapping the SMA stress-strain behavior to the actuation device force-deflection output coordinates through the SMA geometry. The plot can be also created in stress-strain coordinates by mapping the target element force-deflection behavior.

While the force-deflection curve method is a design method for performance prediction for a given set of device design parameters, it does not provide a design process to select design

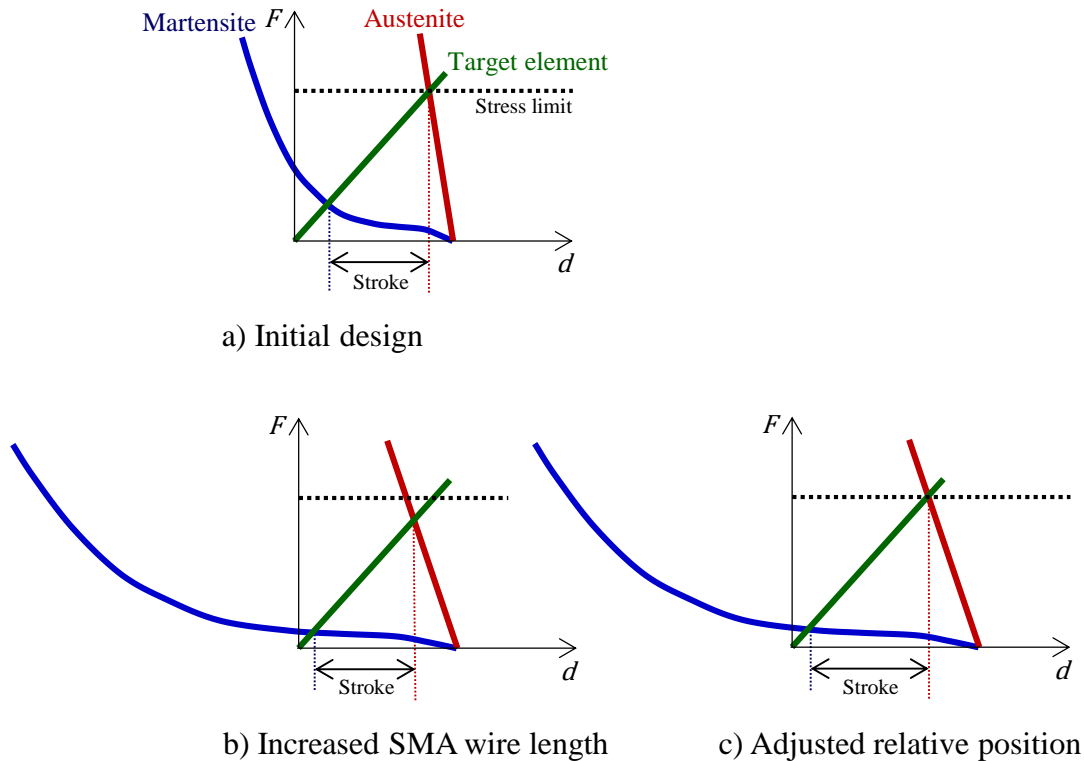


Figure 1.10. Example of non-proportional performance change: effect of increased SMA wire length on actuation stroke.

When a straight SMA wire actuation stroke is smaller than the design requirement, a common design change attempt by a non-expert SMA device engineer is increasing the length of wire. However, the actuation stroke does not always increase proportional to the length change. The actuation stroke of initial design (a) is not improved only by increasing the length of SMA wire (b) because the austenite and martensite equilibria shift at the same time upon the design change. While the actuation stroke can be improved by adjusting the relative position between the SMA and the target element (c), the increased stroke is still not proportional to the SMA wire length increase.

parameters. Moreover, design parameter changes often cause unexpected and non-intuitive changes in actuation performance. For example, when a straight SMA wire actuation stroke is smaller than required, a common design change attempt by a non-expert SMA device engineer is to increase the length of wire under the expectation that the actuation stroke increase is proportional to the length change. However, as shown in Figure 1.10, the actuation stroke does not always increase proportionally to the length change, moreover the actuation stroke might become even smaller with a longer length of wire. The actuation stroke of the initial design (Figure 1.10a) is not improved only by increasing the length of SMA wire (Figure 1.10b) because the austenite and martensite equilibria shift at the same time due to the design change. While the actuation stroke can then be improved by adjusting the relative position between the SMA and the target element (Figure 1.10c), the increased stroke is still not proportional to the SMA wire length increase.

Moreover, while there are several modifications of this method to address complex device structures other than a straight wire form of SMA [22,36,49,50], there is no systematic approach to handle complex device structures.

1.2.3.2. Empirical design method

Another common design approach is empirical-based design, where the actuation behavior is empirically measured with a set of pre-determined configurations and applied to the design [25,51–53]. In the SMA-driven robot finger design example in Figure 1.11, a test setup was built (Figure 1.11a) to characterize the actuation device behavior of 4 candidate configurations (Figure 1.11b). The load-contraction ratio behavior curves of each configuration (Figure 1.11c) are used for robot finger design (Figure 1.11d).

Although this empirical design method is not limited by complex device structures, it is not fully scalable to explore the design space. For example, if the wire diameter is changed, the actuation device behavior must be re-evaluated by repeating the physical experiments. Because this characterization only covers a specific configuration, the re-usability of the research efforts is limited to a specific configuration. Moreover, when the device configuration needs to be modified during the design process, this method provides limited flexibility.

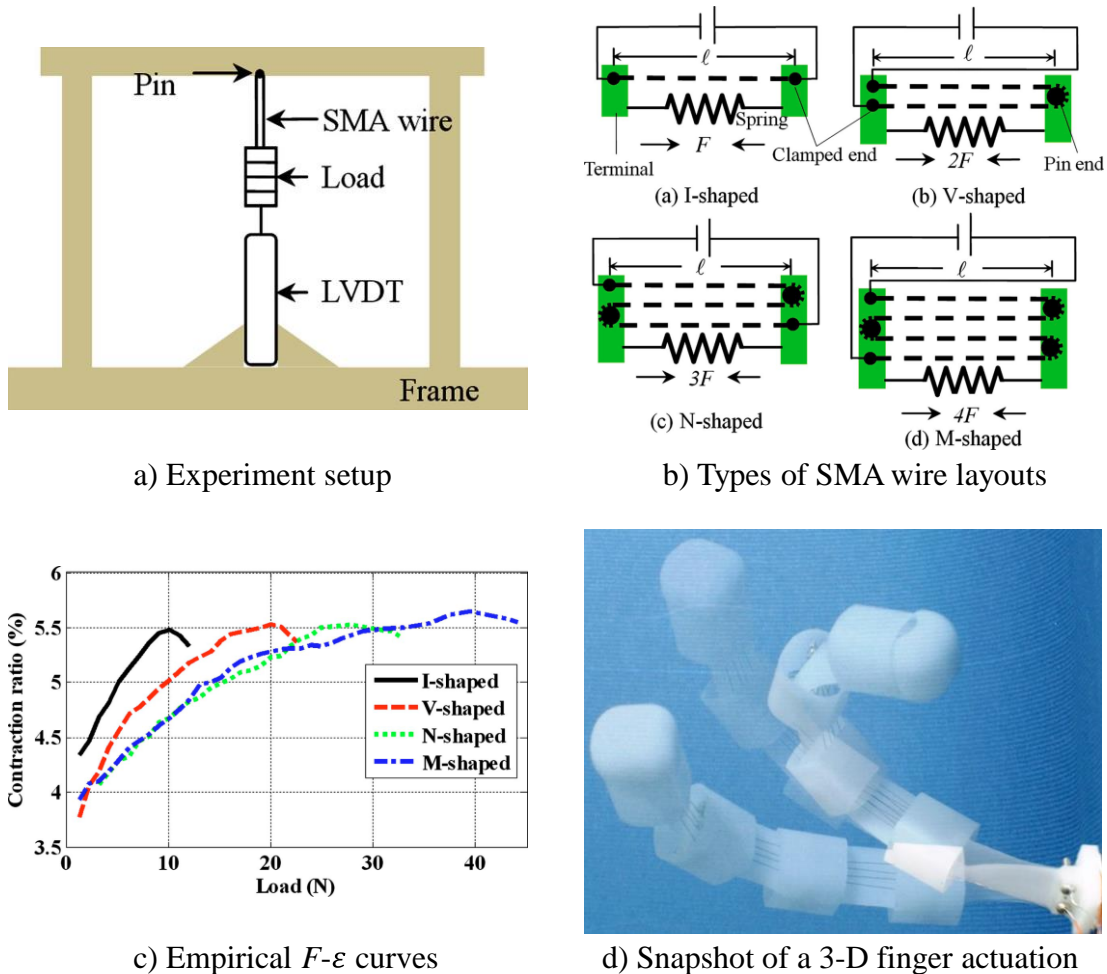


Figure 1.11. Empirical design method example: SMA wire actuated compliant finger [25].

A test setup was built (a) to characterize actuation device behavior of 4 candidate configurations (b). And the load-contraction ratio behavior curves of each configuration (c) are used for robot finger design (d).

1.2.4. SMA actuation device architectures

Designing SMA actuation devices becomes more difficult with SMA architectures due to the complicated interaction between the SMA material and the target element. While SMA actuation has many benefits compared to conventional actuators, the stroke of actuation is usually the limiting factor of using SMA for actuation device design. To overcome the stroke limitation, several SMA architectures (Figure 1.12) has been utilized to amplify the 1 ~ 4 % usable strain of straight SMA wires. For example, the spool packaging technique (Figure 1.12a) is an SMA architecture in which the SMA wire is wrapped around pulleys or mandrels to reduce the length-wise package footprint [54,55]. The SMA web architecture (Figure 1.12b) utilizes the

non-linear leveraging of the web geometry, which is effective to close a long shallow gap [38,56–60]. Another architecture is an SMA driven ratchet actuator (Figure 1.12c) which uses time leveraging of an SMA wire actuator to advance a ratchet to accumulate steps, achieving a large overall stroke of a long rack or continuous rotation of a gear [22,35,37,61]. While these architectures utilize the tensile strain changes, there are also other architectures which use shear strain changes such as SMA cables (Figure 1.12d) [62,63] and SMA helical spring actuators (Figure 1.12e) [27,51,64–77]. While these SMA architectures can overcome the stroke limitation of SMA, the modified interaction between the SMA and target element makes the design of SMA actuation devices even harder because of the additional complexity introduced with the architecture.

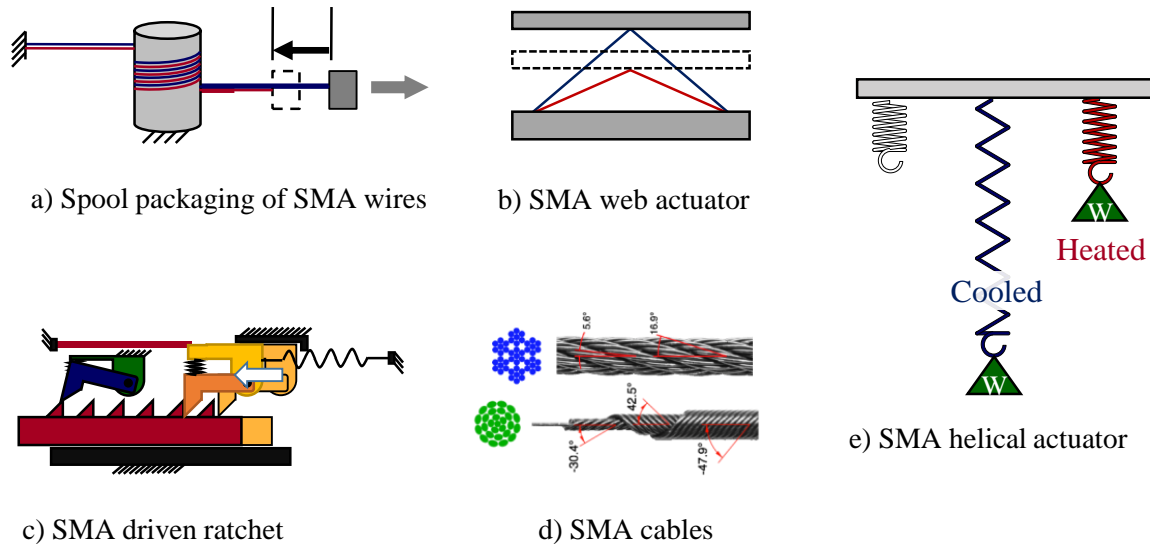


Figure 1.12. Examples of SMA architectures.

To overcome the stroke limitation, several SMA architectures has been utilized to amplify the 1 ~ 4 % usable strain of straight SMA wires.

To discuss the design of SMA actuation devices using sophisticated SMA architectures, two example devices are introduced: the active inner belt seal device and the SMART hood lift reset device. The active inner belt seal device example uses an SMA web actuator (for the in-depth explanation of SMA web actuator, refer to Appendix A), and the SMART hood lift reset device example uses an SMA driven ratchet (Appendix B). Along with the latch release device, these SMA actuation devices will be used as examples throughout the dissertation.

1.2.4.1. SMA web architecture design example: Active inner belt seal device

The active inner belt seal device (Figure 1.13) is an SMA wire actuation device which uses an SMA web actuator to adjust the sealing force of the inner belt seal against the automotive door window. The adjustability of the sealing force mitigates squeal and moan and reduces the required load for the window motor during opening and closing, while maintaining a high sealing force. The web architecture is selected to contain the actuation device within the available shallow form factor package space inside the existing inner belt seal. The SMA wire web actuator is connected between two surfaces of the existing inner belt to actuate the leaf of the inner belt seal to adjust the sealing force on the door window.

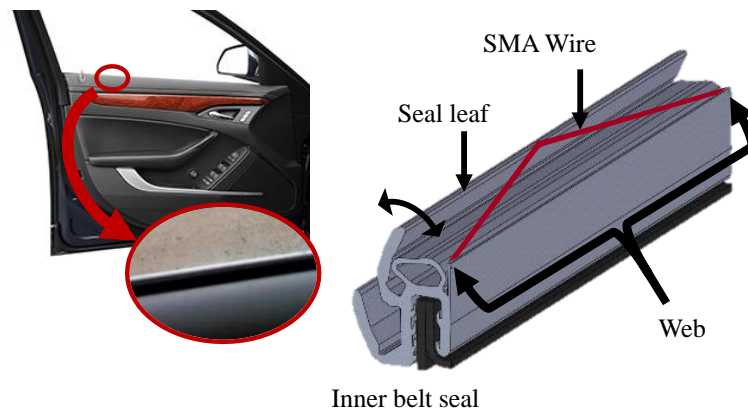


Figure 1.13. Active inner belt seal.

An active inner belt seal device is an SMA wire actuation device which uses an SMA web actuator to adjust the sealing force of the inner belt seal against the automotive door window. The adjustability of the sealing force enables the reduction of the load for the window motor while opening and closing the door window, while maintaining the sealing force when the window is not moving.

An SMA wire web actuator, which zigzags the SMA wire along the width between two surfaces to generate stroke amplification normal to the surfaces (Figure 1.14), has two layers of architectures: the first transformation layer is from SMA material stress-strain to SMA wire tension-elongation (Figure 1.14a), which is same as that of the SMA straight wire, while the second transformation layer is from SMA wire tension-elongation to web actuator force-deflection (Figure 1.14b). Thus, to use the force-deflection design method for SMA web actuator design, the mapping of the target element behavior to the SMA material stress-strain behavior requires a two-step mapping: first mapping to the tension-elongation behavior coordinates, and then to the stress-strain behavior coordinates. Moreover, whenever the web

geometry parameters are updated, the entire mapping must be repeated. Although the web architecture looks like a simple geometric amplification of the SMA wire stroke, it introduces additional complexity in the application of the force-deflection design method.

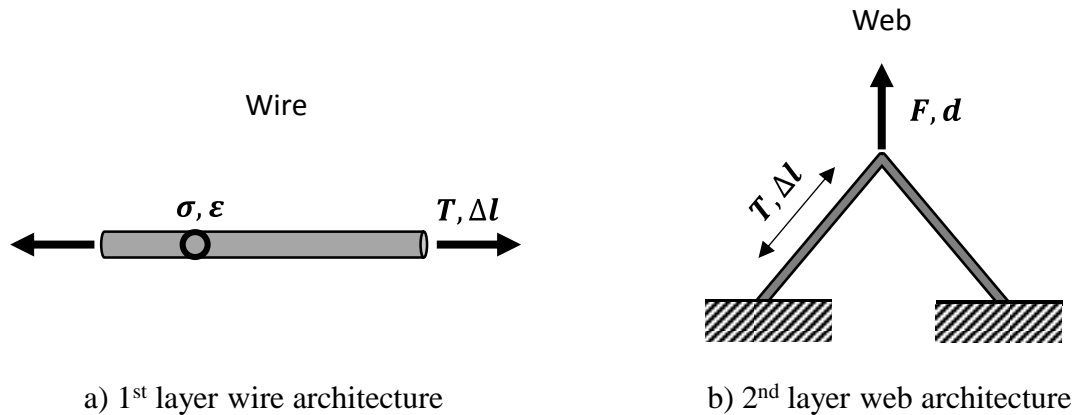


Figure 1.14. Multi-layer structure of the SMA web actuator.

SMA wire web actuator, which zigzags the SMA wire along the width between two surfaces to generate stroke amplification normal to the surfaces, has two layers of architectures: the first transformation layer is from SMA material stress-strain to SMA wire tension-elongation (a), which is same as that of the SMA straight wire, and the second transformation layer is from SMA wire tension-elongation to web actuator force-deflection (b).

1.2.4.2. SMA driven ratchet design example: SMART hood lift reset device

The SMART hood lift (Figure 1.15) is a pedestrian protection device which lifts the hood of an automobile to prevent direct contact between the pedestrian and the engine block. By creating sufficient space between the relatively compliant hood and the rigid engine block, it mitigates head injuries [22]. The lift force is provided by a compression spring which is triggered using an SMA wire driven latch release device. For reusability of the hood lift mechanism, an SMA driven ratchet mechanism is used to compress the spring to the ready state. Due to the extremely large stroke compared to the limited package space inside the hood lift spring, the ratchet mechanism is the only architecture capable of producing the required force and stroke. Although there is a constraint on the overall actuation speed using the ratchet architecture, resetting speed is not critical for the hood lift device.

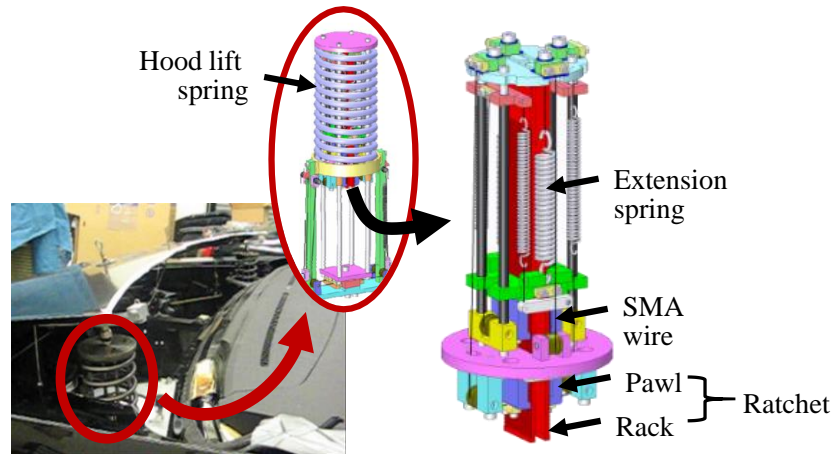


Figure 1.15. SMART hood lift reset device [22].

The SMART hood lift is a pedestrian protection device which lifts the hood of an automotive vehicle to prevent direct contact between the pedestrian and the engine block. The lift force is provided by a compression spring which is triggered using an SMA wire driven latch release device. For reusability of the hood lift mechanism, an SMA driven ratchet mechanism is used to compress the spring to the ready state.

An SMA driven ratchet actuator (Figure 1.16) uses time leveraging of the SMA wire actuator to advance a ratchet to accumulate steps, achieving a large overall stroke of a long rack or continuous rotation of a gear [22,35,37,61]. While mechanical leveraging architectures trade off output force to achieve larger stroke, time leveraging architectures do not sacrifice the output force, rather they require a longer time to achieve the full stroke of many steps. In addition to producing a large stroke or continuous rotation, the SMA ratchet architecture is capable of

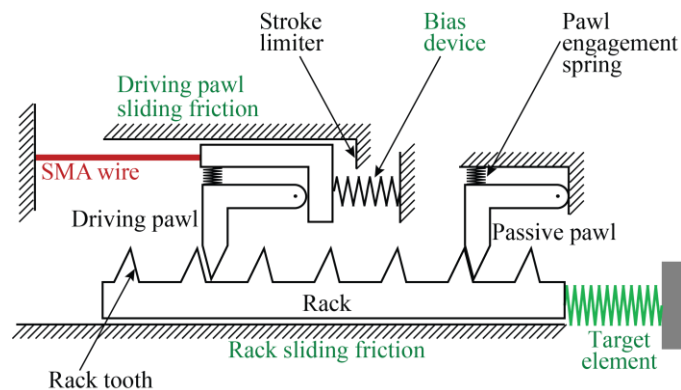


Figure 1.16. SMA wire ratchet mechanism.

An SMA driven ratchet actuator uses time leveraging of SMA wire as an actuator to advance a ratchet to accumulate steps, achieving large overall stroke of a long rack or continuous rotation of a gear.

precisely controlling position in discrete steps, and holding intermediate and/or final positions without requiring power.

Because the SMA wire and the target element are mechanically connected through the rack, the relative position between the SMA wire and the target element resets for each step of actuation due to the accumulated advancement of the rack. Because of the increased relative distance and resulting target element force change, the SMA reaches a new austenite equilibrium position after each step while the martensite equilibrium stays at the same position. Due to this austenite equilibrium position shift, the effective stroke size varies between actuation cycles. To apply the force-deflection curve design method for SMA driven ratchet design, the force-deflection plot must be created for each step, and the mapping of the target element must include the additional interaction forces due to the rack and pawl of the ratchet mechanism.

While there have been systematic design methods since the 1990's, engineers still rely on empirical design methods [25,51–53] because systematic design approaches are hard to use with complex SMA architectures and device structures with many additional elements. Moreover, there are not many SMA applications in the real world because there is a steep learning curve required to design SMA actuation devices. Two design examples show the additional complexity of designing real devices which have complicated SMA architectures and additional device elements. These additional device elements and SMA architectures make the application of existing design methods more difficult, and make the already non-intuitive design parametric sensitivity even harder to predict, forcing engineers to rely on empirical design methods.

1.3. Research Issues

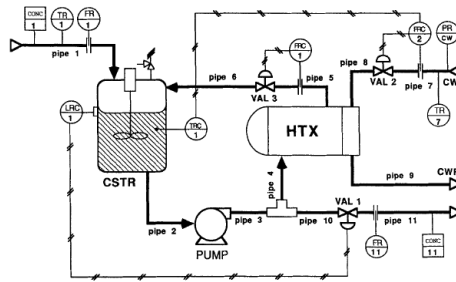
To establish a systematic design approach for SMA actuation devices, there are several areas of research issues to be addressed. First, to handle diverse configurations of actuation device structures such as those shown in the device design examples, there needs to be a systematic approach to describe actuation device structures and to help communication between the stakeholders of actuation device development. Moreover, a reference device structure can provide a baseline to start the exploration of the design options, and enable the establishment of a unified terminology. Second, there should be a set of design methods to support the design decisions which must be applied to complex actuation device structures. Third, a systematic procedure to create a detailed design of an SMA actuation device should be established to

support both expert and non-expert engineers. Forth and last, this SMA design related knowledge should be systematically organized and presented to engineers. However, these research issues are not well explored and addressed in previous research efforts.

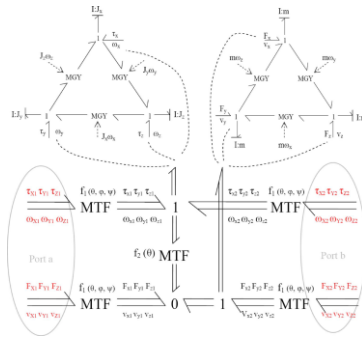
1.3.1. Device grammar

A *device grammar* is a vocabulary and syntax to describe, communicate, and understand a device design. There are commonly used modular system methods to describe systems such as block diagrams, flowcharts, work / system breakdown structures (WBS / SBS), and bond graphs [78–83]. However, these current modular system methods (Figure 1.17) do not well support actuation device design because of their focus on dynamic simulation modeling or system engineering / project management as well as their loose tie between the system representation and physical components and their design parameters.

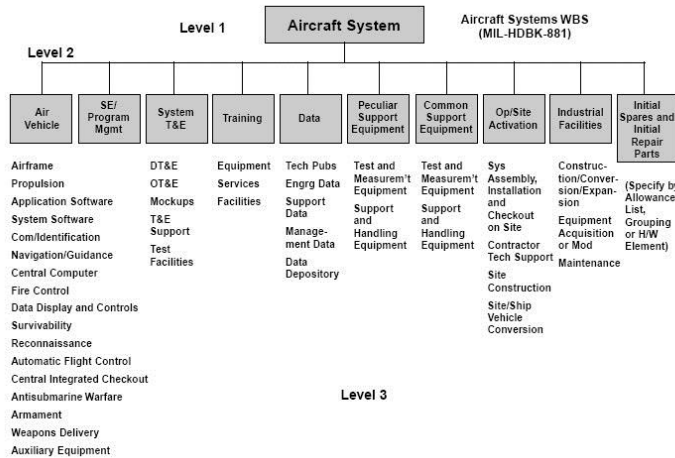
Moreover, there is no reference structure and unified terminology for SMA actuation devices except for those with the most simple structure [48,84]. While these simple conceptual device structures in Figure 1.18 are useful for explaining device operation concepts and validating material constitutive relation models, they are limited in their usefulness for device design because they do not include additional device elements which are commonly used to modify the actuation performance such as stroke limiters or bias (reset) springs. Furthermore, the lack of a unified terminology (for example rotor, stator, and commutator for electric motors) hinders the collaboration between diverse groups of stakeholders and across disciplines. For example, there are two commonly used approaches to define the initial condition of SMA actuation devices. One approach uses the initial stress in the SMA material as the reference parameter, and another approach uses the relative position between the SMA actuation device and the target element before they are mechanically connected together. Moreover, even with these two concepts to set the initial condition, i.e. initial force or initial deflection, different stakeholders may use different design parameters. For example, material scientists tend to evaluate the material behavior in terms of the stress and strain, thus they prefer the pre-strain or pre-stress, while device engineers may use pre-load as a design parameter. System engineers may prefer the relative position to check the geometric interference within the system. Although these parameters are coupled, the different selection of design parameter and corresponding terminology hinders collaboration between different stakeholders and/or research groups. There



a) Flow Chart example: Stirred reactor [81]



b) Generic Bond Graph example: 3 DOF gear [82]



c) Work Breakdown Structure (WBS) example: aircraft system [83]

Figure 1.17. Modular system methods examples.

The current modular system methods to describe systems, such as block diagrams, flowcharts, work / system breakdown structures (WBS / SBS), and bond graphs, do not well support actuation device design because of their focus on dynamic simulation modeling or system engineering / project management as well as their loose tie between the system representation and physical components and their design parameters.

needs to be a device grammar which represents an actuation device system with a strong tie to individual device elements and design parameters, and a reference SMA actuation device

structure which encompasses all the common SMA device sub-components to unify the terminology and educate non-expert SMA engineers.

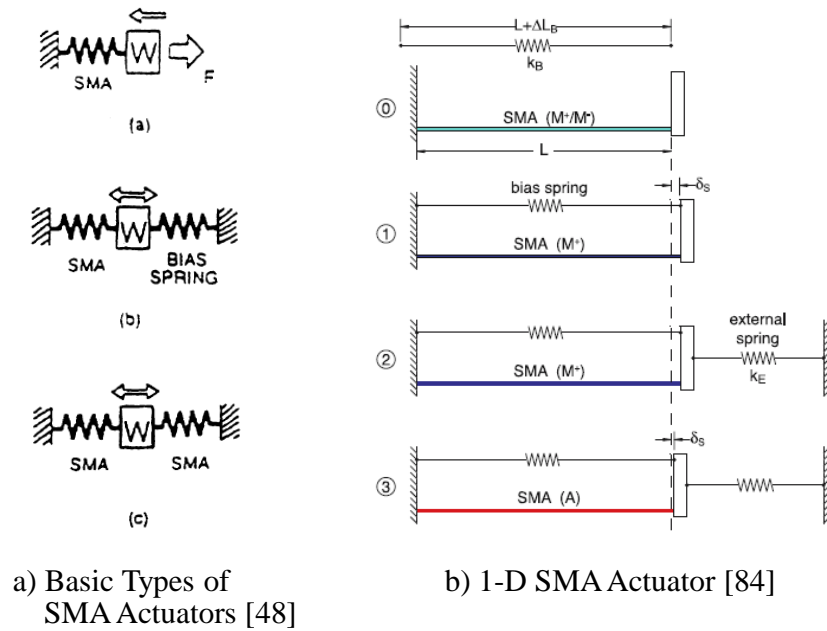


Figure 1.18. Simple conceptual SMA actuator examples.

While these simple conceptual device structures are useful for explaining device operation concepts and validating material constitutive relation models, they are limited in their usefulness for device design because they do not include additional device elements.

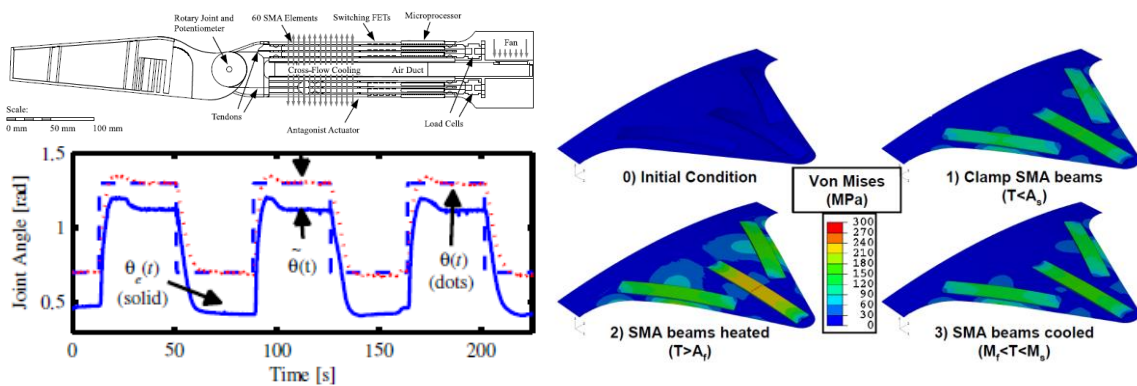
1.3.2. Design methods

Design methods are the means to address particular design tasks. Understanding the actuation device system behavior is necessary to make design decisions at different stages of the design process, and there are three major design tasks for the comprehension of system behavior: modeling, performance prediction, and visualization (presentation) of behaviors and prediction results.

Although there are material constitutive relation models available to predict the stress-strain-temperature coupled material behavior of SMA [31,34,43–45], it is not easy to apply these models for actuation device design which incorporates complex SMA architectures and which involves additional components within real actuation devices. Moreover, SMA architectural transformations impose limitations on performance prediction approaches, but there is no systematic method to integrate architectural models into the system model. Furthermore, most of

the design models developed in previous research are hard to reuse for future design projects due to a lack of modularity [22,26,36]. There needs to be a modular modeling approach using a reference SMA actuation device structure to handle complex SMA architectures and additional components while maintaining the reusability of individual models for device elements.

While performance prediction methods exist to evaluate the actuation device system behavior such as FEA implementation of SMA constitutive models [16,39,46], or equilibrium methods using force-deflection / stress-strain curves [22,48,36,47,50], it is hard to use them for supporting design decisions. Current performance prediction methods require additional parametric studies with expensive computation to evaluate the impact of design parameters of individual components because they often provide only output performance as a performance evaluation result (Figure 1.19). Moreover, the computationally intense performance prediction methods such as FEA limit the interactive exploration of the design space. Furthermore, once a system is modularly modeled to ensure the reusability of individual component models, it is not trivial to combine them to solve the aggregated system model. There needs to be a systematic model aggregation and performance prediction approach to support design decisions by providing a comprehension of the complete actuation device system.



a) SMA driven robot arm angle response [51] b) FEM analysis of Boeing VGC [16]

Figure 1.19. Performance prediction method examples.

Current performance prediction methods requires additional parametric study with expensive computation to evaluate the impact of parameters of individual components because they often provides only output performance as performance evaluation result.

While a heat map-type visualization (Figure 1.19b) is commonly used for the post-processing of FEA methods, and equilibrium methods provide force-deflection / stress-strain

curve plots, these visualizations have limitations to expose the effects of individual device elements and their design parameters, which are required to help diverse groups of stakeholders with interests in different elements and aspects of actuation device systems. For example, material scientists are interested in the effect of material behavior on the actuation performance, while system engineers focus on the effect of the SMA actuation device on the system behavior. For device researchers and device engineers, their interests move throughout the individual device elements while they are deciding appropriate design parameters of each element. Each stakeholder can benefit from a visualization method which shows the effect of the device element of their particular interest. While Shaw and Churchill [85] created design plots to select the bias spring stiffness (Figure 1.20), they only support the selection of one design parameter of an SMA actuation device. A systematic visualization method to expose the effect of individual device elements without expensive parametric studies can help diverse groups of stakeholders with diverse tasks to make design decisions.

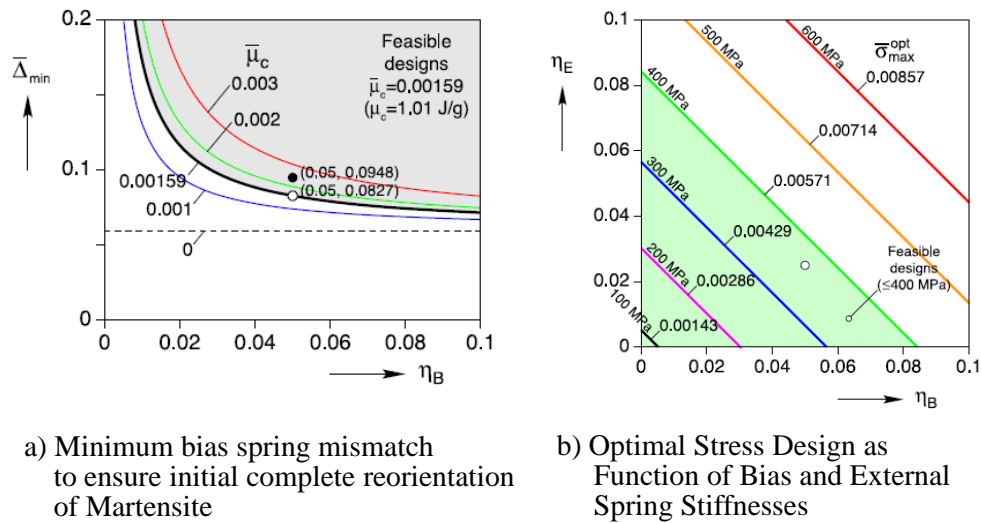


Figure 1.20. Bias spring selection plots [18].

Shaw and Churchill created design plots to select bias spring. a) minimum bias spring mismatch ($\bar{\Delta}_{min}$) as a function of dimensionless bias spring stiffness (η_B) to ensure initial complete reorientation of martensite during initial actuator assembly (cold). b) design stresses as a function of bias spring (η_B) and external spring (η_E) stiffnesses.

1.3.3. Design process

A *design process* is a sequence of design methods to follow through to create a detailed design. While there have been equilibrium design / analysis methods for simple SMA actuation

devices using force-deflection / stress-strain curves since the early 1990's [22,36,47,48,50], there is no systematic design process established around these methods. Empirical design approaches are still applied for SMA application development [25,51–53] because design using other existing design methods is complex and often non-intuitive for real-world SMA actuation devices due to SMA architectures and additional device elements. Moreover, previous research efforts focused on the analysis stage of design, while the full design cycle consists of multiple stages from the early stages that select device concepts and SMA architectures to the later stages that finalize the detailed design parameters using in-depth analysis. Furthermore, the later analysis stages require a detailed design as an input for simulation analysis, which is hard to create for non-expert SMA engineers, and often requires iterative steps even for expert engineers. Although, Langbein and Czechowicz [86] proposed a general procedure to develop a conceptual design of SMA actuator devices (Figure 1.21), their effort is more focused on setting up a regulatory standard rather than guiding engineers through the design process to create a concrete detailed design. There needs to be a step-by-step design process that helps engineers with any level of expertise in SMA technology to identify and make design decisions throughout the design cycle to create a detailed design. The formalization of a step-by-step process to create a

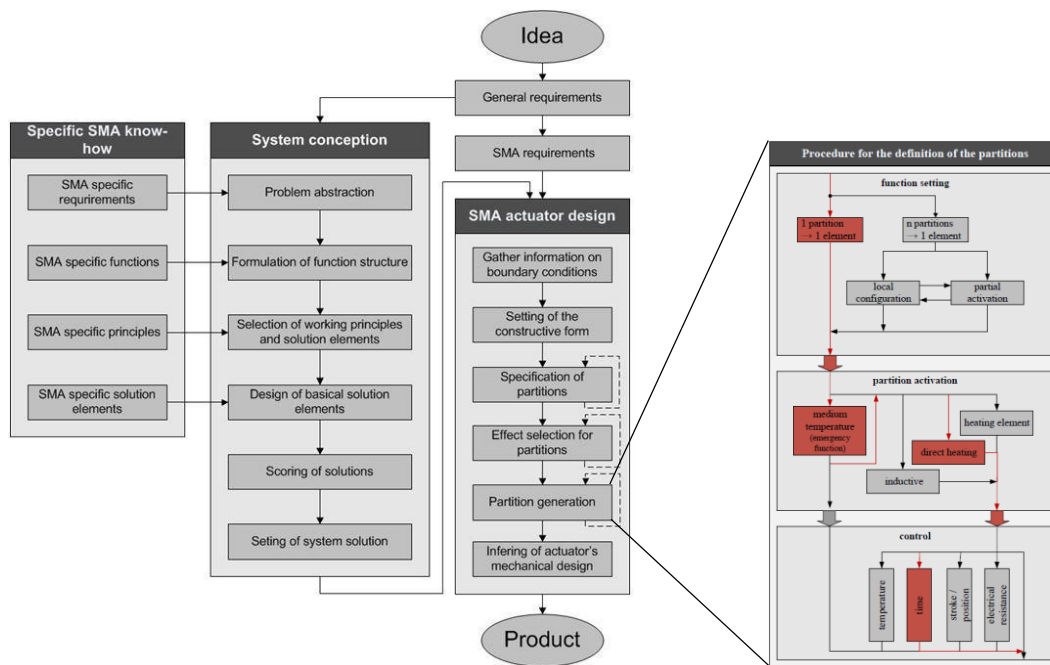


Figure 1.21. Methodical design procedure for developing SMA-based components [84]. Langbein and Czechowicz proposed a general procedure to develop a conceptual design of SMA actuator device.

detailed design helps to complete the device development cycle by providing a means to create a detailed design, which can be used as an input for later stages to finalize the detailed design.

1.3.4. Design framework

A *design framework* is a systematic foundation for SMA actuation device design which helps to make SMA technology available to engineers by organizing and presenting the device grammar, design methods, and design process. A design framework can be implemented as a computer-aided design tool to make SMA technology accessible to diverse groups of stakeholders. While there are research efforts to help engineers by creating computer-aided design software [87–89], these tools have limited scope such as material selection in the planning stage (Figure 1.22), or handling of a single SMA architecture such as straight wires (Figure 1.23) or spool packaging (Figure 1.24). Moreover, these software tools are targeted for design computation support to expedite the analysis portions of the design cycle for expert engineers, i.e. an implementation of a particular design method, but are not capable of guiding non-expert engineers to create a complete detailed design. Such guidance requires design methods to be organized into a design framework including the software platform and user interfaces. An expandable integrative model-based design tool platform to systematically organize the device

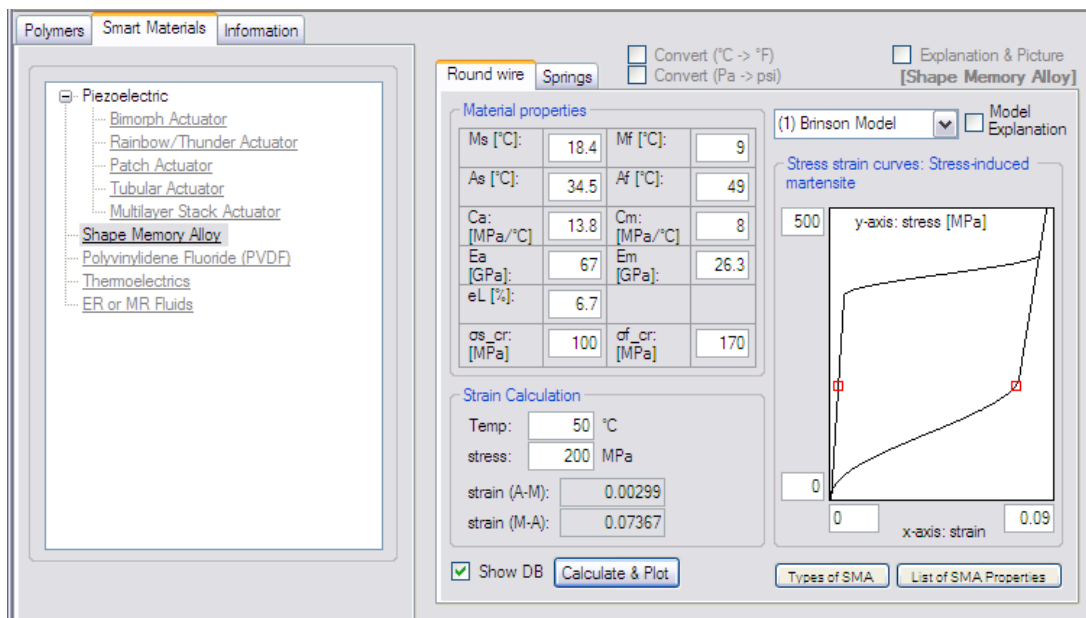


Figure 1.22. Polymers/Smart Materials Database (PSMD) [86].

Park and Washington created a smart material selection tool, which presents material properties and material-level models to expedite the material selection process.

grammar, design methods, and design process is needed to create software design tools to guide non-expert SMA engineers and better support expert SMA engineers throughout the entire process.

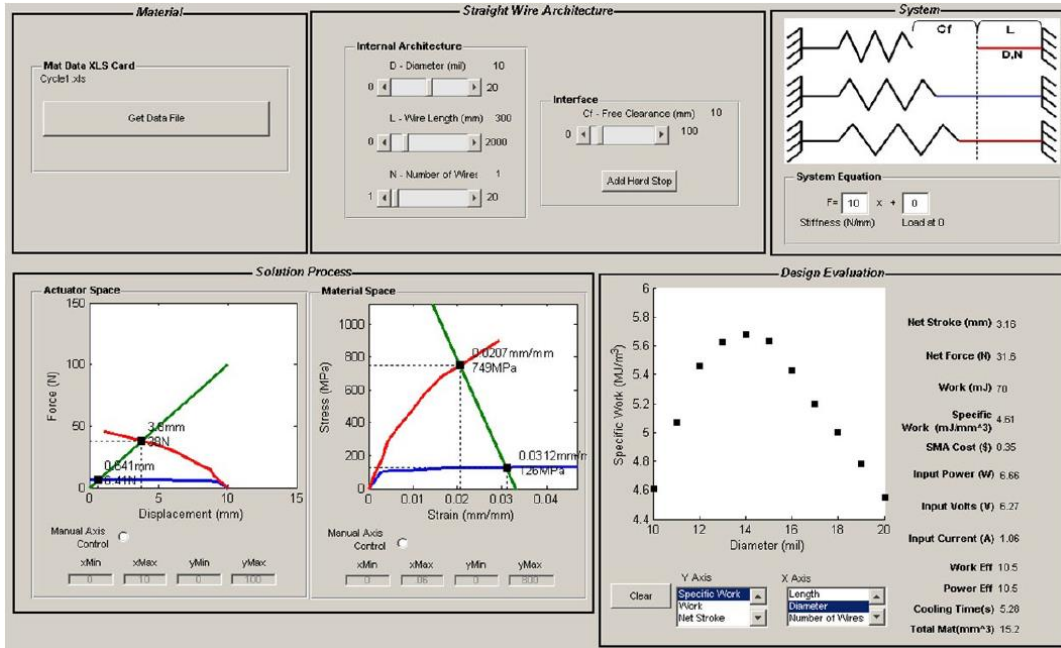


Figure 1.23. SMA straight wire design tool [85].

Luntz et al. developed a design tool to explore the design space for actuation device using straight SMA wires.

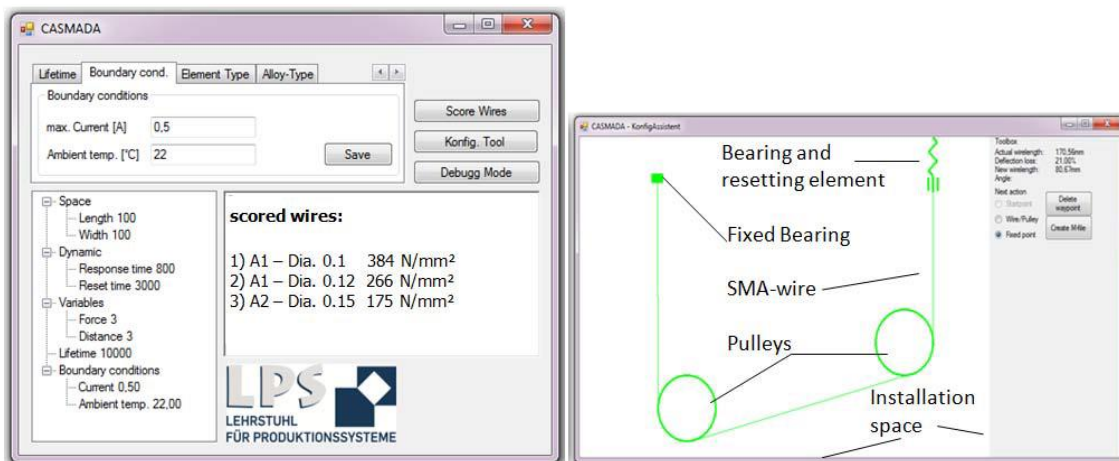


Figure 1.24. Computer-Aided Shape Memory Actuator Development Application (CASMADA) [87].

Meier and Czechowicz created a computer-aided shape memory actuator development application, which helps the routing of SMA wires using spool within a given package space.

1.4. Goal and objectives

The main goal of this research is to develop a systematic design framework for SMA wire device design that incorporates the grammar, design methods, and design process to enable engineers of different backgrounds to make efficient design decisions in different stages of the design process. Four key objectives are identified to realize this goal:

1. **Grammar:** Define a reference SMA device hierarchical structure by establishing an actuation device grammar including basic and macro elements and connectivity rules to set up a common language and enlighten non-expert engineers about necessary elements and their structure.
2. **Methods:** Formalize design methods for modular modeling, model aggregation / performance prediction, and visualization to support design decisions to examine and evaluate the effect of device elements and design parameter variations to serve diverse groups of stakeholders.
3. **Process:** Formalize a design process over various stages of SMA device design to support appropriate decision making with necessary precision at each stage to ensure better design quality, expedite the design cycle, and enable design automation.
4. **Framework:** Create and demonstrate an expandable model-based design tool software platform and user interface that systematically organizes and presents the device grammar, design methods, and design process for diverse expert and non-expert stakeholders.

1.5. Research approach

To achieve the stated goal, individual areas of research issues in device grammar, design methods, and design process are addressed, and the design framework consolidates these three areas. A device grammar is defined to describe actuation device structure and a reference SMA actuation device hierarchical structure is created to describe most SMA actuation devices. Design methods for modeling, performance prediction, and visualization are formalized based on the device grammar and the reference SMA actuation device structure to support design decisions. A design process is established to guide engineers to create a detailed design of an

SMA actuation device. A design framework is created to systematically organize and present the device grammar, design methods, and design process, and is implemented as software design tools.

1.5.1. Device grammar

To set up a common language and enlighten non-expert engineers about the SMA device structure and the necessary basic elements, a reference SMA actuation device hierarchical structure is defined by establishing a general actuation device grammar. The basic elements, which provide unique functionalities to an actuation device system, are first defined as the building blocks for actuation device systems: active elements, reactive elements, modifier elements, and coupling elements. Active elements change their effort-position behavior, such as stress-strain, force-deflection, or force-stretch ratio, upon a signal change. Reactive elements respond to a stimulus following their effort-position behavior. Modifier elements transform an input effort-position behavior into an output effort-position behavior. Coupling elements provide mechanical connections between three or more elements providing position synchronization. Using these basic elements, macro device elements are created along with connectivity rules to form a hierarchical actuation device system structure. Macro device elements provide the means to construct a hierarchical structure to help design decision by creating meaningful conceptual collections of basic elements.

The device grammar defined for general actuation devices is utilized for the standardization of the SMA actuation device structure to provide a foundation to understand and model SMA actuation devices. Common device elements which are universally used for SMA actuation devices are identified, and structured following the actuation device grammar. Typical SMA actuation devices have two macro elements: an SMA active element and a device modifier element. The SMA active element initiates motion using a material behavior change upon a temperature change of the SMA material and transforms it into a force-deflection behavior through the SMA architecture. The device modifier element consists of a series of sub-elements (both basic and macro elements), which transform the SMA active element behavior to achieve a desired force-deflection behavior of the SMA actuation device. The reference SMA actuation device structure provides a framework to understand, document, and model SMA actuation devices.

1.5.2. Design methods

To formalize design methods to support design decisions, a modular modeling approach using the hierarchical actuation device structure is proposed to expose the effect of individual device elements and their design parameters. Common modeling guidelines for each basic element type are suggested. Active and reactive element models define the effort-position relation such as force as a function of deflection or stress as a function of strain. Active element elements initiate actuation which transfers through the system. Modifier element models transform the input effort-position relation into an output effort-position relation. Coupling element models represent the force balance at a mechanical connection.

Model aggregation and performance prediction methods based on the hierarchical device structure are established to support design decisions by evaluating the effect of device elements and design parameter variations. A complete actuation system model for performance prediction is constructed by aggregating individual models for basic elements within the system. A solution coupling element is placed within an actuation device system for model aggregation and performance prediction. The placement of the solution coupling provides options for lumping which enables the separation of device elements from others for the design and analysis of particular design elements.

Visualization methods for actuation device system behavior and performance prediction results are formalized to serve diverse stakeholders and design tasks. Visualization relies on two basic approaches: lumping and projection. Lumping is decided by the placement of the solution coupling for model aggregation. Projection is the mapping of the performance prediction result from the solution coupling element to another potential solution coupling element location to change the coordinates of the visualization. By having various visualization options, engineers can evaluate the effects of individual device elements and their design parameter variations on actuation system behavior, material scientists can evaluate the effect of a new material, and system engineers can integrate an SMA actuation device into a system by selecting interface parameters. These design methods provide the means to support diverse stakeholders to make design decisions.

1.5.3. Design process

A multi-stage design process for SMA actuation devices, which consists of an initial design decision stage, a discrete equilibrium design stage, and an integrated transient behavior evaluation stage, is established to formalize a design process over various stages of SMA device design. In the initial design decision stage, a proper SMA architecture is selected to produce a required force and stroke, and material usage decisions are made. In the discrete equilibrium design stage, an SMA actuation device design is generated using equilibrium assumptions. The focus of this research is on the discrete equilibrium stage to guide non-expert engineers to generate a detailed design without going through an iterative design process. Given a set of initial design decisions, a design process for the discrete equilibrium design stage is broken into three sub-steps which proceed by first meeting the actuation stroke requirement and then meeting the force requirement: the Kinematic design step, the Kineto-static design step, and the Thermomechanical design step. Kinematic actuation maps and a bias design map are created for several SMA architectures and device elements to visualize the design space using the device element models. Once a design is generated in the discrete equilibrium design stage, the design is finalized in the integrated transient behavior evaluation stage using in-depth analysis. This process supports appropriate decision making with necessary precision at each stage to ensure better design quality, expedite the design cycle, and enable design automation.

1.5.4. Design framework

This design framework is demonstrated by a Model-based Design Tool modular platform, and by its implementation as two software design tools tailored for different engineer groups: an expert engineer supporting design tool and a non-expert engineer guiding design tool. To create an expandable model-based design tool software modular platform, major functional modules are identified, defined, and structured following the device grammar, design methods, and design process. Based on this modular platform, a software user interface for a step-by-step design procedure to present an appropriate level of design information to non-expert engineers is created. To minimize the user interaction and unnecessary computation of design parameters which are coupled to other design parameter decisions, parameters suitable for partial design automation are identified, and the design parameter flow is planned throughout the design procedure for design of the step-by-step user interface. While the step-by-step engineer guiding

design tool is useful for non-expert engineers who are not familiar with SMA actuation devices, expert engineers can benefit more from performance prediction and visualization assistance software, which can present all the design information at the same time to explore the design options. This type of expert user support design tool is implemented based on the design methods. The SMA actuation device design framework and its implementations as software design tools provides a systematic foundation to organize and present the device grammar, design methods and design process to engineers to support design decisions.

1.6. Contributions and expected outcomes

The design framework consisting of the device grammar, design methods, and design process supports actuation device design, and has the potential to be expanded to diverse types of actuation devices other than SMA devices. Moreover, individual components of the design framework have their own contributions to actuation device design.

The reference SMA actuation device structure built on the generalized actuation device hierarchical structure works as a reference structure to identify and populate device design options, and to model and analyze the device actuation performance as well as to enlighten non-expert engineers about the essential elements of SMA actuation devices. The unified terminology for SMA actuation devices helps collaboration between different research groups and disciplines. Moreover, the generalized actuation device hierarchical structure and its basic and macro elements and connectivity rules can be used to understand, communicate, analyze, and model a wide range of actuation device systems not limited to SMAs in addition to enabling the modular modeling of actuation devices.

The design methods consisting of modular modeling, model aggregation and performance prediction, and visualization support design decisions to serve diverse sets of stakeholders by exposing the effect of device elements not only for SMA actuation devices, but also for a wide range of other actuation devices. The modular modeling approach which takes advantage of the hierarchical actuation device system structure ensures the re-usability of individual device element models. SMA architectures are one such device element, for which formalized SMA architectural transformations provide a systematic approach to model each type of architecture, revealing the limitations on the evaluation of certain individual elements. The model aggregation and performance prediction methods enable the comprehension of actuation

device systems by providing a means to construct and solve a complete system model from the connected collection of modular device element models. The visualization methods consisting of lumping and projection support design decisions by presenting the device element behaviors and performance prediction results with tailored options for individual stakeholder groups who have their interests in different aspects and elements of an actuation device system.

The formalized design process helps engineers create a complete detailed design while preventing potential design iterations. The multi-stage design process allows engineers to work with models of different types and resolutions at both high and low levels of detail. A three-step discrete equilibrium design procedure prevents potential iteration by decoupling the force and deflection of actuation output behavior, and hides the complexity of material and SMA architectural models from engineers while still exposing the impact of design parameters. Moreover, the formalized systematic design process provides a foundation to automate the design process.

The design framework consisting of the device grammar, design methods, and design process makes SMA related technologies more accessible to engineers with different levels of expertise and roles in device development. A design tool software platform based on this framework enables the creation of computer-aided design tools to support a variety of design tasks. For example, a non-expert design tool guides engineers through the design process while an expert engineer can be supported by a design tool to more effectively explore the design space. Moreover, such tools support diverse visualization options tailored for individual stakeholder groups. The model-based modular design tool platform can be easily expanded not only to incorporate future material and architecture models for SMA actuation devices, but also to create design tools for different types of actuation devices other than SMAs because it is structured following the generalized actuation device structure.

The SMA actuation device design framework consisting of the grammar, design methods, and design process enables engineers of different backgrounds to make efficient and appropriate design decisions in different stages of the design process. This SMA actuation device design framework can increase the acceptance of SMA actuation technology into both research and commercial applications to exploit the promising benefits of SMA actuation, and streamline the device development cycle leading to these applications.

1.7. References

- [1] McDonald Schetky, L., 1991, "Shape memory alloy applications in space systems," *Mater. Des.*, **12**(1), pp. 29–32.
- [2] Chopra, I., 2002, "Review of state of art of smart structures and integrated systems," *AIAA J.*, **40**(11), pp. 2145–2187.
- [3] Kudva, J. N., 2004, "Overview of the DARPA Smart Wing Project," *J. Intell. Mater. Syst. Struct.*, **15**(4), pp. 261–267.
- [4] Sanders, B., Crowe, R., and Garcia, E., 2004, "Defense Advanced Research Projects Agency - Smart Materials and Structures Demonstration Program Overview," *J. Intell. Mater. Syst. Struct.*, **15**(4), pp. 227–233.
- [5] Morgan, N. B., 2004, "Medical shape memory alloy applications--the market and its products," *Mater. Sci. Eng. A*, **378**(1-2), pp. 16–23.
- [6] Brei, D., Luntz, J., Shaw, J., Johnson, N. L., Browne, A. L., Alexander, P. W., and Mankame, N. D., 2007, "General Motors and the University of Michigan smart materials and structures collaborative research laboratory," SPIE, San Diego, California, USA, p. 65270U–12.
- [7] Shaw, J. A., and Kyriakides, S., 1995, "Thermomechanical aspects of NiTi," *J. Mech. Phys. Solids*, **43**(8), pp. 1243–1281.
- [8] Mabe, J. H., Calkins, F. T., and Ruggeri, R. T., 2007, "Full-scale flight tests of aircraft morphing structures using SMA actuators," SPIE, San Diego, California, USA, p. 65251C–12.
- [9] Abel, J., Luntz, J., and Brei, D., 2013, "Hierarchical architecture of active knits," *Smart Mater. Struct.*, **22**(12), p. 125001.
- [10] Dunne, J. P., Pitt, D. M., White, E. V., and Garcia, E., 2000, "Ground demonstration of the Smart Inlet," AIAA, Atlanta, GA.
- [11] Sanders, B., Cowan, D., and Scherer, L., 2004, "Aerodynamic Performance of the Smart Wing Control Effectors," *J. Intell. Mater. Syst. Struct.*, **15**(4), pp. 293–303.
- [12] Martin, C. A., Hallam, B. J., Flanagan, J. S., and Bartley-Cho, J., 2004, "Design, Fabrication, and Testing of a Scaled Wind Tunnel Model for the Smart Wing Project," *J. Intell. Mater. Syst. Struct.*, **15**(4), pp. 269–278.
- [13] Bartley-Cho, J. D., Wang, D. P., Martin, C. A., Kudva, J. N., and West, M. N., 2004, "Development of High-rate, Adaptive Trailing Edge Control Surface for the Smart Wing Phase 2 Wind Tunnel Model," *J. Intell. Mater. Syst. Struct.*, **15**(4), pp. 279–291.
- [14] Kennedy, D. K., Straub, F. K., Schetky, L. M., Chaudhry, Z., and Roznoy, R., 2004, "Development of an SMA Actuator for In-flight Rotor Blade Tracking," *J. Intell. Mater. Syst. Struct.*, **15**(4), pp. 235–248.
- [15] Straub, F. K., Kennedy, D. K., Domzalski, D. B., Hassan, A. A., Ngo, H., Anand, V., and Birchette, T., 2004, "Smart Material-Actuated Rotor Technology - SMART," *J. Intell. Mater. Syst. Struct.*, **15**(4), pp. 249–260.

- [16] Hartl, D. J., and Lagoudas, D. C., 2007, "Characterization and 3-D modeling of Ni60Ti SMA for actuation of a variable geometry jet engine chevron," SPIE, San Diego, California, USA, p. 65293Z–12.
- [17] Utter, B., Luntz, J., Brei, D., Teitelbaum, D., Okawada, M., and Miyasaka, E., 2009, "Design and operation of a fully implantable SMA actuated implant for correcting short bowel syndrome," SPIE, San Diego, CA, USA, p. 72881A–13.
- [18] Furst, S. J., and Seelecke, S., 2014, "Fabrication and characterization of a dual-joint smart inhaler nozzle actuated by embedded SMA wires," *Smart Mater. Struct.*, **23**(3), p. 035008.
- [19] Sugawara, T., Hirota, K., Watanabe, M., Mineta, T., Makino, E., Toh, S., and Shibata, T., 2006, "Shape memory thin film actuator for holding a fine blood vessel," *Sens. Actuators Phys.*, **130-131**, pp. 461–467.
- [20] Browne, A. L., and Johnson, N. L., 2009, "United States Patent: 7498926 - Reversibly opening and closing a grille using active materials."
- [21] Mc Knight, G. P., Massey, C., Herrera, G. A., Barvosa-Carter, W., Johnson, N. L., and Browne, A. L., 2008, "United States Patent: 7429074 - Airflow control devices based on active materials."
- [22] Barnes, B. M., Brei, D. E., Luntz, J. E., Strom, K., Browne, A. L., and Johnson, N., 2008, "Shape memory alloy resettable spring lift for pedestrian protection," SPIE, San Diego, California, USA, pp. 693005–13.
- [23] Bellini, A., Colli, M., and Dragoni, E., 2009, "Mechatronic Design of a Shape Memory Alloy Actuator for Automotive Tumble Flaps: A Case Study," *Ind. Electron. IEEE Trans. On*, **56**(7), pp. 2644–2656.
- [24] Williams, E. A., and Elahinia, M. H., 2006, "Design of a two degree of freedom shape memory alloy actuator for mirror positioning," SPIE, San Diego, CA, USA, pp. 617304–8.
- [25] Lan, C.-C., and Yang, Y.-N., 2009, "A Computational Design Method for a Shape Memory Alloy Wire Actuated Compliant Finger," *J. Mech. Des.*, **131**(2), pp. 021009–9.
- [26] Young Pyo Lee, Byungkyu Kim, Moon Gu Lee, and Jong-Oh Park, 2004, "Locomotive mechanism design and fabrication of biomimetic micro robot using shape memory alloy," pp. 5007–5012 Vol.5.
- [27] Kim, S., Hawkes, E., Choy, K., Joldaz, M., Foley, J., and Wood, R., 2009, "Micro artificial muscle fiber using NiTi spring for soft robotics," *IEEE/RSJ International Conference on Intelligent Robots and Systems, 2009. IROS 2009*, pp. 2228 –2234.
- [28] Hyung-Min Son, Jun-Bum Gu, Se-Hoon Park, Yun-Jung Lee, and Tae-Hyun Nam, 2006, "Design of new quadruped robot with SMA actuators for dynamic walking," pp. 344–348.
- [29] Tanaka, K., Kobayashi, S., and Sato, Y., 1986, "Thermomechanics of transformation pseudoelasticity and shape memory effect in alloys," *Int. J. Plast.*, **2**(1), pp. 59–72.
- [30] Liang, C., and Rogers, C. A., 1990, "One-dimensional thermomechanical constitutive relations for shape memory materials," *J. Intell. Mater. Syst. Struct.*, **1**(2), pp. 207–34.

- [31] Brinson, L. C., 1993, “One-Dimensional Constitutive Behavior of Shape Memory Alloys: Thermomechanical Derivation with Non-Constant Material Functions and Redefined Martensite Internal Variable,” *J. Intell. Mater. Syst. Struct.*, **4**(2), pp. 229–242.
- [32] Boyd, J. G., and Lagoudas, D. C., 1994, “Thermomechanical Response of Shape Memory Composites,” *J. Intell. Mater. Syst. Struct.*, **5**(3), pp. 333–346.
- [33] Chang, B.-C., Shaw, J., and Iadicola, M., 2006, “Thermodynamics of Shape Memory Alloy Wire: Modeling, Experiments, and Application,” *Contin. Mech. Thermodyn.*, **18**(1), pp. 83–118.
- [34] Buravalla, V., and Khandelwal, A., 2008, “Phenomenological Modeling of Shape Memory Alloys,” *AIP Conference Proceedings*, S.M. Sivakumar, V. Buravalla, and A.R. Srinivasa, eds., IIT Madras, Chennai, India, pp. 104–123.
- [35] Utter, B., Barnes, B., Luntz, J., Brei, D., Teitelbaum, D. H., Okawada, M., and Miyasaka, E., 2010, “Design of an SMA Actuated Mechanotransductive Implant for Correcting Short Bowel Syndrome,” *Proceedings of the 2010 Smart Materials, Adaptive Structures, and Intelligent Systems*, Philadelphia, Pennsylvania, USA, pp. 875–892.
- [36] Zhang, X., Yan, X., and Yang, Q., 2013, “Design and Experimental Validation of Compact, Quick-Response Shape Memory Alloy Separation Device,” *J. Mech. Des.*, **136**(1), pp. 011009–011009.
- [37] Kim, W., Utter, B., Luntz, J., Brei, D., Muhammad, H., and Alexander, P., 2013, “Model-based Shape Memory Alloy Wire Ratchet Actuator Design,” *Proceedings of the ASME 2013 Conference on Smart Materials, Adaptive Structures and Intelligent Systems*, ASME, Snowbird, Utah, USA, pp. SMASIS2013–3333–12.
- [38] Kim, W., Thota, M., Luntz, J., and Brei, D., 2012, “Analytical Model and Design Study on Shape Memory Alloy Web Actuator,” *ICAST2012*, Nanjing, China, pp. 031–16.
- [39] Gao, X., Burton, D., Turner, T. L., and Brinson, L. C., 2006, “Finite Element Analysis of Adaptive-Stiffening and Shape-Control SMA Hybrid Composites,” *J. Eng. Mater. Technol.*, **128**(3), pp. 285–293.
- [40] Siddiq Qidwai, M. A., Hartl, D. J., and Lagoudas, D. C., 2008, “Numerical Implementation of an SMA Thermomechanical Constitutive Model Using return Mapping Algorithms,” *Shape Memory Alloys*, pp. 189–231.
- [41] Mangalgi, P. D., and Thakare, A. G., 2010, “Use of SMA Constitutive Model in Finite Element Analysis of Wire-Based Actuators,” *IUTAM Symposium on Multi-Functional Material Structures and Systems*, B. Dattaguru, S. Gopalakrishnan, and V.K. Aatre, eds., Springer Netherlands, pp. 45–53.
- [42] Lewis, N. M., and Seelecke, S., 2011, “FE modeling of multiple SMA wire actuated adaptive structures,” p. 79781D–79781D–10.
- [43] Liang, C., and Rogers, C. A., 1997, “One-dimensional thermomechanical constitutive relations for shape memory materials,” *J. Intell. Mater. Syst. Struct.*, **8**(4), pp. 285–302.
- [44] Boyd, J. G., and Lagoudas, D. C., 1994, “Thermodynamical constitutive model for the shape memory effect due to transformation and reorientation,” *SPIE*, Orlando, FL, USA, pp. 276–288.

- [45] Shaw, J. A., 2002, “A thermomechanical model for a 1-D shape memory alloy wire with propagating instabilities,” *Int. J. Solids Struct.*, **39**(5), pp. 1275–1305.
- [46] Chang, B., 2006, “Thermodynamics of shape memory alloy wire: modeling, experimental calibration, and simulation.”
- [47] Duerig, T. W., Melton, K. N., Stöckel, D., and Wayman, C. M., 1990, *Engineering Aspects of Shape Memory Alloys*, Butterworth-Heinemann.
- [48] Liang, C., and Rogers, C. A., 1997, “Design of shape memory alloy actuators,” *J. Intell. Mater. Syst. Struct.*, **8**(4), pp. 303–13.
- [49] Kim, W., Barnes, B. M., Luntz, J. E., and Brei, D. E., 2011, “Conglomerate Stabilization Curve Design Method for Shape Memory Alloy Wire Actuators With Cyclic Shakedown,” *J. Mech. Des.*, **133**(11), p. 111010.
- [50] Swensen, J. P., and Dollar, A. M., 2013, “Active-Cells for the Construction of Redundant and Configurable Articulated Structures,” ASME 2013 Conference on Smart Materials, Adaptive Structures and Intelligent Systems, American Society of Mechanical Engineers, pp. V001T01A013–V001T01A013.
- [51] Odhner, L., and Asada, H., 2010, “Scaling up shape memory alloy actuators using a recruitment control architecture,” pp. 1675–1680.
- [52] Shydo, J., Garcia, E., and Harris, J. M., 2005, “A remotely activated SMA actuated naval tie-down system,” E.V. White, ed., SPIE, San Diego, CA, USA, pp. 56–64.
- [53] Nishida, M., Tanaka, K., and Wang, H. O., 2006, “Development and control of a micro biped walking robot using shape memory alloys,” pp. 1604–1609.
- [54] Redmond, J. A., Brei, D., Luntz, J., Browne, A. L., and Johnson, N. L., 2008, “Behavioral model and experimental validation for a spool-packaged shape memory alloy actuator,” SPIE, San Diego, California, USA, pp. 693004–13.
- [55] Redmond, J. A., Brei, D., Luntz, J., Browne, A. L., Johnson, N. L., and Strom, K. A., 2010, “The Design and Experimental Validation of an Ultrafast Shape Memory Alloy ResetTable (SMART) Latch,” *J. Mech. Des.*, **132**(6), pp. 061007–14.
- [56] Dynalloy, Inc., 2006, “Comfort Seating,” *Dynalloy Newsl.*, p. 2.
- [57] Grant, D., and Hayward, V., 1997, “Variable structure control of shape memory alloy actuators,” *Control Syst. Mag. IEEE*, **17**(3), pp. 80–88.
- [58] Pathak, A., Brei, D., and Luntz, J., 2009, “Design and preliminary testing of a handheld antagonistic SMA actuator for cancellation of human tremor,” SPIE, San Diego, CA, USA, p. 72881B–13.
- [59] Jiang, C., Uchida, K., and Sawada, H., 2011, “Development of vision based tactile display system using shape memory alloys,” *Advanced Mechatronic Systems (ICAMechS)*, 2011 International Conference on, pp. 570–575.
- [60] Toma, M., Luntz, J., Brei, D., Alexander, P. W., Browne, A. L., and Johnson, N. L., 2012, “Design and Proof-of-Concept Validation of a Latched Arch Active Seal,” *J. Mech. Des.*, **134**(7), p. 075001.

- [61] Park, B., Shantz, M., and Prinz, F. B., 2001, “Scalable rotary actuators with embedded shape memory alloys,” *Smart Structures and Materials 2001: Smart Structures and Integrated Systems*, Newport Beach, CA, United states, pp. 79–87.
- [62] Reedlunn, B., Shaw, J., and Daly, S., 2009, “Shape Memory Alloy Cables: Exploratory Experiments,” ASME, Oxnard, California, USA, pp. 149–160.
- [63] Reedlunn, B., 2012, “Thermomechanical Behavior of Shape Memory Alloy Cables and Tubes.”
- [64] Wen, M., Tu, G. F., Zong, Q. Y., and Xie, C. X., 1994, “A study of NiTi shape memory alloy springs and its application in a new robotic actuator,” *Proceedings of the IEEE International Conference on Industrial Technology*, 1994, pp. 215–219.
- [65] Carrozza, M. C., Lencioni, L., Magnani, B., Dario, P., Reynaerts, D., Trivella, M. G., and Pietrabissa, A., 1996, “A microrobot for colonoscopy,” *Micro Machine and Human Science*, 1996., *Proceedings of the Seventh International Symposium*, pp. 223–228.
- [66] Lee, H. J., and Lee, J. J., 2000, “Evaluation of the characteristics of a shape memory alloy spring actuator,” *Smart Mater. Struct.*, **9**(6), pp. 817–823.
- [67] Johnson, B., Brei, D., and Patera, J., 2002, “Application of SMA technology to auxiliary functions in appliances,” *SPIE*, San Diego, CA, United states, pp. 427–440.
- [68] Khan, M. M., and Lagoudas, D. C., 2002, “Modeling of shape memory alloy pseudoelastic spring elements using Preisach model for passive vibration isolation,” pp. 336–347.
- [69] Morgan, N. B., and Broadley, M., 2004, “Taking the art out of smart! - Forming processes and durability issues for the application of NiTi shape memory alloys in medical devices,” *Proceedings for the Materials and Processes for Medical Devices Conference*, Anaheim, CA, pp. 247–252.
- [70] Menciassi, A., Gorini, S., Pernorio, G., and Dario, P., 2004, “A SMA actuated artificial earthworm,” *2004 IEEE International Conference on Robotics and Automation*, 2004. *Proceedings. ICRA '04*, pp. 3282–3287 Vol.4.
- [71] Kim, B., Lee, S., Park, J. H., and Park, J.-O., 2005, “Design and fabrication of a locomotive mechanism for capsule-type endoscopes using shape memory alloys (SMAs),” *IEEE Trans. Mechatron.*, **10**(1), pp. 77–86.
- [72] Kim, B., Lee, M. G., Lee, Y. P., Kim, Y., and Lee, G., 2006, “An earthworm-like micro robot using shape memory alloy actuator,” *Sens. Actuators Phys.*, **125**(2), pp. 429–437.
- [73] Cho, K.-J., Hawkes, E., Quinn, C., and Wood, R. J., 2008, “Design, fabrication and analysis of a body-caudal fin propulsion system for a microrobotic fish,” *IEEE International Conference on Robotics and Automation*, 2008. *ICRA 2008*, pp. 706–711.
- [74] Dong, Y., Boming, Z., and Jun, L., 2008, “A changeable aerofoil actuated by shape memory alloy springs,” *Mater. Sci. Eng. A*, **485**(1–2), pp. 243–250.
- [75] Mirzaeifar, R., DesRoches, R., and Yavari, A., 2011, “A combined analytical, numerical, and experimental study of shape-memory-alloy helical springs,” *Int. J. Solids Struct.*, **48**(3–4), pp. 611–624.

- [76] An, S.-M., Ryu, J., Cho, M., and Cho, K.-J., 2012, “Engineering design framework for a shape memory alloy coil spring actuator using a static two-state model,” *Smart Mater. Struct.*, **21**(5), p. 055009.
- [77] Czarnocki, I., Kim, W., Utter, B., Luntz, J., Brei, D., and Alexander, P., 2013, “Design of SMA Helical actuators: An experimental study,” ASME 2013 Conference on Smart Materials, Adaptive Structures and Intelligent Systems, American Society of Mechanical Engineers, Snowbird, Utah, USA.
- [78] Blanchard, B. S., and Fabrycky, W. J., 2006, *Systems engineering and analysis*, Pearson Prentice Hall, Upper Saddle River, NJ.
- [79] Karnopp, D., Margolis, D. L., and Rosenberg, R. C., 2006, *System dynamics: modeling and simulation of mechatronic systems*, John Wiley & Sons, Hoboken, N.J.
- [80] IEEE, 2007, “Systems engineering — Application and management of the systems engineering process.”
- [81] Finch, F. E., and Kramer, M. A., 1988, “Narrowing diagnostic focus using functional decomposition,” *AIChE J.*, **34**(1), pp. 25–36.
- [82] Wu, Z., Campbell, M. I., and Fernandez, B. R., 2008, “Bond Graph Based Automated Modeling for Computer-Aided Design of Dynamic Systems,” *J. Mech. Des.*, **130**(4), pp. 041102–11.
- [83] U.S. Department of Defense, 2011, “Work Breakdown Structure for Defense Materiel Items.”
- [84] Shaw, J. A., Chang, B., Iadicola, M. A., and Leroy, Y. M., 2003, “Thermodynamics of a 1D shape memory alloy: modeling, experiments, and application,” SPIE, San Diego, CA, USA, pp. 76–87.
- [85] Shaw, J. A., and Churchill, C. B., 2009, “A reduced-order thermomechanical model and analytical solution for uniaxial shape memory alloy wire actuators,” *Smart Mater. Struct.*, **18**(6), p. 065001.
- [86] Langbein, S., and Czechowicz, A., 2013, “A Multi-Purpose Method for SMA Actuator Development,” Proceedings of the ASME 2013 Conference on Smart Materials, Adaptive Structures and Intelligent Systems, ASME, Snowbird, Utah, USA, pp. SMASIS2013–3053–7.
- [87] Luntz, J., Barnes, B., Brei, D., Alexander, P., Browne, A., and Johnson, N., 2009, “SMA wire actuator modular design framework,” SPIE, San Diego, CA, USA, pp. 729008–12.
- [88] Park, J.-K., and Washington, G., 2011, “Advanced Development of a Smart Material Design, Modeling, and Selection Tool,” ASME 2011 Conference on Smart Materials, Adaptive Structures and Intelligent Systems, ASME, Scottsdale, Arizona, USA, pp. 675–684.
- [89] Meier, H., and Czechowicz, A., 2011, “Computer-Aided Development of Shape Memory Actuators as an Approach Towards a Standardized Developing Method,” ASME 2011 Conference on Smart Materials, Adaptive Structures and Intelligent Systems, pp. 1–6.

Chapter 2.

SMA Device Grammar

A device grammar is a vocabulary and syntax to describe, communicate, and understand a device design. It is important to set up a concrete common language which can serve as a foundation to understand and communicate the design for the discussion on actuation devices driven by SMA. While there are widely used system methods to describe systems such as block diagrams, flowcharts, work / system breakdown structures (WBS / SBS), and bond graphs [1–4], these methods do not well support actuation device design due to their focus on modeling for dynamic simulation, system engineering, or project management. Moreover, most of these methods have loose tie between the system representation and physical components and/or their design parameters. There are also computer-based design synthesis approaches using generative grammars such as graph and spatial grammars [5–11], and their application has been expanded to the areas of structures, consumer products, automotive styling, microelectromechanical systems (MEMS), digital very-large-scale integration (VLSI), and chemical processes [5,12]. However, these approaches are applied through the software implementation and the optimization technique for the automated design synthesis, and thus using these grammars for the training of non-expert engineers has limitations in building design intuitions.

In addition to a proper device grammar, setting up a generalized device structure including the necessary components is important to enlighten engineers who are not familiar with SMA devices. A generalized device structure enables a systematic approach to explore the design space by providing a platform on which to discuss design options. Moreover, a device model derived to design a specific device only serves one configuration of the device, and it is not trivial to reuse the model for later devices. It is desirable to have a systematic means of constructing device models from component model building blocks which can be applied for a variety of devices. Such

a structure can also provide a foundation to formalize a design process which can be implemented for automation of the design. A generalized SMA device structure including key device elements and their mechanical connections needs to be defined to provide the foundation to understand and model SMA devices. There have been several attempts for defining basic SMA device structures. Liang and Rogers [5] introduced three basic actuation devices (one-directional actuator, bias force actuator, and differential SMA actuator) for the application of the model-based design. Chang *et al.* [6] introduced a prototype 1-D SMA actuation device, which is similar to the bias force actuator of Liang and Rogers, for the simulation study of their material constitutive model. Although these simplified actuation device concepts are useful to introduce basic SMA actuation concepts and to demonstrate actuation device performance prediction using material constitutive models, they are not enough to represent realistic SMA device applications. SMA actuation devices often consist of several key device components such as mechanical levers, bias (reset) springs, and/or stroke limiters, and SMA architectures, which are used to transform the SMA behavior into desired device output behavior. Thus these simplified concepts are inadequate to formalize a general SMA device structure which can be used to form an SMA actuation device design platform.

The goal of this chapter is to enable understanding, documentation, and communication of an SMA wire actuation device system design and enlighten non-expert engineers about necessary elements and their structure.

The objectives are

1. Establish an actuation device grammar including basic and macro elements and connectivity rules.
2. Identify common device elements and their mechanical structure in SMA wire devices.
3. Standardize SMA actuation device hierarchical structure to set up a unified common language and enlighten non-expert engineers.

In this chapter, a generalized device structure is introduced using a set of basic elements. Using this generalized device structure, a reference SMA device hierarchical structure is defined to provide a framework to understand and model an SMA actuation device. The hierarchical components provide building blocks for SMA devices. Individual elements are discussed with

example components. Each component provides unique functionality to device operation. This reference SMA device architecture is demonstrated using three example devices.

2.1. Generalized device structure

According to Webster's dictionary, a device is “a piece of equipment or a mechanism designed to serve a special purpose or perform a special function [7]”. Furthermore, it defines an actuator as “a mechanical device for moving or controlling something”. Thus, when we discuss an **actuation device**, it is necessary to discuss the entire system including the “something”, which is defined in this work as a **target element** to emphasize that it is part of an actuation device system and it is the subject of actuation. For the example solenoid-spring actuation device system (Figure 2.1), the solenoid is an actuation device which moves the compression spring, which is something in the definition. It is especially important to include target element when we discuss the SMA actuation devices because the actuation performance of the SMA device is highly coupled to the target element behavior.

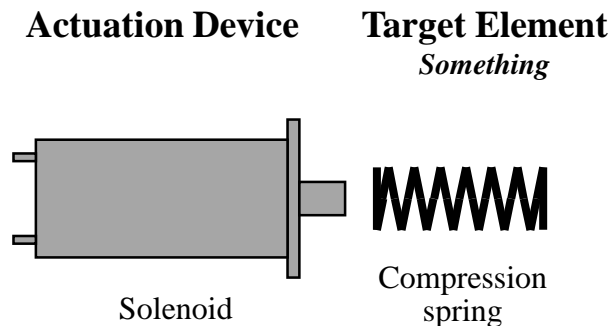


Figure 2.1. Actuation device system.

The solenoid is an actuation device which moves the compression spring, which is a target element. It is important to include target element in the system to discuss the actuation device design. It is especially important to include target element for the SMA actuation device system because the actuation performance of the SMA device is highly coupled to the target element behavior.

From a global point of view, the **system** consists of three major elements: the actuation device, the target element, and the interface between these two elements. While the system can be analyzed as three major elements from this global point of view, both the actuation device and the target element can be analyzed further by decomposing into sub-elements to aid the analysis of the system, and these sub-elements can have a hierarchical structure. However, for the design of

actuation devices, the target element is often regarded as a single macro element because it is not necessary to decompose the target element.

Actuation devices consist of several elements which provide unique functionalities, and these elements can be categorized for the modeling and the understanding of the device. This work defines a generalized hierarchical actuation device structure composed of three types of basic elements: behavior definition elements, modifier elements, and coupling elements. There are two sub-types of **behavior definition elements**: active elements and reactive elements. An *active element* changes its *effort-position* relation (*e.g.* force-deflection, stress-strain, force-stretch ratio, *etc.*) upon input signal change. A *reactive element* responds to a stimulus following its own effort-position behavior. A **modifier element** transforms the original effort-position behavior of the behavior definition element (*i.e.* active or reactive element) into a desired effort-position behavior. A **coupling element** provides the mechanical connection between the three or more elements providing behavior synchronization. An actuation device can be composed of multiple active elements, reactive elements, modifier elements, and coupling elements, and the basic elements can be grouped hierarchically into macro active elements, macro reactive elements, and/or macro modifier elements. These macro elements can have multiple layers of hierarchical structure. This hierarchical structure helps device design, modeling, and analysis by providing a tool for lumping device elements to isolate a macro or basic element which is the particular subject of interest.

2.1.1. Basic element types

The three types of basic elements (behavior definition elements, modifier element, and coupling element) serve as the building blocks for the hierarchical structure of actuation devices. These basic elements are categorized based on their function within the device, and may not directly match with specific physical components because some components provide more than one function while it maintains the connection to the design parameters of physical components and preserves the direct connection using macro element concept.

2.1.1.1. Behavior definition elements

Behavior definition elements defines their unique effort-position behavior initiating the behavior flows. While basic reactive elements have one effort-position behavior, active elements have multiple effort-position behaviors for different values of the input signal.

2.1.1.1.1. Active element

Active elements change their effort-position behavior upon input signal change. They are multi-state elements which change their behavior depending on the input signal. An actuation device must have at least one active element to initiate the motion, and the input signal can be either energy input or control signal input depending on the scope of design task. For example, a solenoid can have a voltage input or a simple on/off input. For SMA actuation devices, the input can be direct austenite/martensite phase control, temperature which decides the material phase (austenite/martensite), or input current for resistive heating (to increase the temperature to induce the material phase change). Active elements are represented diagrammatically as two half-rounded rectangles, representing the multiple states, with a block arrow on top, representing the input signal, and a behavior line emanating from the squared end (Figure 2.2).

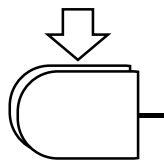


Figure 2.2. Active element.

Active elements change their effort-position behavior upon input signal change.

2.1.1.1.2. Reactive element

Reactive elements respond to a stimulus following their effort-position behavior. A reactive element may have direction-dependent effort-position behavior, e.g. asymmetric loading/unloading behavior. Examples of reactive elements include energy storage elements such as springs and hydraulic or pneumatic accumulators. Reactive elements are represented diagrammatically as a single half-rounded rectangle, and a behavior line emanating from the squared end (Figure 2.3).



Figure 2.3. Reactive element.

A reactive element responds to a stimulus following its effort-position behavior.

2.1.1.2. Modifier element

Modifier elements transform an input effort-position behavior into a modified output effort-position behavior. They therefore have a single input port and a single output port, and are represented diagrammatically using a rectangular shape (Figure 2.4). In general, a modifier can transform an effort-position behavior in either direction, although the transformation might be asymmetric.



Figure 2.4. Modifier element.

Modifier elements transform an input effort-position relation into a modified output effort-position relation. They therefore have a single input port and a single output port.

There are three types of modifier elements: kinematic modifier elements, geometric modifier elements, and interface modifier elements. **Kinematic modifiers** transform a force-deflection relation into another force-deflection relation. One simple example is a mechanical lever which trades off force and deflection to obtain a desired output performance. Other examples of kinematic modifiers include gear trains, linkages, friction, and stroke limiters.

Geometric modifiers transform an effort-position relation in a distributed form such as stress-strain, through the geometry of a physical component such as a cantilever beam, circular rod, or torsional tube: *e.g.* stress-strain to force-deflection, stress-strain to force-stretch ratio, or force-stretch ratio to force-deflection. In the case of non-homogeneous stress-strain distributions over the geometry of a physical component, the modifier transformation may not be reversible as it is with a simple kinematic modifier element such as a mechanical lever; it may not be possible for a geometric modifier to transform the force-deflection relation into a stress-strain relation. Because the geometry change is dependent on the distributed stresses and strains within the material, the transformation from force-deflection to stress-strain (*i.e.* the reverse transformation) is only possible for a representative point and/or a representative distributed stress-strain range. Irreversible modifier elements are represented diagrammatically by a rectangular shape with a thick vertical band on one end to represent the heterogeneously distributed effort-position behavior (Figure 2.5).



Figure 2.5. Irreversible modifier element.

In the case of non-homogeneous stress-strain distributions over the geometry of a physical component, the modifier transformation may not be reversible as it is with a simple kinematic modifier element such as a mechanical lever. Irreversible modifier elements are represented diagrammatically by a rectangular shape with a thick vertical band on one end to represent the heterogeneously distributed effort-position behavior.

Interface modifier elements define the relative position between two device elements, and match the coordinate systems. The interface modifier elements defines the initial condition of the system by providing the installation condition of the actuation device. It is more important for SMA actuation device system because the SMA actuation is produced by changing the force balance between the SMA material and the target element. There should be at least one interface modifier element between two active and/or reactive elements, and they are diagrammatically represented by a square with a thin line above them with one input port and one output port (Figure 2.6).

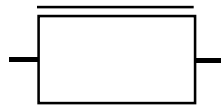


Figure 2.6. Interface modifier element.

Interface modifier elements define the relative position between two device elements, and match the coordinate systems.

2.1.1.3. Coupling element

Coupling elements represent the mechanical connection between three or more elements. A coupling element represent a simple mechanical connection; all other transformations which may be required must be handled by modifiers. For example, if there is a mechanical connection between one active element which generates a rotation and another active element which generates a linear motion, these behaviors initiated from active and reactive elements cannot be directly connected using coupling element. There must be a modifier element to transform the rotation into a linear motion or vice versa, and an interface modifier element to define the relative position

between them. Coupling elements provide the additional function of combining efforts from multiple active and/or reactive elements while maintaining a consistent position among the connected behaviors. Thus the coordinate systems of all the inputs and outputs must be matched using interface modifier elements. Couplings are represented diagrammatically by a circle in the diagram (Figure 2.7).



Figure 2.7. Coupling element.

Coupling elements represent the mechanical connection between three or more elements.

2.1.2. Connectivity rules

Connectivity must preserve behavior flows which originate at active and/or reactive elements, pass through the modifier elements, merge at coupling elements, and interact with the target element through the interface modifier element. The basic rules to compose a system using the basic elements are

- 1) Each port of individual basic elements must be connected to a port of another basic element through the behavior flow lines,
- 2) All behavior flows start from active and/or reactive elements,
- 3) There must be at least one interface modifier element between active and/or reactive elements,
- 4) The coordinate systems (i.e. dimension) of behavior flows should match at coupling elements, and
- 5) There should not be any closed loop of behavior flow in the system.

Active elements and reactive elements have their own effort-position behavior, which provides a particular relation between the effort variable and the position variable such as force-deflection, tension-stretch ratio, or stress-strain. The behaviors are modified by modifier elements to achieve desired behavior, and synchronized at coupling elements. The system finds equilibrium by balancing the forces and the corresponding synchronized position initiating from all the active

and reactive elements. The equilibrium change due to the state-dependent active element behavior change upon input signal change produces the actuation.

The simplest possible system structure is a system consisting of one active element and one reactive element, and an interface modifier element to define the relative position between them. An example of such a system (Figure 2.8) is a solenoid actuation device acting against a helical compression spring target element. The solenoid converts electric energy into motion, and the helical compression spring responds to the stimulus from the solenoid while storing potential energy. The initial offset between the two behavior definition elements is represented by an interface modifier element. The active and reactive elements define force-deflection behaviors; the solenoid has its own force-deflection behavior which changes upon the input signal (electric current) change, and the helical compression spring target element has a linear stiffness which defines its force-deflection behavior. The interface modifier element matches the coordinate systems of the two behavior definition elements by shifting the origin of the solenoid force-deflection coordinate system to the origin of the helical compression spring coordinate system.

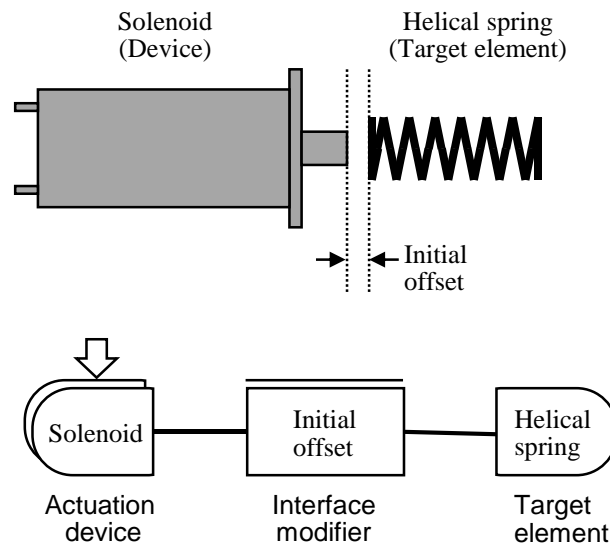


Figure 2.8. Simple actuator device example.

2.1.3. Macro elements

Macro elements can be composed by grouping several basic elements to help in the understanding and modeling of a system. The type of a macro element is determined by the number of input ports and output ports in the same way as basic elements. If there is an input signal and one output port in a macro element, it is a macro active element, which must contain at least one basic active element. If there is only one output port, it is a macro reactive element. Similarly, if a macro element has one input and one output port, it is a macro modifier element even if it contains a basic active and/or reactive element. Macro coupling elements do not exist because coupling elements only represent simple mechanical connections. Figure 2.9 shows a simple macro behavior definition element example which adds a mechanical lever modifier element to the simple example in Figure 2.8. In this case the actuation device consists of a basic active element (solenoid) and a basic modifier element (mechanical lever), which together can be grouped as a single macro active element, which is represented diagrammatically as a double-lined active element shape. It may be convenient for system engineer to think of this macro element as a single unit with its own (combined) force-deflection behavior.

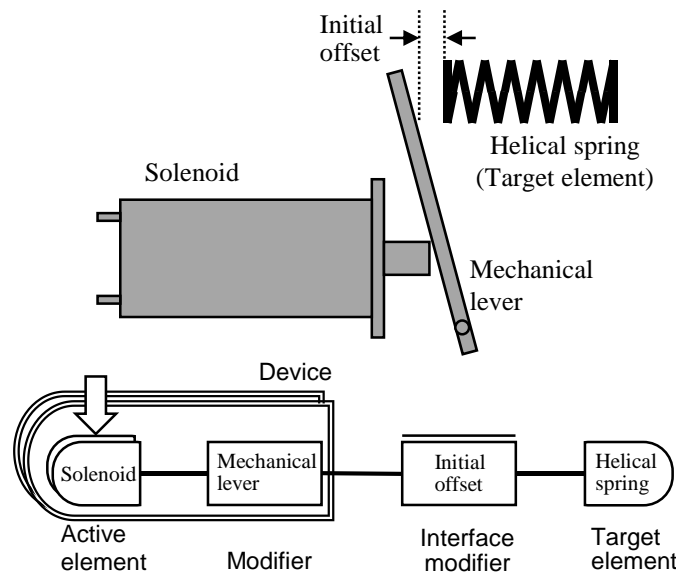


Figure 2.9. Macro behavior definition element example.

Macro elements can have multiple layers of hierarchal structure. For example, an entire actuation device can be composed as one single macro active element, and the device macro active

element can have several macro active, reactive, and/or modifier elements as sub-components. The powertrain of an automobile is a good example of a multi-layer hierarchical structure (Figure 2.10). A powertrain consists of two major macro elements: the engine and the drivetrain. The engine macro active element initiates the motion, and the drivetrain transforms the high speed motion from the engine to provide proper speed and torque. In the engine macro element, each cylinder, which is a basic active element, converts chemical energy into linear motion. Connecting rods transform linear motion into rotation at the crank shaft. If the individual elements are not the subject of interest, each cylinder and its corresponding connecting rod can be composed as a single macro cylinder assembly element, which converts chemical energy into rotation directly. Depending on the design and/or analysis task, the drivetrain can be decomposed into sub-components. For example, the engine, containing all four cylinder assemblies and the crank shaft, can be grouped as a single macro element for final drive design, while the individual element of the drivetrain are decomposed to separate the final drive from the other components. Similarly,

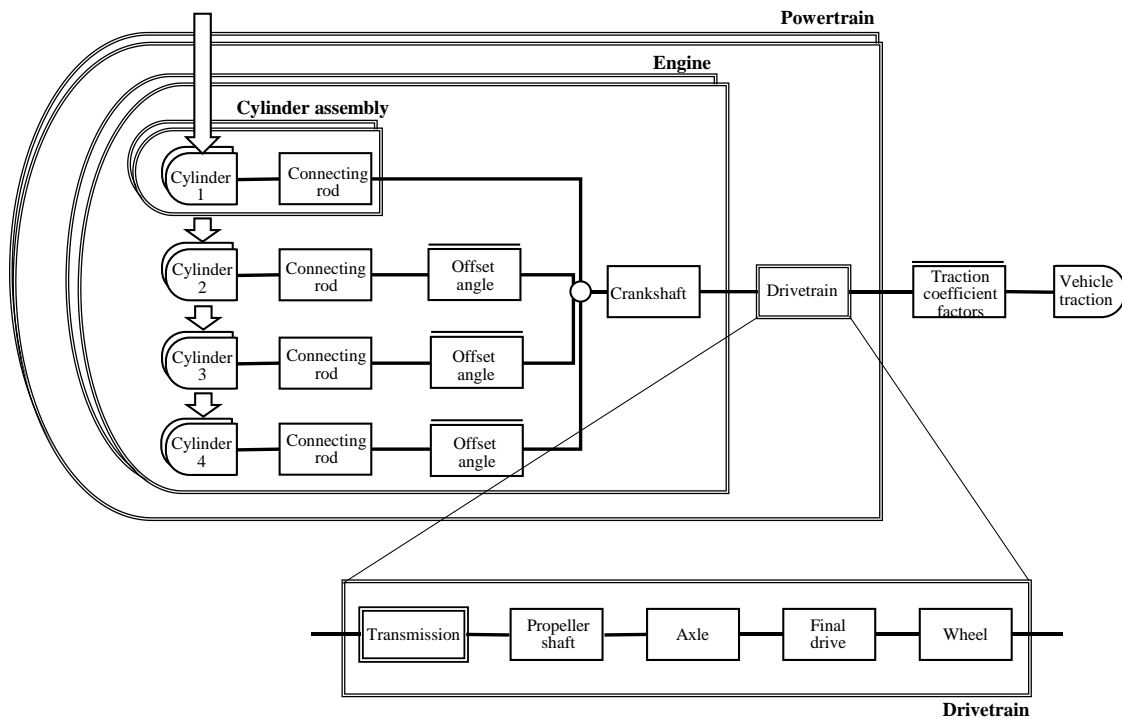


Figure 2.10. Multi-layer hierarchical structure of automotive powertrain.

Macro elements can have multiple layers of hierarchal structure. For example, an entire actuation device can be composed as one single macro active element, and the device macro active element can have several macro active, reactive, and/or modifier elements as sub-components.

the transmission can be decomposed for design of its individual parts, while it is considered as single macro modifier element for the design of other drivetrain components. The powertrain example demonstrates the multi-layer hierarchical structure, and it also shows that the grouping of the macro elements can be re-organized based on the design and/or analysis task.

Another example of a macro element is the target element. Although a target element consists of basic elements and it is also possible to analyze it as several layers of macro elements, the target element is considered as a macro reactive element for the design and analysis of the actuation device system. However, when the actuation performance can be improved by modifying the target element, a system level engineer can analyze the target element by decomposing it into multiple layers of macro elements.

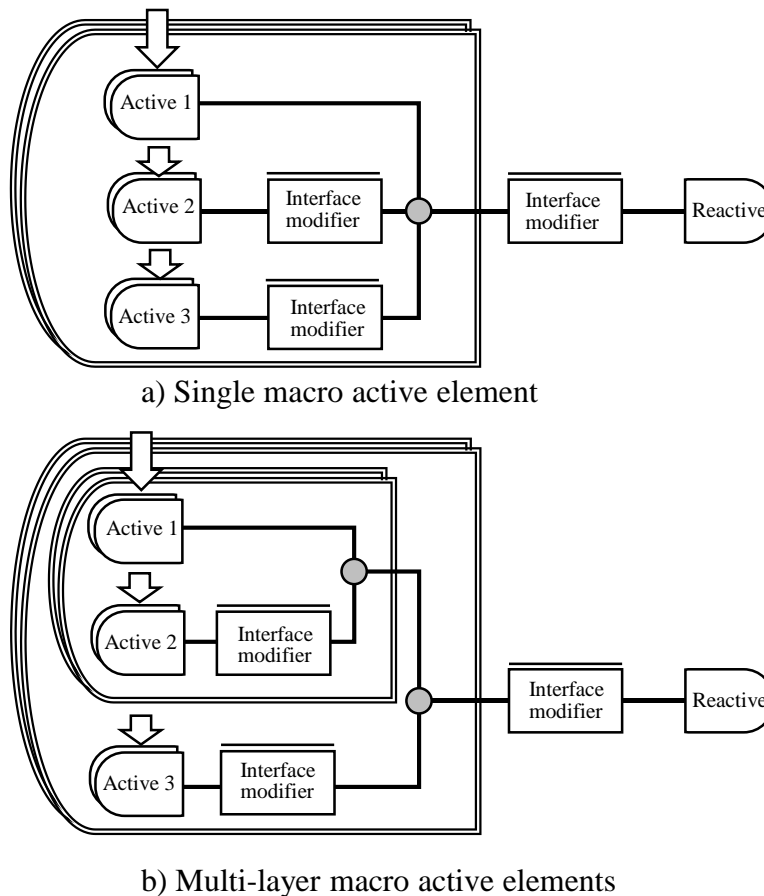


Figure 2.11. Macro element regrouping using coupling decomposition.

Macro elements can be re-organized by splitting and re-grouping coupling elements. by decomposing the gray colored coupling in (a), Active element 3 in (b) can be isolated from Active elements 1 and 2 (which together creating a macro active element) by creating a multi-layer structure for the design and analysis of individual components.

Macro elements can be re-organized by splitting and re-grouping coupling elements. Coupling elements having three or more inputs can be divided into coupling elements each having fewer inputs. This separation enables the flexible grouping of macro elements. For example, by decomposing the gray colored coupling element in Figure 2.11a, Active element 3 in Figure 2.11b can be isolated from Active elements 1 and 2 (which together creating a macro active element) by creating a multi-layer structure for the design and analysis of individual components.

2.2. SMA device hierarchical structure

To provide a common language to understand and set up a foundation to model SMA devices, a reference SMA actuation device hierarchical structure (Figure 2.12) is defined based on the generalized device structure and the device grammar defined in section 2.1. An **SMA actuation device** consists of two major macro device elements: an **SMA active element** and a **device modifier** macro element. The **SMA active element**, which is a macro active element, generates actuation motion using changes in the SMA material properties upon temperature changes through the SMA architecture. The **device modifier** macro element transforms the SMA active element force-deflection behavior into a modified force-deflection behavior, which then interacts with the target element through the interface modifier element. Although the interface modifier element is not technically part of the SMA actuation device, it defines the installation position of the SMA device relative to the target element and is an important design parameter because it affects the actuation equilibria by changing the target element force interaction with the SMA actuation device.

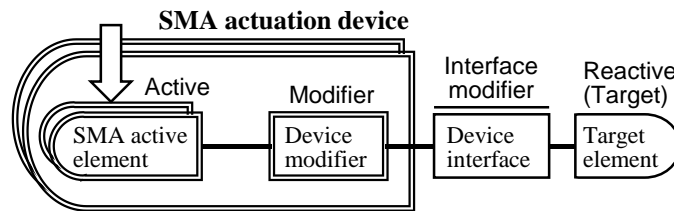


Figure 2.12. A reference SMA actuation device system.

2.2.1. SMA active element

The SMA active element, which works as the main macro active element in the SMA device, produces actuation by transforming energy into motion. In common SMA wire actuation devices which use electric Joule heating, this transformation is a two-step transformation: first, electric energy is transformed into heat, and second, thermal energy is transformed into motion through the changes in the SMA material properties between the cold compliant martensite phase and the hot stiff austenite phase. This chapter focuses on the second transformation because it determines the characteristics of the motion produced, whereas the first transformation determines the actuation timing.

The SMA active element is a macro element, which consists of two sub-elements (Figure 2.13): the SMA material (active element) and the SMA architecture (modifier element). The **SMA material** has its stress-strain constitutive relations defined in the austenite and martensite phases. The **SMA architecture** transforms the stress-strain behavior of the SMA material into force-deflection behavior through the geometric form of the architecture. For example, a straight wire produces a different force-deflection behavior output than that from a helical spring. The SMA architecture element can be a macro modifier element consisting of multiple layers of transformation.

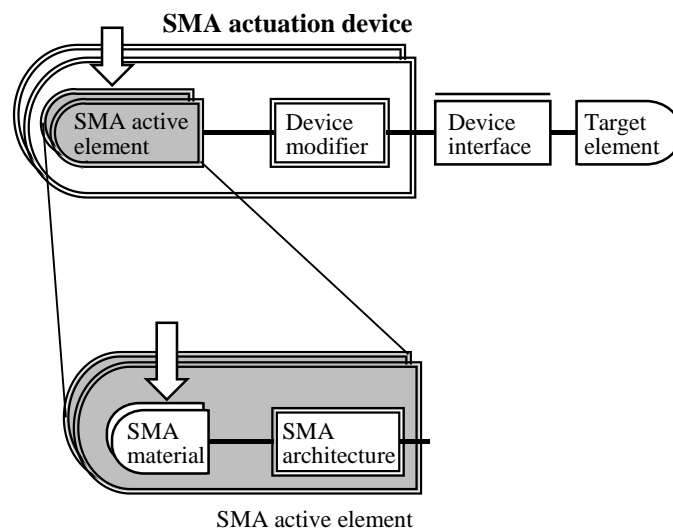


Figure 2.13. SMA active element.

The SMA active element is a macro element, which consists of two sub-elements: the SMA material (active element) and the SMA architecture (modifier element).

2.2.1.1. SMA material

The stress-strain-temperature dependent material properties of SMA enable actuation stroke. SMA actuation is produced using the equilibrium shift between the low temperature martensite phase and the high temperature austenite phase. Because the actuation is produced between two equilibria, the material properties such as recoverable strain, material stiffness in the martensite and austenite phases, and transformation temperatures decide the actuation characteristics. Due to the stress-strain-temperature coupled nature of SMA, it is important to capture and represent the constitutive relations of SMA in each phase to predict the material behavior during actuation.

In addition to the drastic material property changes between the two material phases, the material properties also vary due to many reasons such as the material composition, previous cold work, and operation history [8]. Although this material variation affects the performance of SMA actuation devices, it is possible to mitigate the effects of the material variations using various device architectures such as stroke limiters (Appendix C).

2.2.1.2. SMA architectures

As a modifier, the SMA architecture transforms the SMA material stress-strain behavior into the actuation force-deflection behavior through the SMA architecture geometry. For example, a simple straight wire architecture directly transforms the SMA stress-strain behavior into force-deflection behavior through a simple architectural transformation: the force is proportional to the cross-sectional area of the SMA wire and the deflection is proportional to the length of the SMA wire. The SMA architecture may have multiple layers of transformation. For example, the SMA wire web actuator introduced with active inner belt seal example in Section 1.2.4.1, which zigzags the SMA wire along the width between two surfaces to generate stroke amplification normal to the surfaces (Figure 2.14), has two layers of transformation: the first transformation layer is from SMA material stress-strain behavior to SMA wire tension-elongation behavior (Figure 2.14a), which is same as that of the SMA straight wire, and the second transformation layer is from SMA wire tension-elongation behavior to web actuator force-deflection behavior (Figure 2.14b). This multi-layer SMA architecture is a modular device architecture (Figure 2.14c), which means that each architectural layer can be replaced by another compatible architecture. For example, the first SMA wire layer can be replaced by SMA helical springs, SMA tubes or SMA ribbons.

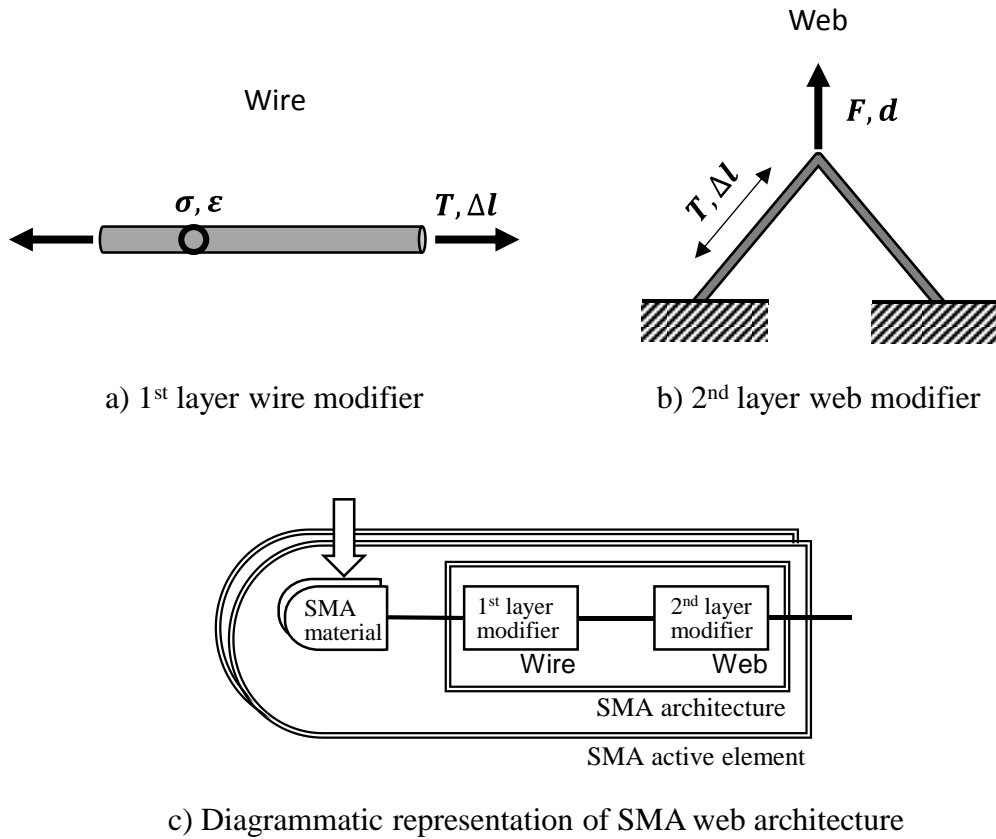


Figure 2.14. Multi-layer structure of the SMA web actuator.

The SMA architecture may have multiple layers of transformation. For example, the SMA wire web actuator, which zigzags the SMA wire along the width between two surfaces to generate stroke amplification normal to the surfaces, has two layers of transformation: the first transformation layer is from SMA material stress-strain behavior to SMA wire tension-elongation behavior (a), which is same as that of the SMA straight wire, and the second transformation layer is from SMA wire tension-elongation behavior to web actuator force-deflection behavior (b).

Not all transformations are as straightforward as the straight wire or web architecture. Depending on the stress distribution over the geometry, the architectures may produce complex transformations coupled to the heterogeneous material behavior over the architecture (Figure 2.5). These **material dependent** architectures are different from **material independent** architectures because the internal architecture geometry change during actuation is affected by the material properties. Moreover, the stress-strain distribution within a material dependent architecture is heterogeneous over the architecture geometry, requiring complex modeling such as the integration of the heterogeneous strain to predict the net stroke. These architecture transformation

characteristics also affect the performance prediction and its visualization as well as the design process, which will be discussed in the following chapters.

2.2.2. Device modifiers

Device modifiers provide the interaction force and/or deflection modification between the SMA active element and the target element (Figure 2.15). There are a number of modifier elements which commonly appear as sub-elements of the device modifier macro element. The **bias** provides the bias force to adjust the austenite and martensite equilibrium stresses and the corresponding actuation strain. **Stroke limiters** may be implemented to limit the actuation stroke to provide consistent actuation stroke and mitigate functional and structural fatigue [9–16]. A **device leverage** enables a force deflection tradeoff. The **friction** from the moving components of the SMA device is combined into a single device modifier element to simplify modeling and performance prediction. A **stroke accumulator** modifier such as a ratchet accumulates the stroke over multiple actuation cycles while resetting the relative position between the SMA device and the target element. While these device modifier elements are illustrated in a particular sequence (Figure 2.15), the order is generally arbitrary and can be changed depending on the design and analysis purpose.

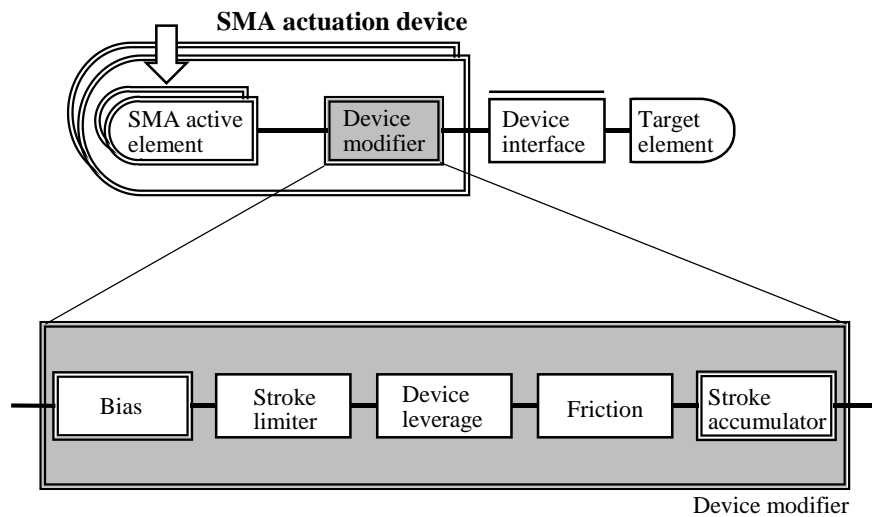


Figure 2.15. Device modifier macro element.

Device modifiers provide the interaction force and/or deflection modification between the SMA active element and the target element. While these device modifier elements are illustrated in a particular sequence, the order is generally arbitrary and can be changed depending on the design and analysis purpose.

2.2.2.1. Bias

The bias modifies the actuation force initiating from the SMA active element by providing bias force to adjust the austenite and martensite equilibrium stresses and corresponding strain. The SMA active element pulls target element when it is hot, and the target element pulls back the SMA active element when the SMA is cold. This force balance shift produces the actuation stroke. However, in some cases target element fails to restore the cold martensitic SMA active element due to friction in the target element and/or in the SMA device, or stiff target element, resulting in a reduction in stroke. By using a bias modifier, the bias force helps the target element to restore the martensitic SMA active element. By providing the bias force, the bias adjusts the apparent stiffness of the target element relative to the SMA active element, which determines the equilibria. Moreover, the martensite stress determines the martensite transformation temperatures, which should be kept above the ambient temperature to ensure a complete austenite to martensite transformation because most SMA devices rely on natural convective heat transfer for cooling of the SMA.

For device design, considering the bias as a modifier to the SMA active element rather than as a modifier to the target element allows effective grouping of macro element as a SMA actuation device. From this point of view, the bias modifies the SMA active element to be more easily restored to the desired martensite equilibrium rather than modifying the target element to be more effective at restoring the SMA active element. This places the design focus on the SMA actuation device rather than the target element. It is also possible to group the bias macro modifier element with the SMA active element creating a macro active element (Figure 2.16). However, in this

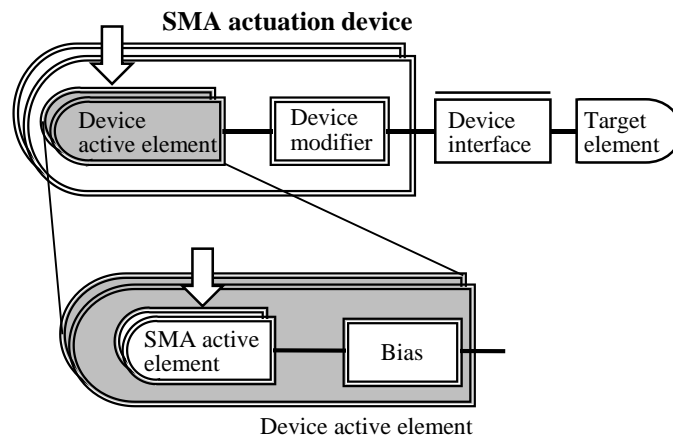


Figure 2.16. Device behavior definition macro element.

study, the bias macro modifier element is categorized as part of the device modifiers, adjusting the force initiating from the SMA active element.

The bias macro modifier element consists of a bias device macro reactive element and a bias device interface modifier element (Figure 2.17). The bias device produces a bias reactive force which modifies the SMA active element behavior, and the bias device interface defines the initial relative position between the bias device and the SMA active element.

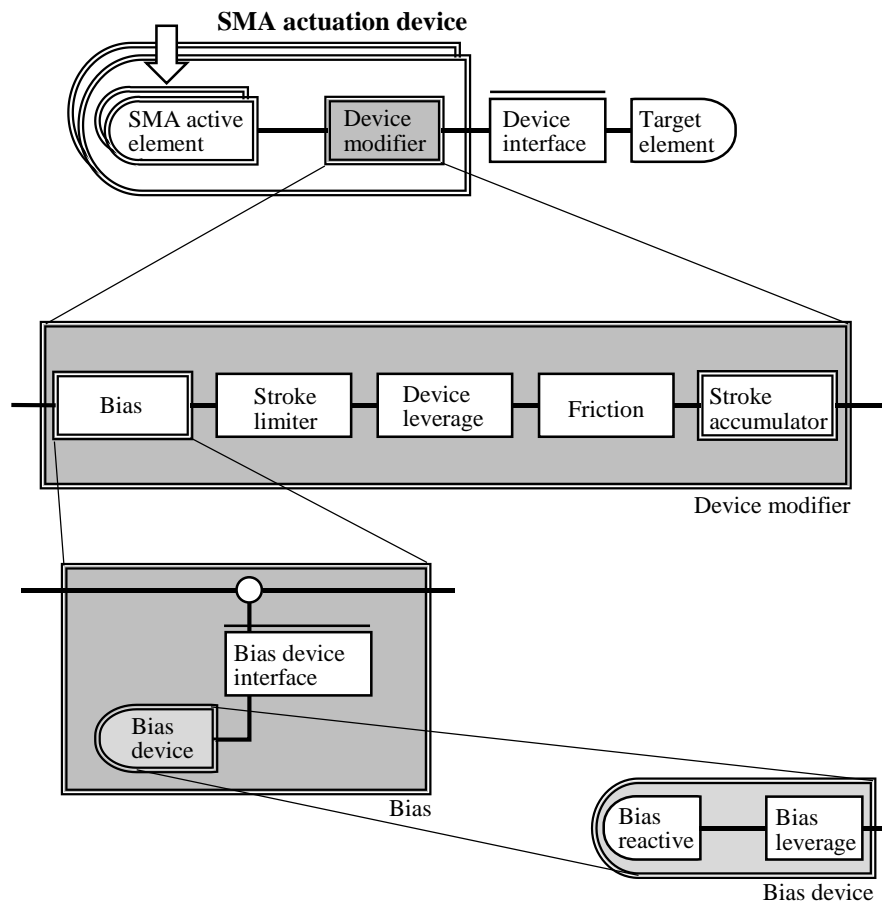


Figure 2.17. Bias macro modifier element.

2.2.2.1.1. Bias device

The bias device, which is a macro reactive element within an SMA device, produces a bias reactive force to adjust the SMA active element force (Figure 2.17). A mechanical coil spring is the most common form of bias reactive element. Although elastic potential energy is the source of the bias force, it is desired to keep the stiffness of the bias reactive element as low as possible

because the bias device increases both the martensite and the austenite stresses. The increased austenite stress reduces the available output force to the target element assuming a fixed maximum SMA stress limit. For many SMA device designs, the selection of an available bias behavior definition element to satisfy a certain operating condition is the most important design task, and bias modifiers are used to overcome limitations of commercially available bias reactive elements under particularly given package constraints. Because bias reactive elements are selected from a discrete set in spring catalogs in most cases, a bias leverage can adjust the bias force, although it requires additional mechanical structure. Therefore, the bias device is often composed of the bias reactive element and the bias leverage modifier element.

2.2.2.1.2. Bias device interface

The bias device interface is an interface modifier element which determines the actual bias force produced by the bias device when a position-dependent bias device (such as a linear spring) is employed. By setting the initial stretch of the bias device (spring), the initial force of the device bias is determined. The bias device interface defines the relative position between the active element and the device bias. By setting the relative position and matching the coordinate system, the bias device deflection at the martensite and austenite equilibria are determined. By modifying the initial pre-tension (pre-load) on the SMA wire, the resulting martensite and austenite deflections decide the bias device forces at each equilibrium. The bias device interface is constrained by the available package space, while the selection of the bias reactive element, bias modifier, and bias device interface are coupled together to provide the required bias device force.

2.2.2.2. Stroke limiters

The austenite and martensite strains, which determine the usable net actuation strain, vary over actuation cycles under certain conditions due to functional fatigue (also known as *shakedown*) [9–16]. Over consecutive actuation cycles, the austenite and martensite strains change resulting in a decrease in actuation stroke due to the different rates of change of the martensite and austenite strain. Functional fatigue negatively impacts the stability of actuation device performance because of the stroke reduction during product life. Moreover, strain shakedown which is the increase of austenite and martensite strain during actuation cycles, can shift the relative interface position between the target element and the SMA active element, thereby changing the performance.

Functional fatigue itself is, in turn, affected by the austenite and martensite stress and strain experienced during actuation, as is structural fatigue (failure) [9–16]. It is a common approach to limit actuation strain by employing stroke limiters to ensure reliable actuation position and mitigate functional fatigue [9,16]. Moreover, stroke limiters are useful for accounting for the material behavior variation due to the reasons stated in Section 2.2.1.1 [8]. The most common stroke limiters are mechanical hard stops which are generally used to limit the martensite strain, and position-based heating current cutoffs which are commonly used to limit the austenite strain. A mechanical hard stop modifies the force-deflection behavior originating from the SMA active element creating pseudo-infinite force by holding the target element force at deflections beyond the cold martensite stop position. A position-based heating current cutoff modifies the force-deflection originating behavior from the SMA active element by changing the state of the SMA active element at deflections beyond the hot cutoff position. Thus, stroke limiter modifier elements are grouped into the device modifier macro element, and it is possible to use both mechanical hard stop and position-based heating current cutoff modifier in a same actuation device.

2.2.2.2.1. Mechanical hard stop

A **mechanical hard stop** constrains the martensite strain by blocking the moving part of the SMA device at the cold actuation end at a preset position which corresponds to the desired martensite strain limit. When the moving part rests on the hard stop, the hard stop holds the target element force, thus the SMA wire is relieved from the target element force. At this hard stop position, further stretching of the SMA material is prevented by the mechanical stroke limiter. This fixed hard stop position can be used as a stable interface position between the SMA device and the target element to ensure a consistent position at each cycle over the device lifetime.

While it is possible to implement a mechanical hard stop to constrain the austenite strain at the hot actuation end, it is not desirable because the mechanical hard stop induces a higher stress than the austenite actuation stress without a hard stop. Since the SMA material is not fully transitioned to the austenite phase when it reaches the mechanical hard stop, the remaining SMA material transformation to the austenite phase induces a blocked stress due to the mechanical stroke limiter.

2.2.2.2.2. Position-based heating current cutoff

A **Position-based heating current cutoff** is a technique to limit the austenite strain by cutting off the Joule heating current to stop the martensite to austenite material phase transformation without inducing the block stress. A position-based switch (either physical or logical) is implemented to terminate the heating current supply when the moving part of the SMA device reaches at a preset position which corresponds to the desired austenite strain limit. The main benefit of implementing a position-based heating current cutoff for the austenite end of the actuation is that this technique protects the SMA material from overheating which also contributes to functional and structural fatigue [17,18]. Moreover, it prevents the higher actuation stress resulting from a mechanical stroke limiter. This stress at the austenite end is considered one of the major factors which cause functional and structural fatigue [9,18–21]. However, the drawback of this technique is the need for additional components such as sensors or switches rather than a simple mechanical stop.

2.2.2.3. Device leverage

The device leverage modifier element allows a tradeoff between force and deflection, although leveraging requires additional device components. When the required force is small with a large required stroke, it is a very challenging design problem for an SMA device because small forces generally produce small displacements and larger forces generally produce larger displacements due to the larger strain difference between the austenite and the martensite equilibria at higher stress levels. Using an external leverage, however, the small force from the target element is amplified to a larger stress in the SMA to produce a larger strain difference from the SMA, which is further amplified to produce an even larger output stroke. Although leveraging in the other direction is also possible, it is generally not called for because the force from SMA is easily scalable by using more and/or thicker wires.

2.2.2.4. Friction

Friction is an unavoidable element during actuation device operation. Friction is important for SMA devices because friction not only causes output force loss, but also shifts the austenite and martensite equilibrium positions, reducing actuation stroke. Friction can be modeled as a single independent device modifier element although it is actually the sum of friction originating from multiple moving components. It acts to modify the force originating from the SMA active

element by adding to it while cooling (austenite to martensite transformation) and subtracting from it while heating (martensite to austenite transformation). Accounting for friction is more important at the martensite equilibrium because the target element may not produce enough force to overcome friction while re-stretching the martensitic SMA wire. A proper bias design can accommodate this issue by providing the resetting force to overcome the friction.

2.2.2.5. Stroke accumulator

A **stroke accumulator macro modifier element** is a time leveraging mechanism which accumulates stroke over multiple cycles to produce a large overall stroke beyond the typical 1 ~ 4 % SMA net strain. The accumulation of stroke is accomplished by updating the internal offset after each actuation step. One example of stroke accumulator macro element is an SMA ratchet mechanism (Figure 2.18), which uses the force originating from the SMA active element to advance a pawl, achieving large overall stroke of a long rack or continuous rotation of a gear. When the SMA wire advances the ratchet, the internal free clearance is also updated within the device free clearance update modifier element.

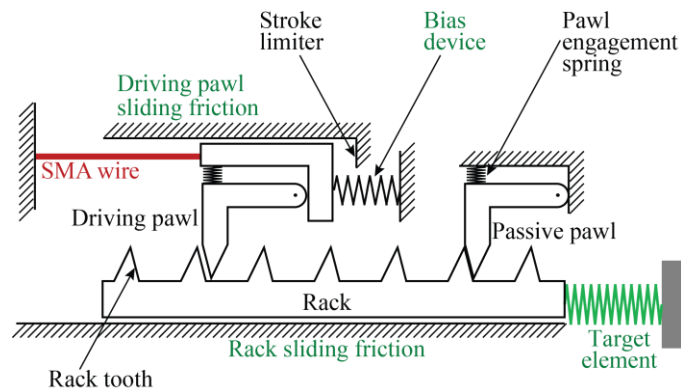


Figure 2.18. SMA wire ratchet mechanism.

2.2.3. Target element

The SMA actuation device system cannot be analyzed without considering the entire system because the SMA actuation is determined by its coupling with the target element. The elements outside of the SMA device macro element are the device interface and the target element. The target element is a macro reactive element which is subject to the SMA device actuation. While, it can be a simple single element or a complex hierarchical macro element, for the design

of an SMA device, it is considered as a single macro element. In some cases, however, the target element and the SMA actuation device can be designed simultaneously to improve performance, where the decomposing the target element into multiple layers of macro elements is useful.

2.3. SMA device architecture examples

Three SMA devices with distinct device architectures, which were introduced in Chapter 1, are presented to help the understanding of the generalized device structure and the SMA device hierarchical structure. A latch release device demonstrates a simple straight wire architecture. An active inner belt seal demonstrates a multi-layer SMA web architecture. The SMART hood lift reset device demonstrate the multi-mode stroke accumulator modifier element. The generalized SMA device structure has been applied to describe these example devices, and these examples will be followed through the rest of this dissertation.

2.3.1. Latch release device: straight wire example

A latch release device (Figure 1.7) is an SMA wire actuation device which uses a straight wire architecture to release a trunk latch in an automobile. An SMA wire actuation device is connected to a latch mechanism through a mechanical lever, and a bias device provides the resetting force during the restoration stage of the actuation.

The physical configuration of the latch release device can be modeled using the SMA device hierarchical structure (Figure 2.19). The actuation device consists of an SMA active element (macro active element) and a device modifier element (macro modifier). In the SMA active element, the stress-strain behavior of the SMA material (SMA active element) is transformed to the force-deflection behavior of the SMA active element through the straight wire SMA architecture. The bias macro modifier element transforms the force-deflection behavior of the SMA active element using the bias device reactive force, which is connected through the bias device interface at the coupling element inside the bias macro element. The device leverage element again transforms the force-deflection behavior, and the SMA actuation device output force-deflection behavior interacts with the target element, which is the latch in this example, through the device interface modifier element. The hierarchical structure allows the design and analysis of particular portion of a device separate from the rest of the device by grouping other elements into macro elements. For example, the bias spring, bias lever, and bias device interface

can be grouped into a single bias macro modifier element, which can also be grouped together with device leverage element creating a macro device modifier element, simplifying the analysis while designing the SMA active element.

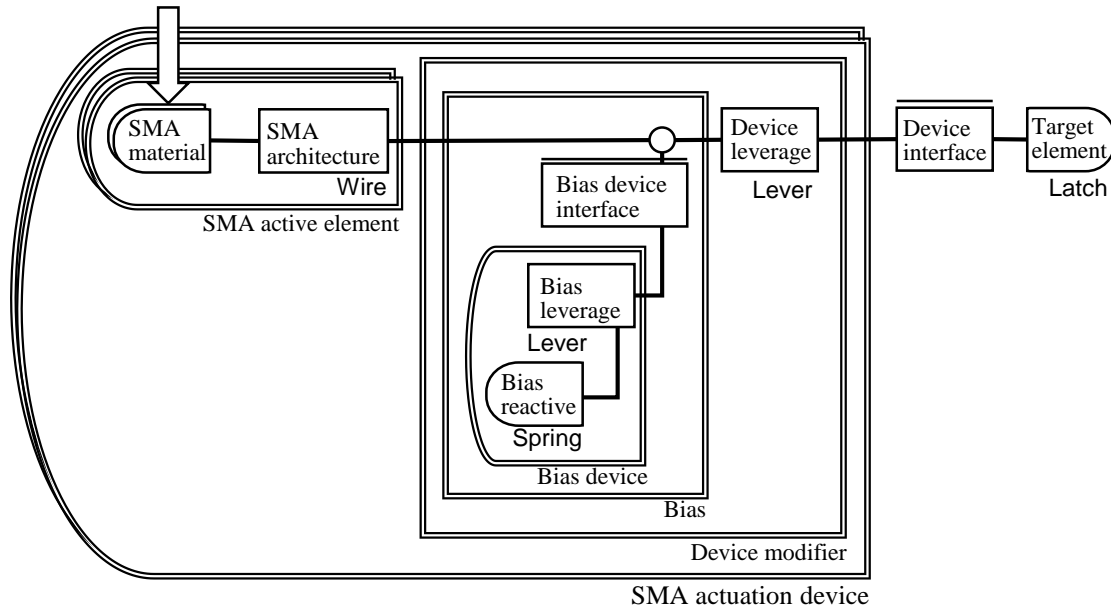


Figure 2.19. Latch release device hierarchical structure.

2.3.2. Active inner belt seal device: web actuator example

An active inner belt seal device (Figure 1.13) is an SMA wire actuation device which uses an SMA web actuator to adjust the sealing force of the inner belt seal against the automotive door window. The adjustability of the sealing force mitigates the squeal and moan while opening and closing the door window in addition to the load reduction for the window motor, while maintaining the sealing force when the window is not moving. The web architecture is selected to enclose the actuation device within the available shallow form factor package space inside the existing inner belt seal (For further explanation of the SMA web actuators, refer Appendix A. The SMA wire web actuator is connected between two surfaces of the inner belt to actuate the leaf of the inner belt seal to adjust the sealing force on the door window.

The structural diagram shows that the SMA active element itself is the actuation device (Figure 2.20); the device does not have any macro modifier element. However, the macro SMA active element itself has a hierarchical structure; the SMA architecture element consists of two

layers of architecture modifier elements: the wire geometry layer, and the web geometry layer. Grouping these two SMA architecture modifier elements into a single macro SMA architecture macro modifier element allows proper design approach.

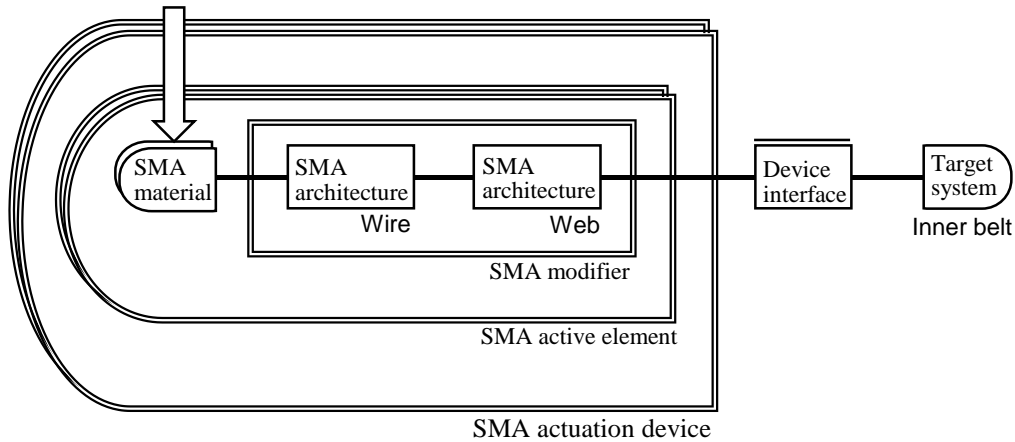


Figure 2.20. Active inner belt seal hierarchical structure.

2.3.3. SMART hood lift reset device: ratchet example

The SMART hood lift (Figure 1.15) is a pedestrian protection device which lifts the hood of an automotive vehicle to prevent direct contact between the pedestrian and the engine block. By creating sufficient space between the relatively compliant hood and the rigid engine block, it mitigates head injuries [22]. The lift force is provided by a compression spring which is triggered using an SMA wire driven latch release device. For reusability of the hood lift mechanism, an SMA driven ratchet mechanism is used to compress the spring to the ready state. Due to the extremely large stroke compared to the limited package space inside the hood lift spring, the ratchet mechanism is the only architecture capable of producing the required force and stroke. Although there is a constraint on the overall actuation speed using the ratchet architecture, resetting speed is not critical for the hood lift device.

The actuation device consists of an SMA active element and a device modifier element. The active element of the hood lift reset device is a bundle of SMA straight wires similar to the active element of the latch release device (Figure 2.21). The device modifier macro element consists of a bias macro modifier element (similar to that in the latch release device, without a bias leverage), and a stroke accumulator modifier macro element. This stroke accumulator element,

which is shaded in gray on the diagram, provides the unique capability of accumulating stroke of the individual step to create a large overall stroke. Because the connection between elements and the force interaction within the stroke accumulator modifier element changes between the heating and the cooling cycles during a single step, the system needs to be analyzed separately for each individual operation mode because the device elements interaction is different for each mode (For further explanation on ratchet mechanism, refer to Appendix B).

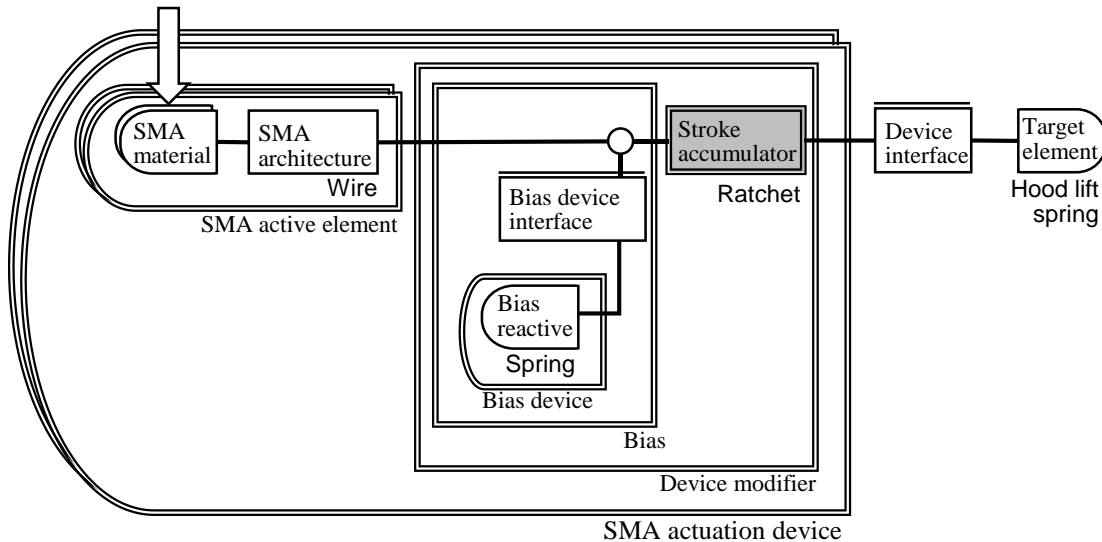


Figure 2.21. SMART hood lift reset device hierarchical structure.

Figure 2.22 shows two different modes of the ratchet operation in the gray stroke accumulator macro modifier element. During the **primary actuation mode**, the SMA active element advances the target element through the driving pawl and linear rack while overcoming the interaction force from the passive pawl (Figure 2.22a). The passive pawl modifies the force initiating from the SMA active element by adding a friction-like interaction force between the rack tooth and the floating passive pawl, which is pressed against the rack by the passive pawl spring. During the **driving pawl restoration mode**, the target element is held by the passive pawl while the driving pawl is restored by the bias device (Figure 2.22b). During the restoration of the driving pawl, the entire system is divided into two disconnected sub-systems because the stroke accumulator macro modifier element is divided into two disconnected macro reactive elements. One sub-system is the passive pawl, which works as a macro reactive element, holding the target element, and the other is the bias device working as a temporary target element (macro reactive

element) to restore the SMA active element. Re-grouping of the macro elements effectively helps the understanding and modeling of the system during the different modes of operation.

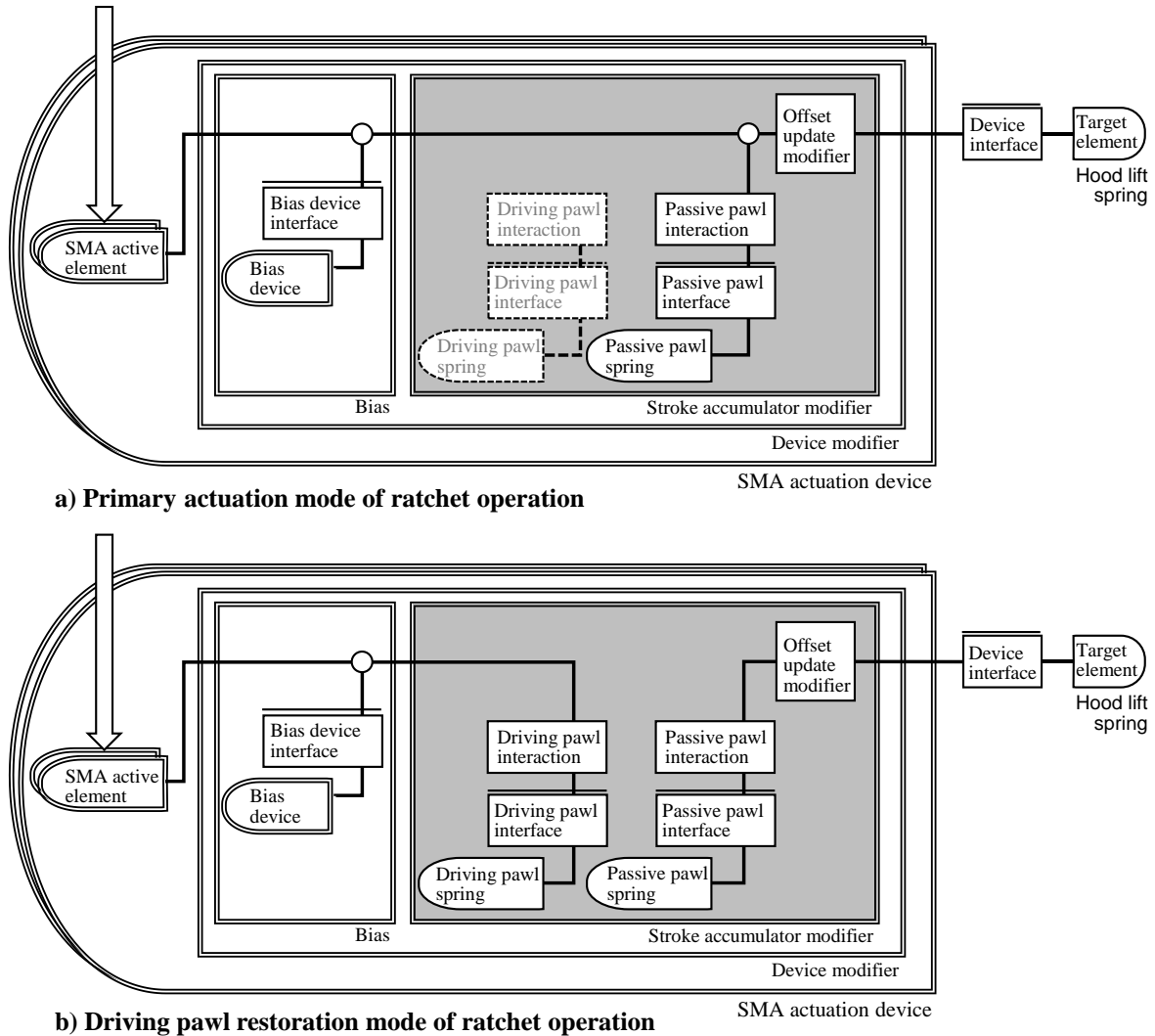


Figure 2.22. Two operation modes of SMART hood lift reset device.

2.4. Conclusions

Hierarchical device architecture provides a foundation to understand and model the SMA actuation devices, and to develop a design framework. The generalized device structure defines a common language to understand actuation devices, identify the design parameters, and discover possible design options. Basic elements work as building blocks of the actuation devices. Active elements initiate the motion by converting a form of energy defining the force-deflection or stress-strain relation. Active elements change its effort-position behavior, such as stress-strain, force-

deflection, or force-stretch ratio, upon signal change (multi-state element). Reactive elements respond to a stimulus following their effort-position behavior, and they may have direction-dependent effort-position behavior. Modifier elements transform a force-deflection or stress-strain input behavior into a desired force-deflection output behavior. Coupling elements provide mechanical connections between the three or more elements providing behavior synchronization. Macro elements enable flexible grouping of meaningful conceptual sets of basic elements to form a hierarchical actuation device system structure while designing and analyzing the device.

A reference SMA hierarchical structure using the generalized device structure and device grammar enables a framework to generate design concepts of SMA actuation devices. Typical SMA actuation device has two macro elements: SMA active element and device modifier element. SMA active element initiates motion using material behavior change upon temperature change of SMA material and transforms into force-deflection behavior through SMA architecture. Device modifier element consists of a series of sub-elements (both basic and macro elements), which transform SMA active element behavior to achieve desired force-deflection behavior of SMA actuation device. By presenting common device elements of the SMA actuation devices, the reference SMA device hierarchical structure helps engineers to understand the role and common usage of the individual element, and formulate the design concepts. Moreover, the engineers can expect the constraints during the design process because the characteristics of each element constrain the specific method for performance prediction, visualization, and modeling. Three device examples are presented to demonstrate the SMA hierarchical structure and three SMA architectures, and will be used in the following chapters (Table 2.1). The reference SMA actuation device structure provides a framework to understand, document, and model SMA actuation devices.

Table 2.1. Hierarchical architectures of three device examples

	Latch release	Inner belt seal	Hood lift reset
SMA architecture	Wire	1 st layer: wire 2 nd layer: web	Wire
Stroke limiter	Yes	N/A	N/A
Bias device	Extension spring Mechanical leverage	N/A	Extension spring
Device leverage	Mechanical leverage	N/A	N/A
Device interface	Fixed	Fixed	Ratchet

2.5. References

- [1] Blanchard, B. S., and Fabrycky, W. J., 2006, *Systems engineering and analysis*, Pearson Prentice Hall, Upper Saddle River, NJ.
- [2] Karnopp, D., Margolis, D. L., and Rosenberg, R. C., 2006, *System dynamics: modeling and simulation of mechatronic systems*, John Wiley & Sons, Hoboken, N.J.
- [3] IEEE, 2007, “Systems engineering — Application and management of the systems engineering process.”
- [4] U.S. Department of Defense, 2011, “Work Breakdown Structure for Defense Materiel Items.”
- [5] Liang, C., and Rogers, C. A., 1997, “Design of shape memory alloy actuators,” *Journal of Intelligent Material Systems and Structures*, **8**(4), pp. 303–13.
- [6] Chang, B.-C., Shaw, J., and Iadicola, M., 2006, “Thermodynamics of Shape Memory Alloy Wire: Modeling, Experiments, and Application,” *Continuum Mechanics and Thermodynamics*, **18**(1), pp. 83–118.
- [7] “Device,” Merriam-Webster.
- [8] Shaw, J. A., Churchill, C. B., and Iadicola, M. A., 2008, “Tips and Tricks for Characterizing Shape Memory Alloy Wire: Part 1; Differential Scanning Calorimetry and Basic Phenomena,” *Experimental Techniques*, **32**(5), pp. 55–62.
- [9] Sun, H., Pathak, A., Luntz, J., Brei, D., Alexander, P. W., and Johnson, N. L., 2008, “Stabilizing shape memory alloy actuator performance through cyclic shakedown: an empirical study,” SPIE, San Diego, California, USA, p. 69300Q–11.
- [10] Bertacchini, O. W., Schick, J., and Lagoudas, D. C., 2009, “Parametric study and characterization of the isobaric thermomechanical transformation fatigue of nickel-rich NiTi SMA actuators,” SPIE, San Diego, CA, USA, p. 72890P–12.
- [11] Miyazaki, S., Mizukoshi, K., Ueki, T., Sakuma, T., and Liu, Y., 1999, “Fatigue life of Ti-50 at.% Ni and Ti-40Ni-10Cu (at.%) shape memory alloy wires,” *Materials Science and Engineering A*, **273-275**, pp. 658–663.

- [12] Wilkes, K., Liaw, P., and Wilkes, K., 2000, “The fatigue behavior of shape-memory alloys,” *JOM Journal of the Minerals, Metals and Materials Society*, **52**(10), pp. 45–51.
- [13] Tobushi, H., Pieczyska, E., Ejiri, Y., and Sakuragi, T., 2009, “Thermomechanical properties of shape-memory alloy and polymer and their composites,” *Mechanics of Advanced Materials and Structures*, **16**(3), pp. 236–247.
- [14] Furuichi, Y., Tobushi, H., Ikawa, T., and Matsui, R., 2003, “Fatigue properties of a TiNi shape-memory alloy wire subjected to bending with various strain ratios,” *Proceedings of the Institution of Mechanical Engineers, Part L: Journal of Materials: Design and Applications*, **217**(2), pp. 93–99.
- [15] Cheung, G. S. P., and Darvell, B. W., 2007, “Fatigue testing of a NiTi rotary instrument. Part 1: strain-life relationship,” *International Endodontic Journal*, **40**(8), pp. 612–618.
- [16] Kim, W., Barnes, B. M., Luntz, J. E., and Brei, D. E., 2011, “Conglomerate Stabilization Curve Design Method for Shape Memory Alloy Wire Actuators With Cyclic Shakedown,” *Journal of Mechanical Design*, **133**(11), p. 111010.
- [17] Otsuka, K., and Wayman, C. M., 1999, *Shape Memory Materials*, Cambridge University Press.
- [18] Mabe, J. H., Ruggeri, R. T., Rosenzweig, E., and Yu, C.-J. M., 2004, “NiTiNol performance characterization and rotary actuator design,” SPIE, San Diego, CA, USA, pp. 95–109.
- [19] Churchill, C. B., and Shaw, J. A., 2008, “Shakedown response of conditioned shape memory alloy wire,” SPIE, San Diego, California, USA, p. 69291F–12.
- [20] Churchill, C. B., and Shaw, J. A., 2009, “Thermo-Electro-Mechanical Shakedown Response of Conditioned Shape Memory Alloy Wires,” pp. 137–148.
- [21] Bo, Z., and Lagoudas, D. C., 1999, “Thermomechanical modeling of polycrystalline SMAs under cyclic loading, Part III: evolution of plastic strains and two-way shape memory effect,” *International Journal of Engineering Science*, **37**(9), pp. 1175–1203.
- [22] Barnes, B. M., Brei, D. E., Luntz, J. E., Strom, K., Browne, A. L., and Johnson, N., 2008, “Shape memory alloy resettable spring lift for pedestrian protection,” SPIE, San Diego, California, USA, pp. 693005–13.

Chapter 3.

SMA Design Methods

Design methods are means to address particular design tasks. Among diverse design tasks, understanding the actuation device system behavior is necessary to make design decisions at different stages of the design process. There are three major design tasks for the comprehension of system behavior: modeling, performance prediction, and visualization (presentation) of behaviors and prediction results.

Although there are material constitutive relation models available to predict the stress-strain-temperature coupled material behavior of SMA [1–5], it is not easy to apply these models for actuation device design which incorporates complex SMA architectures and which involves additional components within real actuation devices. Moreover, SMA architectural transformations impose limitations on performance prediction approaches, but there is no systematic method to integrate architectural models into the system model. Furthermore, most of the design models developed in previous research are hard to reuse for future design projects due to a lack of modularity [6–8]. There needs to be a modular modeling approach using a reference SMA actuation device structure to handle complex SMA architectures and additional components while maintaining the reusability of individual models for device elements.

While performance prediction methods exist to evaluate the actuation device system behavior such as FEA implementation of SMA constitutive models [9–11], or equilibrium methods using force-deflection / stress-strain curves [7,8,12–14], it is hard to use them for supporting design decisions. Current performance prediction methods require additional parametric study with expensive computation to evaluate the impact of parameters of individual components because they often provide only output performance as the performance evaluation result (Figure 1.19).

Moreover, the computationally intense performance prediction methods such as FEA limit the interactive exploration of the design space. Furthermore, once a system is modularly modeled to ensure the reusability of individual component models, it is not trivial to combine them to solve the aggregated system model. There needs to be a systematic model aggregation and performance prediction approach to support design decisions by providing a comprehension of the complete actuation device system.

While a heat map-type visualization (Figure 1.19) is commonly used as output post-processing for FEA methods, and equilibrium methods provide force-deflection / stress-strain curve plots, these visualizations have limitations to expose the effect of individual device elements and their design parameters, which are required to help diverse groups of stakeholders with interests in different elements and aspects of actuation device systems. For example, material scientists are interested in the effect of material behavior on the actuation, while system engineers focus on the effect of the SMA actuation device on the system behavior. For device researchers and device engineers, their interests move throughout the individual device elements while they are deciding appropriate design parameters of each element. Each stakeholder can benefit from a visualization method which shows the effect of the device element of their particular interest. While Shaw and Churchill [15] created design plots to select a bias spring (Figure 1.20), they only support design of one component of an SMA actuation device. A systematic visualization method to expose the effect of individual device elements without expensive parametric studies can help diverse groups of stakeholders with diverse tasks to make design decisions.

The goal of this chapter is to enhance the comprehension of an SMA wire actuation device system behavior by evaluating and presenting the effect of device elements and design parameter variations to support diverse groups of stakeholders to make design decisions.

The objectives are

1. Formalize general modeling approaches for typical SMA wire actuation device system elements including SMA materials, SMA architectural and basic modifier elements, and target elements transformations.
2. Formalize model aggregation and performance prediction approach for the understanding of SMA wire actuation device system behavior.

3. Develop visualization methods to expose the design parameter sensitivity of individual device elements.

In this chapter, to formalize design methods to support design decisions, a modular modeling approach using the hierarchical actuation device structure is proposed to expose the effect of individual device elements and their design parameters. Common modeling guidelines for each basic element type are suggested. Active and reactive element models define the effort-position relation such as force as a function of deflection or stress as a function of strain. Upon an input signal change, active elements initiate actuation, which transfers through the system. Modifier element models transform an input effort-position relation into an output effort-position relation. A coupling element model represents the force balance at a mechanical connection. An actuation system model is constructed by aggregating individual models for basic elements within the system.

Model aggregation and performance prediction methods based on the hierarchical device structure are established to support design decisions by evaluating the effect of device elements and design parameter variations. A solution coupling element is placed within an actuation device system for model aggregation and performance prediction. Placement of the solution coupling provides options for grouping which enables the separation of device elements from others for the design and analysis of particular design elements.

Visualization methods for actuation device system behavior and performance prediction results are formalized to serve diverse stakeholders and design tasks. The visualization relies on two basic approaches: grouping and projection. Projection is the mapping of a performance prediction result from the solution coupling element to another potential solution coupling location to change the coordinates of the visualization. By having various visualization options, engineers can evaluate the effect of individual device elements and their design parameter variations on actuation system behavior, material scientists can evaluate the effect of new materials, and system engineers can integrate an SMA actuation device into a system by selecting interface parameters. These design methods provide the means to support diverse stakeholders to make design decisions.

3.1. General modeling approach

The hierarchical device structure provides a framework for modeling and performance prediction. Individual basic elements are modeled following their unique modeling approach based on element type. A macro element model is constructed by combining basic element models, and a device model is constructed by combining macro and/or basic element models. For example, the model for the macro active element in Figure 2.9 can be constructed by combining the model for the basic active element (solenoid) and the basic modifier element (mechanical lever). The modular modeling approach using a hierarchical structure enables the design and analysis of individual device elements.

Each type of basic element has its unique modeling approach which reflects its nature. Active and reactive element models define their effort-position relations. A modifier element model is constructed to numerically describe the effort-position relation transformation from input to output. Coupling elements provide effort-position behavior synchronization to merge the behavior flows originating at multiple basic active and reactive elements. A solution coupling is placed for performance prediction of a system, and the behavior flows are routed to be terminated at the solution coupling.

3.1.1. Behavior definition elements (active and reactive elements)

Active and reactive element models define effort-position behaviors. The generalized form of the active or reactive element model is

$$F = f(d) \quad \text{or} \quad \sigma = f(\varepsilon). \quad (3.1)$$

An active or reactive element model may have the form of an analytical equation model, a virtual computer aided engineering (CAE) model, or an empirical look up table. For the example system in Figure 2.1, the helical compression spring (target element) can be modeled as a simple analytical equation using the spring stiffness (k) as

$$F = k d. \quad (3.2)$$

While basic reactive elements have one effort-position behavior, active elements have multiple effort-position behaviors for multiple **states** for different values of the input signal. It is

worth to be mentioned that there must always be an OFF state for an active element regardless of the number of the intermediate states.

The form of the model may limit the performance prediction approach. For example, both analytical equations and look up tables can be used for predicting equilibrium, however, numerical implementation of analytical equations and CAE models can be used for dynamic transient behavior prediction which is not possible using look up tables.

While basic reactive elements have only one effort-position behavior, macro reactive elements may have asymmetric behaviors for loading (OFF \rightarrow ON) and unloading (ON \rightarrow OFF) because of the engagement of asymmetric friction and/or device elements. In this case, the loading and unloading directions of macro reactive elements need to be accounted for and synchronized with the ON and OFF states of active elements.

3.1.2. Modifier elements

Modifier elements modify effort-position behaviors to achieve a desired performance. By passing through a series of modifiers, the effort-position behavior originating at an active element is transformed to a required actuation to work against the target element. A typical geometric modifier element model has the form of

$$F_{output} = f(\sigma_{input}, \varepsilon_{input}), \quad d_{output} = g(\sigma_{input}, \varepsilon_{input}), \quad (3.3)$$

and a typical kinematic modifier element model has the form of

$$F_{output} = f(F_{input}, d_{input}), \quad d_{output} = g(F_{input}, d_{input}). \quad (3.4)$$

In general, inverse transformations exist for modifier element models, but for some modifier elements, the inverse transformation may exist in a limited way or not exist at all. For example, the kinematic modifier (mechanical lever) in Figure 2.9 can be modeled with a simple algebraic equation, and the inverse form of the model exists. However, the inverse transformation of some geometric modifier elements only exists for a special condition such as for the equilibrium state due to the non-homogeneous stress-strain distribution over the geometry (There will be a further discussion on the irreversible transformation in Section 3.4.3.1.2.). There are also some kinematic modifiers without inverse transformations such as a bistable mechanism.

3.1.3. Coupling elements

A coupling element model represents force (effort) equality at a connection point. The coordinate system of each input and output port of a coupling element must match with its connected element, and they all must be the same. For coupling elements, the sum of all input forces at each compatible deflection position equals the output force following

$$\sum_{i=1}^n F_{input}^i = F_{output}. \quad (3.5)$$

3.2. Model aggregation and performance prediction

For performance prediction, the models for individual device elements must be systematically combined, and a coordinate system needs to be selected for the force balance solution. This is accomplished by the placement of the solution coupling which aggregates the system model by setting direction of the behavior flows. The actuation performance of the device can be predicted at the solution coupling using two different approaches: the discrete equilibrium approach and the integrated dynamic approach. The **discrete equilibrium approach** assumes an actuation device to actuate between the ON and OFF equilibrium states, and ignores the transient response between the two states. The **integrated dynamic approach** predicts the continuous force balance state of the device during actuation including the transient response. The discrete equilibrium approach allows fast iteration of design changes because it requires a relatively short computation time, while the integrated dynamic approach can capture the transient behavior analysis but requires more intensive computation. The discrete equilibrium approach is useful to explore the design space and set initial design parameters, while the integrated dynamic approach is useful to finalize the design.

3.2.1. Solution coupling and model aggregation

One **solution coupling** element exists in a system, where the system behavior is predicted by solving the effort balance and corresponding position. The solution coupling can be placed among behavior connections between basic elements, which are diagrammatically represented using straight lines. A solution coupling is a special type of coupling which has two input ports

and no output port, and is not necessarily a physical coupling. The behavior is predicted by finding the force balance using

$$\sum_{i=1}^2 F_{input}^i = 0. \quad (3.6)$$

The hierarchical structure of the device does not require directionality of the connections between the elements, however, performance prediction requires that the behavior flow direction originates at the active or reactive element. The behavior flow direction is diagrammatically represented as arrows between elements. Once the solution coupling is placed, the behavior flow direction is obvious because all the behavior flows terminate at the solution element. However, it is possible to adjust the input and output ports of modifier and coupling elements to relocate the solution coupling element for the design and analysis of a particular macro or basic element (Figure 3.1).

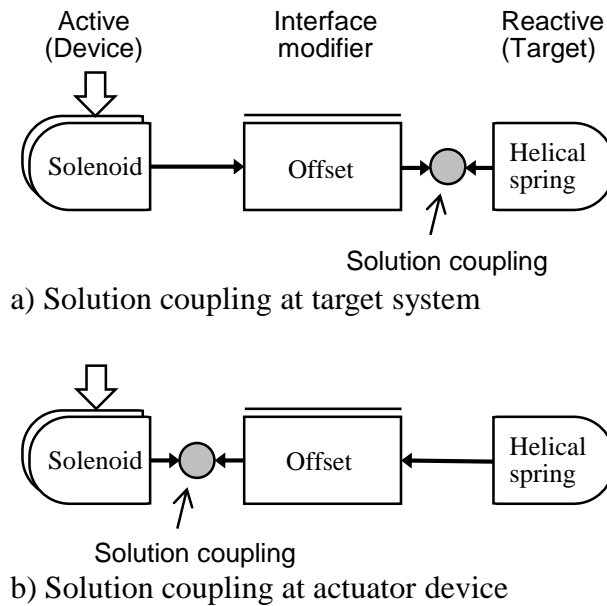


Figure 3.1. Relocating solution coupling element.

However, there are limitations on the placement of the solution coupling due to the irreversible transformations of heterogeneous geometric modifier element transformations. A

solution coupling cannot be placed before irreversible transformation modifiers (Figure 3.2), because the irreversible modifiers do not provide a general form of inverse transformation.

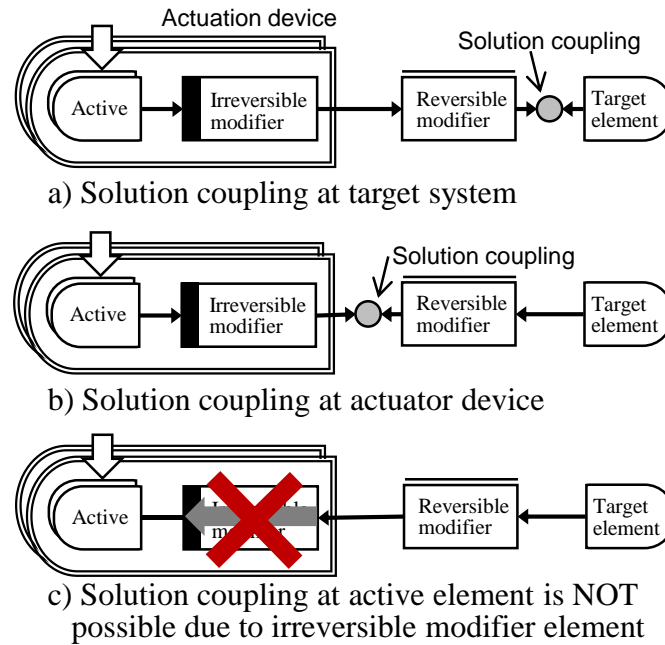


Figure 3.2. Limitation on selecting solution coupling due to irreversible modifier.

3.2.2. SMA actuator device performance prediction approaches

The discrete equilibrium approach and the integrated dynamic approach are applied to the prediction of SMA actuator device performance. As the discrete equilibrium approach for general actuation devices uses the ON and OFF states for performance prediction, the SMA actuator device discrete equilibrium performance prediction approach uses two pre-set temperatures to evaluate the material stress-strain behavior. These two temperatures are usually set to ensure that the SMA has fully transformed to the austenite and the martensite states. For the integrated dynamic performance prediction approach, the temperature evolution of the SMA material between the two pre-set temperatures is first evaluated, and the temperature coupled stress-strain behavior of the SMA material is continuously evaluated to capture the transient behavior of the actuator device. The performance prediction of a simple SMA actuator device system (Figure 3.3) consisting of a straight SMA wire actuation device and a helical extension spring target

element is demonstrated using both the discrete equilibrium approach and the integrated dynamic approach.

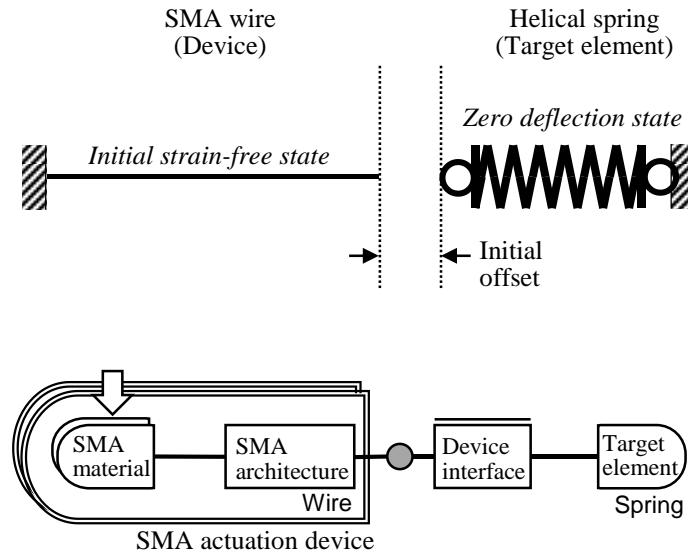


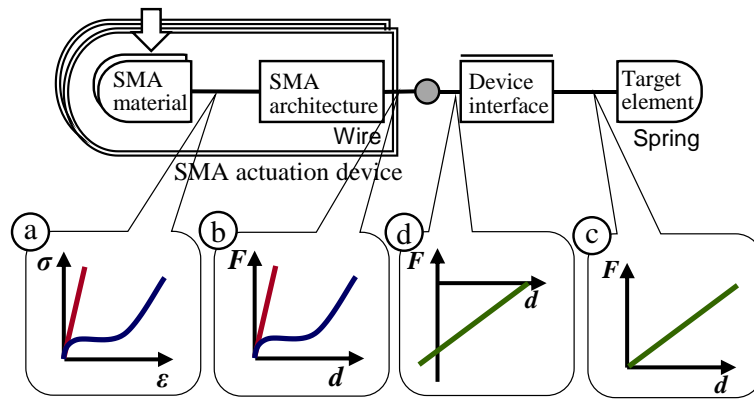
Figure 3.3. A simple straight SMA wire actuator device example.

3.2.2.1. Discrete equilibrium performance prediction approach

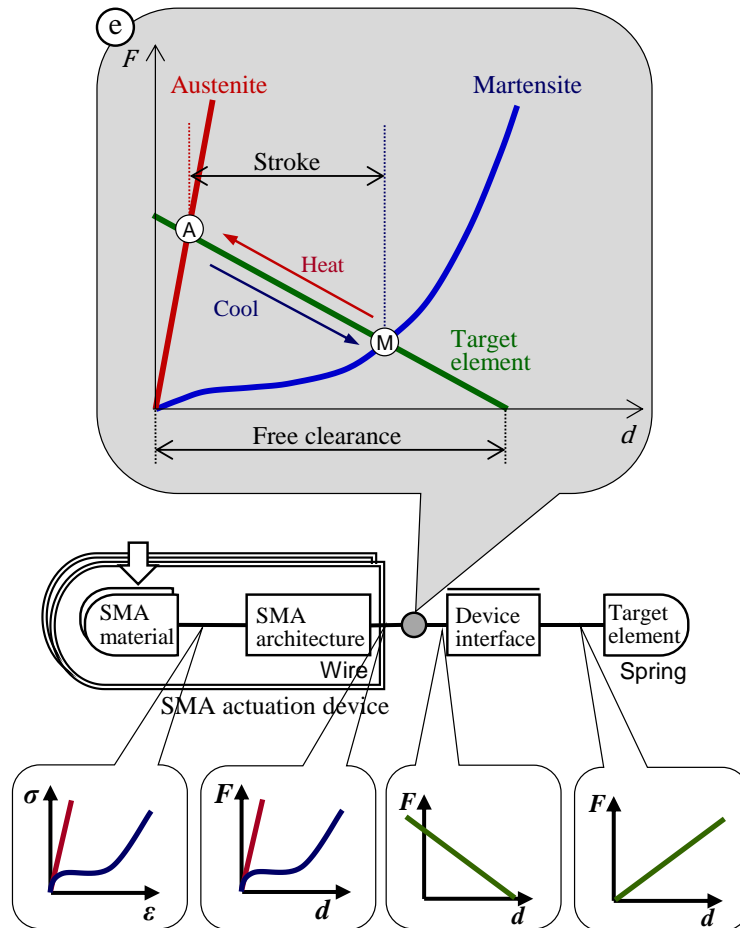
In the discrete equilibrium approach, the pre-evaluated effort-position behavior of every active and reactive element passes through the device elements following the flow direction to the solution coupling element. The modifier elements modify the effort-position relation using the transformation models, and the coupling elements provide the synchronization and summation of the multiple behavior flows. At the solution coupling element, the system performance is predicted by finding the equilibria in the ON and OFF states.

For the example system in Figure 3.3, the material stress-strain behavior and the system force-deflection behavior are evaluated independently under quasi-static assumptions, *i.e.* both the material behavior and the target element behavior are evaluated without accounting for transient or dynamic effects. The austenite and martensite state stress-strain behaviors of the SMA material are evaluated at two pre-set temperatures (Figure 3.4a). The SMA device force-deflection behavior can be predicted by transforming the SMA material stress-strain behavior into the coordinates of the device force-deflection output through the modifier transformations (Figure 3.4b). The target element behavior curve is also pre-evaluated using quasi-static assumptions

(Figure 3.4c), and the interface modifier element transforms it by shifting the origin with the initial offset distance and matching the deflection direction which was defined in the opposite direction



A) Visualization of active and reactive element behavior and interface modifier transformation



B) Modified visualization of discrete equilibrium approach

Figure 3.4. Discrete equilibrium performance prediction approach.

(Figure 3.4d). However, the visualization of the behavior in the matched coordinate system is hard to use for finding the force balance (Figure 3.4A). Thus, a modified visualization is created to show the force balance effectively by changing the direction of the effort on the plot while keeping the matched position (Figure 3.4B), and this modified visualization will be used throughout the entire dissertation. The equilibria in both the martensite and austenite states are evaluated at the gray colored solution coupling (Figure 3.4e), which are visualized as the intersections of the overlaid force-deflection curves. Although the solution coupling can be moved to other locations, the material curves and the target element curve are not required to be re-evaluated. The intersection solution at the new solution coupling location is found only after applying the modifier element transformations which should produce the same performance prediction result. Thus, the discrete equilibrium performance prediction approach is efficient for exploring the design space by changing design parameters and evaluating their performance changes. However, because the actuation device performance is only evaluated for the martensite and austenite state equilibria, the transient behavior of the actuator device is not evaluated using the discrete equilibrium approach.

3.2.2.2. Integrated dynamic performance prediction approach

While the discrete equilibrium approach uses the pre-evaluated effort-position relations to find and evaluate the equilibrium states, the integrated dynamic approach predicts the device performance throughout the entire actuation sequence. Instead of passing the entire pre-evaluated force-deflection relations, the point by point force-deflection is passed through the same device elements (*i.e.* the discrete equilibrium approach and the integrated dynamic approach use the same actuator device structure). The integrated dynamic approach usually employs some form of numerical implementation of the system model such as a computer aided engineering (CAE) software model or a mathematical software model. By evaluating the point-by-point balance of forces, the dynamics of the system interaction can be captured.

While the discrete equilibrium performance prediction approach conceptually passes the pre-evaluated material stress-strain relations and target element force-deflection relation between the device components and transforms them into modified force-deflection behaviors to find the austenite and martensite equilibria, the integrated dynamic performance prediction approach passes the point-by-point force-deflection relation to find the equilibrium at each point in time

while the system transitions through the entire actuation motion. The SMA material transformation is simulated by evaluating the thermo-mechanical temperature evolution. Figure 3.5 shows the integrated dynamic performance prediction result using a MATLAB Simulink model implementation for Figure 3.3 example system. The bottom plateau values of the displacement and force correspond to the martensite equilibrium from the discrete equilibrium performance prediction approach, and the top plateau values correspond to the austenite equilibrium. The temperature evolution is evaluated using Joule heating and convective cooling, and the corresponding material transformation is evaluated in terms of the martensite phase fraction. The force and deflection at the output of the SMA actuation device is evaluated using updated material stress-strain relations at every martensite phase fraction state.

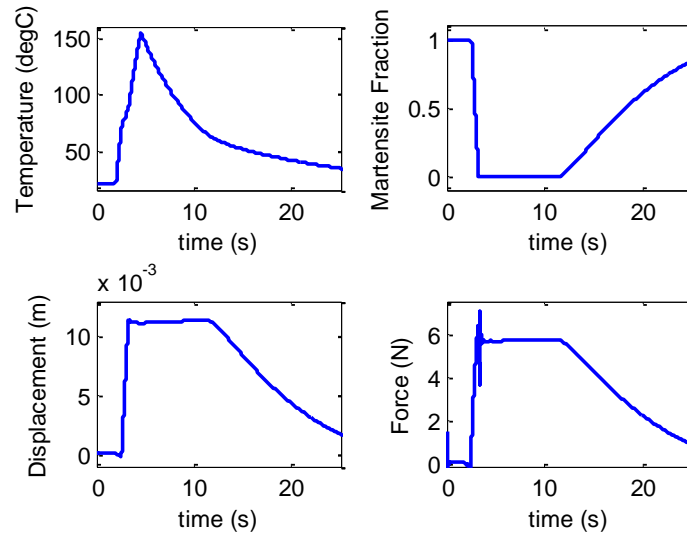


Figure 3.5. Integrated dynamic performance prediction results of a simple SMA actuation device system.

3.3. Visualization of actuation device system behavior

The generalized device structure provides the foundation for modeling and performance prediction. Visualization of the result of the discrete equilibrium performance prediction relies on the generalized device structure to set the grouping of behavior flows originating at the active and/or reactive elements and passing through the modifier and coupling elements. The grouping of the behavior flows enables the isolation of a particular behavior flow which contains a subject element of interest during design and analysis. Because the subject of interest changes throughout

the design process, the grouping of the behavior flows and the corresponding visualization change can help with individual design tasks during the entire design process, and support diverse stakeholders.

While the grouping of the behavior flows is determined by the placement of the solution coupling and the subject element of interest, the coordinates of the visualization can be changed to check design considerations such as the maximum stress and/or the actuation strain during actuation. The coordinate change can be done through the projection of behaviors and of the performance prediction result plot. Projection is the mapping of a performance prediction result from the solution coupling element to another potential coupling element location to change the coordinates of the visualization.

3.3.1. Solution coupling

Visualization of the discrete equilibrium performance prediction result at the solution coupling can help with design and analysis by systematically presenting design information. Moreover, each potential solution coupling can provide different types of design information during SMA actuation device design. For the example system consisting of a straight SMA wire actuation device and a helical extension spring target element in Figure 3.6, there are three potential solution coupling locations, and the visualization at each coupling provides design information of a unique aspect. Performance prediction visualization in material stress-strain coordinates (Figure 3.6a) shows the stress and strain in the austenite and martensite equilibria, and

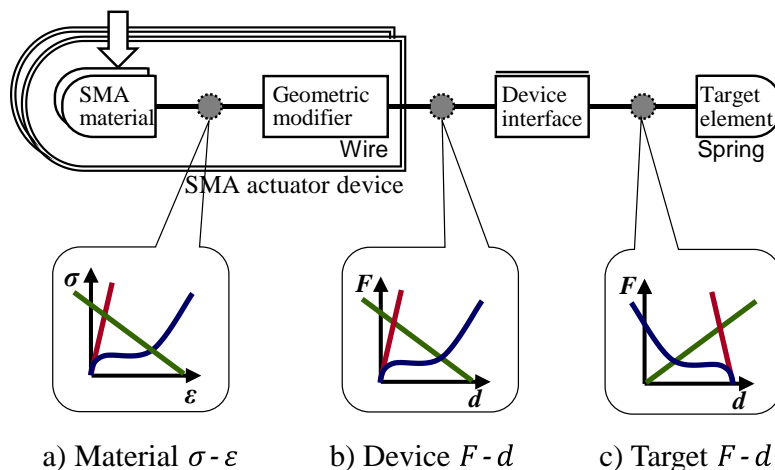


Figure 3.6. Diverse discrete equilibrium performance prediction visualization.

helps evaluate the maximum stress, and the maximum and actuation net strain. Visualization in device macro element force-deflection coordinates (Figure 3.6b) shows the actuation device force and deflection in both equilibria, while visualization in target element force-deflection coordinates (Figure 3.6c) shows the target element force and deflection.

3.3.2. Behavior flow grouping

For an actuation device which has multiple active and/or reactive elements and corresponding behavior flows, the diverse solution coupling placement and visualization options can provide even more valuable design information by separating the effects of one behavior flow from the others for the design and analysis of particular design elements. Grouping is accomplished by placing the solution coupling at a location such that the subject element of interest lies one side of the solution coupling while the remainder of the system is lumped together in the other side of the solution coupling. This enables the visualization of the behavior of one portion of the system against the other. Although the performance predictions using diverse grouping options produce the same result, the direct reading from the visualization plot helps to investigate

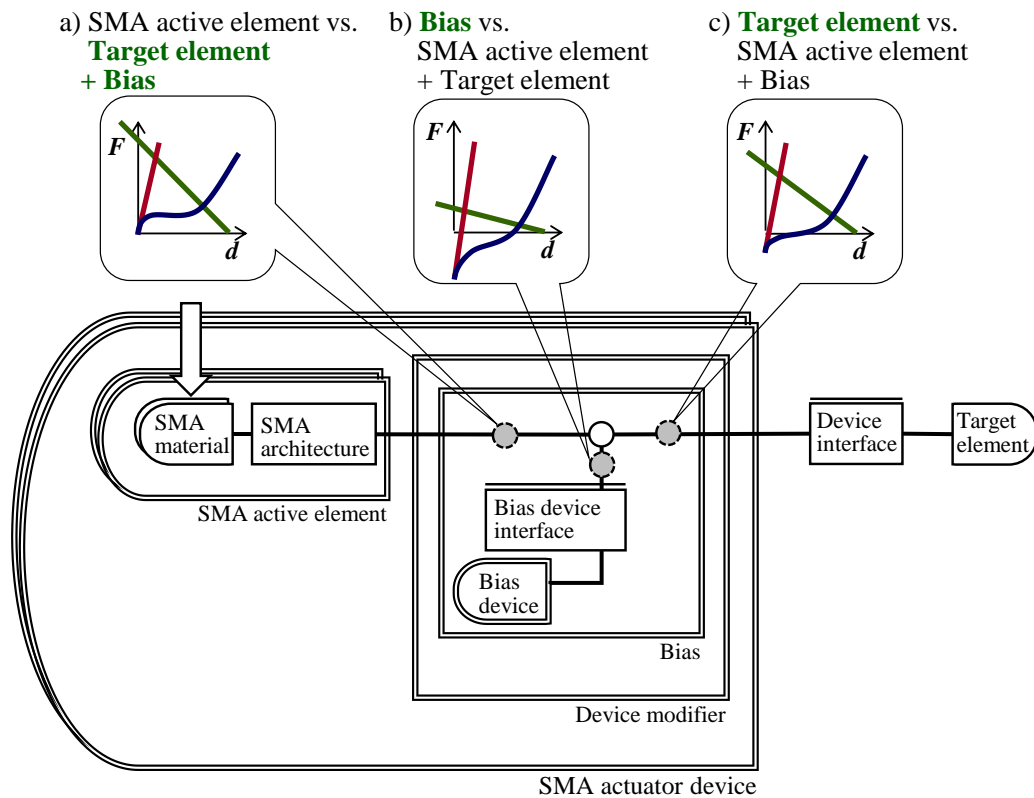


Figure 3.7. Diverse grouping of behavior flows at a single solution coupling element.

diverse aspect of the design. For the example SMA actuation device in Figure 3.7 which contains a bias device macro reactive element within the bias macro modifier element, the three performance prediction visualizations in Figure 3.7 using three grouping options help to evaluate the effect of three active and reactive elements: the SMA active element (Figure 3.7a), the bias device (Figure 3.7b), and the target element (Figure 3.7c). The force-deflection behavior of the individual active and reactive elements are directly presented using these visualizations, and the lumped curves helps to evaluate the sensitivity of each active or reactive element.

3.3.3. Performance prediction projection

While the diverse grouping options of behavior flows provide valuable design intuition, the visualization of the discrete equilibrium performance prediction can be further improved by projecting a visualization plot to another potential solution coupling location (Figure 3.8). The major benefit of projecting the performance prediction result is that the performance prediction can be illustrated in a different coordinate system, and thus the design parameters can be modified using the coordinate system natural to a particular device element. While both visualizations in

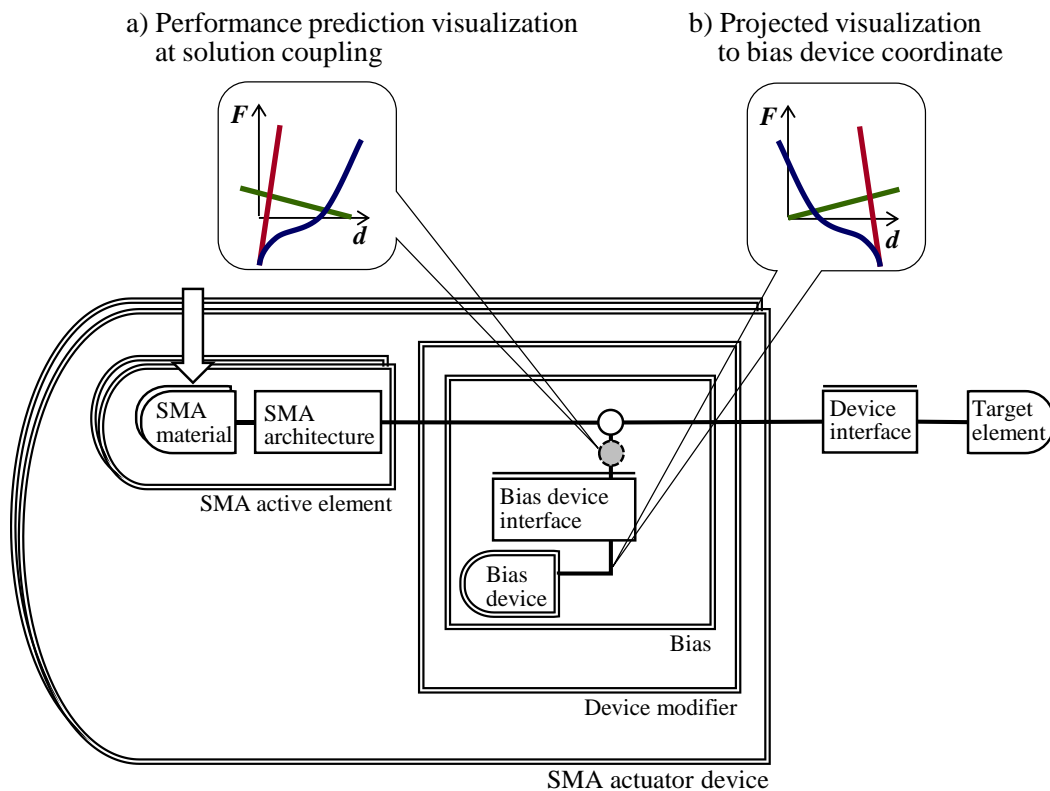


Figure 3.8. Projection of performance prediction visualization.

Figure 3.8 show the effect of the bias device on the actuation device performance, the visualization in Figure 3.8b is easier to use to adjust the design parameters related to the bias device.

Although projection can produce the same visualization plot as moving the solution coupling, it is different from shifting the solution coupling because projection is not limited by irreversible transformation modifier elements. While the solution coupling cannot be placed between an active element and an irreversible transformation modifier element, the result can be projected to the coupling between the active element and the irreversible transformation modifier element to show a representative prediction in the natural coordinate system of the active element (*e.g.* SMA material stress-strain coordinate system).

3.4. SMA device modeling approach

The hierarchical structure provides a foundation for modular modeling of SMA devices. Because the models for the individual device elements are modular, the model for an SMA actuation device is constructed by combining these modular models. However, this does not mean that the actuation performance of the individual device elements is decoupled. The performance prediction must be done after the entire device model is constructed by aggregating the device element models.

The type of each component determines the modeling approach. Modeling of active and reactive elements focuses on how to capture the unique stress-strain or force-deflection behavior. A modifier element model addresses the transformation of an input behavior into a modified output behavior. A coupling model accounts for the combination of multiple behavior flows.

3.4.1. SMA material (active element) models

SMA material models represent the stress-strain-temperature coupled behavior of SMA. The performance prediction of an SMA actuation device must capture the multiple states of the SMA material behavior at multiple temperatures. For example, the discrete equilibrium performance prediction approach requires at least two states for the SMA material representation, typically in the full austenite state and the full martensite state, which can be evaluated by setting the temperature at two fixed values. The integrated dynamic performance prediction approach requires the evaluation of the temperature evolution, and the stress-strain behavior is evaluated at each temperature to analyze the transient behavior of the system.

While several types of material models exist for SMA, there needs to be a distinction between the material behavior and the representation of the behavior. Although diverse types of representations of the material behavior may have different forms, they represent the same material behavior. However, the material properties of the SMA material varies due to many reasons including material composition, previous cold work, and operation history [17]. It is desirable to characterize the material behavior of a specific material to be used for a particular device design, however, it may not be possible to characterize all the materials for mass production of a device, which may require multiple batches of SMA material. Moreover, there always is some disagreement between the model prediction of the material behavior and the actual performance. Thus, it is practical to allow a safety margin to accommodate material behavior variations and/or model disagreement.

3.4.1.1. Empirical representation

The material behavior of SMA can be represented as a set of stress-strain relations. The empirical stress-strain relation can be measured using a single straight SMA wire which is subject to dead weight tensile loading tests under single heating/cooling cycles (Figure 3.9). Although there needs to be many stress-strain relations to represent the SMA behavior over a wide temperature range for integrated dynamic performance prediction, the discrete equilibrium performance prediction approach only requires two temperatures which capture the full austenite and full martensite behaviors. A fresh wire needs to be used for each applied load in a series of loads to prevent functional fatigue during the measuring process [18].

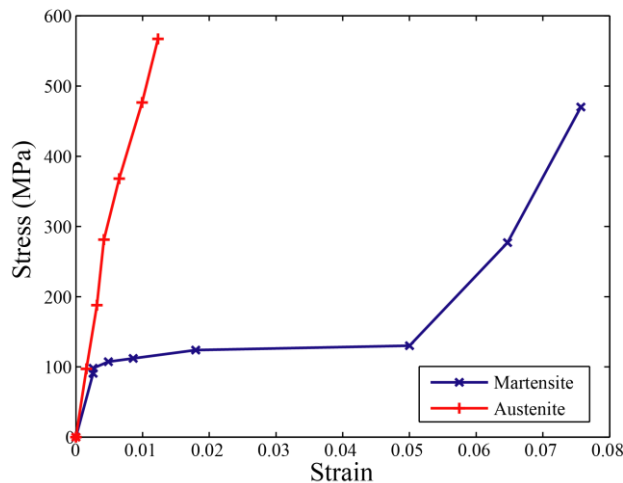


Figure 3.9. Empirical stress-strain measurement along with a curve fit.

3.4.1.2. Constitutive models

Modeling of the SMA material behavior is an on-going research area; the categorization and review of these models are not the focus of this study and will not be attempted. Any type of SMA behavior model which can capture the stress-strain-temperature coupling of the material can be used for SMA device design. Most SMA constitutive models use the martensite phase fraction to capture changes in material properties due to crystal structure changes. The martensite phase fraction is tracked as a function of the SMA stress and temperature. The temperature evolution is computed coupled with the martensite phase fraction and SMA stress. Popular SMA constitutive models include those by Liang [19], Brinson [2], Chang and Shaw [20], Lagoudas [21], and several variations of these models. For example, Liang's model, one of the most commonly used material models, provides a stress(σ)-strain(ϵ)-temperature(T) coupled form of the constitutive relation using the martensite phase fraction (ξ) as

$$\sigma - \sigma_0 = D(\epsilon - \epsilon_0) + \Omega(\xi - \xi_0) + \Theta(T - T_0), \quad (3.7)$$

where $D(\epsilon, \xi, T)$ is the modulus of the SMA material, $\Omega(\epsilon, \xi, T)$ is the transformation tensor, $\Theta(\epsilon, \xi, T)$ is the thermal expansion coefficient for the SMA material, and σ_0 , ϵ_0 , ξ_0 , and T_0 represent the initial state [19]. The transformation tensor is expressed using the SMA material modulus D and the maximum residual strain ϵ_L as

$$\Omega = -\epsilon_L D. \quad (3.8)$$

The martensite phase fraction from the austenite state to the martensite state is described by

$$\xi = \frac{1 - \xi_0}{2} \cos \left[a_M \left(T - M_f - \frac{\sigma}{C_M} \right) \right] + \frac{1 + \xi_0}{2} \quad (3.9)$$

for $C_M(T - M_s) < \sigma < C_M(T - M_f)$,

while the reverse transformation from martensite to austenite is expressed as

$$\xi = \frac{\xi_0}{2} \left\{ \cos \left[a_A \left(T - A_s - \frac{\sigma}{C_A} \right) \right] + 1 \right\} \quad (3.10)$$

for $C_A(T - A_f) < \sigma < C_A(T - A_s)$,

where M_s and M_f are the austenite to martensite transformation start and finish temperatures, A_s and A_f are the martensite to austenite transformation start and finish temperatures, and the constants C_M and C_A are material properties for the relationship between temperature and the critical stress required to induce transformation. The constants a_M and a_A are defined as

$$a_M = \frac{\pi}{M_s - M_f}, \quad a_A = \frac{\pi}{A_f - A_s}. \quad (3.11)$$

Brinson improved this model by separating the martensite phase fraction (ξ) into the temperature induced martensite phase fraction (ξ_T) and the stress induced martensite phase fraction (ξ_S), and by updating the constitutive relation and corresponding constant definitions [2]. Using a numerical implementation of a variation of an example constitutive model [5], the stress-strain relations at several discrete temperature are evaluated as shown in Figure 3.10.

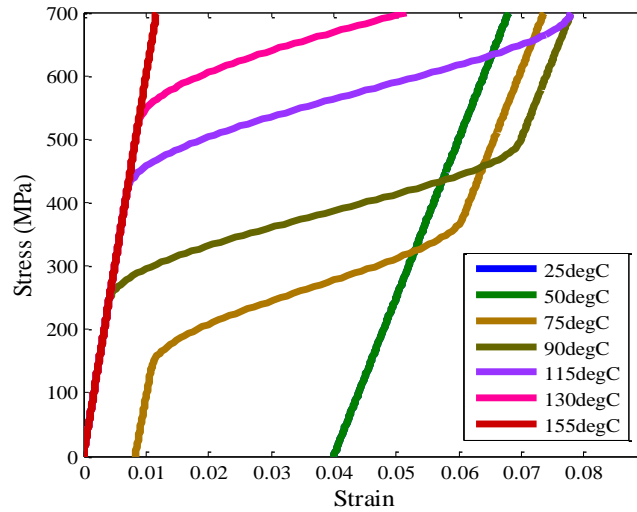


Figure 3.10. Stress-strain behavior prediction using a modified Brinson type model.

While empirical representations of SMA material behavior have limitations to capture the transient behavior, the numerical implementation of constitutive SMA models enable various options for SMA actuation device performance prediction.

3.4.2. Reactive element models

Since SMA material models provide stress-strain relations only, they require SMA architectures as modifier elements to transform to force-deflection relations, which can then

interact with reactive element models which provide force-deflection curve directly. Because a bias reactive element is implemented in a bias device as a linear stiffness spring, a simple analytical model is usually used for its representation. For the target element, if there is a physical prototype available, it is possible to directly measure the force-deflection behavior to generate an empirical representation. It is also possible to assume the target element is a simple constant load or a linear stiffness system in the early design stages. Computer aided engineering (CAE) models can also be built for in-depth analysis of target element behavior. Similar to SMA material models, some forms of representation impose limitations on available performance prediction approaches.

3.4.2.1. Empirical representation

An empirical representation of a target element is only practical when an SMA device is designed to actuate a target element which exists as a physical prototype. While it is possible to measure the dynamic behavior of a target element, it is more practical to measure the point by point quasi-static force-deflection response in multiple equilibrium positions over a range of force or deflection. However, a set of equilibrium force-deflection behavior profiles cannot be used to represent the dynamic behavior of the target element. Moreover, this form of target element representation is hard to aggregate into a combined system model including the SMA device to simulate transient interaction. However, it is possible to use a curve fit model as a surrogate model or a look up table for simulation although only the SMA behavior can be simulated dynamically in this case.

3.4.2.2. Analytical model

The target element can be represented as a simple constant load or a linear stiffness, when the design information is limited in the early design stage. A more sophisticated analytical representation of the target element can also be used which may or may not include dynamic aspects of the target element. Analytical models can be easily implemented into a combined system model including the SMA device for both the discrete equilibrium and the integrated dynamic performance prediction approaches.

3.4.2.3. CAE model

During the later stage of the design process, the target element is often built as a virtual prototype both for fabrication of a physical prototype and for CAE analysis. The most common

types of analysis methods are the finite element method (FEM) for stress and deflection analysis, and multi-body dynamic analysis methods. Both types of models enable a variety of options for SMA device design, although technical issues related to the implementation of SMA constitutive models and/or co-simulation between the target element model and the SMA material model need to be properly addressed.

When a CAE model is used for the discrete equilibrium performance prediction approach, a surrogate model or a look up table is created by pre-simulation over an operable range. This procedure is similar to direct measurement for an empirical representation of a physical prototype. Instead of using a physical prototype, a virtual prototype is used for pre-simulation to evaluate the effort-position behavior.

While the material behavior and reactive element behaviors including the target element can be evaluated using different methods for the discrete performance prediction approach, representations for the SMA material and the reactive elements need to be of the same type or at least computationally compatible with each other (software compatibility). This is necessary to allow concurrent simulation with interaction between the material model and the reactive element representations in the integrated dynamic performance prediction approach. Moreover, empirical material and/or reactive element models limit the accuracy of the integrated dynamic performance prediction approach because the empirically modeled portions of the system return quasi-static responses to the dynamically simulated portions of the system.

3.4.3. Modifier element models

Modifier elements transform the original force-deflection or stress-strain behavior of an active or reactive element into a desired force-deflection behavior. SMA architectures (Geometric modifier elements) transform the stress-strain behavior of the SMA material to the force-deflection behavior of the SMA active element through the architecture geometry. Kinematic modifier elements represent the device elements which transform a force-deflection relation into another force-deflection relation.

3.4.3.1. SMA architecture (Geometric modifier element)

SMA architectures transform stress-strain relations into force-deflection relations through the architecture geometry. The architectural transformation is categorized as either a

homogeneous geometric modifier element transformation or a heterogeneous geometric modifier element transformation. The geometry change in a heterogeneous geometric modifier element transformation is affected by the material behavior while that in a homogeneous geometric modifier element transformation is mainly governed by the geometry.

3.4.3.1.1. Homogeneous geometric modifier element transformation

A homogeneous geometric modifier element transformation is a function of only geometric variables and is a fully bi-directional transformation which does not require material behavior information. For the example actuation device system with a straight SMA wire connected to target element, the target element force-deflection behavior can be transformed to stress-strain coordinates through the wire architectural transformation (Figure 3.6a). Alternatively, the material stress-strain behavior can be transformed to force-deflection coordinates (Figure 3.6c). The motion solution can be found using either one of these potential solution coupling placements. In this case, the transformation is simple where force-deflection maps directly to stress-strain through the area and length of the wire. This bi-directional transformation is possible because the stress distribution over the SMA architecture geometry is homogeneous.

Homogeneous geometric modifier element transformation example (straight wire): The simplest example of an architectural transformation is that of the SMA straight wire actuator (Figure 3.3). The SMA material is interacting with the target element through the geometry of the straight wire. The stress is transformed into a force through the cross-sectional area of the wire, and the strain is transformed into a deflection through the length of the wire.

Multi-layer homogeneous geometric modifier element transformation example (web actuator): An example of a homogeneous geometric modifier element architecture is a web (or bow string) actuator (Figure 3.11) [22]. In the SMA web actuator architecture, the SMA in wire form is connected between a stationary and a moving surface in a zigzag pattern. The SMA web actuator architecture operates in three states: the reference strain-free state, the austenite equilibrium state, and the martensite equilibrium state. Actuation is the movement between the austenite equilibrium state and the martensite equilibrium state. The first state, the **reference strain-free state** (Figure 3.11a), defines the reference geometry of the web: width of the web segment (W), gap between the fixed base and the moving attachment point (G), length of the SMA wire (l), and the initial offset (C_0). The initial offset is defined as the relative position between the web and the origin of

the target element (simplified here as a spring), using the heated unloaded wire before they are attached. In the second state, the *austenite equilibrium state* (Figure 3.11b), the target element is attached to the web in the austenite phase at an equilibrium position with an austenite equilibrium gap G_A , where the force from the web balances the force from the target element. In the third state, the *martensite equilibrium state* (Figure 3.11c), the SMA wire is cooled to the compliant martensite phase, and the target element force stretches the web to a new equilibrium position with a martensite equilibrium gap G_M . The actuation stroke is defined as the difference in the gaps ($\delta_{Stroke} = G_M - G_A$) when the wire is heated and cooled between the martensite and austenite equilibrium states. The primary benefit of using this architecture is that it exploits the wide length of the packaging space, and amplifies and redirects the stroke of the SMA wire perpendicular to its length without any additional mechanisms. While the straight wire architecture only has one layer of transformation, the web architecture has two layers of transformations; the material stress-strain relation is transformed to a wire tension-elongation relation, which is the same transformation through area and length as the straight wire transformation, then this wire tension-elongation relation is transformed to a web force-deflection relation through the web geometry. In reverse, the transformation of the target element force-deflection is done by the web architectural transformation to the wire tension-elongation relation, and then by the wire architectural transformation to the material stress-strain relation.

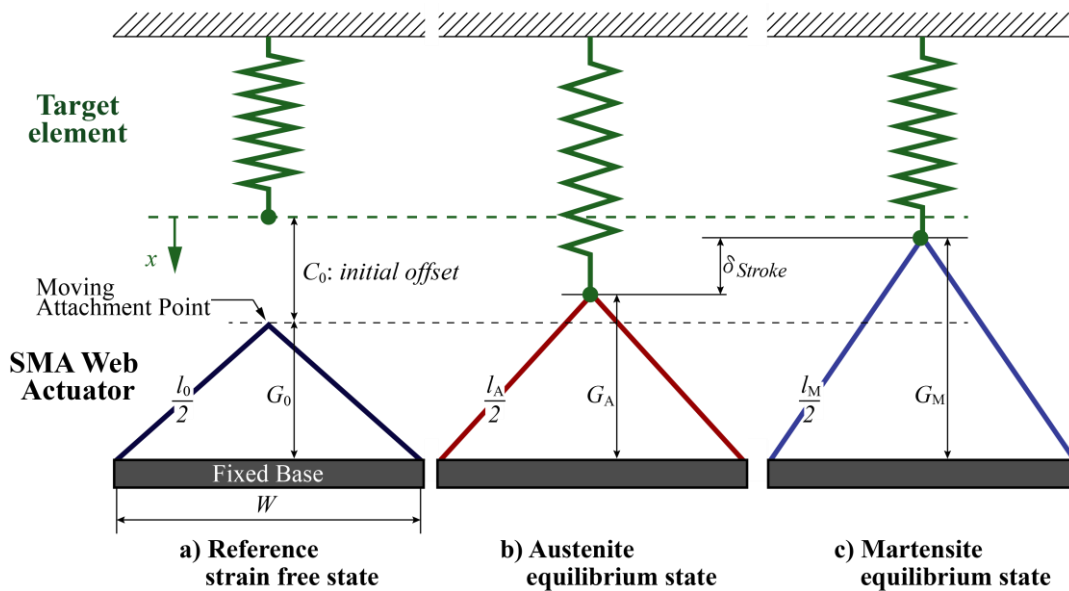


Figure 3.11. Multi-layer homogeneous geometric modifier element transformation: web

This transformation can be modeled as one combined macro element transformation to solve the motion in either material stress-strain coordinates or system force-deflection coordinates (Figure 3.12). However, by having separate layers of the wire architectural transformation and the web architectural transformation, the wire tension-elongation relation enables additional analysis during design. Moreover, multi-layer architectures can be modified with different one layer architectures without modifying the other layers. For example, the web architecture can be used with other forms for the 1st layer modifier such as SMA ribbon or cables by substituting the SMA wire architectural transformation with other transformations. For further explanation on the SMA web architecture, refer to Appendix A.

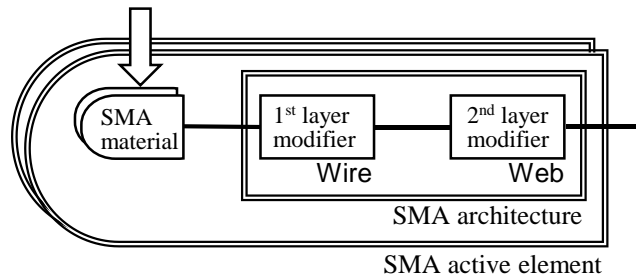


Figure 3.12. Hierarchical structure of the SMA web actuator.

3.4.3.1.2. Heterogeneous geometric modifier element transformation

A heterogeneous geometric modifier element transformation is coupled to the material behavior as the stress-strain and/or force-deflection is not uniformly distributed over the SMA architecture because the geometry changes are constrained by the material behavior during actuation. For example, although the material is in the same geometric form factor as a straight wire, the transformation of a bent SMA wire is not a homogeneous geometric modifier element transformation due to the stress-strain variation over the wire diameter direction; the exact shape of the bent wire depends on the distribution of stresses and the material constitutive behavior. While the forward transformation from the input material stress-strain relation to the output force-deflection relation is a fully defined transformation, the backward transformation is a limited transformation because it is coupled to the material behavior and heterogeneously distributed. A representative backward transformation can be used for a particular force-deflection value which projects to a range of distributed stress-strain or to a representative value such as the maximum. The motion solution must be found in the system force-deflection coordinates because the

representative backward transformations must use the motion solution result to project to the stress-strain coordinates.

Heterogeneous geometric modifier element transformation example (spool packaging): An example of a heterogeneous geometric modifier element architecture is the spool packaging architecture (Figure 3.13) in which the SMA wire is wrapped around pulleys or mandrels to reduce the package footprint [23]. While the transformation from the material stress-strain relation to the active element force-deflection output through the wire tension-elongation relation is similar to the homogeneous geometric modifier element transformation, the tension-elongation and the stress-strain distribution is not homogeneous across the architecture geometry. This spool packaging architecture modifier model is a multi-layer heterogeneous geometric modifier element transformation which is not fully reversible (Figure 3.14). This transformation requires the material stress-strain relations to be integrated over the cross-sectional area and the wire length to predict the overall output performance.

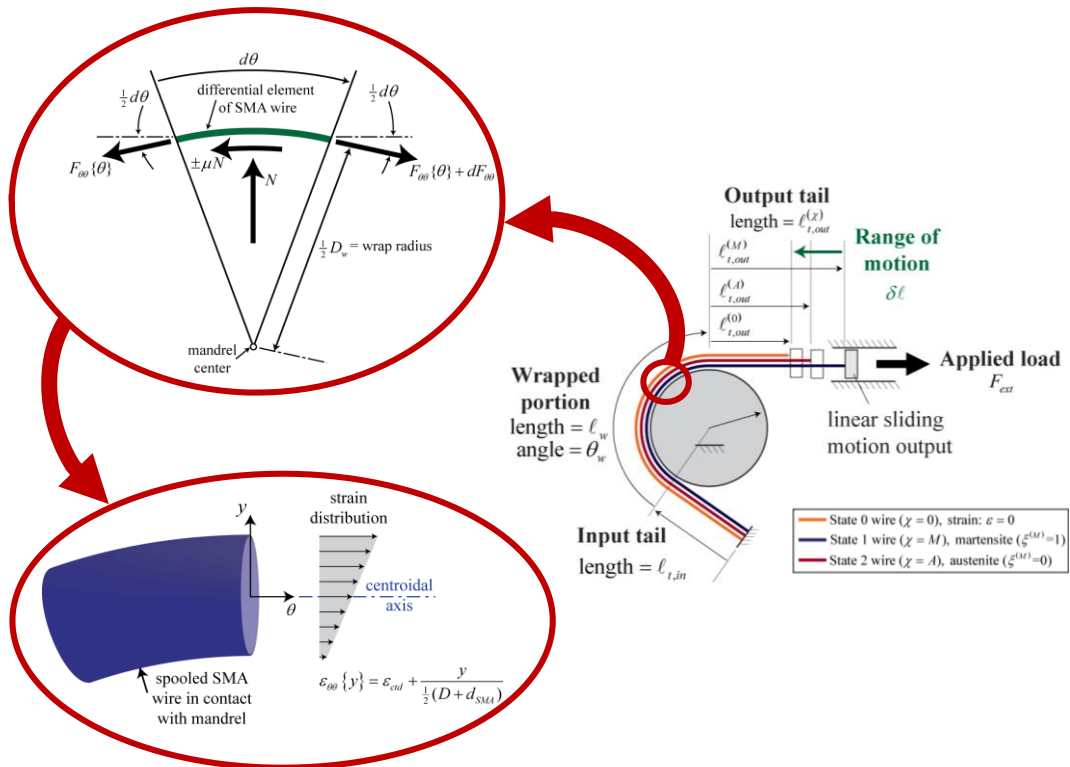


Figure 3.13. Heterogeneous geometric modifier element transformation example: spool

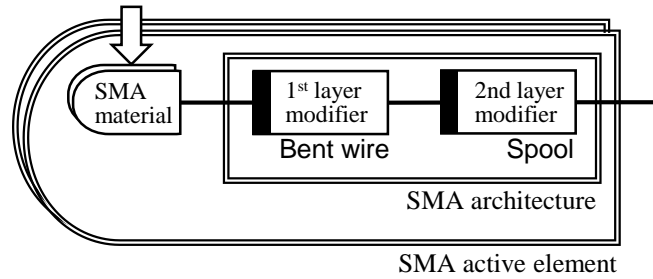


Figure 3.14. Hierarchical structure of the SMA spooling.

Because the tension-elongation and the stress-strain distribution is not homogeneous, the transformation from the higher layer to the lower layer, for this example from the force-deflection coordinates to the wire tension-elongation coordinates and from the wire tension-elongation coordinates to the material stress-strain coordinates, is only possible for a range of distributed stress-strain over the wrap angle (Figure 3.15). Because the projected stress-strain distribution only represents the maximum and minimum stress and strain during actuation, the motion solution can be found only after the SMA architecture macro modifier element.

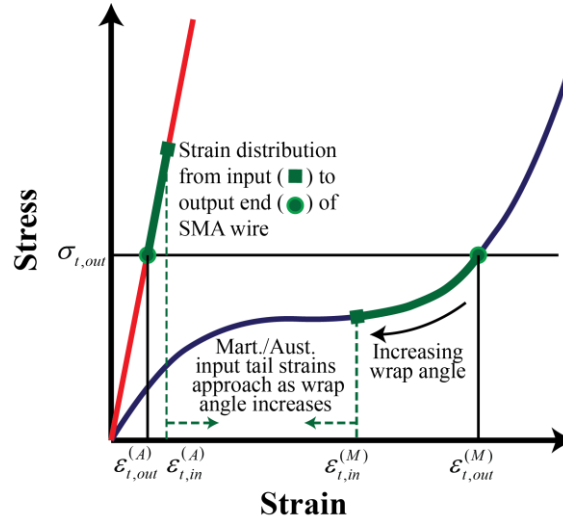


Figure 3.15. Stress-strain distribution over the spool packaged SMA wire [6].

3.4.3.2. Kinematic modifiers

Kinematic modifiers transform the force-deflection behavior flow originating from the SMA active element to achieve a desired force-deflection behavior. Stroke limiters constrain the actuation stroke to control the material strain during actuation. A mechanical leverage trades off

between force and deflection to produce the desired performance. Friction captures mechanical losses in the SMA device.

3.4.3.2.1. Stroke limiters

When stroke limiters are applied, the material stress-strain model becomes a piecewise model to capture the discontinuous force interaction inside the SMA device. For a martensite mechanical stroke limiter (hard stops), the target element force seen by the SMA active element is relieved by the stroke limiter. In Figure 3.16, the martensite stroke limiter is represented as a vertical line of the actuation device behavior curve in the martensite state, or a vertical line of the target element behavior curve depending on the solution coupling position. If an austenite mechanical stroke limiter is applied, the mechanical stroke limiter imposes a blocking force to the SMA wire, resulting in high stresses, which is not desirable due to the issues with functional and structural fatigue.

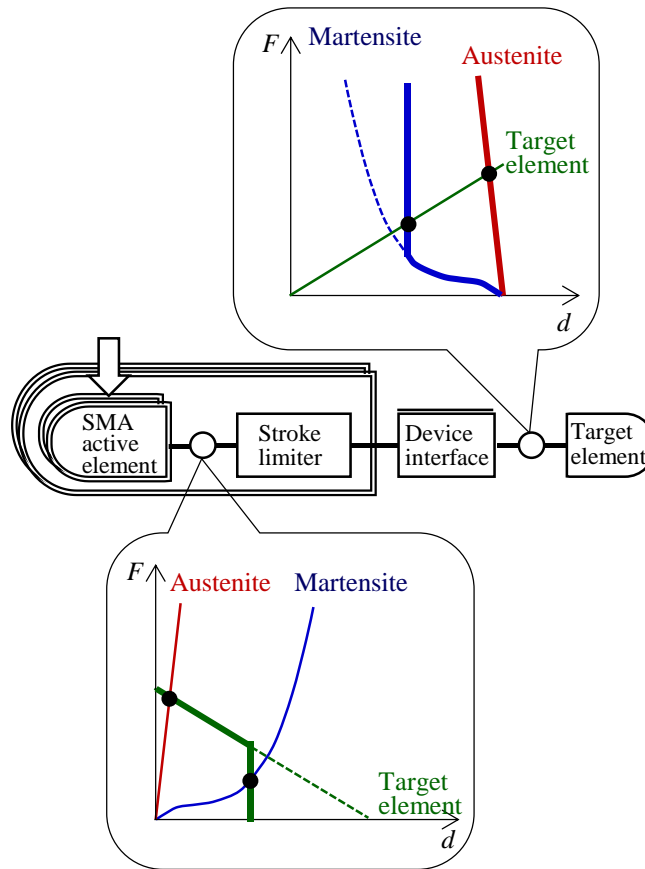


Figure 3.16. Martensite mechanical stroke limiter.

A position-based heating current cutoff is modeled as an actuation position check, which also adds another piece to the actuation device force-deflection output curve. Because the position-based heating current cutoff modifies the material behavior through temperature, this modifier does not allow a backward transformation to be applied to the target element behavior. In Figure 3.17, the position-based heating current cutoff switch is represented as a vertical line in the austenite state. While the actuation motion performance is predicted similarly, the heated temperature needs to be found separately to match the cutoff switch position to predict the thermo-mechanical behavior of the device.

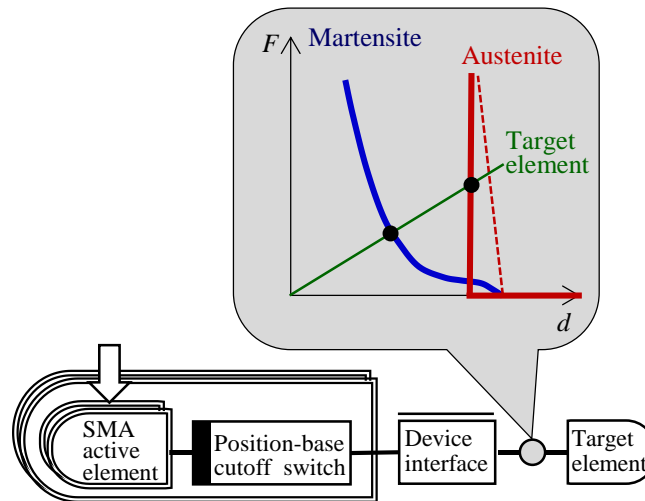


Figure 3.17. Position-based heating current cutoff switch.

3.4.3.2.2. Mechanical leverage

A mechanical leverage can be implemented as a device modifier and/or a bias modifier, and it enables a force-deflection tradeoff. A model of a mechanical leverage can be implemented as a simple arithmetic equation. The amplification ratio needs to be carefully defined for book keeping purposes because it is often confused; it should be clearly defined as either force amplification ratio or deflection amplification ratio. Figure 3.18 shows the effect of a mechanical leverage. Note that the interface offset is also affected by the mechanical leverage when the solution coupling is shifted to the SMA active element.

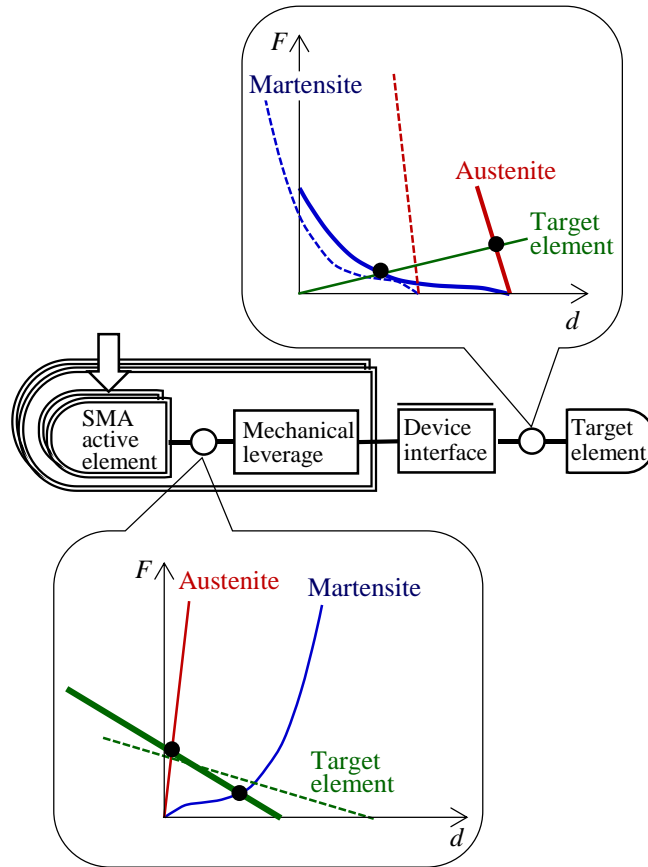


Figure 3.18. Mechanical leverage.

3.4.3.2.3. Friction

Although actual friction is the sum of friction from all moving components of the device, it is easier to model and/or measure friction as a single total friction. Friction works in different directions for actuation loading and unloading, which requires two model states. Figure 3.19 shows the effect of friction at solution couplings both at the target element and at the SMA active element. The friction force is subtracted from the austenite force output and it is added to the martensite force output at the target element coupling. Alternatively, it is added to the target element force during loading, and subtracted from the target element force during unloading.

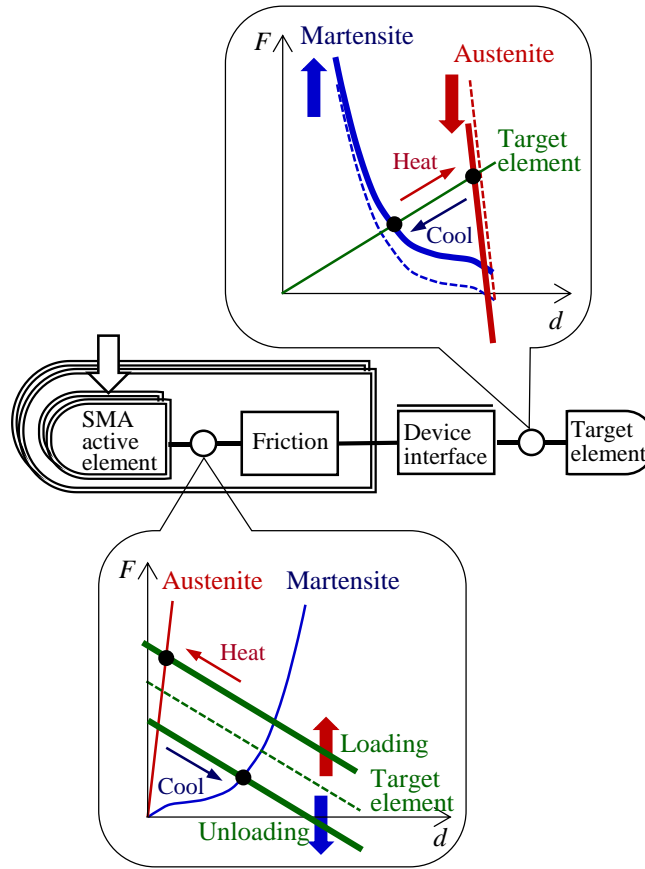


Figure 3.19. Two modes of friction modifier.

3.4.3.2.4. Interface modifier transformation

The interface modifier transformation is the conversion of the coordinates of the target element to match with the device coordinates with an offset of the origin to reflect the initial distance between the target element and the device (Figure 3.4). For the device bias, the bias device interface defines the distance between the device bias and the SMA active element, and the transformation is same as the device interface element.

3.4.3.2.5. Stroke accumulator transformation

A stroke accumulator macro modifier element is a time leveraging mechanism which accumulates stroke over multiple cycles to produce a large overall stroke beyond the typical 1 ~ 4 % SMA net strain. The main challenge for performance prediction with a time leveraging mechanism is that the target element force changes at each individual actuation step, affecting the martensite and austenite equilibria. This macro modifier element can be modeled as an interface

update transformation to account for the target element force change due to the accumulated stroke. By updating the internal offset, the force from the target element is modified for consecutive actuation steps.

Stroke accumulator transformation example (ratchet actuator): One example of a stroke accumulator architecture is an SMA ratchet actuator which uses a ratchet mechanism to accumulate SMA actuation stroke over multiple steps. SMA wire ratchet actuators consist of a linear rack or rotating gear, a driving pawl including an SMA wire actuator, and a passive pawl. The linear rack or rotating gear provides the mechanical connection between the driving pawl and the target element. The driving pawl, which advances the linear rack or rotating gear, is connected to the SMA wire and accompanying bias device, which antagonistically actuates and restores the driving pawl. The passive pawl holds the rack or gear during restoration of the driving pawl. The actuation sequence of a linear SMA wire ratchet actuator is illustrated in Figure 3.20a. In the martensite equilibrium state (Figure 3.20b), the target element force is supported by the passive pawl, and the driving pawl is in the equilibrium position between the cold compliant martensitic SMA wire and the bias device. This martensite equilibrium position is affected by the pre-tension from the bias device, which is determined by the stiffness of the bias device k_{bias} and the bias

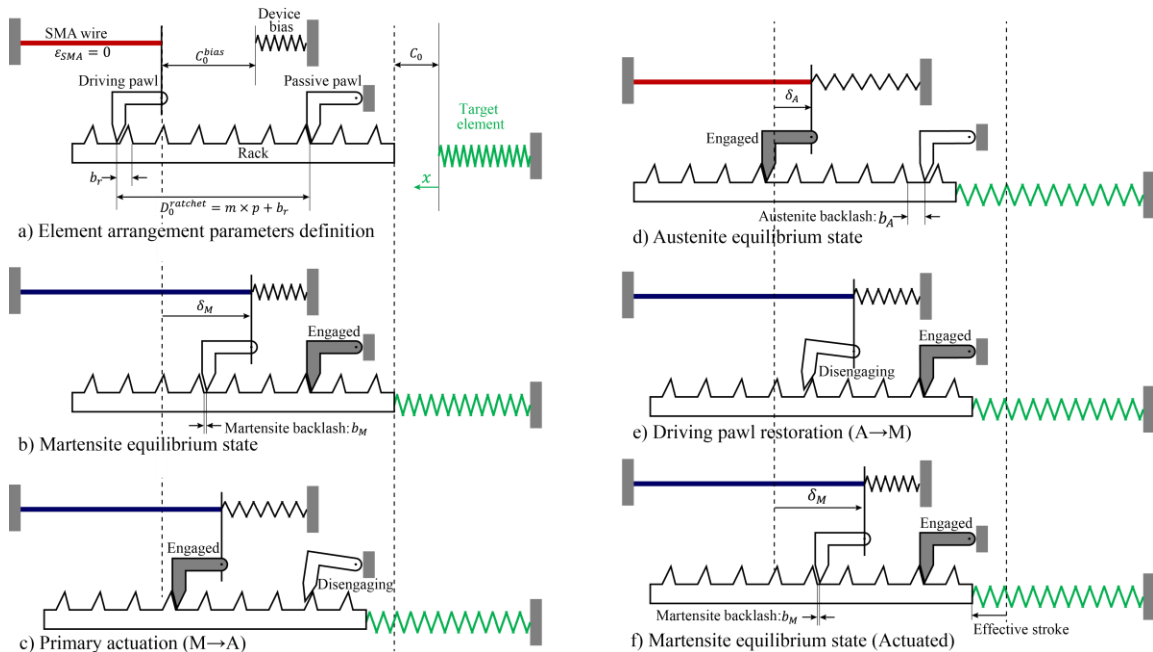


Figure 3.20. Stroke accumulator transformation example: ratchet actuator.

interface C_0^{bias} . The bias interface is defined as the relative separation between the bias device and the SMA wire in the austenite strain-free state before they are connected.

When the SMA wire is heated, the driving pawl first moves from the martensite equilibrium position, which may lie between rack teeth, to the nearest rack tooth position, engaging the rack. This free sliding distance, which is named as the *martensite backlash* b_M , does not contribute to the output stroke because the rack is not moving during this lost portion of SMA wire stroke. Once the driving pawl engages the rack, the SMA wire pulls the target element F_{ext} along with the rack while overcoming the bias device force F_{bias} , the rack sliding friction $F_{friction}^{rack}$, the driving pawl sliding friction $F_{friction}^{driving}$, and the disengagement interaction force between the passive pawl and the rack tooth $F_{ratchet}^{passive}$ (Figure 3.20c). This disengagement interaction force occurs when the passive pawl is climbing the rack tooth to allow passage of the rack under the pawl. When the SMA wire is fully transformed to the hot stiff austenite state, the driving pawl reaches the austenite equilibrium position (Figure 3.20d). This austenite equilibrium position is affected by the target element force F_{ext} , which is a function of its deflection x . At this austenite equilibrium position, which increases after each actuation cycle, the target element deflection is the sum of the rack sliding distance and the device interface.

Upon cooling of the SMA wire, the driving pawl and rack retract until the passive pawl engages the rack and holds the target element at the actuated position. This sliding distance, which is named as the *austenite backlash* b_A , is another loss from the SMA wire stroke because the rack is moving backward. At this point, the rack is shifted by the *effective stroke*, which is the stroke of the driving pawl from the austenite equilibrium position to the martensite equilibrium position after subtracting the austenite and martensite backlashes. Because each actuation step starts and ends in the condition of the passive pawl engaging the rack tooth and holding the target element, the effective stroke advances a discrete distance, which is multiple of the tooth pitch length. Once the passive pawl holds the rack, the bias device moves the driving pawl while overcoming the martensitic SMA wire force F_{SMA}^M , the driving pawl sliding friction force $F_{friction}^{driving}$ and the disengagement interaction between the driving pawl and the rack tooth $F_{ratchet}^{driving}$ (Figure 3.20e). When the SMA wire is fully transformed to the cold compliant martensite phase, the driving pawl is restored to the martensite equilibrium position, and this process completes one *step* (Figure

3.20f). By repeating the heating and cooling of the SMA wire, the SMA wire ratchet actuator accumulates steps, and the *overall stroke* of the actuator output is the sum of the effective strokes of each step.

Ratchet modeling for performance prediction involves evaluating the SMA actuation stroke by finding the martensite and the austenite equilibria by solving the force balance models, and evaluating the effective stroke by subtracting the backlash from the SMA actuation stroke to update the offset for the next step. The force balance model of the SMA wire ratchet actuator is complicated by the mechanical coupling of the device elements during actuation, which separates two modes of operation. During the first mode in the martensite equilibrium, the passive pawl holds the external system, and the bias device (F_{bias}) stretches the cold martensite SMA wire (F_{SMA}^M) moving the driving pawl to the equilibrium position while working against the driving pawl sliding friction $F_{friction}^{driving}$ and the disengagement interaction force between the driving pawl and the rack tooth $F_{ratchet}^{driving}$ (Figure 3.20b),

$$F_{bias} = F_{SMA}^M + F_{friction}^{driving} + F_{ratchet}^{driving}. \quad (3.12)$$

Upon heating, in the second mode, the hot stiff austenite SMA wire (F_{SMA}^A) pulls the external system (F_{ext}) through the driving pawl while overcoming the rack sliding friction force $F_{friction}^{rack}$, the driving pawl sliding friction forces $F_{friction}^{driving}$, the disengagement interaction force between the passive pawl and the rack tooth $F_{ratchet}^{passive}$, and the bias device F_{bias} (Figure 3.20d),

$$F_{SMA}^A = F_{ext} + F_{friction}^{rack} + F_{friction}^{driving} + F_{ratchet}^{passive} + F_{bias}, \quad (3.13)$$

where the external system force F_{ext} is a function of the external system deflection x

$$F_{ext} = F(x). \quad (3.14)$$

There are additional challenges to be addressed to predict the SMA ratchet actuator performance, which are the force interaction change between the ratchet components for the heating and cooling stages, and the friction-like interaction disengaging force when the rack tooth passes under the pawl tip. For further explanation on the SMA ratchet mechanism, refer to Appendix B.

3.5. SMA device modeling examples using discrete equilibrium performance prediction

Three SMA devices with distinct device architectures which were introduced in the previous chapter are utilized to demonstrate their modeling. Although the device architecture is applicable to both the discrete equilibrium performance prediction approach and the integrated dynamic performance prediction approach, the examples are introduced using the discrete equilibrium performance prediction approach to better demonstrate the interaction between the device components.

3.5.1. Latch release device: straight wire example

For discrete equilibrium performance prediction of the latch release device, the SMA material behavior is characterized as two stress-strain curves in the austenite and martensite states (Figure 3.21a), and transforms into two force-deflection curves through the straight wire geometry (b). This transformation is done by multiplying the cross-sectional area and the length of the SMA wire to the stress and the strain respectively. The bias device is characterized as a straight force-deflection line (c), and is combined at the coupling with the SMA wire force-deflection curves through the bias leverage and the bias interface. The bias device interface defines the relative position between the active element (straight SMA wire) and the bias device, and matches the coordinate system (d). The visualization of the combined behavior flows (e) shows the reduced martensite state force, which requires smaller resetting force. A mechanical leverage is used to trade off the output force and stroke to reduce the SMA wire length to reduce the package length (f). The device interface determines the pre-tension on the SMA wire from the latch mechanism. The target element is also characterized as a linear stiffness system (g), and overlaid with the SMA device force-deflection curves at the solution coupling to find the austenite and martensite equilibria (h). This process demonstrates the predictive design methods, which can further tailored for individual design task by applying grouping and projection.

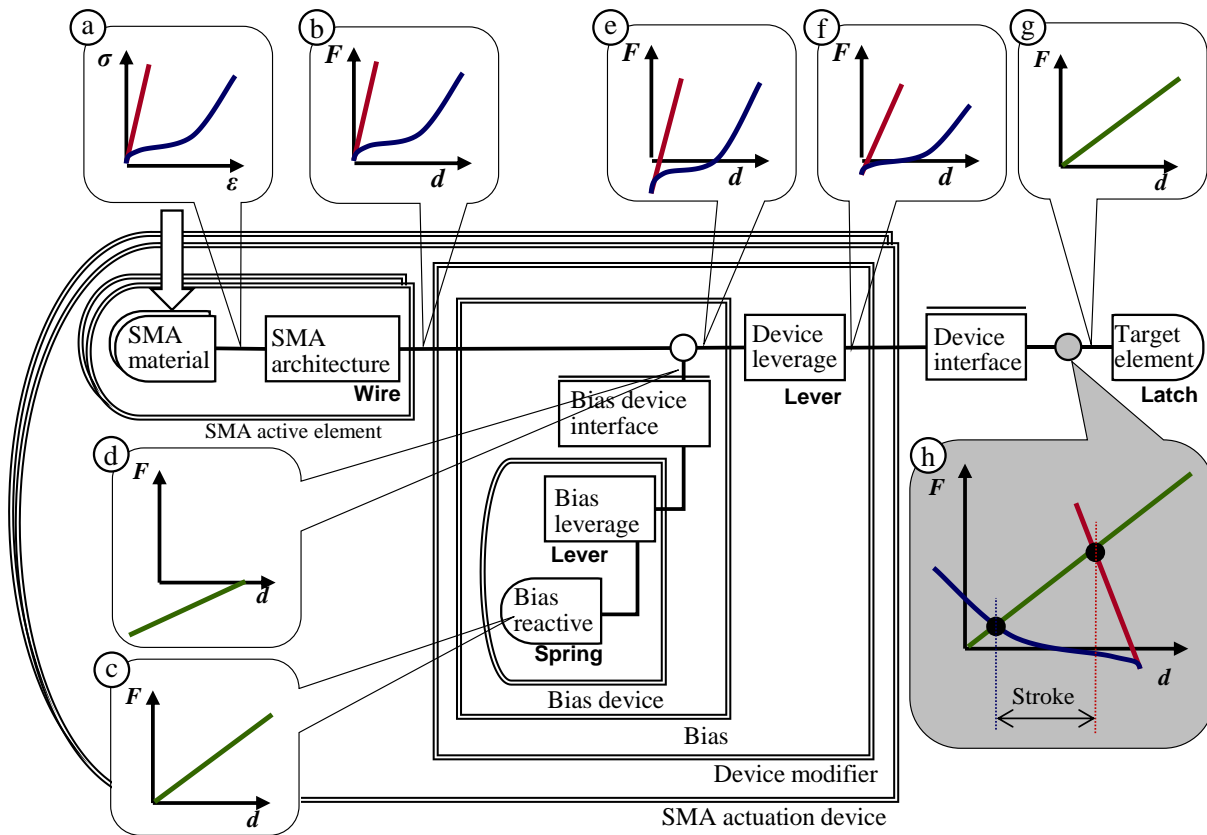


Figure 3.21. Discrete equilibrium performance prediction of latch release device.

3.5.2. Active inner belt seal device: web actuator example

For discrete equilibrium performance prediction of the active inner belt seal device (Figure 3.22), the SMA material stress-strain curves are first transformed into the tension-elongation curves of the SMA wire, and then transformed into the force-deflection output curves of the SMA wire web actuator architecture. The first layer transformation is the same as the straight SMA wire transformation in the latch release device example, and the second layer transformation accounts for the non-linear leveraging of the geometric stroke amplification. Although it is possible to model the macro SMA modifier element as a combined model, which directly transforms the stress-strain curves into the SMA wire web actuator output force-deflection curves, the modular structure of the multi-layer transformation model enables reusability of the model. If the SMA wire layer is replaced with another SMA architecture, *e.g.* a SMA helical spring architecture, the modifier model for a web architecture is still usable only requiring a new model for a helical spring architecture. After being modified by the interface element, the SMA wire web actuator output

force-deflection curves are overlaid with the target element force-deflection curve, which is measured directly from the prototype.

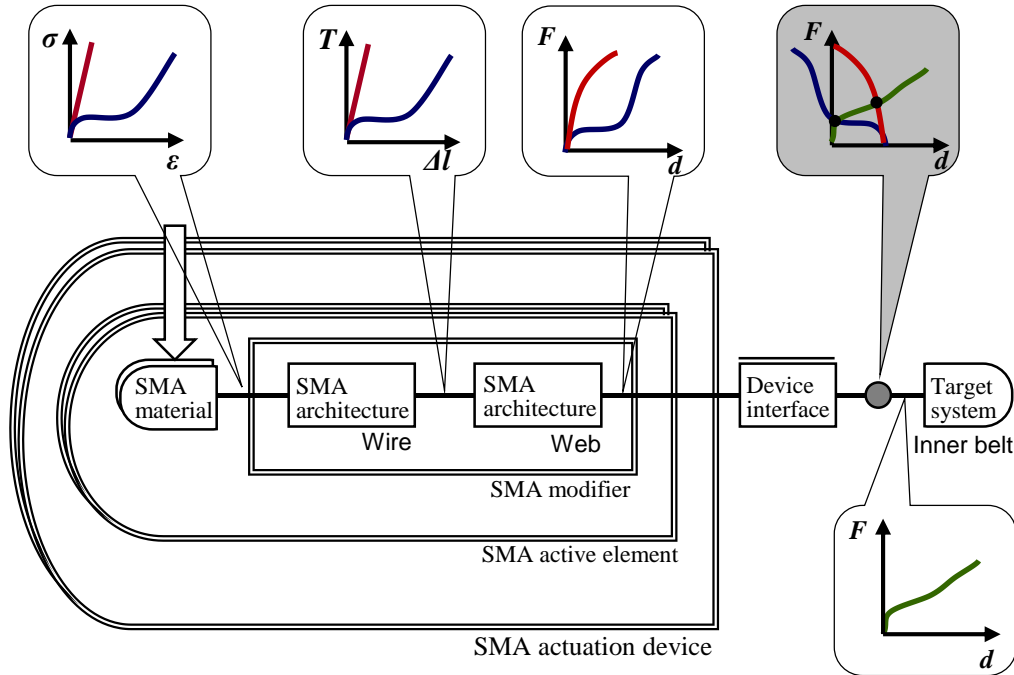
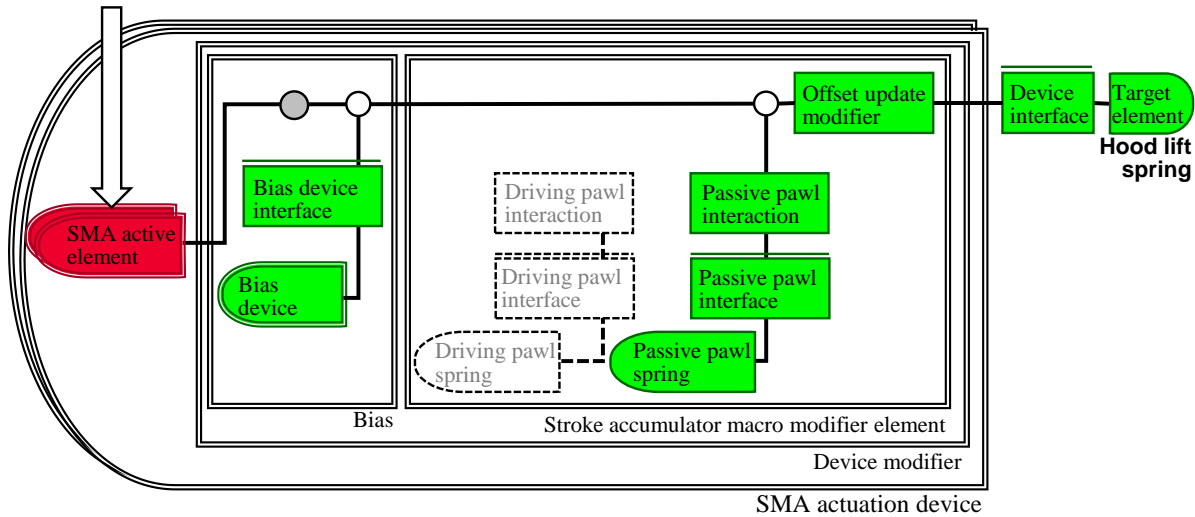


Figure 3.22. Discrete equilibrium performance prediction of active inner belt seal.

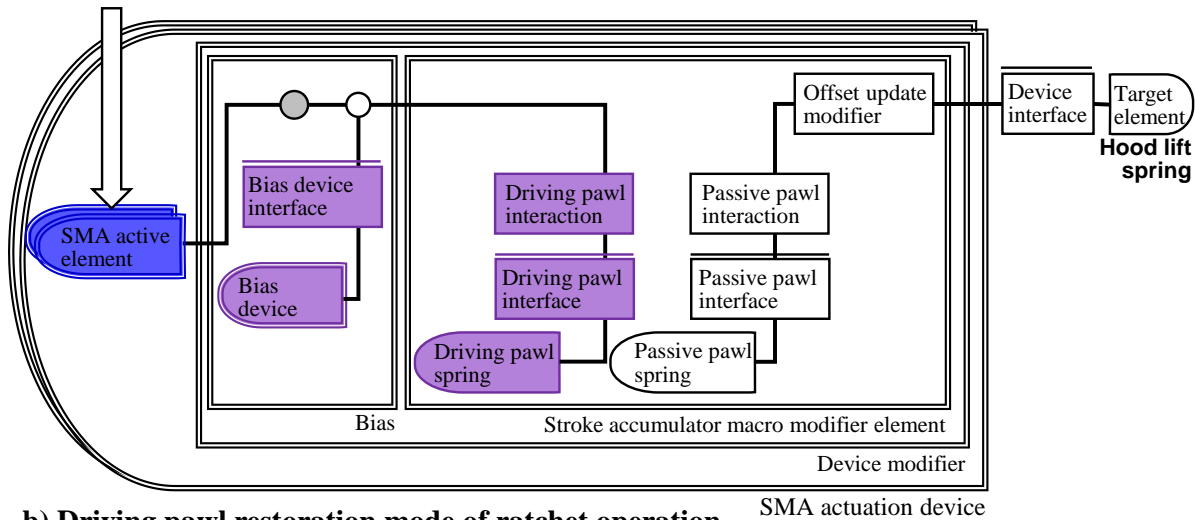
3.5.3. SMART hood lifter reset device: ratchet example

The ratchet mechanism accumulates the limited stroke of the SMA wires to produce a large stroke within the limited package space inside the helical compression spring. The linear rack provides a mechanical connection between the driving pawl and the helical compression spring. Figure 3.23 shows two different modes of ratchet operation. During primary actuation, the SMA active element advances the target element through the driving pawl and linear rack while overcoming the interaction force from the passive pawl (Figure 3.23a). The target element is held by the passive pawl while the driving pawl is restored by the bias device (Figure 3.23b). During restoration of the driving pawl, the system is divided into two disconnected sub-systems, which divides the stroke accumulator macro modifier element into two macro reactive elements. One sub-system is the passive pawl, which works as a macro reactive element, holding the target element fixed in place, and the other is the bias device providing the main driving force (macro

reactive element) to actuate the SMA active element which works as a target element. This shows that the re-organization of the macro elements effectively helps the understanding and modeling of the system during the different modes of operation.



a) Primary actuation mode of ratchet operation



b) Driving pawl restoration mode of ratchet operation

Figure 3.24 effectively visualize the system behavior during both the primary actuation mode (Figure 3.23a) and the driving pawl restoration mode (Figure 3.23b). The color of the behavior curves are matched with the color of the device elements in Figure 3.23. The offset between the SMA actuator and the helical spring is updated after each step of SMA actuation. In addition to the force interaction change throughout the actuation stages during each step of the actuation, the stroke accumulator introduces an additional complication due to the changes in

interaction between the SMA actuator and the target element, which leads to a possible austenite equilibrium position change.

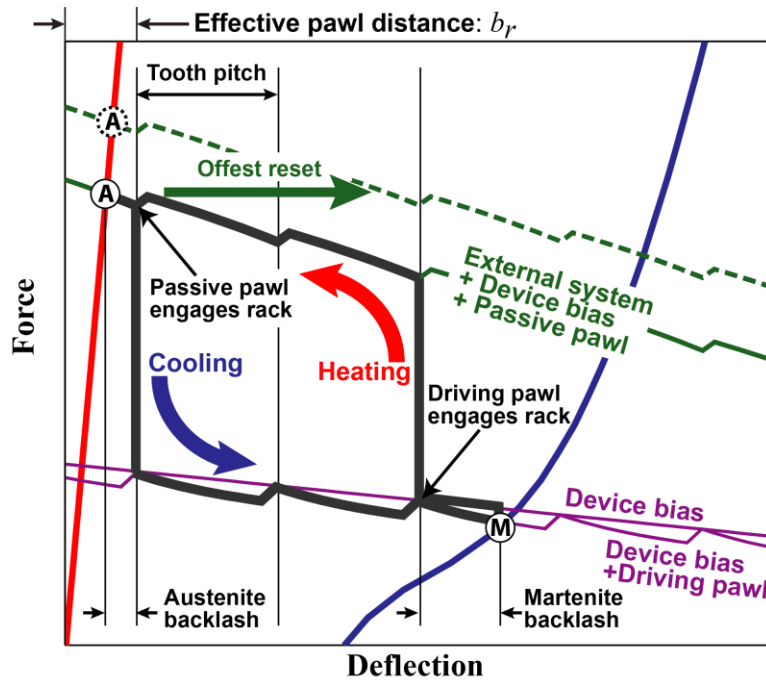


Figure 3.24. Ratchet actuator loading / unloading path of a single actuation step.

3.6. Conclusions

The design methods consisting of modular modeling, model aggregation and performance prediction, and visualization approaches support design decisions to serve diverse sets of stakeholders by exposing the effect of device elements not only for SMA actuation devices, but also for a wide range of other actuation devices. The modular modeling approach which takes advantage of the hierarchical actuation device system structure ensures reusability of individual device element models. SMA architectures are one such device element, for which formalized SMA architectural transformations provide a systematic approach to model each type of architecture, revealing the limitations on the application of performance prediction methods. The model aggregation and performance prediction approaches enable a comprehension of actuation device systems by providing a means to construct and solve a complete system model from the connected collection of modular device element models. The visualization methods consisting of

grouping and projection support design decisions by presenting the device element behaviors and performance prediction results with tailored options for individual stakeholder groups who have their interests in different aspects and elements of an actuation device system.

These systematic design methods expose the effects of individual device elements on the actuation device system behavior, provide design metrics to select the design parameters of individual elements, and prevent potential design iteration by exposing the individual element effects. By applying these design methods, a diverse group of stakeholders including design engineers can make better design decisions using model-based design evaluation and visualization of actuation device behavior tailored for individual stakeholder groups and design tasks.

3.7. References

- [1] Liang, C., and Rogers, C. A., 1997, “One-dimensional thermomechanical constitutive relations for shape memory materials,” *Journal of Intelligent Material Systems and Structures*, **8**(4), pp. 285–302.
- [2] Brinson, L. C., 1993, “One-Dimensional Constitutive Behavior of Shape Memory Alloys: Thermomechanical Derivation with Non-Constant Material Functions and Redefined Martensite Internal Variable,” *Journal of Intelligent Material Systems and Structures*, **4**(2), pp. 229–242.
- [3] Boyd, J. G., and Lagoudas, D. C., 1994, “Thermodynamical constitutive model for the shape memory effect due to transformation and reorientation,” SPIE, Orlando, FL, USA, pp. 276–288.
- [4] Shaw, J. A., 2002, “A thermomechanical model for a 1-D shape memory alloy wire with propagating instabilities,” *International Journal of Solids and Structures*, **39**(5), pp. 1275–1305.
- [5] Buravalla, V., and Khandelwal, A., 2008, “Phenomenological Modeling of Shape Memory Alloys,” AIP Conference Proceedings, S.M. Sivakumar, V. Buravalla, and A.R. Srinivasa, eds., IIT Madras, Chennai, India, pp. 104–123.
- [6] Young Pyo Lee, Byungkyu Kim, Moon Gu Lee, and Jong-Oh Park, 2004, “Locomotive mechanism design and fabrication of biomimetic micro robot using shape memory alloy,” pp. 5007–5012 Vol.5.
- [7] Barnes, B. M., Brei, D. E., Luntz, J. E., Strom, K., Browne, A. L., and Johnson, N., 2008, “Shape memory alloy resetable spring lift for pedestrian protection,” SPIE, San Diego, California, USA, pp. 693005–13.
- [8] Zhang, X., Yan, X., and Yang, Q., 2013, “Design and Experimental Validation of Compact, Quick-Response Shape Memory Alloy Separation Device,” *J. Mech. Des.*, **136**(1), pp. 011009–011009.

- [9] Hartl, D. J., and Lagoudas, D. C., 2007, “Characterization and 3-D modeling of Ni60Ti SMA for actuation of a variable geometry jet engine chevron,” SPIE, San Diego, California, USA, p. 65293Z–12.
- [10] Gao, X., Burton, D., Turner, T. L., and Brinson, L. C., 2006, “Finite Element Analysis of Adaptive-Stiffening and Shape-Control SMA Hybrid Composites,” *J. Eng. Mater. Technol.*, **128**(3), pp. 285–293.
- [11] Chang, B., 2006, “Thermodynamics of shape memory alloy wire: modeling, experimental calibration, and simulation.”
- [12] Liang, C., and Rogers, C. A., 1997, “Design of shape memory alloy actuators,” *Journal of Intelligent Material Systems and Structures*, **8**(4), pp. 303–13.
- [13] Duerig, T. W., Melton, K. N., Stöckel, D., and Wayman, C. M., 1990, *Engineering Aspects of Shape Memory Alloys*, Butterworth-Heinemann.
- [14] Swensen, J. P., and Dollar, A. M., 2013, “Active-Cells for the Construction of Redundant and Configurable Articulated Structures,” ASME 2013 Conference on Smart Materials, Adaptive Structures and Intelligent Systems, American Society of Mechanical Engineers, pp. V001T01A013–V001T01A013.
- [15] Shaw, J. A., and Churchill, C. B., 2009, “A reduced-order thermomechanical model and analytical solution for uniaxial shape memory alloy wire actuators,” *Smart Materials and Structures*, **18**(6), p. 065001.
- [16] Magnetic Sensor Systems, Inc., 2005, “Tubular Pull Type Solenoid S-69-38.”
- [17] Shaw, J. A., Churchill, C. B., and Iadicola, M. A., 2008, “Tips and Tricks for Characterizing Shape Memory Alloy Wire: Part 1; Differential Scanning Calorimetry and Basic Phenomena,” *Experimental Techniques*, **32**(5), pp. 55–62.
- [18] Kim, W., Barnes, B. M., Luntz, J. E., and Brei, D. E., 2011, “Conglomerate Stabilization Curve Design Method for Shape Memory Alloy Wire Actuators With Cyclic Shakedown,” *Journal of Mechanical Design*, **133**(11), p. 111010.
- [19] Liang, C., and Rogers, C. A., 1990, “One-dimensional thermomechanical constitutive relations for shape memory materials,” *Journal of Intelligent Material Systems and Structures*, **1**(2), pp. 207–34.
- [20] Chang, B.-C., Shaw, J., and Iadicola, M., 2006, “Thermodynamics of Shape Memory Alloy Wire: Modeling, Experiments, and Application,” *Continuum Mechanics and Thermodynamics*, **18**(1), pp. 83–118.
- [21] Boyd, J. G., and Lagoudas, D. C., 1996, “A thermodynamical constitutive model for shape memory materials. Part I. The monolithic shape memory alloy,” *International Journal of Plasticity*, **12**(6), pp. 805–842.
- [22] Kim, W., Thota, M., Luntz, J., and Brei, D., 2012, “Analytical Model and Design Study on Shape Memory Alloy Web Actuator,” ICAST2012, Nanjing, China, pp. 031–16.
- [23] Redmond, J. A., Brei, D., Luntz, J., Browne, A. L., and Johnson, N. L., 2012, “Spool-Packaging of Shape Memory Alloy Actuators: Performance Model and Experimental Validation,” *Journal of Intelligent Material Systems and Structures*, **23**(2), pp. 201–219.

Chapter 4.

SMA Design Process

Designing SMA actuator devices is not as straight forward as designing devices using conventional actuators. While conventional actuators such as electromagnetic actuators or hydraulic actuators are *selected* for devices, SMA actuators are *designed* for individual projects. Designing an SMA actuator is even more complicated due to the non-linear nature of its performance due to the stress-strain-temperature coupled material properties. While there have been equilibrium performance prediction methods for simple SMA actuation devices using force-deflection / stress-strain behavior curves since the early 90's [1–5], there is no systematic design process established to create a detailed design using these methods. Empirical design approaches are still applied for SMA application development [6–9] because the design process is complex and often non-intuitive due to SMA architectures and additional device elements of real SMA actuation devices. Moreover, previous research efforts focused on performance prediction and analysis methods for the later analysis stage of design, while the full design cycle consists of multiple stages from the early stages that select device concepts and SMA architectures to the later stages that finalize the detailed design parameters using in-depth analysis. Furthermore, the later analysis stages require a detailed design as the input for simulation analysis, which is hard to create for non-expert SMA engineers, and often requires iterative steps even for expert engineers. Although, Langbein and Czechowicz [10] proposed a general procedure to develop a conceptual design of SMA actuator device (Figure 1.21), their effort is more focused on generating a conceptual design and setting up a regulatory standard rather than guiding engineers through the design process to create a concrete detailed design. An et al. [11] proposed a design framework for SMA coil spring actuators (Figure 4.1), but their scope is limited to one type of SMA active element which is only part of a whole actuation

device system. There needs to be a step-by-step design procedure that helps engineers with any level of expertise in SMA technology to identify and make design decisions throughout the design cycle to create a detailed design of whole actuation device system.

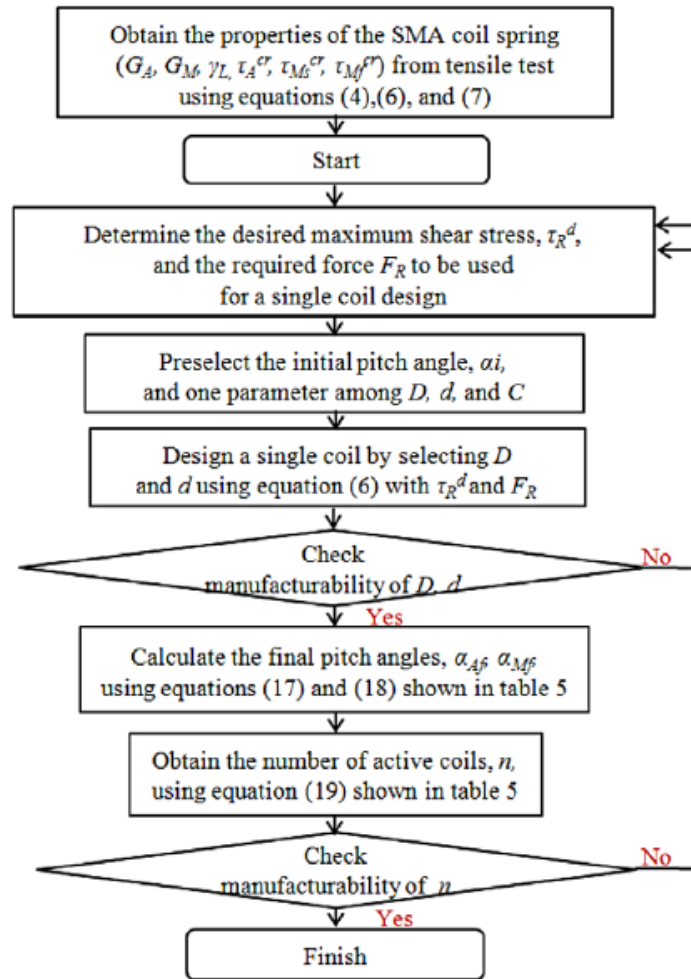


Figure 4.1. Design process of SMA coil spring actuator [11].

An et al. proposed an engineering design framework for a shape memory alloy coil spring actuator using a static two-state model.

The design task differs at each stage of the design cycle. For example, in the early design stage, the SMA actuation device engineer needs to choose a proper SMA architecture which can produce required force and stroke within given constraints. Along with SMA architecture selection, several design decisions related to SMA material usage also need to be made

considering material fatigue, operation temperature, and manufacturing tolerance. Once SMA architectures are chosen and material usage decisions are made, engineers explore many device design options to find better candidate designs. In this early stage, a faster evaluation is more important than the accuracy of the performance prediction. However, once a candidate design is selected from the early design stage, precise performance evaluation is required especially in transient behavior analysis to capture the interdependency and path-dependent material behavior. To facilitate these different needs for different design stages, a multi-stage design process is desirable to provide tailored support to device engineers.

The goal of this chapter is to formalize a design process over various stages of SMA device design to support appropriate decision making with necessary precision at each stage to ensure better design quality, expedite the design cycle, and enable design automation.

The objectives are

1. Formalize a multi-stage design process to identify the design task for each stage of the device design cycle.
2. Establish a discrete equilibrium design procedure which helps engineers to create a good detailed design without iterative processes.
3. Create visualization methods to explore the design space for given SMA architectures.
4. Demonstrate the design process for common actuator architectures.

In this chapter, a **multi-stage design process** is formalized to support the different design tasks for different stages of the SMA device design cycle. The first stage is **the initial design decision** stage where a proper SMA architecture is selected to produce the required force and stroke, and material usage decisions are made. The second stage is **the discrete equilibrium design** stage where the SMA device design is generated using quasi-static equilibrium assumptions through three steps: the Kinetic design step, the Kineto-static design step, and the Thermo-mechanical design step. The three steps of the discrete equilibrium design stage are formalized which can guide a novice engineer to create a concrete detailed design of SMA device and can be implemented as a design automation tool. The third and last stage is **the**

integrated transient behavior evaluation stage where the interactive transient behavior of the SMA device and the target element is evaluated.

A multi-stage design process is necessary in the SMA device design cycle as the design methods based on both the discrete equilibrium performance prediction approach and the integrated dynamic performance prediction approach are useful to different stages of the SMA device design cycle. However, most research efforts focused on design methods for the later stage integrated transient behavior evaluation through numerical implementation of SMA models, which are essentially analysis methods rather than design methods [12–14]. Although these tools are critical to finalize a detailed design through optimization and transient behavior analysis, the lack of a formalized procedure to create a detailed design as well as supporting methods for the earlier stages of SMA device design hinders the adoption of SMA technology. To use the existing methods for the later stages of design, a feasible design of an SMA device is critical because analysis tools do not work with a non-feasible design. However, creating a feasible design is not an easy task for an engineer who is not familiar with SMA technology. In this research, the focus is on the discrete equilibrium design stage because the integrated transient behavior evaluation stage is already in a mature state thanks to the previous research efforts. The formalization of the second stage helps to complete the device development cycle by providing a means to create a detailed design, which can be used as an input for the transient behavior evaluation stage to finalize the detailed design. The three-step discrete equilibrium design procedure is demonstrated using the three device examples introduced in previous chapters.

4.1. Initial design decisions

The first step of the design process is to select an SMA architecture for producing the required actuation motion, and to make material usage decisions. To determine the SMA architecture, basic design requirements need to be collected: the required force and stroke, and the available package space. The feasibility of using straight SMA wires for producing the required stroke with the required force depends on the actuation strain and the maximum stress in the SMA material. The maximum actuation strain and the maximum stress are **material usage decisions** which should be made as part of the initial design decisions considering the expected lifetime and the tolerable material shakedown (degradation over cycles) [15–21]. SMA wire net strain is the net actuation strain produced by the SMA wire, which is the difference

between the austenite strain and the martensite strain. Although the SMA wire net strain can be controlled using stroke limiters such as a mechanical hard stop and/or a position-based heating current cutoff switch, it cannot exceed the maximum strain achieved by the SMA material stress-strain behavior. By comparing the required stroke with the product of the available package length and the actuation net strain, the feasibility to use straight SMA wires can be evaluated because it is not hard to satisfy the stress constraints by adding more wires in most cases.

If the straight wire architecture is not feasible, engineers can explore several other options to produce the required force and stroke. An architecture suggestion map (Figure 4.2) is created to qualitatively illustrate the output performance tradeoff options of several SMA architectures. The x-axis shows the output stroke relative to the package length, and the y-axis shows the output force relative to the straight wire force with the same cross-sectional area. The dark gray square area represents the achievable straight wire output performance. The first option to overcome the stroke limitation of straight SMA wires is to use a mechanical lever as a device modifier. A mechanical lever enables a tradeoff between force and stroke, as shown by the blue triangular area on the architecture suggestion map. The point where the gray straight wire square and the blue mechanical lever triangle meet is where the mechanical lever ratio is 1. Usually, a stroke limitation can be overcome at the cost of force reduction. Although the opposite tradeoff is possible, it will be rarely used because the output force can be easily scaled by increasing the total cross-sectional area of SMA wires. Another option to overcome a stroke limitation is to use the spooling technique to package longer lengths of SMA wire within a limited package length [22]. While there are stroke losses due to friction between the SMA wire and the mandrel, and design limitations regarding the wrap angle and the diameter ratio between the SMA wire and the mandrel, spool packaging allows a larger output stroke within a limited package length without sacrificing output force. If the package space has a shallow form factor where the required actuation motion is in the direction normal to the longest package dimension, a web architecture can be a good candidate because it exploits the geometric stroke amplification obtained by using a zigzag shaped SMA wire connected between two surfaces [23]. Another architecture to overcome a stroke limitation without a large loss in output force is a ratchet architecture where the limited stroke of SMA is accumulated over multiple actuation steps [24,25]. While it is possible to produce an extremely large stroke using a ratchet, there are limitations related to the actuation time and the package volume due to the additional parts such

as the rack and pawls. Other possible architectures include SMA helical spring actuators [11,26,27] and SMA cables [28], although they are not illustrated on the map.

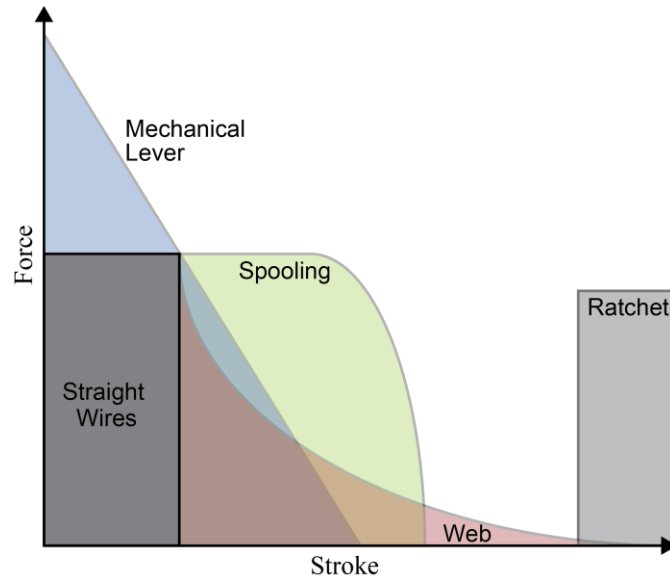


Figure 4.2. Architecture suggestion map.

An architecture suggestion map is created to approximately illustrate the output performance tradeoff options of several SMA architectures. The x-axis show the output stroke relative to the package length, and the y-axis shows the output force relative to the straight wire force with the same cross-sectional area.

Once an SMA architecture is selected, additional system requirements are collected such as required operation cycle time (heating and cooling time), operation ambient temperature, expected life cycle, and robustness. These additional system requirements are used to determine the additional material usage decisions: safety margin, maximum strain during actuation, and martensite transformation temperature and corresponding martensite stress. The martensite transformation temperature must be set above the operation ambient temperature to ensure restoration of the actuation device during the cooling portion of the cycle. The martensite transformation temperature is determined by the martensite stress [29–32], which is set as a material usage decision. The net actuation strain and the maximum strain are determined considering the desired device lifetime. Although there are still ongoing efforts to investigate the relationship between lifetime and actuation and/or maximum strain, it is commonly agreed that the values of both should be lowered to increase the expected lifetime of the SMA [15–21]. A safety margin can be applied in terms of a strain shift to account for material property variations

and unexpected disturbances. Partly because of the lack of understanding of SMA material such as the exact effect of acutation stress and strain on lifetime, it is not yet possible to completely systemize the initial design decision stage.

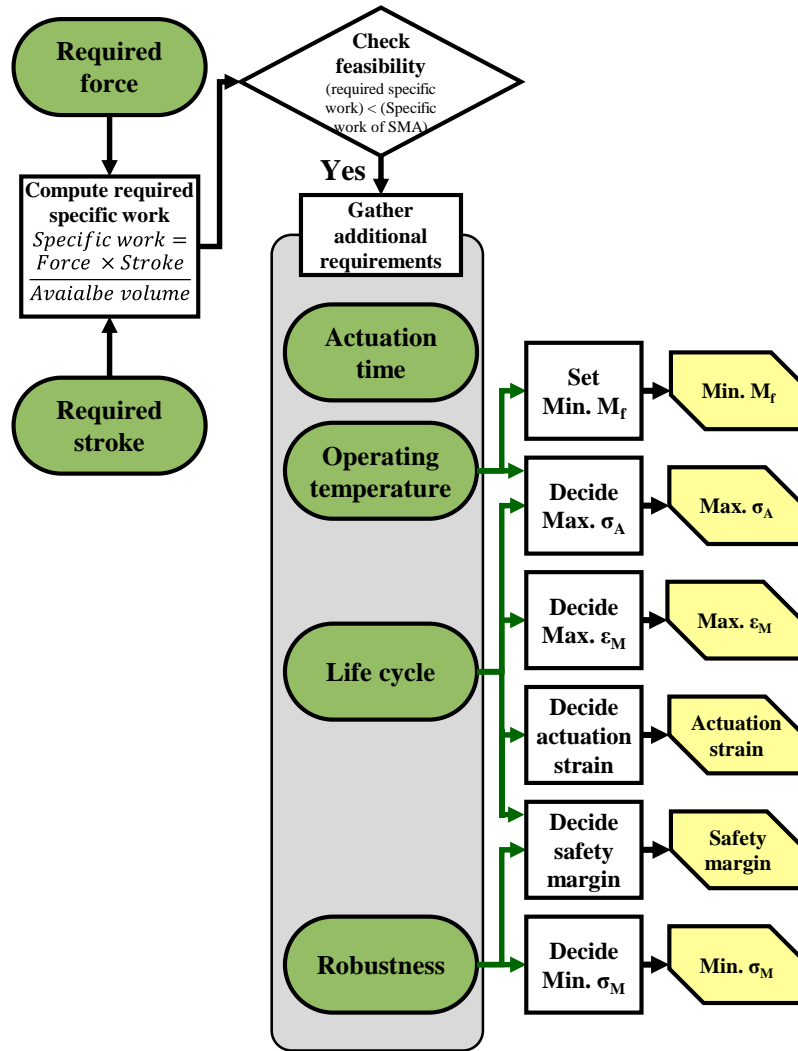


Figure 4.3. Initial design decision stage flow.

To determine the SMA architecture, the basic requirements need to be collected: the required force and stroke, and the available package space. The feasibility of using straight SMA wire for producing the required stroke with the required force depends on the actuation strain and the maximum stress in the SMA material. Once an SMA architecture is selected, additional system requirements are collected such as required operation cycle time (heating and cooling time), operation ambient temperature, expected life cycle, and robustness. These additional system requirements are used to determine the additional material usage decisions: safety margin, maximum strain during actuation, and martensite transformation temperature and corresponding martensite stress.

4.2. Discrete equilibrium design method

A systematic design process for SMA actuation devices is required to reduce the design iteration due to the non-intuitive sensitivity to design parameters. Because the SMA actuation is produced using the equilibrium change which comes from the temperature dependent material properties, design parameter changes often cause unexpected changes in actuation performance. For example, when the straight SMA wire actuation stroke is smaller than the design requirement, a common design change attempt by a non-expert SMA actuator device engineer is to increase the length of wire under the expectation that the actuation stroke increases proportionally to the length increase. However, this is not always the case, as shown in Figure 4.4. The actuation

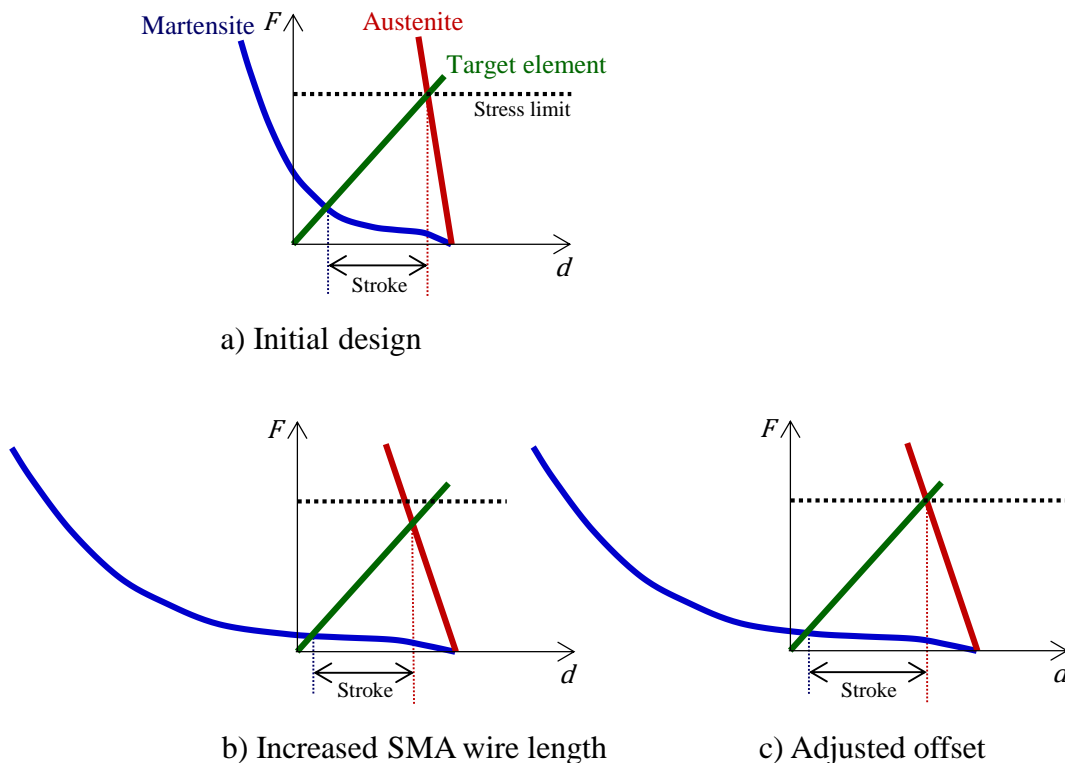


Figure 4.4. Effect of longer length of SMA wire.

When a straight SMA wire actuation stroke is smaller than the design requirement, a common design change attempt by a non-expert SMA device engineer is increasing the length of wire. However, the actuation stroke does not always increase proportional to the length change. The actuation stroke of initial design (a) is not improved only by increasing the length of SMA wire (b) because the austenite and martensite equilibria shift at the same time upon the design change. While the actuation stroke can be improved by adjusting the relative position between the SMA and the target element (c), the increased stroke is still not proportional to the SMA wire length increase.

stroke of the initial design (Figure 4.4a) is not improved by only increasing the length of the SMA wire (Figure 4.4b) because the austenite and martensite equilibria shift at the same time upon the design change. While the actuation stroke can be slightly improved by adjusting the offset (Figure 4.4c), the increased stroke is still not proportional to the SMA wire length increase.

Since an increased SMA wire length does not produce a much larger actuation stroke, the next most obvious attempt would be to increase the total cross sectional area of the SMA wire under the expectation of producing a larger force to pull the target element further (Figure 4.5). However, the increased cross sectional area of SMA wire does not produce a larger stroke due to the equilibrium shifts in both the austenite and martensite states. The increased cross-sectional area makes the austenite and martensite equilibrium stresses lower, and the lower equilibrium stresses reduce the actuation strain.

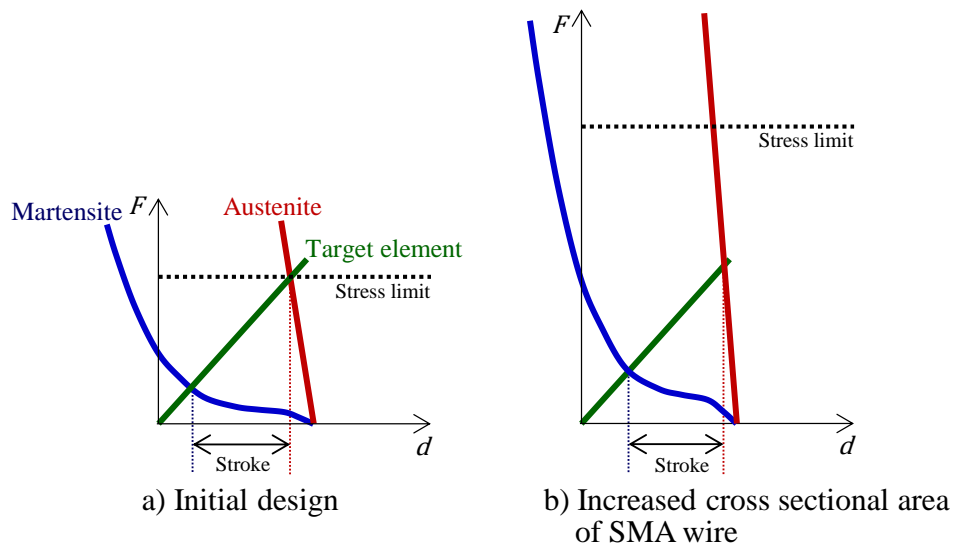


Figure 4.5. Effect of larger cross sectional area of SMA wire.

The increased cross sectional area of the SMA wire does not produce a larger stroke due to the equilibrium shifts in both the austenite and martensite states. The increased cross-sectional area makes the austenite and martensite equilibrium stresses lower, and the lower equilibrium stresses reduce the actuation strain.

Because the actuation stroke changes non-intuitively upon design parameters changes, it is desired to decouple the effects of individual design parameters. However, it is not always possible to decouple the effect of every design parameter input. Moreover, the modifier elements within the SMA actuator device make it even harder to decouple the effects of design

parameter inputs. Thus, an alternative approach is to decouple the force and deflection of the actuation output performance and the corresponding design parameters which affect them.

If the actuation strain is regulated by using stroke limiters, it is possible to decouple the force and deflection because the martensite equilibrium is no longer determined by the SMA material behavior although the material behavior still constrains the maximum actuation strain. It is a desirable approach to regulate the actuation strain using stroke limiters not only because the actuation strain should be limited to mitigate functional and structural fatigue [15–21,33], but it also provides a stable interface position between the SMA actuation device and the target element [33].

Given a set of initial design decisions, a design procedure for the early discrete equilibrium design stage is broken into three sub-stages which proceed by meeting first the actuation stroke requirement, and then the force requirement. Step 1: In the **Kinematic Design** step, the actuation stroke related design parameters are selected using the material usage decisions which are made during the feasibility check stage, and the interface offset is set for the desired actuation positions. Step 2: In the **Kineto-static Design** step, the force related design parameters are selected such as the SMA wire total cross-sectional area under the set maximum allowable stress. During this Kineto-static design step, the device bias can be designed to meet the material usage decisions such as the martensite transformation temperature and stress. Step 3: In the **Thermo-mechanical Design** step, the number and diameter of SMA wires are decided based on the selected cross-sectional area considering the heating and cooling times, and the device operation parameters such as power and cooling medium are determined.

One advantage of this discrete design approach is that engineers can explore many design candidates because the fast computation of the discrete approach enables interactive motion prediction upon design parameter changes. This is enabled by the pre-evaluation of the quasi-static behavior of both the target element and the SMA material behavior before exploring the design space. Moreover, the graphical representations used in this discrete approach provide intuition about design parameter sensitivity using the diverse lumping and projection options of the behavior visualization method in Chapter 3.

Another advantage of this approach is that engineers can combine different methods to evaluate the material behavior and the target element behavior. For example, the material

behavior can be predicted using pre-simulation using an analytical model, while the target element behavior can be evaluated using a direct measurement of its force-deflection behavior at the intended interface point with an SMA actuation device. However, the transient behavior of the actuator cannot be evaluated with this discrete approach. Moreover, heterogeneous geometric transformation architectures, such as the bent SMA wire in spool packaging, limit the use of the discrete design approach because the pre-evaluation of the SMA active element performance is not scalable with the geometric design parameters. Thus, additional iterations are required to design heterogeneous geometric transformation architectures although the design process still follows the same overall procedure.

4.2.1. Kinematic design step

The first step of the discrete equilibrium design stage is to set the design parameters to get the required stroke and to set the interface offset for the desired actuation positions (Figure 4.6). The required stroke is the main objective of this design step, and the available package space serves as the primary constraint. The net actuation strain is the governing material usage decision in this step, and the safety margin, the maximum martensite strain, and the maximum austenite stress affect the available net actuation strain. The sum of the net actuation strain, the strain at the maximum austenite stress and the safety margin should not exceed the maximum martensite strain. The device interface is the relative position between the SMA actuator and the target element, and it affects the austenite and martensite equilibrium. For example, if the target element needs to be actuated from its zero deflection position, the interface must be set to match the zero deflection position to the maximum strain, which is the sum of the net actuation strain and the austenite strain (austenite strain corresponding to the maximum stress). If the target element needs to be actuated between certain deflection positions, the interface needs to be adjusted to match the off-state deflection to the maximum strain.

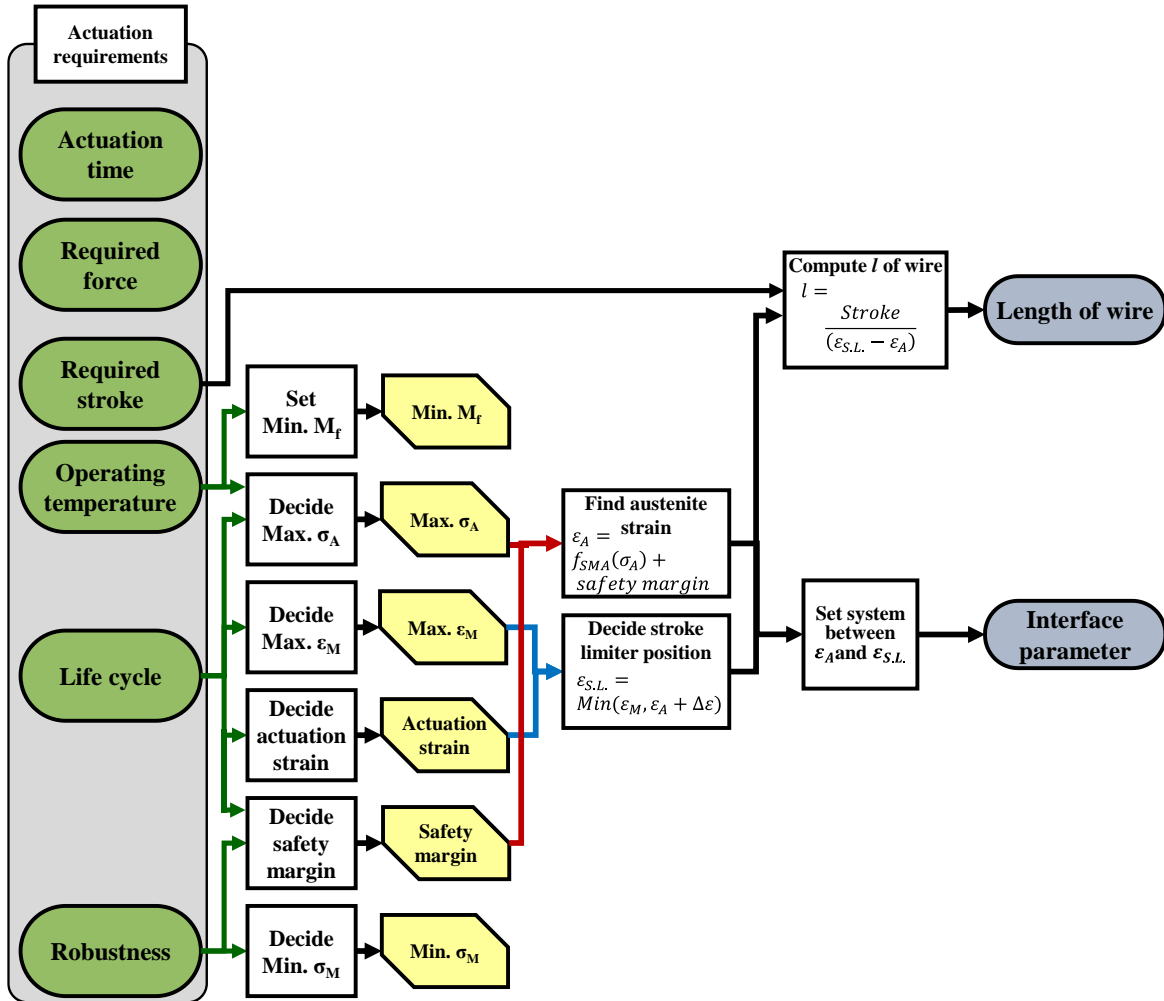


Figure 4.6. Kinematic design step flow for straight SMA wires.

First step of the discrete equilibrium design stage is setting the design parameters to get the required stroke. The required stroke is the main objective of this design step, and the available package space works as the primary constraint. The net actuation strain is the governing material usage decision in this step, and the safety margin, the maximum martensite strain, and the maximum austenite stress affect the available net actuation strain. The sum of the net actuation strain, the strain at the maximum austenite stress and the safety margin should not exceed the maximum martensite strain.

For a straight wire architecture example, it is a very simple arithmetic operation: the length of the SMA wire can be calculated by dividing the required stroke by the net actuation strain. However, more complex architectures such as the web or the ratchet actuators in Appendices A and B require additional considerations due to the architectural transformations. For the application of an architectural model, creating a **Kinematic Actuation Map** is useful to

show the design space as demonstrated in Figure 4.7 for a mechanical leverage. The x-axis of the map is the actuation net strain. The y-axis of the map is a non-dimensional geometric parameter specific to a particular SMA architecture. For example, the stroke amplification ratio (lever ratio) is selected as the y-axis for the mechanical leverage in Figure 4.7. The device strain, which is represented as the diagonal contours is defined as the ratio of the device output stroke to the initial strain-free SMA wire length. The contours are computed using the transformation of particular device element(s), for which the Kinematic Actuation Map is created to visualize the design space. The thick vertical lines are the strain limitation lines where the material does not produce an internal SMA wire net actuation strain larger than the limitation lines for the given maximum stress limits due to the stress-strain behavior of the material. Because the SMA actuation is produced using the force balance shift between the austenite and martensite states, the actuation strain cannot exceed the strain difference at a given stress.

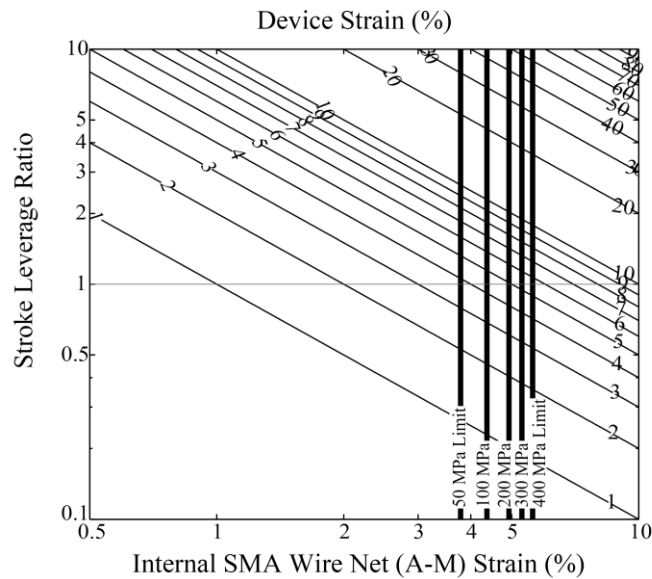


Figure 4.7. Kinematic Actuation Map for mechanical leverage.

The x-axis of the map is the actuation net strain, and the y-axis of the map is the stroke amplification ratio (lever ratio). The device strain, which is represented as the diagonal contours is defined as the ratio of the device output stroke to the initial strain-free SMA wire length. The thick vertical lines are the strain limitation lines where the material does not allow to use the internal SMA wire net actuation strain larger than the limitation lines for given maximum stress limits.

The SMA web actuator architecture creates a more complex but interesting Kinematic Actuation Map (Figure 4.8), and the details of the map is explained in Section 4.1 of Appendix A.

The x-axis is again the actuation net strain, and the y-axis is the width to gap ratio, which is the main geometric design parameter for the SMA web architecture. The active element package strain, which is represented by the diagonal contours is defined as the ratio of the active element stroke to the package length in the actuation direction. The active element package strain contours on the map indicate that higher width / gap ratios and larger SMA wire net strains provide larger amplification resulting in larger package strains. The gray triangular region on the top right side of the map shows the geometric limitation of SMA web actuators, where the active element strain contours approach 100 % and the shape of the web becomes completely flat in the

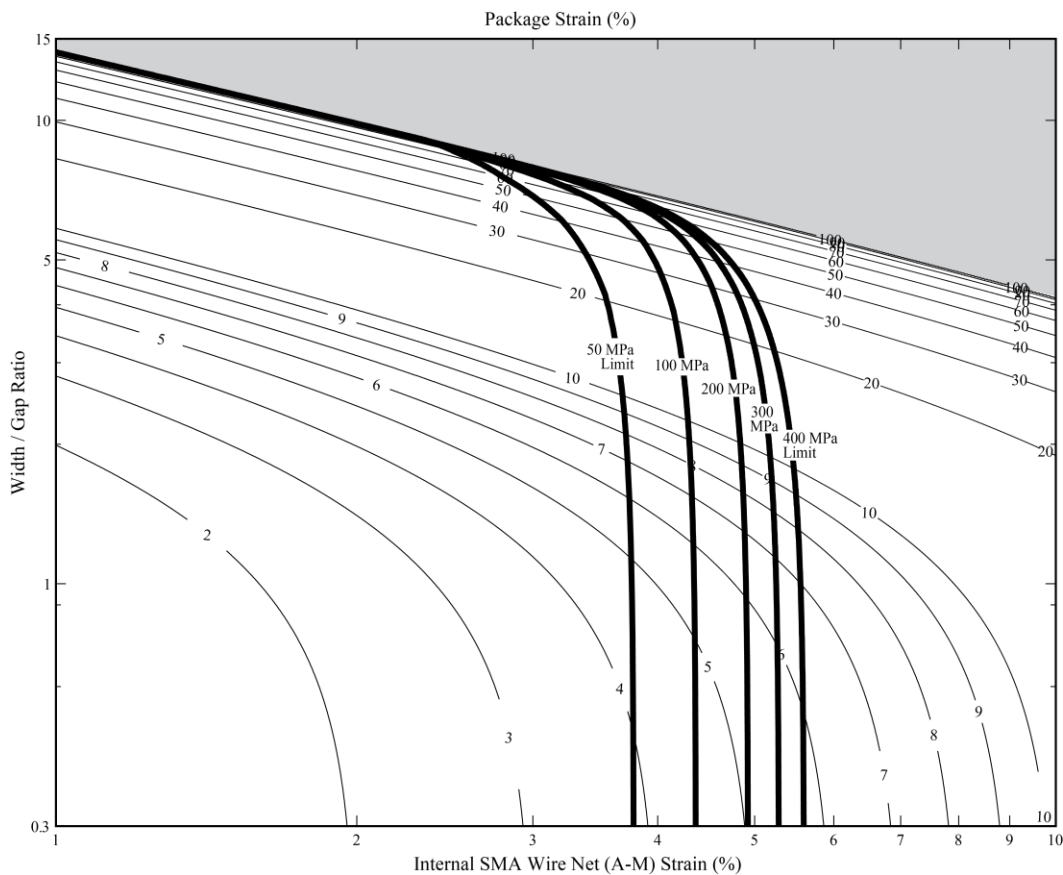


Figure 4.8. Kinematic Actuation Map for SMA web actuator.

The x-axis is the actuation net strain, and the y-axis is the width to gap ratio, which is the main geometric design parameter for SMA web architecture. The active element package strain, which is represented as the diagonal contours is defined as the ratio of the active element stroke to the package length in the actuation direction. The gray triangular region on the top right side of the map shows geometric limitations of SMA web actuators, where the shape of the web becomes completely flat. The thick vertical curved lines show material limitations due to the SMA properties when different maximum allowable stresses are applied. Only designs on left side of these limitation lines are feasible.

austenite state. The thick vertical curved lines show the material limitations due to the SMA properties when different maximum allowable stresses are applied (for further explanation, refer to Figure 7 in Appendix A). Only designs on the left side of these limitation lines are feasible.

Both for the mechanical lever and the web architecture, material limitation lines need to be re-evaluated for different materials due to possible material property variations. However, because the internal SMA wire net actuation strain is usually selected during the initial design decision stage to be smaller than the material limitations to mitigate functional and structural fatigue, the material limitation lines rarely affect the actual design.

Once the actuation stroke is set, the interface offset needs to be determined to set the actuation positions. The design of actuation is not just to produce a certain amount of stroke, but to actuate a target element from a desired deflection position in the OFF state (martensite) to a desired deflection position in the ON state (austenite). The interface offset defines the relative position between the SMA actuation device and the target element to set the SMA actuation device to actuate the target element between the desired deflection positions. The device interface is an interface modifier element, and determines the installation condition of an SMA actuation device.

4.2.2. Kineto-static design step

The next step of the discrete equilibrium design stage is to decide the design parameters to provide the required force while meeting the material usage decisions. The required force is the main objective in this step and the maximum austenite stress serves as the primary constraint. For simple straight wires, the cross-sectional area of the wires can be calculated by dividing the required maximum force by the maximum stress. The device bias can be designed to ensure actuation between the desired actuation positions by avoiding the martensite plateau, or to meet material usage decisions such as the martensite transformation temperature and stress.

The visualization of actuation device system behavior and performance prediction results which has been described in Section 3.3 is useful for this discrete equilibrium design method; the actuation behavior of the device and target element is predicted by finding the equilibria, which are the intersections of the target element curve (green curve) and the material curves (red and blue solid curves) in Figure 4.9. The material behavior curves, which are generally evaluated as stress-strain relations, can be mapped to force-deflection behavior curves through the SMA

architecture to find the equilibrium points with the target element behavior curve, which is evaluated as a force-deflection relation. Alternatively, the target element curve can be mapped to a stress-strain relation through the SMA architecture. For either approach, the material curves and the target element curve are generated independently, and then the intersections are found to predict the device actuation. These visualization plots effectively illustrate the SMA and target element behavior and evaluate the actuation device system behavior. For the example actuation device system in Figure 4.9, the SMA actuation device fails to produce the required stroke because of an insufficient target element force at the planned martensite equilibrium resulting in an inactive stroke limiter. The plot helps to evaluate the difference between the planned actuation strain and the actual actuation strain by showing the SMA behavior and the target element behavior in the same coordinates. Moreover, these plots show the stiffness of the target element relative to the SMA active element, and provide a rough estimation of the parametric sensitivity of the major design parameters.

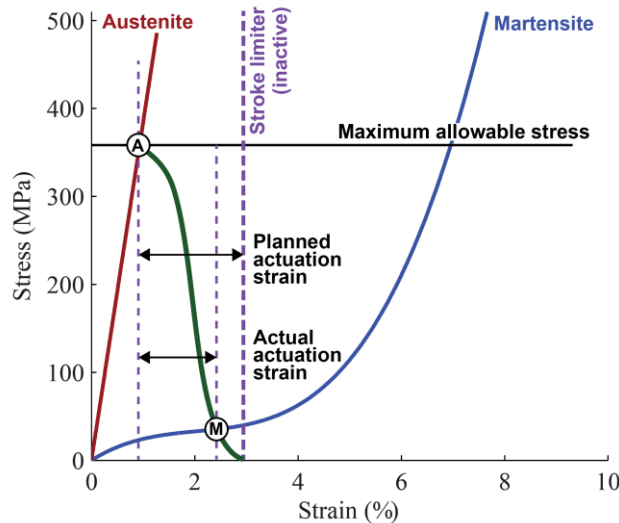


Figure 4.9. Visualization of actuation device system behavior and performance prediction results for discrete equilibrium design method.

The visualization of actuation device system behavior and performance prediction results is very useful for this equilibrium design method; the actuation behavior of the device and target element is predicted by finding the equilibria, which are the intersections of the target element curve (green curve) and the material curves (red and blue solid curves). These visualization plots effectively illustrate the SMA and target element behavior and evaluates the actuation device system. For this example actuation device system, the SMA actuation device fails to produce the required stroke because of the insufficient target element force at planned martensite equilibrium resulting inactive stroke limiter.

Once the total cross-sectional area is set, the martensite stress can be checked to meet the material usage decisions. There are two possible cases which require the use of a device bias to ensure the desired actuation performance. One case is when the target element force at the initial deflection is too low to restore the SMA actuator to the martensite equilibrium; the device bias can provide additional resetting force to bring the SMA to the desired martensite equilibrium position. The other case is when the martensite stress is too low to restore the SMA actuator under a relatively high ambient temperature; the martensite stress (and therefore the martensite transformation temperature) can be increased by increasing the total cross-sectional area of the SMA wire along with the bias force level, thus reducing the target element stiffness relative to the SMA actuator. In the example in Figure 4.9, the actual actuation stroke is smaller than the planned actuation stroke, which is intended to be set using a stroke limiter, because the stroke limiter is inactive as the martensitic SMA wire achieves equilibrium with the target element before it reaches the stroke limiter. Moreover, this martensite equilibrium prevents actuation from the zero deflection position of the target element, which might be a critical constraint in some design problems. Furthermore, the martensite equilibrium stress might be also too low to ensure the actuation at higher ambient temperatures.

The selection procedure of the bias stiffness can be formalized, and Shaw and Churchill [34] proposed a systematic approach and supporting map to select a minimum bias spring mismatch as a function of a dimensionless bias spring stiffness assuming a linear stiffness target element. A bias design procedure which applies to a general non-linear target element requires a direct non-dimensionless approach, which also can be devised to work with a spring database to select among available springs.

The design of the device bias has two steps: decreasing the stress difference between the austenite and martensite equilibria, and restoring the austenite equilibrium stress using the bias device (Figure 4.10). By increasing the cross-sectional area, the SMA becomes stiffer relative to the target element, and the stress difference between the austenite equilibrium and the martensite equilibrium becomes smaller, thus allowing room to increase the martensite stress (Figure 4.10a). Although the stress difference becomes smaller when the cross-sectional area is increased, both the austenite and the martensite stresses are lowered, and there needs to be a device bias to restore the austenite stress to the set maximum allowable stress and increase the martensite stress.

By restoring the austenite stress, the stroke limiter becomes active, and the martensite stress is increased to ensure actuation at higher ambient temperatures (Figure 4.10b).

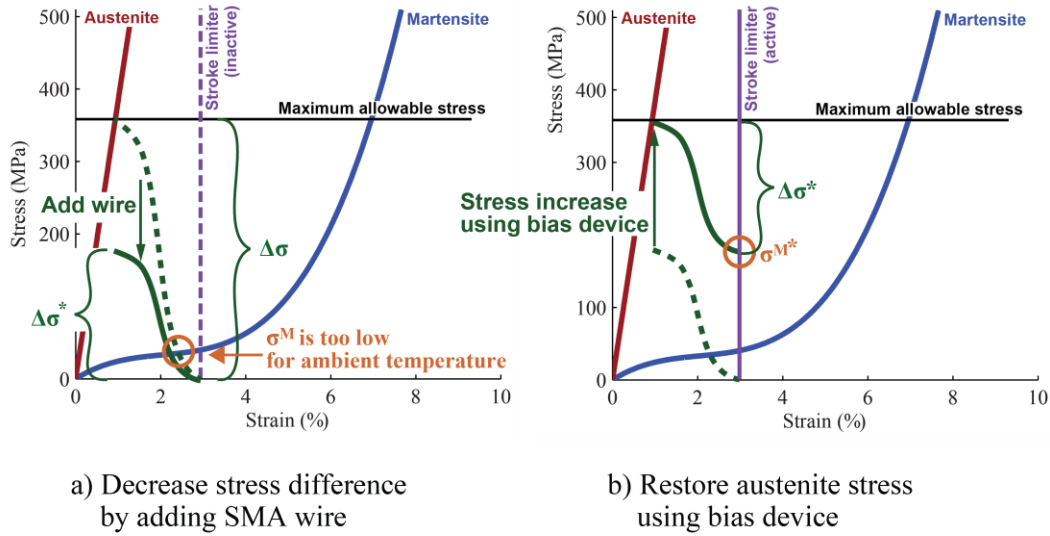


Figure 4.10. Adjusting the target element stiffness using bias device to ensure the operation at high ambient temperature.

In Figure 4.10b, the solid green curve represents the desired lumped stress-strain behavior of the target element and the bias modifier element. The desired cross-sectional area of the SMA wire (A_{SMA}^*) can be selected using the initial stress difference ($\Delta\sigma$), the desired stress difference ($\Delta\sigma^*$), and the initial cross-sectional area (A_{SMA}) as

$$A_{SMA}^* = \frac{\Delta\sigma}{\Delta\sigma^*} A_{SMA}. \quad (4.1)$$

Because the stress in the austenite state is the pre-determined maximum allowable stress (σ_{max}), the desired cross-sectional area of the SMA wire (A_{SMA}^*) can be expressed using the target element force in the austenite equilibrium (F_{target}^A) and the bias element force in the austenite equilibrium (F_{bias}^A) as

$$A_{SMA}^* \cdot \sigma_{max} = F_{target}^A + F_{bias}^A. \quad (4.2)$$

Because the bias element force in the austenite equilibrium can be expressed using the bias element force in the martensite equilibrium (F_{bias}^M), the bias stiffness (k_{bias}), and the actuation stroke (δ_{stroke}), Equation 4.2 can be expressed as

$$A_{SMA}^* \cdot \sigma_{max} = F_{target}^A + F_{bias}^M + \delta_{stroke} \cdot k_{bias}. \quad (4.3)$$

In martensite equilibrium, the desired martensite stress (σ^{M^*}) can be expressed using the target element force (F_{target}^M), the bias element force (F_{bias}^M), and the desired SMA wire cross-sectional area (A_{SMA}^*) as

$$A_{SMA}^* \cdot \sigma^{M^*} = F_{target}^M + F_{bias}^M. \quad (4.4)$$

By substituting the bias element force using Equation 4.4, Equation 4.3 can be rewritten to show the desired bias stiffness for a given SMA wire cross-sectional area as

$$k_{bias} = \frac{1}{\delta_{stroke}} \cdot (A_{SMA}^* \cdot \Delta\sigma^* - \Delta F_{target}), \quad (4.5)$$

where $\Delta\sigma^* = \sigma_{max} - \sigma^{M^*}$ and $\Delta F_{target} = F_{target}^A - F_{target}^M$. However, the bias element should produce enough force to modify the target element force. The maximum force requirement of the bias element in the austenite state can be found by substituting Equation 4.5 into Equation 4.2 as

$$F_{bias}^A = \frac{\sigma_{max}}{\Delta\sigma} \cdot (\Delta F_{target} + \delta_{stroke} \cdot k_{bias}) - F_{target}^A. \quad (4.6)$$

Thus, a spring which satisfies Equations 4.5 and 4.6 as well as the packaging constraints can be selected from a spring catalog.

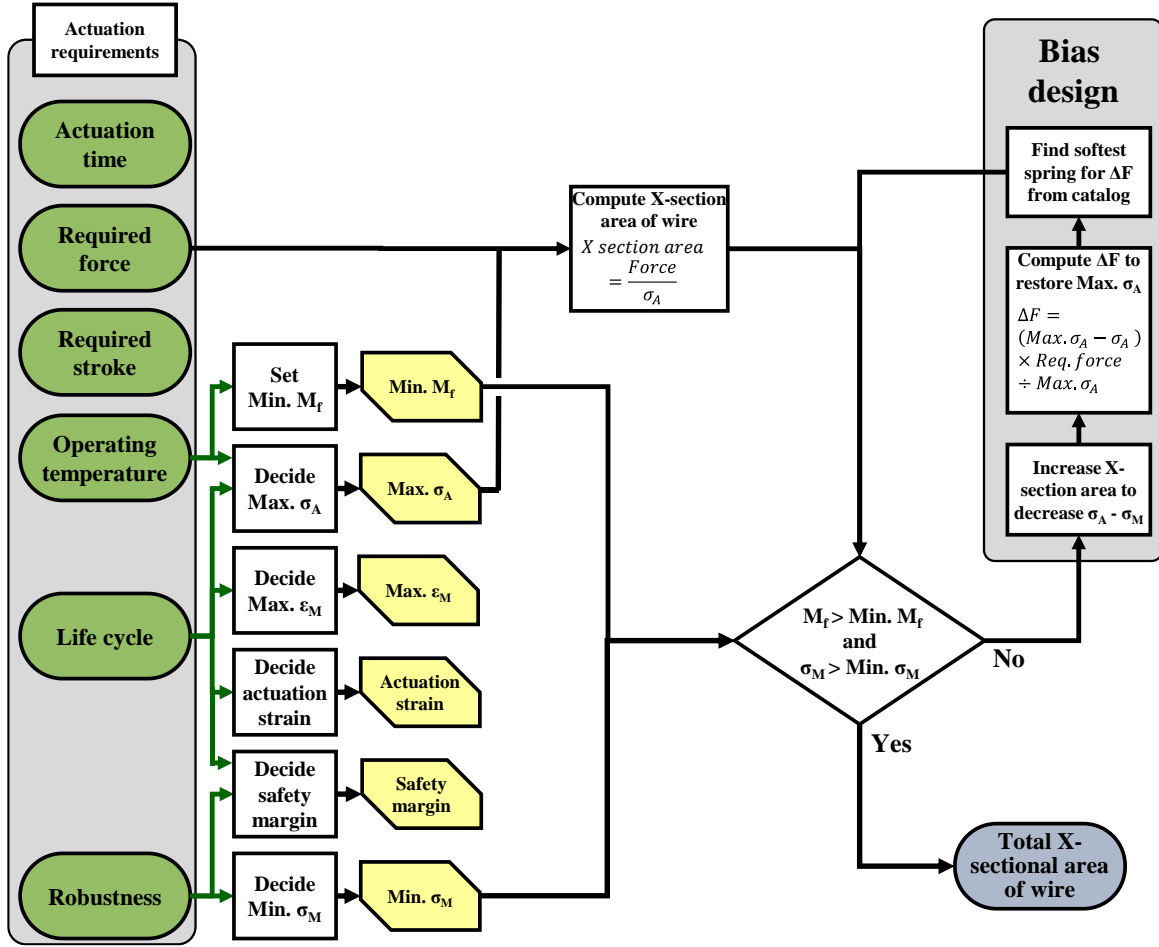


Figure 4.11. Kineto-static design step flow for straight SMA wires.

The required force is the main objective in this step and the maximum austenite stress works as the primary constraint. For the simple straight wires, the cross-sectional area of the wires can be calculated by dividing the required maximum force with the maximum stress.

To avoid an iterative bias design procedure, a bias design map (Figure 4.12) can be created using Equations 4.5 and 4.6. Given the target element force at austenite equilibrium F_{target}^A , the maximum allowable stress σ_{max} , the actuation stroke δ_{stroke} , the target martensite equilibrium force $F_{target}^{M^*}$, and the target martensite stress σ^{M^*} , the desired SMA wire cross-sectional area A_{SMA}^* and the required bias force at the austenite equilibrium F_{bias}^A for a range of bias stiffness k_{bias} can be calculated. There are two infeasible areas on the bias design map. The vertical lines on the map indicate the maximum bias stiffness allowed at a given SMA wire cross-sectional area. If the bias stiffness is higher than the vertical line (the right side of the vertical line), the bias force between the austenite and martensite equilibria becomes too large,

and thus either the maximum allowable stress limit is violated when the martensite stress meets the target stress or the martensite stress becomes too low when the austenite stress is constrained to be the target maximum allowable stress limit. The other feasibility condition is the required bias spring force for a given bias stiffness, represented as the diagonal line on the map, given that real springs selected from a catalog have maximum allowable forces. If a bias spring can not produce enough force for its stiffness (the gray area on the map), the bias force will limit the stroke when set to meet the desired martensite stress. Using this bias design map, a bias spring can be easily selected by plotting the available bias spring options from a catalog on the map.

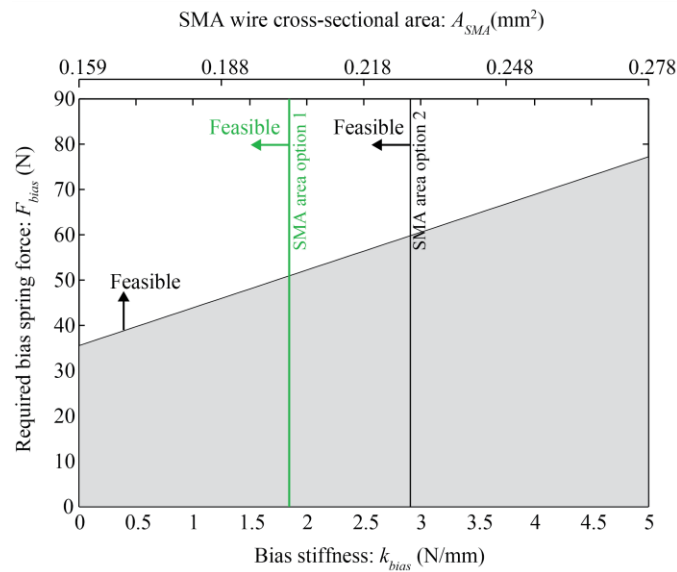


Figure 4.12. Bias design map example.

4.2.3. Thermo-mechanical design step

As the last step of the discrete equilibrium design stage, the number and diameter of SMA wires with the selected total cross-sectional area can be chosen from many combinations based on available wire diameters and required actuation cycle time. During actuation, SMA goes through a temperature evolution upon heating and cooling, and the temperature evolution initiates the stress-strain behavior change due to the material transformation between the martensite and austenite phases. Because the material transformation happens at asymmetric transformation start and finish temperatures, the temperature-stress behavior during actuation shows a hysteresis (Figure 4.13). When heating starts, the actuator does not start to actuate until

the SMA reaches the austenite start temperature (⑥→①). During the martensite to austenite transformation (①→②), actuation occurs. After the material phase transformation is completed, temperature increases (②→③) with accompanying thermal expansion, which counters actuation by small amount. Upon cooling, the backward transformation (austenite to martensite transformation) does not start at the austenite finish temperature (②). Thus, the device does not move until it reaches the martensite start temperature (④). The retraction of the device occurs between the martensite start temperature and the martensite finish temperature (④→⑤). The actuation time is usually regarded as the heating time from the initial temperature (⑥) to the austenite finish temperature (②). The cooling time starts at the heated temperature (③) and ends at the martensite finish temperature (⑤).

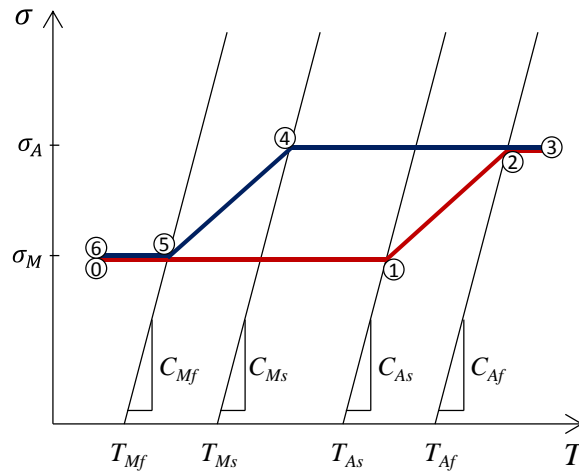


Figure 4.13. Temperature-stress behavior during the actuation.

The transformation temperatures and stress-temperature coupling sensitivities are the material properties which vary due to the material composition, previous cold work, and operation history [35]. The transformation temperatures as shown in Figure 4.13 are calculated as

$$T_{Mf} @ \sigma_M = T_{Mf}@ 0 + \frac{\sigma_M}{C_{Mf}}, \quad (4.7)$$

$$T_{Ms}@ \sigma_A = T_{Ms}@ 0 + \frac{\sigma_A}{C_{Ms}}, \quad (4.8)$$

$$T_{As}@ \sigma_M = T_{As}@ 0 + \frac{\sigma_M}{C_{As}}, \quad (4.9)$$

$$T_{Af}@ \sigma_A = T_{Af}@ 0 + \frac{\sigma_A}{C_{Af}}. \quad (4.10)$$

Due to the stress-temperature coupling, the actuation time is affected by the austenite and martensite equilibrium stresses, which vary with design changes.

While the actuation cycle time is the sum of the heating time and the cooling time to induce temperature dependent material phase changes, the heating time is usually less critical than the cooling time because it can be reduced by increasing the applied voltage and current. The cooling time imposes a more critical constraint affecting the geometric design parameters because it is coupled to the diameter of the SMA wire and the environmental medium, which in many cases not easy to change. The diameter of the SMA wire is selected to meet the required cooling time, which can be approximated using a lumped simple heat transfer model accounting for the specific heat of the material (C_0) and the latent heat of the martensite to austenite phase transformation (Λ_{AM}), and convective heat transfer from the wire (film coefficient h). This model is described by the differential equation,

$$\begin{aligned} \rho V_{SMA} C_0 \frac{\partial T}{\partial t} + \rho V_{SMA} \Lambda_{AM} \frac{\partial \xi}{\partial T} \frac{\partial T}{\partial t} \\ = -h A_{surface} (T(t) - T_\infty) + P, \end{aligned} \quad (4.11)$$

where ρ is the density of the SMA, V_{SMA} is the volume of the SMA wire, T_0 is the temperature of the SMA wire when the cooling starts, T_{Ms} and T_{Mf} are the start and finish temperatures of the austenite to martensite transformation, $A_{surface}$ is the surface area of the SMA wire, and T_∞ is the ambient temperature. By assuming the latent heat is distributed evenly between the martensite start temperature and the martensite finish temperature, i.e. assuming $\Lambda_{AM} \partial \xi / \partial T$ is constant over the entire transformation temperature range, a simple closed-form analytical solution can be found. The transformation temperatures are increasing functions of the austenite

and martensite stresses (Equations 4.7-10). For a given heated temperature T_0 , this equation can be solved for the time to cool to the martensite finish temperature T_{Mf} , such that

$$t_{cooling} = \frac{\rho d_{SMA}}{4h} C_0 \ln\left(\frac{T_0 - T_\infty}{T_{Ms} - T_\infty}\right) + \frac{\rho d_{SMA}}{4h} \left(C_0 + \frac{\Lambda_{AM}}{T_{Ms} - T_{Mf}}\right) \ln\left(\frac{T_{Ms} - T_\infty}{T_{Mf} - T_\infty}\right), \quad (4.12)$$

where, d_{SMA} is the diameter of the SMA wires. The thermo-mechanical material properties (ρ , Λ_{AM} , C_0 , T_{Ms} , and T_{Mf}) can be characterized from the material, and the film heat transfer coefficient (h) can be empirically measured [36]. While a smaller diameter wire is desirable for a faster cooling time, there are limitations for using smaller diameter wires due to an increased complexity related to making mechanical and electrical connections to a larger number of wires. Moreover, using multiple smaller diameter wires requires more power than using a single larger diameter wire due to the increased heat transfer, which may or may not be a driving constraint.

After setting the diameter of the wire, the heating power is determined to meet the required actuation time to heat the wire to the austenite state. The heating time is evaluated similar to the cooling time with an additional Joule heating term as

$$t_{Heating} = \frac{\rho V_{SMA}}{I^2 R} (C_0 (T_{As} - T_\infty)) - h A_{SMA} \left(\frac{T_{As} - T_\infty}{\ln\left(\frac{T_{As}}{T_\infty}\right) - T_\infty} \right) + \frac{\rho V_{SMA}}{I^2 R} (C_0 (T_{Af} - T_{As}) + \Lambda_{MA}) - h A_{SMA} \left(\frac{T_{Af} - T_{As}}{\ln\left(\frac{T_{Af} - T_\infty}{T_{As} - T_\infty}\right)} \right), \quad (4.13)$$

where I is the heating electric current, R is the resistance of the SMA wire, T_{As} and T_{Af} are the austenite transformation start and finish temperatures, and Λ_{MA} is the latent heat of the martensite to austenite transformation. The resistance of the SMA wire, and therefore the power for a given current, can be found using the resistivity of the SMA material. However, deciding an appropriate heating power is not trivial because the heating time varies depending on the

power. The minimum heating power to maintain the heated temperature can provide a starting point to adjust the heating current, which can be calculated as

$$P_{steady}(= I^2R) = \rho V_{SMA}(C_0(T_0 - T_\infty)) - hA_{SMA}(T_0 - T_\infty). \quad (4.14)$$

The heating time can be reduced by increasing the heating electric current beyond this point while accounting for limitations in available power.

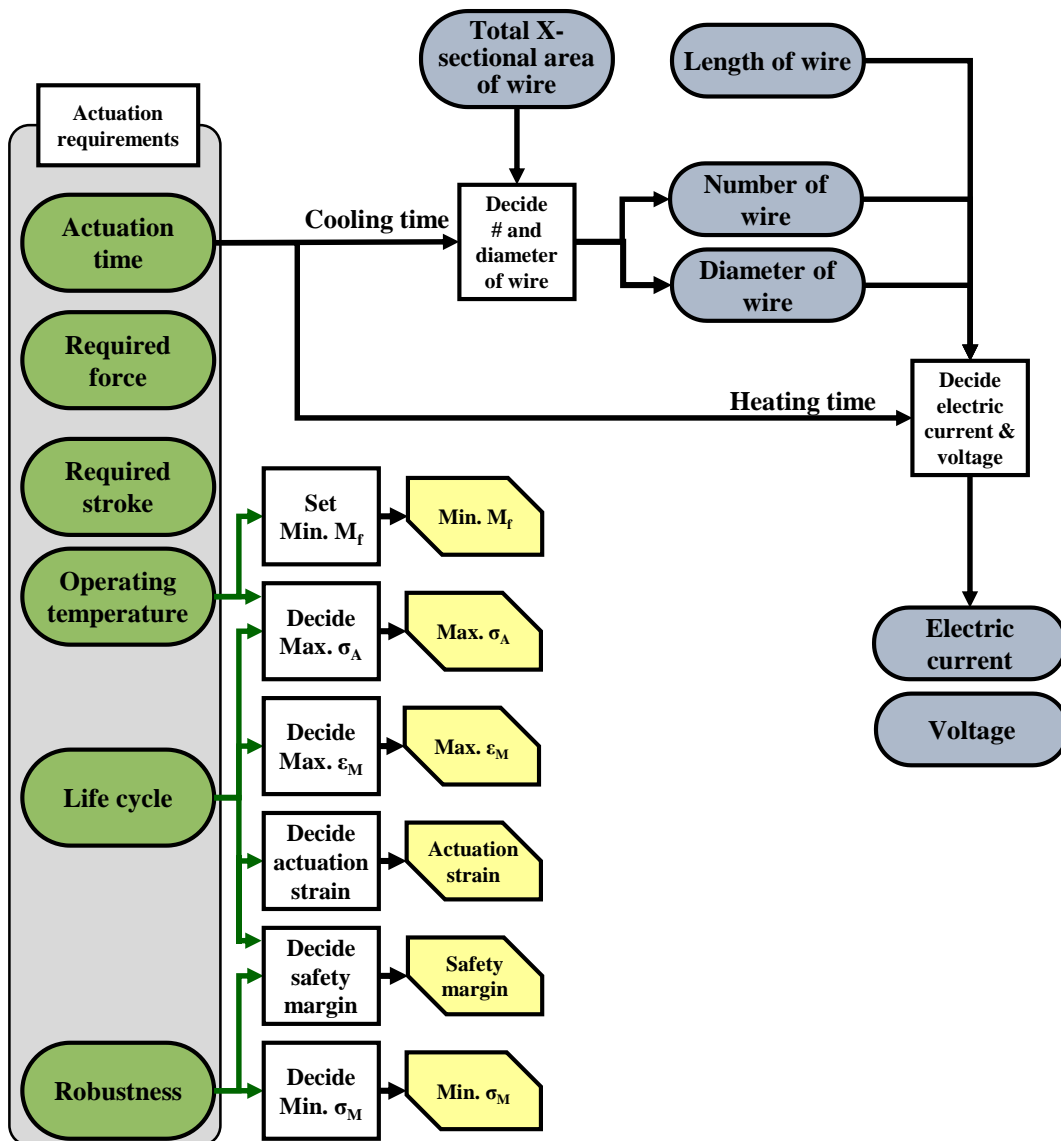


Figure 4.14. Thermo-mechanical design step flow.

The required force is the main objective in this step and the maximum austenite stress works as the primary constraint. For the simple straight wires, the cross-sectional area of the wires can be calculated by dividing the required maximum force with the maximum stress.

4.3. Integrated transient behavior evaluation

To capture the full transient behavior of an SMA wire device, the integrated transient behavior evaluation design method is useful in the later design stage. The material and target element representations are integrated first, and then evaluated to predict the actuation behavior by solving the target element motion and the SMA wire transformation concurrently. While the material curves and target element curve can be generated using different methods for the discrete design method, the representations for the material and target elements need to be of the same type or at least computationally compatible with each other for the integrated design method to allow concurrent interaction between the material model and the target element representation. For example, if the SMA material representation and the modifier elements in the actuation device are implemented in Simulink for the transient behavior simulation, the target element model should also be implemented in Simulink as part of an entire system model, or there must be a connector between the SMA actuation device Simulink model and the other CAE tool which is used for the target element model.

The advantage of this integrated method is the accurate full transient evaluation of the path dependent actuator behavior. For example, when the temperature evolution of the SMA wire is evaluated with the discrete method, the latent heat is assumed to be uniformly spread over the temperature range between the austenite start temperature and the austenite finish temperature at the maximum stress. However, the actual phase transformation starts at a lower temperature than the austenite start temperature at the maximum stress because the actual stress when the phase transformation starts is lower than the maximum stress. Thus, the temperature range over which the phase transformation actually happens is bigger than the temperature range used by the discrete method. By simulating the target element and the material transformation concurrently, the transient behavior can be evaluated more accurately overcoming the limitations of the discrete method. However, the full transient evaluation requires longer computation time, as this method does not allow pre-evaluation as does the discrete design method, slowing the design cycle. Moreover, this method does not provide an intuitive visualization or the evaluation of the impact of individual elements in the device, and thus it requires a more intensive process to evaluate the design parameter sensitivity. Furthermore, the integrated design process requires a set of feasible initial design parameters to start the design iteration, but it is hard for non-expert engineers of SMA actuators to create a feasible initial design. Thus, the discrete equilibrium

design stage works in conjunction with the integrated transient behavior evaluation stage to complete the device development cycle by providing a means to create a detailed design, which can be used as a starting point for the integrated transient behavior evaluation stage.

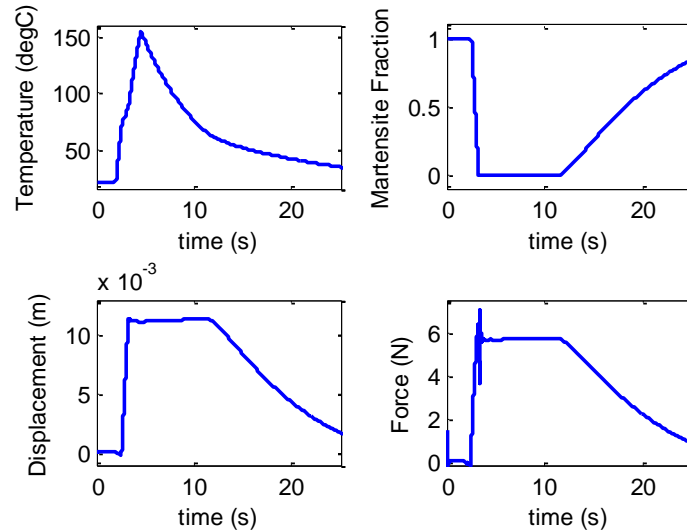


Figure 4.15. Integrated transient behavior evaluation (Simulink) example of an SMA wire-extension spring system.

By simulating the target element and the material transformation concurrently, the transient behavior can be evaluated more accurately overcoming the limitations of the discrete method.

4.4. Common SMA actuator architecture design examples

Three device design examples introduced in the previous chapters are used to demonstrate the discrete equilibrium design procedure. The latch release device example demonstrates the design process for a generalized SMA device structure using a simple straight wire architecture. The active inner belt example demonstrates the design process for a multi-layer SMA active element in a simple device structure, which is only composed of an SMA web actuator and a target element. The hood lifter reset device example demonstrates the design process for a stroke accumulator modifier architecture (SMA ratchet). Although each architecture requires a tailored application of the design procedure, all three examples follow the generalized procedure which consists of three major steps: Kinematic design, Kineto-static design, and Thermo-mechanical design.

4.4.1. Latch release device: straight wire example

The design process for a latch release device starts with initial design decisions, where the basic operation requirements are collected, the SMA architecture is decided, and the material usage decisions are made (Figure 4.16). Using the initial design decisions, a detailed design is produced in the discrete equilibrium design stage. In the Kinematic design step, the length of the SMA wire is selected using the required stroke and the actuation strain, and the interface offset is set to position the SMA actuation device to release the latch properly. In the Kineto-static design step, the total cross-sectional area is selected, and the device bias is designed to ensure actuation at a given operation ambient temperature. In the Thermo-mechanical design step, the actual diameter and number of wires are selected to meet the cooling time requirement, and the resistive heating power is selected to meet the heating time requirement.

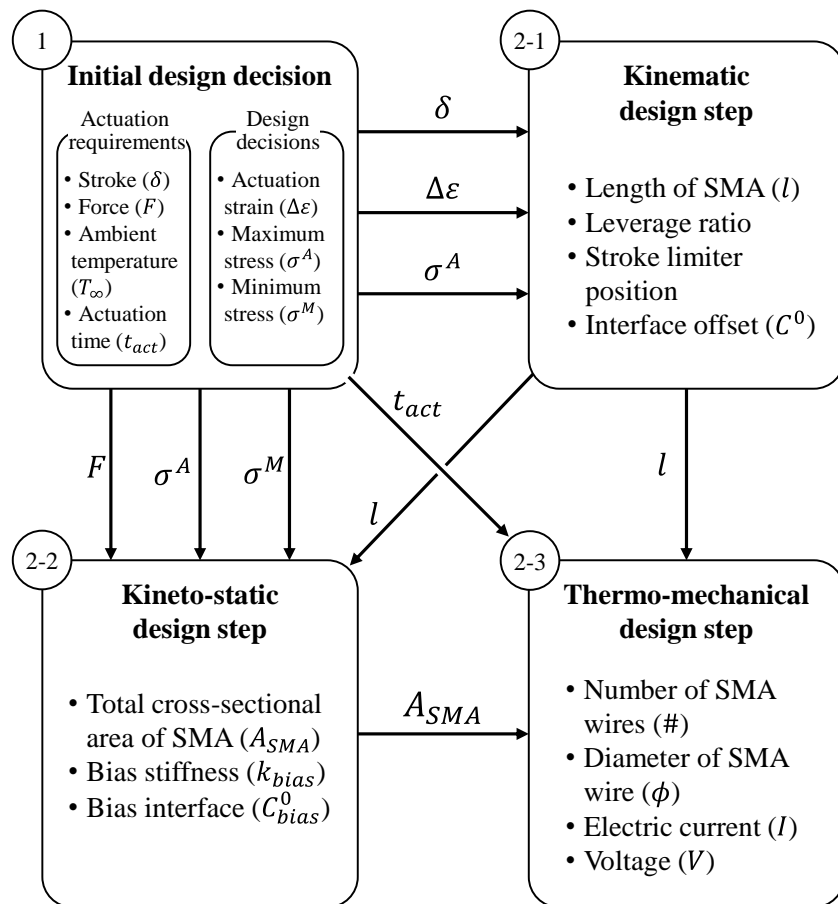


Figure 4.16. Design process for latch release device.

4.4.1.1. Initial design decision stage

The actuation requirements are collected; the latch release device requires 6 mm stroke with force varying linearly from 0 to 10 N. The package space for this device is limited to 200 mm length to be practically housed within the trunk door, and the maximum operation ambient temperature is 60 °C. The feasibility of producing the required force and stroke using SMA wires should be evaluated. For feasibility evaluation, the material usage decisions should be made; the maximum stress on the wire is set to be 350 MPa, and the net actuation strain is selected as 1.5 % to ensure sufficient lifetime. Because the package space is relatively long, it is likely possible to use straight SMA wires for the latch release device design to produce the required force and stroke. Although the high ambient temperature might impose a martensite transformation temperature constraint which is hard to meet, the maximum austenite stress is high enough to set the martensite transformation finish temperature to ensure the restoration at the operation ambient temperature.

Table 4.1. Initial design decisions for latch release device.

Actuation requirements		Material usage decisions	
Stroke	6 mm	Maximum austenite stress	350 MPa
Maximum force	10 N	Actuation net strain	1.5 %
Operation ambient temperature	60 °C	Minimum martensite stress	224 MPa
Packaging limit	200 mm		

4.4.1.2. Discrete equilibrium design stage

In the discrete equilibrium design stage, a detailed design is created using the initial design decisions. First, the stroke related design parameters, i.e. the length of the SMA wires in this example, and the interface offset are set to meet the required stroke and actuation position. Then the force related design parameter, i.e. the total cross-sectional area, is selected along with the device bias design to ensure restoration under the operation ambient temperature by setting the minimum martensite stress. The heating and cooling time related parameters, i.e. the number and the diameter of the SMA wires, are selected along with the heating power parameters, i.e. the electric current and the voltage.

4.4.1.2.1. Kinematic design step

The first step of the design is the kinematic design, where the required length of the SMA wire is calculated using a simple arithmetic equation as

$$\frac{6 \text{ mm}}{1.5 \%} = 400 \text{ mm.} \quad (4.15)$$

Because the 400 mm length wire exceeds the packaging limit, a mechanical leverage can amplify the stroke to reduce the required SMA wire length. To reduce the 400 mm SMA wire length to 200 mm while maintaining the 6 mm required stroke, 3 % active element package strain is required, and thus a 2 times stroke amplification lever is implemented (Figure 4.17). Due to the stroke amplification, the required SMA wire force output becomes 20 N.

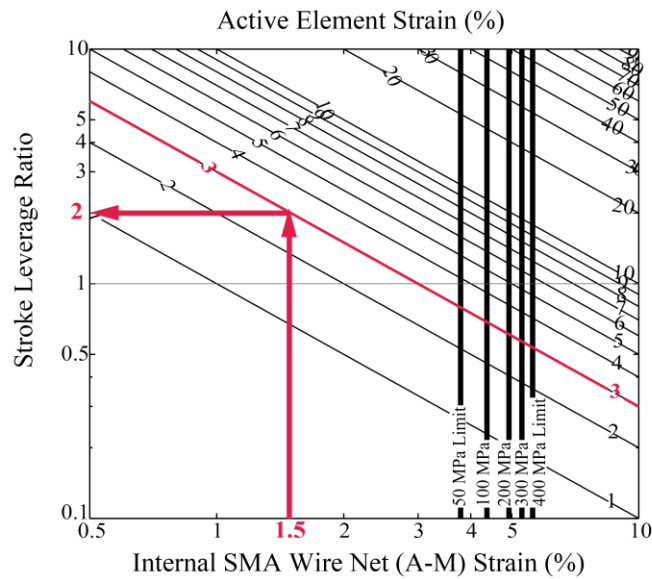


Figure 4.17. Mechanical leverage actuation map example.

4.4.1.2.2. Kineto-static design step

After setting the length of the SMA wire, the second step is to compute the required cross-sectional area of the SMA wire using the maximum stress and the required output force:

$$\frac{20 \text{ N}}{350 \text{ MPa}} = 5.714 \times 10^{-8} \text{ m}^2. \quad (4.16)$$

The cross-sectional area of the SMA wire can be easily converted to the diameter of the SMA wire. While it is possible to have infinite numbers of SMA wire diameter and number combinations which satisfy the computed cross-sectional area, an even number of SMA wires reduces the installation complexity, and it is easier to mount a smaller number of wires. Thus, if the number of SMA wires is set to 2, the diameter of the SMA wire can be calculated as

$$\sqrt{\frac{5.714 \times 10^{-8} \text{ m}^2 \times 4}{\pi \times 2}} \times 39.3701 \text{ in}/\text{m} = 7.509 \times 10^{-3} \text{ in.} \quad (4.17)$$

From the set of commercially available diameters, 8 mil (8/1000 in) wire is selected. The actual cross-sectional area becomes $6.486 \times 10^{-8} \text{ m}^2$, thus the actual austenite stress becomes 308 MPa, which is less than the maximum allowable stress of 350 MPa.

If the latch force is a constant force, the martensite stress is same as the austenite stress, which makes the martensite finish temperature 72 °C:

$$28 \text{ }^\circ\text{C} + \frac{308 \text{ MPa}}{7 \text{ MPa}/^\circ\text{C}} = 72 \text{ }^\circ\text{C}. \quad (4.18)$$

However, if the latch force is a linear stiffness force, which has 10 N / 6 mm = 1.667 N/mm stiffness, then the martensite finish temperature is 28 °C which is below the ambient temperature. Moreover, since the force at zero deflection is zero, the martensitic SMA may not be restored to its zero position. In this case, a device bias needs to be implemented to increase the martensite finish temperature and to provide a restoring force.

The device bias applies an additional force to the SMA wire to increase the stress. However, the cross-sectional area of the SMA wire is computed only to account for the latch force, thus the cross-sectional area needs to be increased to allow room for the device bias not to exceed the maximum allowable stress. The minimum increase in the cross-sectional area can be calculated using the desired stress difference between austenite and martensite. The desired martensite stress can be computed by setting the minimum martensite finish temperature to be above the operation ambient temperature:

$$(60 \text{ }^\circ\text{C} - 28 \text{ }^\circ\text{C}) \times 7 \text{ MPa}/^\circ\text{C} = 224 \text{ MPa}. \quad (4.19)$$

Thus, the maximum stress difference between austenite and martensite is 126 MPa (350 MPa – 224 MPa). Thus the minimum cross-sectional area of the SMA wire is

$$5.714 \times 10^{-8} \text{ m}^2 \times \frac{350 \text{ MPa}}{126 \text{ MPa}} = 1.587 \times 10^{-7} \text{ m}^2. \quad (4.20)$$

Thus the minimum diameter of the two strands of the SMA wire is

$$\sqrt{\frac{1.587 \times 10^{-7} \text{ m}^2 \times 4}{\pi \times 2}} \times 39.3701 \text{ in}/\text{m} = 12.515 \times 10^{-3} \text{ in}. \quad (4.21)$$

From a set of commercially available diameters, 15 mil (15/1000 in) wire is selected, which provides a cross-sectional area of $2.280 \times 10^{-7} \text{ m}^2$. Using Equation 4.5, the bias element stiffness limit is calculated as

$$\begin{aligned} k_{bias} &= \frac{1}{3\text{mm}} \times (2.280 \times 10^{-7} \text{ m}^2 \times 126 \text{ MPa} - 20 \text{ N}) \\ &= 2.910 \text{ N}/\text{mm}. \end{aligned} \quad (4.22)$$

The required bias element force in the austenite equilibrium state is calculated using Equation 4.6 as

$$\begin{aligned} F_{bias}^A &= \frac{350\text{MPa}}{126\text{MPa}} \times (20 \text{ N} + 3 \text{ mm} \times 2.910 \text{ N}/\text{mm}) - 20 \text{ N} \\ &= 59.806 \text{ N}. \end{aligned} \quad (4.23)$$

This bias element design procedure can be simplified using the bias design map (Figure 4.18). While the minimum cross-sectional area of SMA wire is calculated as 0.159 mm^2 , the bias stiffness should be 0 N/mm for this case which means a dead weight bias element. There are two reasonable options for selecting the SMA wires to allow a linear extension spring bias element. The individual red dots on the map represent extension springs from a catalog with a range of spring stiffness and maximum forces. The springs located on the left side of the vertical line and in the white feasible area are viable options among the springs which meet the stiffness and force requirements. The softest of these springs allows a reduction of the maximum stress at the

austenite equilibrium while keeping the martensite equilibrium stress at the target value to ensure full retraction of the actuator device at higher ambient temperatures. Thus the spring which has 1.03 N/mm stiffness and 57.8 N maximum force is the best option for either four 10 mil SMA wires or two 15 mil wires. However, if the packaging length of the bias spring is required to be less than 2 inches, the spring options are narrowed down to the springs with blue circles on the map, and the spring which has 2.10 N/mm stiffness and 57.8 N maximum force becomes the best option. Moreover, the SMA wire combination is forced to be two 15 mil wires because no feasible spring exists for the four 10 mil wires to create enough stress difference between the austenite and martensite equilibria.

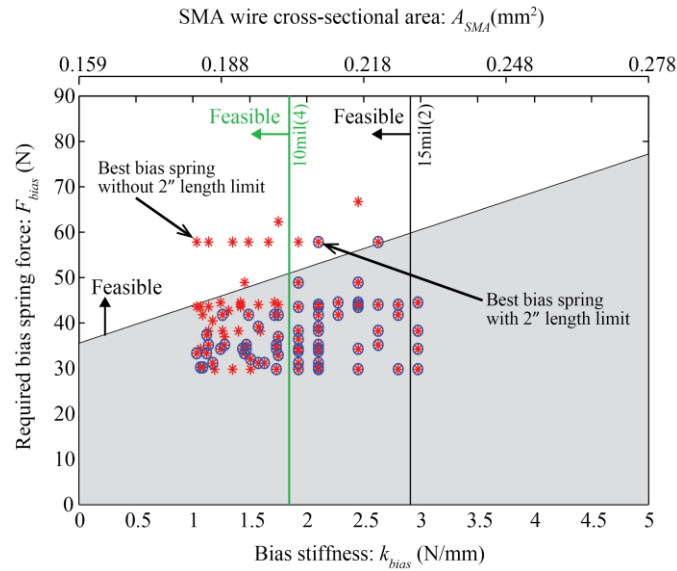


Figure 4.18. Latch release device bias design map example.

4.4.1.2.3. Thermo-mechanical design step

Assuming the 2.10 N/mm stiffness device bias is applied, the transformation temperatures of the SMA wire are calculated using the austenite and the martensite stresses; T_{Mf} : 60 °C, T_{Ms} : 99 °C, T_{As} : 93°C, T_{Af} : 107°C. For a given heated temperature of 120 °C to ensure full austenite transformation, the minimum heating current for a given ambient temperature of 25 °C is calculated as 0.74 A with a total wire resistance of 5.06 Ω. Using the material properties provided by one manufacturer of commercially available SMA wire [37] and the film heat transfer coefficient measured by Pathak [38], the cooling time is evaluated as 1.9

second, and the heating time is 0.45 second. If the ambient temperature is changed to 60 °C, the required minimum heating current reduces to 0.59 A because the heat loss becomes smaller, and the cooling time increases to 15 second, with a heating time of 0.44 second. In addition, by increasing the heating current to 1 A for 25 °C case, the heating time becomes 0.25 second, while the cooling time stays the same.

4.4.2. Active inner belt seal device: web actuator example

The design process for the active inner belt seal device starts with initial design decisions, where the basic operation requirements are collected, the SMA architecture is decided as the web architecture, and the material usage decisions are made. Using the initial design decisions, a detailed design is produced in the discrete equilibrium design stage (Figure 4.19): In the Kinematic design step, the width to gap ratio is selected to create the required stroke, and the length of SMA wire is computed using the width to gap ratio and the given package footprint, and the interface offset is set. In the Kineto-static design step, the total cross-sectional area is selected using the selected width to gap ratio. In the Thermo-mechanical design step, the actual diameter and number of wires are selected to meet the cooling time requirement, and the resistive heating power is selected to meet the heating time requirement in the same manner as the straight wire design example. For further reference, a more detailed design procedure and design tradeoff study are explained in Sections 4 and 5 of Appendix A.

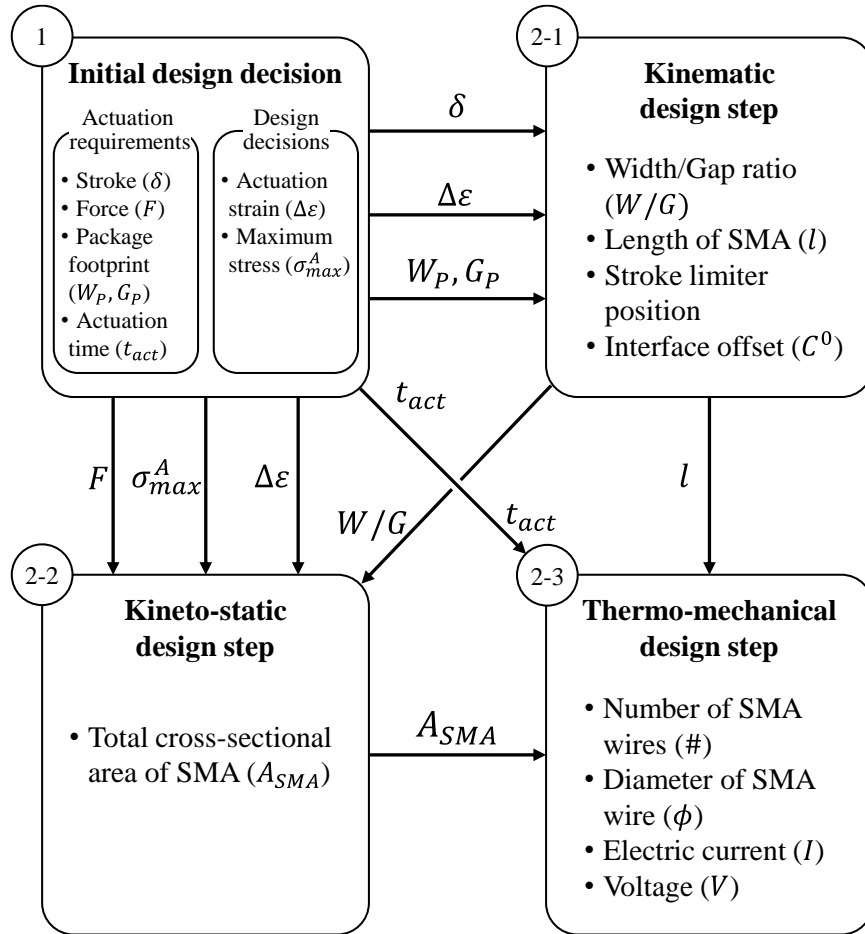


Figure 4.19. Design process for active inner belt seal.

4.4.2.1. Initial design decision stage

The active inner belt seal requires 5 mm stroke with 2.8 N force output to adjust the normal force on the door window. The actuator needs to be packaged within a 12 mm gap inside the existing inner belt seal. The maximum stress on the wire is set to be 200 MPa, and the net actuation strain is selected as 3 %.

4.4.2.2. Discrete equilibrium design stage

In the discrete equilibrium design stage, a detailed design is created using the initial design decisions. First, the stroke related design parameters are set, i.e. the width to gap ratio of the web geometry. The length of the SMA wire is computed using the set width to gap ratio and the available package constraint. Then, the force related design parameters, i.e. the total cross-

sectional area in this example, is selected using the chosen width to gap ratio during the Kinematic design step. The heating and cooling time related parameters, i.e. the number and the diameter of the SMA wires, are selected along with the heating power parameters, i.e. the electric current and the voltage in this example.

4.4.2.2.1. Kinematic design step

The first step is to check the feasibility to produce 5 mm stroke within the 12 mm gap, and set the design parameters related to the stroke. The SMA Web Actuator Kinematic Actuation Map is utilized to check the feasibility and find the required width/gap ratio to achieve a 40 % active element package strain. The actuation map helps the engineer to explore the design space and examine the effects of the diverse design options (Figure 4.20). This map quantifies the non-linear leveraging of the web architecture which transforms the internal SMA wire actuation to the output actuation. The active element package strain ($\epsilon_{Act.} = \delta_{Stroke}/G_M$) is defined as the ratio of the actuator stroke to the initial martensite gap (G_M). The map shows the active element package strain for a range of packaging configurations and internal SMA wire strains. By projecting the 3 % SMA wire net actuation strain to the 40 % active element package strain curve, a 6.26 width/gap ratio is selected using the actuation map.

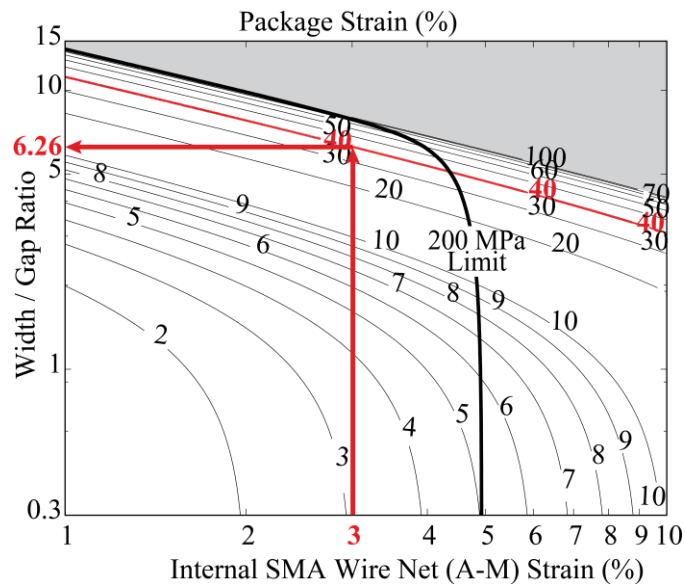


Figure 4.20. SMA web actuator design using Kinematic Actuation Map.

4.4.2.2.2. Kineto-static design step

The second step of the design process is to determine the total cross-sectional area of the SMA wires to carry the required target element force based on the width/gap ratio and the maximum allowable stress. Because the width/gap ratio is defined in the martensite state and the stress in the wire increases to a maximum in the austenite state, it is required to relate target element force to the tension (and resulting stress) on the wire in the martensite state and also in the austenite state. The required cross-sectional area of the SMA wire to avoid exceeding a specified maximum stress ($\sigma_{max.}$) in the austenite state for a constant force ($F = F_A = F_M$) target element is calculated using the web kinematics along with the stress developed in the wire due to the applied load as

$$A_{SMA} = \frac{F}{\sigma_{max.}} \times \frac{1}{2} \frac{\sqrt{1 + R_M^2 - \varepsilon_{SMA}}}{\sqrt{\left(\sqrt{1 + R_M^2 - \varepsilon_{SMA}}\right)^2 - R_M^2}}, \quad (4.24)$$

where R_M is the half of the width/gap ratio at the martensite equilibrium ($R_M = W/2G_M$).

However, for a typical position dependent target element and due to the non-linear leveraging coupled to the web geometry, the cross-sectional area of the SMA wire and the interface offset need to be calculated numerically. The cross-sectional area of the SMA is expressed using the web leverage in the austenite state and the experimentally measured force from the target element evaluated at the austenite position $F(x_A)$ as

$$A_{SMA} = \frac{F(x_A)}{\sigma_{max.}} \times \frac{1}{2} \sqrt{1 + R_A^2}. \quad (4.25)$$

This cross-sectional area needs to be determined through an iterative numerical process along with the interface offset ($x_A = C_0 - (G_A - G_0)$), which affects both the maximum stress in the austenite state and the martensite stress during actuation. For this example, the 6 mil (6/1000 in) SMA wire diameter is selected. The design is verified by performance prediction and actuation system behavior visualization in target element coordinates (Figure 4.21).

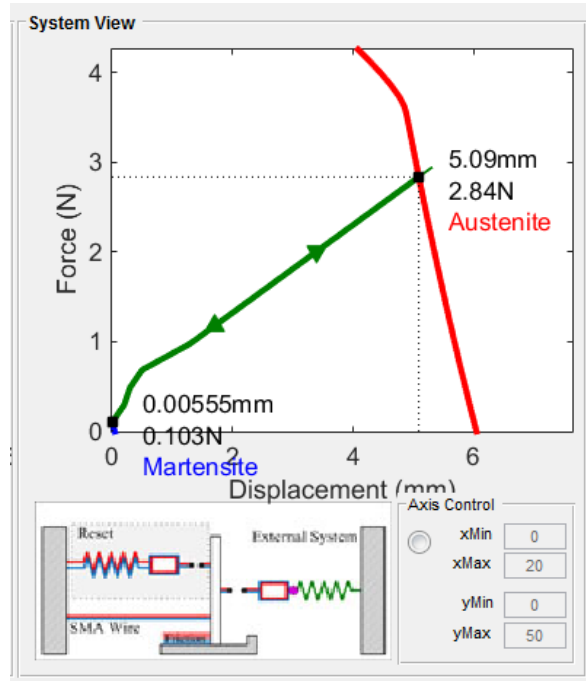


Figure 4.21. Verification of SMA web actuator design using target element coordinates.

4.4.3. SMART hood lifter reset device: ratchet example

The design process for the SMART hood lifter reset device (Figure 4.22) starts with initial design decisions, where the basic operation requirements are collected, the use of ratchet mechanism is decided, and the material usage decisions are made. The geometry of the rack and pawl of the ratchet to carry the required force is designed in this stage [1,24] but not included in this example because it is out of the scope of this SMA actuation device design. Using the initial design decisions, a detailed design is produced in the discrete equilibrium design stage. In the Kinematic design step, the maximum length of SMA wire to fit in the given package space is selected to complete individual actuation steps, and the offset is set. In the Kineto-static design step, the total cross-sectional area is selected along with the bias device to restore the driving pawl. In the Thermo-mechanical design step, the actual diameter and number of wires are selected, and the resistive heating power is selected to meet the heating time requirement in the same manner as the straight wire design example.

The design of a ratchet device is unique because the design for step stroke and the design for overall stroke is done differently. The design for step stroke is done by selecting the length of SMA wire which can complete steps given a rack and pawl geometry overcoming backlash.

The design for overall stroke is highly related to the design for required force. Because the ratchet accumulates the individual step strokes to produce the overall stroke, if the SMA wire can produce the maximum target element force during actuation, the ratchet can meet the overall stroke requirement. In the Kinematic design step, the design parameters related to step stroke are selected, and the design parameters related to overall stroke and force are selected in the Kineto-static design step. Further explanation for the ratchet design model and design study are in Appendix B.

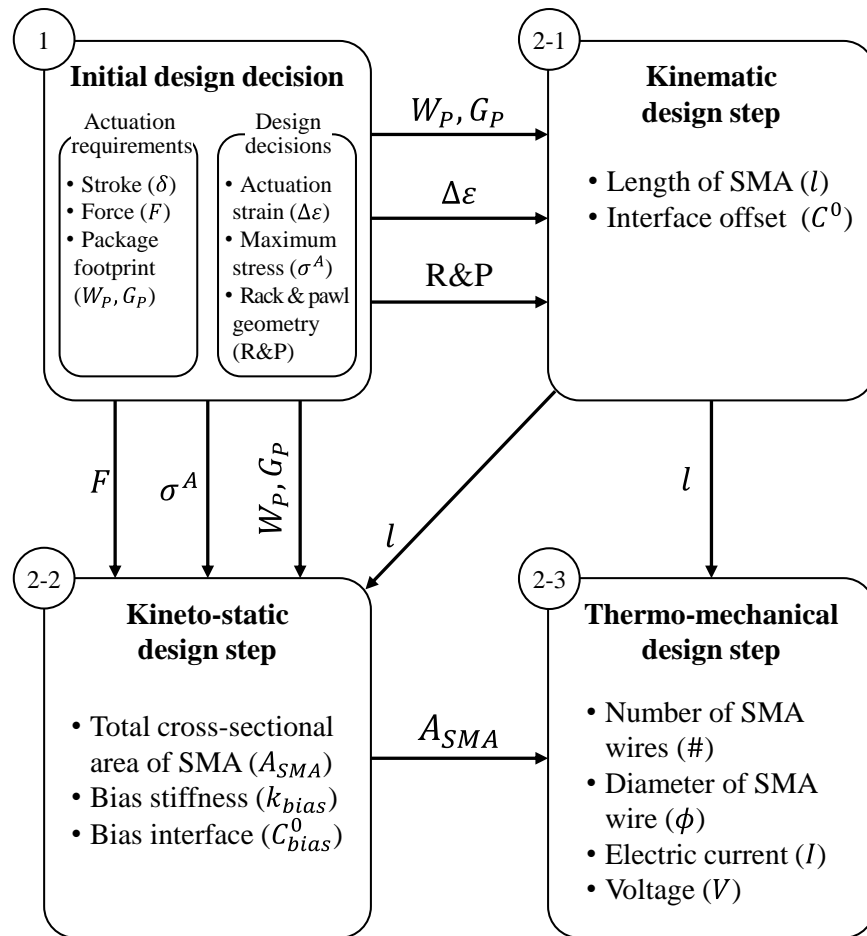


Figure 4.22. Design process for SMART hood lifter reset device.

4.4.3.1. Initial design decision stage

The SMART hood lift reset device restores the pedestrian protection system after operation by compressing the main spring, which requires 125 mm stroke and 1375 N maximum

force. The packaging space for the SMA wire is 160 mm, and the packaging space for the bias spring only allows a spring diameter smaller than 12.7 mm (0.5”).

Even if 4 % actuation strain of the SMA wire is used for actuation, 3125 mm length SMA wire is required to produce 125 mm stroke. Because the actuation time is less critical to reset the SMART hood lift, a ratchet mechanism can be a good candidate to fit the reset mechanism inside the hood lift spring while producing 125 mm stroke. The maximum stress in the SMA wire is set to be 350 MPa and the actuation net strain at the maximum stress is set to be 2 %. The actuation net strain is selected at the maximum stress because the SMA does not see the maximum austenite stress in every cycle due to the nature of the ratchet mechanism. For the low stress early steps, the 2 % actuation net strain limit is not necessary, and limits overall stroke. The net strain during the earlier steps (when the stress is low) would exceed the 2 %, but will be close to the 2 % during the later steps (when the stress becomes close to the 350 MPa limit).

The next step is to design the rack and pawl geometry to support the actuation requirements. Once the geometry parameters are set, a device bias to restore the driving pawl is selected. Using CAE software, a right triangle shape 1 mm pitch width and height rack tooth is designed to carry the 1375 N required maximum force [1].

4.4.3.2. Discrete equilibrium design stage

For the ratchet design, the design parameters related to the step stroke are selected. If the packaging space is unlimited, the longer the SMA wires are the fewer steps are required to complete the overall actuation cycle (for the further design study, refer to Appendix B). Thus, the maximum length which can be housed within the given package space is usually selected. However, the possibility of completing actuation steps overcoming backlash using a given rack and pawl geometry should be evaluated in the Kinematic design step. In the Kineto-static design step, the overall cross-sectional area of SMA wire is selected to produce the maximum force using the maximum stress design decision. If the SMA can produce the maximum force while completing actuation steps overcoming backlash, the overall stroke can be accumulated. During the discrete equilibrium design stage, engineers benefit from a ratchet actuation system behavior visualization (Figure 4.23) which overlays the behavior visualization of individual steps (Figure 3.29).

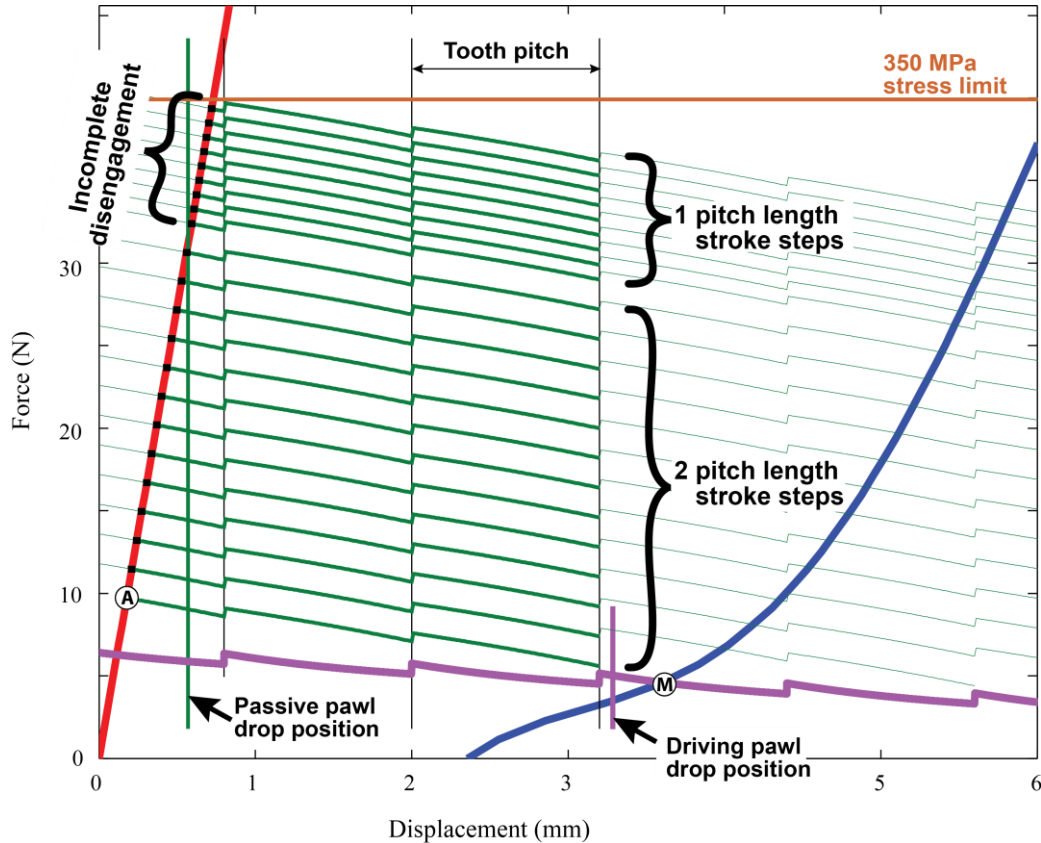


Figure 4.23. SMA ratchet actuator performance evaluation.

For performance evaluation, the effective stroke is found by counting the number of pitch lengths between the austenite and martensite equilibria. The effective stroke also indicates the overall actuation cycle time because the heating / cooling cycle takes almost the same time for a 1 pitch length stroke actuation and a 2 pitch length actuation. The plot also shows the quantitative and qualitative actuation characteristics at the same time such as the number of steps to reach the maximum stress limit and the effective stroke variation during overall actuation. For example, the actuator stroke changes after 13 steps from 2 pitch length strokes to 1 pitch length strokes when the passive pawl fails to fully disengage the rack tooth. This incomplete disengagement is visualized using the vertical black dotted passive pawl drop position line, which also shows the safety margin of the actuation. The effects of key design parameters can be evaluated with this plot. For example, by changing the bias interface, the martensite equilibrium position is changed, and if the equilibrium position moves to the left of the driving pawl drop position, the actuator loses 1 pitch length of effective stroke. The plot also shows the zero effective stroke condition, where the SMA wire stroke is completely lost to backlash, along with the design parameter changes to avoid this condition. This interactive evaluation using SMA wire view design method enables engineers to make better design decisions.

4.4.3.2.1. Kinematic design step

Given the rack and pawl geometry parameters, the first step is to select the SMA wire length to ensure the effective stroke for each step throughout the actuation. The minimum length of SMA wire can be calculated similarly as calculating the straight wire length by setting the required stroke as the pitch of the rack tooth including backlash to ensure each actuation step. Because the actuation does not require precise intermediate position control, and faster actuation is better for this application, the SMA wire length is set to be the maximum available package length, which is 160 mm for this example.

4.4.3.2.2. Kineto-static design step

The next step is to design the overall cross-sectional area of the SMA wires and a bias modifier element to ensure restoration of the driving pawl. The total cross-sectional area to produce 1375 N using 350 MPa stress is computed first to provide a starting point. However, the SMA should produce the force not only to actuate the target element but also to overcome the bias element force. By setting the overall cross-sectional area temporarily, engineers can evaluate the minimum stress (and the equivalent force) to restore the active pawl. The procedure to select the bias element stiffness follows the same procedure for the latch release device. To ensure ratchet restoration during actuation, the martensite equilibrium stress should be higher than 20 MPa. The Bias Design Map is created for a given SMA wire length and the temporary overall cross-sectional area (Figure 4.24), and a spring database is plotted on the map. Due to the package constraint, the outer diameter of the spring should be smaller than 12.7 mm. Because of the symmetric parallel design of the device, a set of springs of 0.39 N/mm stiffness and 97.86 N force is selected among the springs, which satisfies the requirements (Figure 4.24). The number of wires is selected as 21 strands of 20 mil (20/1000 inch) wires to meet the modified cross-sectional area of SMA.

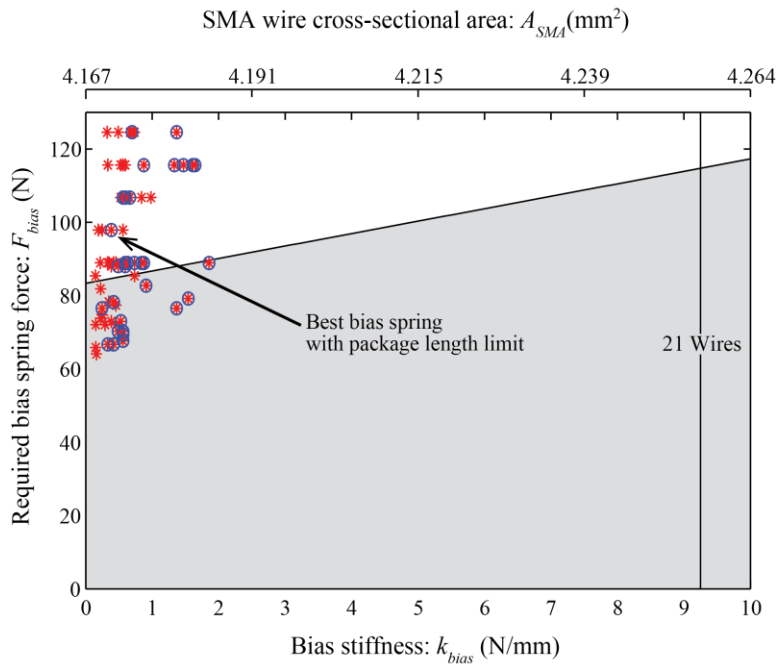


Figure 4.24. SMART hood lifter reset device bias design map.

The final design is evaluated using the ratchet actuation system behavior visualization (Figure 4.23). Using the visualization, engineers can evaluate the completion of individual actuation steps over the entire actuation cycle, the number of steps to complete the overall actuation, the stroke length of individual steps, and possible design improvement by adjusting bias interface. The final design of the ratchet actuation device can produce 128 mm stroke with 101 actuation steps (Figure 4.25). The initial steps are 3 pitch lengths long, but during the actuation cycle it is reduced to 2 pitch lengths after hitting the passive pawl backlash drop position.

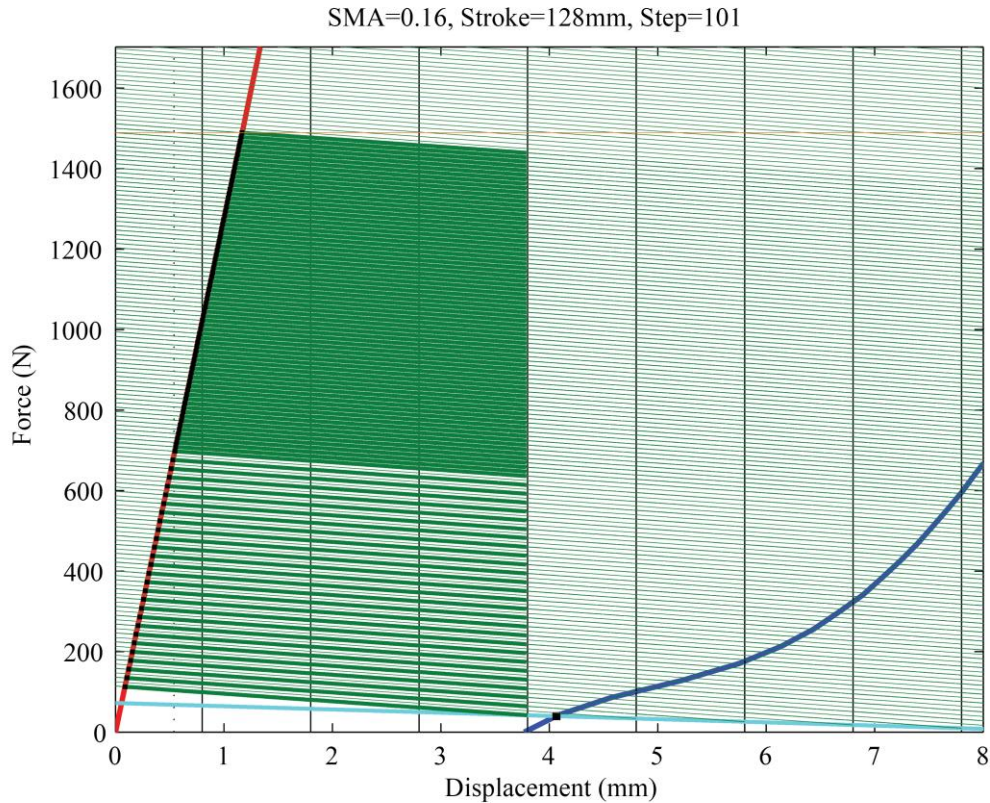


Figure 4.25. Actuator performance evaluation for hood lift reset device.

4.5. Conclusions

The formalized design process helps engineers create a good detailed design while preventing potential design iterations. The multi-stage design process allows engineers to work with models of different types and resolutions at both high and low levels of detail. A three-step discrete equilibrium design procedure prevents potential iteration by ordering design steps to decouple the force and deflection of actuation output behavior, identifying and presenting only the appropriate design variables at each step. This can be visually verified following the information flow in the design process diagrams for the examples (Figures 4. 16, 19, 21). Moreover, the process hides the complexity of material and SMA architectural models from engineers while still exposing the impact of design parameters, and helps engineers to overcome the non-intuitive design parameter sensitivity. Furthermore, the formalized systematic design process provides a foundation to automate the design process.

4.6. References

- [1] Barnes, B. M., Brei, D. E., Luntz, J. E., Strom, K., Browne, A. L., and Johnson, N., 2008, "Shape memory alloy resetable spring lift for pedestrian protection," SPIE, San Diego, California, USA, pp. 693005–13.
- [2] Zhang, X., Yan, X., and Yang, Q., 2013, "Design and Experimental Validation of Compact, Quick-Response Shape Memory Alloy Separation Device," *J. Mech. Des.*, **136**(1), pp. 011009–011009.
- [3] Duerig, T. W., Melton, K. N., Stöckel, D., and Wayman, C. M., 1990, *Engineering Aspects of Shape Memory Alloys*, Butterworth-Heinemann.
- [4] Liang, C., and Rogers, C. A., 1997, "Design of shape memory alloy actuators," *Journal of Intelligent Material Systems and Structures*, **8**(4), pp. 303–13.
- [5] Swensen, J. P., and Dollar, A. M., 2013, "Active-Cells for the Construction of Redundant and Configurable Articulated Structures," ASME 2013 Conference on Smart Materials, Adaptive Structures and Intelligent Systems, American Society of Mechanical Engineers, pp. V001T01A013–V001T01A013.
- [6] Shydo, J., Garcia, E., and Harris, J. M., 2005, "A remotely activated SMA actuated naval tie-down system," E.V. White, ed., SPIE, San Diego, CA, USA, pp. 56–64.
- [7] Nishida, M., Tanaka, K., and Wang, H. O., 2006, "Development and control of a micro biped walking robot using shape memory alloys," pp. 1604–1609.
- [8] Lan, C.-C., and Yang, Y.-N., 2009, "A Computational Design Method for a Shape Memory Alloy Wire Actuated Compliant Finger," *J. Mech. Des.*, **131**(2), pp. 021009–9.
- [9] Odhner, L., and Asada, H., 2010, "Scaling up shape memory alloy actuators using a recruitment control architecture," pp. 1675–1680.
- [10] Langbein, S., and Czechowicz, A., 2013, "A Multi-Purpose Method for SMA Actuator Development," Proceedings of the ASME 2013 Conference on Smart Materials, Adaptive Structures and Intelligent Systems, ASME, Snowbird, Utah, USA, pp. SMASIS2013–3053–7.
- [11] An, S.-M., Ryu, J., Cho, M., and Cho, K.-J., 2012, "Engineering design framework for a shape memory alloy coil spring actuator using a static two-state model," *Smart Materials and Structures*, **21**(5), p. 055009.
- [12] Hartl, D. J., and Lagoudas, D. C., 2007, "Characterization and 3-D modeling of Ni60Ti SMA for actuation of a variable geometry jet engine chevron," SPIE, San Diego, California, USA, p. 65293Z–12.
- [13] Gao, X., Burton, D., Turner, T. L., and Brinson, L. C., 2006, "Finite Element Analysis of Adaptive-Stiffening and Shape-Control SMA Hybrid Composites," *J. Eng. Mater. Technol.*, **128**(3), pp. 285–293.
- [14] Chang, B., 2006, "Thermodynamics of shape memory alloy wire: modeling, experimental calibration, and simulation."

- [15] Sun, H., Pathak, A., Luntz, J., Brei, D., Alexander, P. W., and Johnson, N. L., 2008, “Stabilizing shape memory alloy actuator performance through cyclic shakedown: an empirical study,” SPIE, San Diego, California, USA, p. 69300Q–11.
- [16] Bertacchini, O. W., Schick, J., and Lagoudas, D. C., 2009, “Parametric study and characterization of the isobaric thermomechanical transformation fatigue of nickel-rich NiTi SMA actuators,” SPIE, San Diego, CA, USA, p. 72890P–12.
- [17] Miyazaki, S., Mizukoshi, K., Ueki, T., Sakuma, T., and Liu, Y., 1999, “Fatigue life of Ti-50 at.% Ni and Ti-40Ni-10Cu (at.%) shape memory alloy wires,” *Materials Science and Engineering A*, **273-275**, pp. 658–663.
- [18] Wilkes, K., Liaw, P., and Wilkes, K., 2000, “The fatigue behavior of shape-memory alloys,” *JOM Journal of the Minerals, Metals and Materials Society*, **52**(10), pp. 45–51.
- [19] Tobushi, H., Pieczyska, E., Ejiri, Y., and Sakuragi, T., 2009, “Thermomechanical properties of shape-memory alloy and polymer and their composites,” *Mechanics of Advanced Materials and Structures*, **16**(3), pp. 236–247.
- [20] Furuichi, Y., Tobushi, H., Ikawa, T., and Matsui, R., 2003, “Fatigue properties of a TiNi shape-memory alloy wire subjected to bending with various strain ratios,” *Proceedings of the Institution of Mechanical Engineers, Part L: Journal of Materials: Design and Applications*, **217**(2), pp. 93–99.
- [21] Cheung, G. S. P., and Darvell, B. W., 2007, “Fatigue testing of a NiTi rotary instrument. Part 1: strain-life relationship,” *International Endodontic Journal*, **40**(8), pp. 612–618.
- [22] Redmond, J. A., Brei, D., Luntz, J., Browne, A. L., and Johnson, N. L., 2012, “Spool-Packaging of Shape Memory Alloy Actuators: Performance Model and Experimental Validation,” *Journal of Intelligent Material Systems and Structures*, **23**(2), pp. 201–219.
- [23] Kim, W., Thota, M., Luntz, J., and Brei, D., 2012, “Analytical Model and Design Study on Shape Memory Alloy Web Actuator,” *ICAST2012*, Nanjing, China, pp. 031–16.
- [24] Utter, B., Barnes, B., Luntz, J., Brei, D., Teitelbaum, D. H., Okawada, M., and Miyasaka, E., 2010, “Design of an SMA Actuated Mechanotransductive Implant for Correcting Short Bowel Syndrome,” *Proceedings of the 2010 Smart Materials, Adaptive Structures, and Intelligent Systems*, Philadelphia, Pennsylvania, USA, pp. 875–892.
- [25] Kim, W., Utter, B., Luntz, J., Brei, D., Muhammad, H., and Alexander, P., 2013, “Model-based Shape Memory Alloy Wire Ratchet Actuator Design,” *Proceedings of the ASME 2013 Conference on Smart Materials, Adaptive Structures and Intelligent Systems*, ASME, Snowbird, Utah, USA, pp. SMASIS2013–3333–12.
- [26] Liang, C., and Rogers, C. A., 1993, “Design of Shape Memory Alloy Springs With Applications in Vibration Control,” *J. Vib. Acoust.*, **115**(1), p. 129.
- [27] Churchill, C. B., and Shaw, J., 2011, “Thermo-Mechanical Modeling of a Shape Memory Alloy Heat Engine,” pp. 641–650.
- [28] Reedlunn, B., 2012, “Thermomechanical Behavior of Shape Memory Alloy Cables and Tubes.”

- [29] Shaw, J. A., 2002, "A thermomechanical model for a 1-D shape memory alloy wire with propagating instabilities," *International Journal of Solids and Structures*, **39**(5), pp. 1275–1305.
- [30] Buravalla, V., and Khandelwal, A., 2008, "Phenomenological Modeling of Shape Memory Alloys," *AIP Conference Proceedings*, S.M. Sivakumar, V. Buravalla, and A.R. Srinivasa, eds., IIT Madras, Chennai, India, pp. 104–123.
- [31] Boyd, J. G., and Lagoudas, D. C., 1994, "Thermodynamical constitutive model for the shape memory effect due to transformation and reorientation," *SPIE*, Orlando, FL, USA, pp. 276–288.
- [32] Brinson, L. C., and Huang, M. S., 1996, "Simplifications and comparisons of shape memory alloy constitutive models," *Journal of Intelligent Material Systems and Structures*, **7**(1), pp. 108–118.
- [33] Kim, W., Barnes, B. M., Luntz, J. E., and Brei, D. E., 2011, "Conglomerate Stabilization Curve Design Method for Shape Memory Alloy Wire Actuators With Cyclic Shakedown," *Journal of Mechanical Design*, **133**(11), p. 111010.
- [34] Shaw, J. A., and Churchill, C. B., 2009, "A reduced-order thermomechanical model and analytical solution for uniaxial shape memory alloy wire actuators," *Smart Materials and Structures*, **18**(6), p. 065001.
- [35] Shaw, J. A., Churchill, C. B., and Iadicola, M. A., 2008, "Tips and Tricks for Characterizing Shape Memory Alloy Wire: Part 1; Differential Scanning Calorimetry and Basic Phenomena," *Experimental Techniques*, **32**(5), pp. 55–62.
- [36] Pathak, A., Brei, D., and Luntz, J., 2010, "Transformation strain based method for characterization of convective heat transfer from shape memory alloy wires," *Smart Materials and Structures*, **19**(3).
- [37] Dynalloy, Inc., 2010, "Technical and Design Data for FLEXINOL Wire from Dynalloy, Inc." [Online]. Available: <http://www.dynalloy.com/TechData.html>. [Accessed: 16-Feb-2010].
- [38] Pathak, A., 2010, "The Development of an Antagonistic SMA Actuation Technology for the Active Cancellation of Human Tremor.," University of Michigan.

Chapter 5.

SMA Design Framework

A *design framework* is a systematic foundation for SMA actuation device design which helps to make SMA technology available to engineers by organizing and presenting the device grammar, design methods, and design process. A design framework can be implemented as a computer-aided design tool to make SMA technology accessible to diverse groups of stakeholders. While there are research efforts to help engineers by creating computer-aided design software [1–3], these tools have limited scope such as material selection in the planning stage (Figure 1.22), or handling of a single SMA architecture such as straight wires (Figure 1.23) or spool packaged wires (Figure 1.24). Moreover, these software tools are targeted for design computation support to expedite the analysis portions of the design cycle for expert engineers, i.e. an implementation of a particular design method, but they are not capable of guiding non-expert engineers to create a detailed design. Such guidance requires design methods and processes to be organized into a design framework including a software platform and user interfaces. An expandable integrative model-based design tool platform to systematically organize the device grammar, design methods, and design processes is needed to create software design tools to guide non-expert SMA engineers and better support expert SMA engineers throughout the entire design process.

The goal of this chapter is to systematically organize and present the SMA design knowledge including device grammar, design methods, and design process for diverse expert and non-expert stakeholders.

The objectives are

1. Formalize the comprehensive design activity using design framework components, i.e. grammar, methods, and process

2. Create an expandable integrative model-based design software platform to realize the design framework for SMA devices
 - 2-1. Develop a design process guider to provide a step-by-step procedure to assist engineers to identify an effective order to make design decisions
 - 2-2. Develop a behavior evaluator to model, predict performance, and visualize the actuation device system behavior to support design decisions
 - 2-3. Develop an actuation device system structure module to represent the device elements and connections between the actuation device system
3. Demonstrate the software platform as well as the design framework with example design tool software

In this chapter, the design framework is demonstrated by a model-based design tool modular platform, and by its implementation as two software design tools tailored for different engineer groups: an expert engineer supporting design tool and a non-expert engineer guiding design tool. To create an expandable model-based design tool software modular platform, major functional modules are identified, defined, and structured following the device grammar, design methods, and design process. Based on this modular platform, a software user interface for a step-by-step design procedure to present an appropriate level of design information at each step to non-expert engineers is designed following the discrete equilibrium design procedure formalized in Chapter 4. For design of the step-by-step user interface, a design parameter flow is identified to follow the design procedure. While a step-by-step guiding design tool is useful for non-expert engineers who are not familiar with SMA actuation devices, expert engineers can benefit more from performance prediction and visualization assistance software, which can present all the design information at once to explore the design options. This type of expert user supporting design tool is implemented using the design methods introduced in Chapter 3. The SMA actuation device design framework and its implementations as software design tools provide a systematic foundation to organize and present the device grammar, design methods and design process to engineers to support design decisions.

5.1. Model-based design tool modular platform

The model-based design tool modular platform consists of four major functional modules: the actuation device system modular structure, the evaluation manager module, the design decision manager module, and the user interface (Figure 5.1). The **device modular structure** consists of instances of basic element objects, which work as building blocks of the actuation device structure. Instances of individual device elements are aggregated as a device structure through the evaluation manager module by setting the port connectivity of individual elements. The **evaluation manager module** predicts the performance of the actuation device system, evaluates design metrics, and generates behavior visualization. The **design decision manager module** guides non-expert engineers to create a detailed design by updating the user interface and actuation device system modular structure to present and manage the three-step discrete equilibrium design process. The **user interface** provides a software user interface to set the device structure, select the design parameters, and present the performance prediction results.

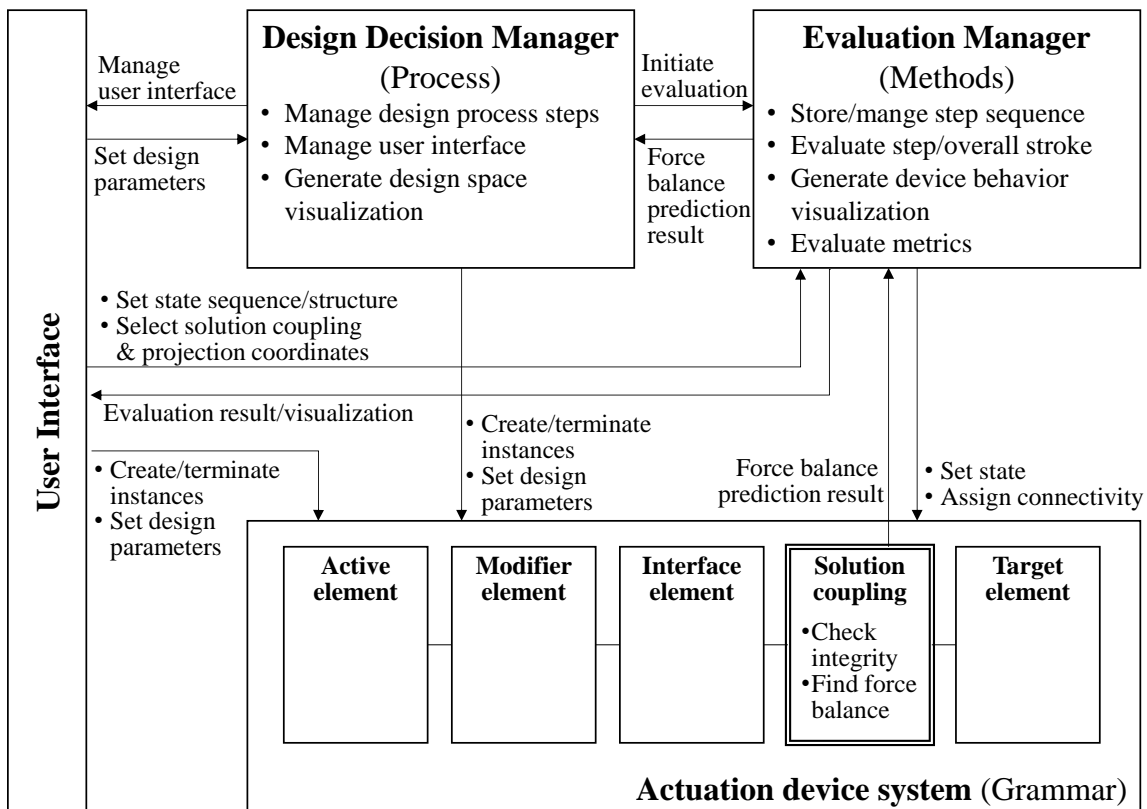


Figure 5.1. Model-based Design Tool modular platform.

Model-based design tool modular platform consists of four major parts: actuation device system modular structure, evaluation manager modules, design decision manager module, and user interface.

5.2. User interface work flows

The design tool user interface provides a graphical user interface to allow engineers to address design tasks using the design tool software. The design tool user interface needs to be created specifically for the design decision manager and evaluation manager modules as part of an individual design tool software implementation. This study suggests two types of design tool implementations: an expert user supporting design tool and a non-expert user guiding design tool. In this section, two types of design tool user interfaces are discussed in terms of engineer interaction scenarios (Appendix D).

The expert engineer supporting design tool interface (Figure 5.2) makes the design methods from Chapter 3 available to engineers to help make design decisions. The expert engineer supporting tool interface is highly related to the evaluation manager module, which manages the performance prediction, design metric evaluation, and visualization. The non-expert engineer guiding design tool interface (Figure 5.3) presents the design decisions which are to be made in each step of the discrete equilibrium design procedure, and proceeds to the next step by updating the user interface following the design information flows from Chapter 4. This design procedure is managed by the design decision manager module, which updates the user interface and the actuation device system modular structure as the design procedure proceeds.

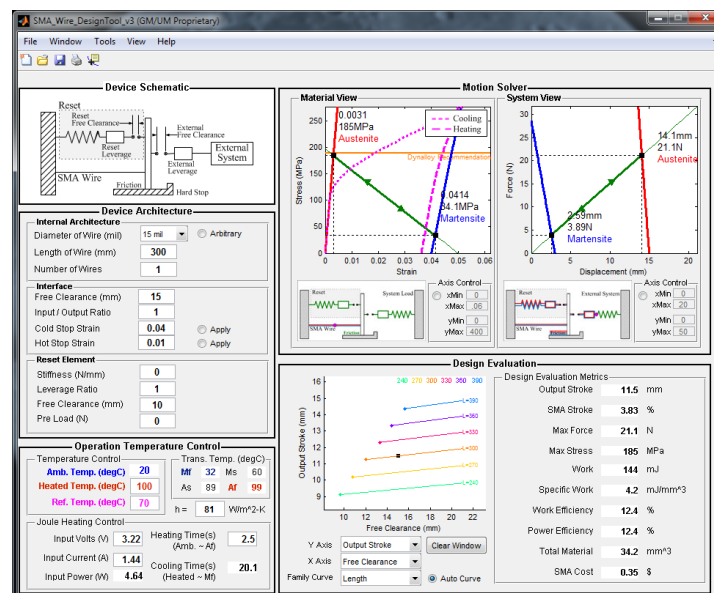


Figure 5.2. Example of expert user supporting design tool interface.

Expert engineer supporting design tool interface makes design methods in Chapter 3 available to engineers to help making design decisions.

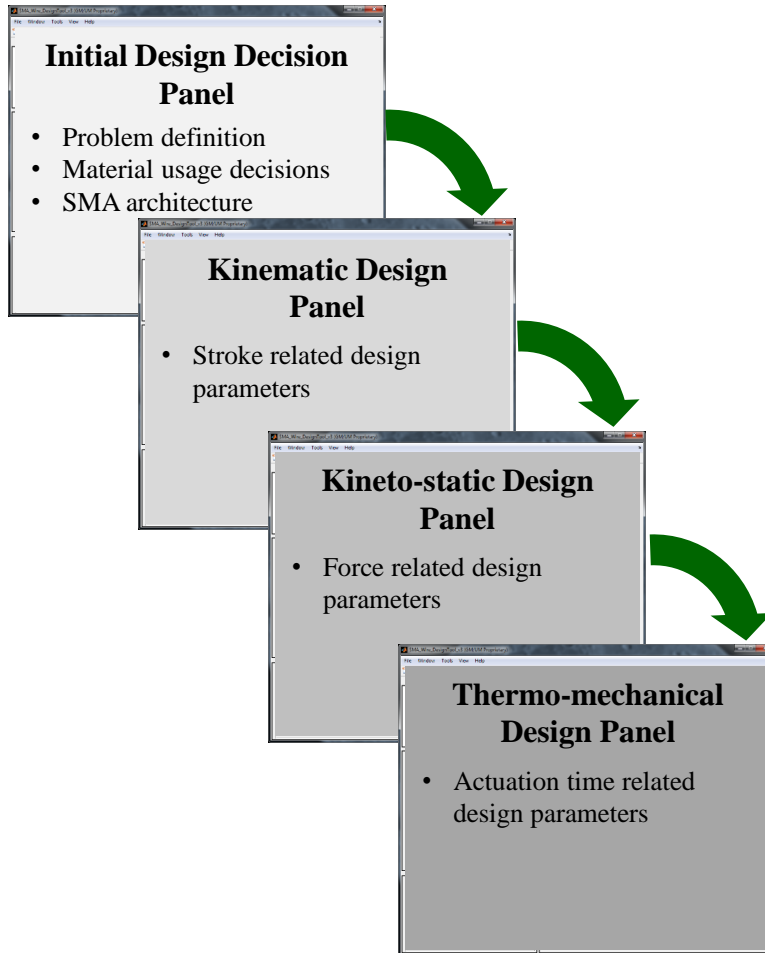


Figure 5.3. Concept of non-expert user guiding design tool interface.

Non-expert engineer guiding design tool interface presents design decisions to make in each step of discrete equilibrium design process, and proceeds the next step by updating user interface following the design process in Chapter 4.

5.2.1. Expert engineer supporting design tool interface

The expert engineer supporting design tool interface provides an interface to define the design problem and the material behavior, select an SMA architecture, set actuation device system structure and design parameters, plan actuation state sequence and related parameters, set evaluation and visualization options, and update the design parameters, as well as presenting related design information such as actuation device system behavior visualization and design metrics. Expert engineers can explore the design space interactively without having to iterate through manual design evaluations.

5.2.1.1. Design problem definition and initial design decisions

Engineers start a design project by defining the design problem. With the expert engineer supporting tool, engineers define the design problem by first setting the target element behavior. The user interface presents available options to define the target element behavior such as importing an empirical data set, defining an analytical model, or connecting a CAE model of the target element. Once the target element behavior is defined, engineers set the starting and ending points of actuation, and the design decision manager module evaluates the actuation requirements such as the maximum force and the actuation stroke. After the design problem is defined, engineers set the SMA material behavior by selecting from the options presented on the user interface such as importing an empirical data set, or using a constitutive model. Engineers need to set the behavior of the material which is going to be used for a specific design project by importing empirically characterized material behavior using a specific SMA wire or by setting the model parameters for a specific SMA wire. The next step is to select an SMA architecture which fits to the given design problem. The user interface presents the available SMA architecture options and corresponding Kinematic Actuation Maps to allow engineers to evaluate the feasibility of applying an SMA architecture. Along with the SMA architecture selection, engineers need to make material usage decisions such as the maximum stress and the actuation net strain.

5.2.1.2. Setting device structure

The expert engineer supporting design tool interface presents a list of available device elements with the corresponding design parameters. When a device element is selected, an instance of the selected basic element object is created in the device structure. While engineers set the structure of the actuation device system on the user interface, the evaluation manager module stores the connectivity corresponding to the structure currently in effect. During or after setting the actuation device system structure, engineers select the design parameters of individual device elements and update the instances of the basic element objects through the user interface. The user interface collects and presents the list of design parameters corresponding to the chosen device elements.

5.2.1.3. Planning state sequence and evaluation

Once an actuation device structure is set, engineers plan the state sequence for the overall actuation cycle. If the actuation device system has only one active element, the state sequence is

as simple as ON and OFF (or austenite and martensite). However, if there are more than two active elements, engineers need to plan the state sequence accordingly. Moreover, some actuation device systems, such as ratchet mechanisms, change the connectivity of some elements during actuation depending on the direction of motion and the corresponding active element state. Engineers must update the state-dependent actuation device system structure by reassigning the connectivity, and the evaluation manager module stores the connectivity definition per each state. While updating the actuation device system structure, engineers must place the solution coupling(s) within the actuation device system structure for performance prediction. The user interface searches for all of the potential solution coupling locations, and presents them to engineers to select among. Engineers may select multiple solution coupling locations and/or projection coordinates for the visualization of the actuation device system behavior. This information is stored in the evaluation module, which updates the actuation device system structure corresponding to the states which are in effect while the performance prediction proceeds. The performance prediction results, design metrics, and visualizations of actuation device system behavior generated by the evaluation manager module are presented through the user interface, and the user interface provides an interactive design platform to update the actuation device design using the evaluation results.

5.2.2. Non-expert engineer guiding design tool interface

The non-expert engineer guiding design tool interface provides a series of user interface document panels to guide engineers to create a detailed design. The non-expert engineer guiding design tool consists of four document panels corresponding to the initial design decision and the three sub-steps of the discrete equilibrium design procedure from Chapter 4. Each document panel contains the necessary design information corresponding to each design step, and the later design step panels are activated only after the design decisions from the previous step are made.

5.2.2.1. Problem definition and initial design decisions

The initial design decision step is the same for both the expert engineer supporting design tool and the non-expert engineer guiding design tool. Using the initial design decision panel, non-expert engineers define the target element and the SMA material behavior, select an SMA architecture, and make material usage decisions in the same way as expert engineers in the previous section. However, the SMA material behavior definition may be optional because it may not be an easy task to characterize and/or set constitutive models for non-expert engineers. Instead,

providing a default SMA material behavior with an appropriate safety margin is preferable for non-expert engineers. Once the initial design decision step is completed, the Kinematic design panel is activated to guide engineers to the next step of the design procedure.

5.2.2.2. Kinematic design

The Kinematic design panel presents a list of stroke related design parameters for a given SMA architecture along with the Kinematic Actuation Map. The design decision manager module collects the list of stroke related design parameters and generates the Kinematic Actuation Map for a given individual SMA architecture. Engineers select the design parameter values which can produce the required stroke under the actuation net strain material usage decision. The design decision manager module updates the actuation device system, and asks the evaluation manager module to verify the actuation stroke related design parameter decision.

5.2.2.3. Kineto-static design

The Kineto-static design panel is activated when the Kinematic design panel step is completed, and it presents a list of force related design parameters for the given SMA architecture. Once engineers make design decisions regarding the force related design parameters, the design decision manager module updates the actuation device system and asks the evaluation manager module to evaluate the design metrics and generate the actuation device system behavior visualization. While there are many lumping and projection options available for behavior visualization, it is desirable to limit the solution coupling location and the projection coordinates to the natural coordinates of the target element. If a bias macro modifier element is needed, the Kineto-static design panel presents the Bias Design Map created by the design decision module specific to the device structure and design parameters currently in effect to help engineers select a bias spring.

5.2.2.4. Thermo-mechanical design

The Thermo-mechanical design panel is activated following the Kineto-static design step, and it presents a set of diameter and number of wire combinations, which satisfy the total cross-sectional area of SMA wires selected during the Kineto-static design step. The cooling time for each wire diameter is evaluated and presented along with the diameter / number combinations to help engineers to make a design decision. Once the diameter and number of SMA wires are selected, the minimum electric current and voltage to reach the target heated SMA wire

temperature to ensure full transformation to the austenite state is computed and presented. Heating time evaluation using a range of currents and voltages above the minimum values is useful to provide reference metrics to engineers to select heating parameters. Once a detailed design is completed to produce the required actuation, the expert engineer supporting design tool is activated to allow engineers to further explore the design space.

5.3. Design decision manager module

The design decision manager module manages the design procedure steps, updates the user interface and actuation device system, initiates the performance evaluation through the evaluation manager module, and generates design space visualizations such as the Kinematic Actuation Map and the Bias Design Map. During the initial decision stage, the design decision manager module creates the target element behavior visualization to set the starting and ending points of the actuation, evaluates the maximum force and actuation stroke requirements using the set starting and ending points, and generates the Kinematic Actuation Map for a given SMA architecture.

For the Kinematic design step, the design decision manager module updates the user interface and the actuation device system to limit the design scope only to the actuation stroke. The total cross-sectional area of the SMA wires is set by the design decision manager to match the maximum austenite stress material usage decision. A dummy target element instance is created with a constant force load using the maximum required force determined during the initial design decision stage, and an interface element instance is automatically created to match the actuation starting and ending points which were set during the initial design decisions. With the dummy target element and the interface element, the design decision manager assigns the connectivity for a basic actuation device system structure, and provides a default martensite-austenite-martensite state sequence to the evaluation manager for actuation stroke evaluation.

When the design tool transitions to the Kineto-static design panel, the design decision manager module terminates the dummy target element instance, and reassigns the connectivity to the real target element instance. While engineers make design decisions regarding the force related parameters, the user interface overrides the SMA architecture parameters with the user-selected parameters. During the Kineto-static design step, the design decision manager module generates the Bias Design Map using the method stated in Section 4.2.2. The design decision manager can be connected to a mechanical spring supplier database to show the commercially available options

for the bias reactive element, and a filtering function can be used to narrow down the options based on available packaging space.

The design decision manager module generates a set of diameter and number of wire combinations, and the cooling time for each wire diameter is evaluated. After engineers select a particular combination, the design decision manager module evaluates the minimum electric current / voltage to reach the target heated SMA wire temperature to ensure full transformation to the austenite state.

5.4. Evaluation manager module

The evaluation manager module predicts the actuation device system performance by aggregating the system model and finding the force balance at the solution coupling, evaluates the design metrics, and generates device behavior visualization. For performance prediction, the evaluation manager module stores the state sequence information and corresponding state/direction dependent device elements and system structure, and updates the actuation device system throughout the overall actuation cycle.

The evaluation manager stores and manages the state sequence for the overall actuation cycle, and the corresponding state/direction dependent device elements and system structure. The state sequence is defined by engineers through the user interface, or the design decision manager module provides a pre-set default state sequence. In the case of an engineer-defined state sequence, engineers are able to update the actuation device system structure per each state, and select among the functions associated with direction-dependent device elements such as friction and/or asymmetric target element behavior. Engineers place solution coupling element(s) per each state in the actuation device system, and select projection coordinates. Following the state sequence defined, the evaluation manager module reassigns the connectivity corresponding to each state, and assigns the state to the actuation device system structure currently in effect. Each time the evaluation manager reassigns the state and connectivity, the solution coupling element(s) perform an integrity check verifying that the actuation device system is solvable.

The solution coupling evaluates the force balance equilibrium after checking the integrity of the actuation device system structure. The actuation stroke is evaluated by finding the force balance difference between the states. Once the actuation per a single step is evaluated, the evaluation manager updates internal variables of any necessary device elements such as an offset

update modifier element (ratchet mechanism) which accumulates the overall actuation stroke and keeps track of the rack advancement to update the interaction between the SMA active element and the target element. The evaluation module then repeats the state sequence, and evaluates the actuation stroke to determine the completion of the overall actuation cycle. If a step actuation does not produce any stroke or the overall output stroke is the same as the previous step, and all the internal variables remain the same, the evaluation module stops the performance prediction, and evaluates all the design metrics and generates the actuation device system behavior visualization.

The system behavior visualization is created by first overlaying two behavior curves at two input ports of the solution coupling, and then overlaying the system behavior curves of each state together. The visualization curves are then projected to the projection coordinates by transforming through the intervening modifier elements, which may not be the same as the behavior modifier transformations.

5.5. Actuation device system modular structure

The actuation device system modular structure consists of instances of device elements and solution coupling element objects. There is a library of available device element objects with pre-defined behavior definitions or transformations, and the user interface and/or the design decision manager module create and terminate the instances of device elements, and the evaluation manager module manages the instance of the solution coupling element object. The actuation device system structure is created by assigning the port connectivity of the individual instances, which is managed manually by engineers (expert interface) or by the design decision manager module (non-expert interface) through the evaluation manager module.

5.5.1. Basic element objects

Basic element objects are defined to represent the basic elements of the actuation device system. Depending on the type of basic elements they represent, individual basic element objects have functions defined for active/reactive behavior definition, modifier element transformation, and behavior flow synchronization at compatibility couplings, and, some modifier element transformations (irreversible modifier element transformations) impose restrictions on the placement of the solution coupling element. Each basic element object has a different number of ports depending on the element type; active/reactive element objects have one port, modifier

element objects have two ports, and coupling element objects have three or more ports. Each port is assigned to connect to some other port in a different basic element object.

5.5.1.1. Active and reactive element objects

An active/reactive element object has functions to define the effort-position behavior. While there are various ways to define the effort-position behavior, the main role of an active/reactive element object in the actuation device system is to initiate the effort-position behavior flow through its port. An instance of an active element object contains multiple state-dependent effort-position behavior definitions, and the particular effort-position behavior to output through the port is chosen by the state assigned by the evaluation manager module. An instance of a reactive element object may have two direction-dependent effort-position behavior definitions. The direction-dependent effort-position behavior is coordinated with the state of the active element object by engineers through the evaluation manager module.

There are three types of methods to define the effort-position behavior of an active/reactive element object. One method is to import an empirical representation, where the effort-position relations in array form are stored in the instance of the active/reactive element object. This method is useful for importing empirically characterized active/reactive element effort-position behaviors such as the stress-strain behavior of SMA (wire), force-elongation behavior of SMA helical springs, or force-deflection behavior of target elements. While it is only applicable to the discrete states for which the behavior is empirically characterized, and limits the application of some design methods, this method allows the use of the design framework before the development and/or implementation of analytical models for particular active/reactive elements. Another method is to use an analytical model implementation, where the effort-position relation is generated using an analytical model for an active/reactive element. The benefit of this method is that the instances of active/reactive element objects using this method can generate intermediate state behavior such as the SMA stress-strain behavior at temperatures between the austenite start and austenite finish temperatures during the heating cycle, for example, to decide upon the heating current cutoff level. The other method is to use connectors for computer aided engineering (CAE) models, where the active/reactive element object provides an interface for CAE pre-simulation and stores the results. This method is similar to the empirical representation method, and it is useful for working with target element CAE models which allow engineers to change the target element design parameters

and update the behavior evaluation. This active/reactive element object needs to be implemented for each CAE software platform.

5.5.1.2. Modifier element objects

A modifier element object defines the transformation of effort-position behavior from input port to output port. The modifier element has two ports, and they are assigned as one input port and one output port by the evaluation manager module when the solution coupling is placed. Depending on the solution coupling placement, the input port and output port are interchangeable except for directional modifier element objects (irreversible modifier elements - heterogeneous geometric modifier elements and heating current cutoff modifier elements). In general, a modifier element object contains four transformation functions: two functions for one direction, and two for the opposite direction. However, heterogeneous geometric modifier elements have two equations for complete transformation in one direction, but the other two equations are only reference transformations for some representative distributed effort-position behavior for visualization projection. Similarly, the heating current cutoff modifier element has reverse transformations only for projection. The solution coupling also needs to check for directional modifier elements because the solution coupling cannot be placed between the active/reactive element and a directional modifier element. The evaluation manager module must keep track of the modifier elements' direction assignment because the projection method may require the reversal of modifier transformations.

5.5.1.3. Compatibility coupling objects

Compatibility coupling objects merge multiple effort-position behavior inputs into one output. The input and output ports are assigned by the evaluation manager module when the solution coupling is placed. The compatibility coupling object functions are defined to merge the forces from multiple inputs while the deflections are synchronized. However, the ranges over which the input effort-position behaviors are defined may not match; the compatibility coupling object needs to know whether each input deflection range was set to reflect the motion constraint of the physical elements or just set arbitrarily (for active/reactive elements which use the analytical model implementation method). For the former case, the deflection range should be restricted to reflect the physical constraint. For the latter case, the deflection range should be extended to match the deflection range of the other behavior flows.

5.5.2. Solution coupling object

The solution coupling object performs an integrity check of the actuation device system structure, finds the force balance equilibrium at each state, and works as an intermediate connector between the instances of the basic element objects in the actuation device system structure and the evaluation manager module. The solution coupling is placed through the evaluation manager module by engineers (expert engineer supporting design tool) or by the design decision manager module (non-expert engineer guiding design tool). The placement of the solution coupling determines the behavior flow lumping of a complex actuation device system, which contains one or more compatibility coupling elements.

The integrity of an actuation device system modular structure is evaluated before the solution coupling element object finds the force balance equilibrium of the system. An actuation device system should not have any closed loops, which are connected through two or more compatibility coupling elements, because a loop prohibits the evaluation of force balance equilibrium by over constraining the system. The dimension of the connected ports of two elements should match to preserve physical consistency. For example, the stress-strain behavior at the SMA material element should not be connected to the force-deflection port at the target element. All the active instances of basic element objects in the actuation device system should connect to a solution coupling through any intervening modifier and coupling elements. There are certain device elements which cause separation of the actuation device system during operation such as a ratchet mechanism. In such a case, a secondary solution coupling must be placed in the secondary subsystem, which is separated from the primary subsystem.

5.6. Design tool use case examples

The expert engineer supporting design tool in Figure 5.2 has been implemented using MATLAB and applied to several SMA actuation device design projects. Two of them will be discussed in this dissertation as use case examples of the design framework. One example case is a classroom design project of DESC 501/ME 455 Analytical Product Design at the University of Michigan. One team used an SMA helical spring actuation device driven ratchet mechanism to implement an automated vent for home air conditioning systems. None of the team members had prior experience with SMA actuation device design, and the team followed the three-step discrete equilibrium design process using the expert engineer supporting design tool as an alternative to

the non-expert engineer guiding tool which has not been implemented. The other example case is an automotive vehicle component development project, where engineers identified manufacturing issue of a prototype to debug the design. For this case, the engineers had extensive experience in SMA actuation device design, and they created a final detailed device design without the help of the design tool. However, the prototype did not operate as designed, and the design tool helped to identify the issue, and to communicate with suppliers.

5.6.1. Non-expert engineer use case: classroom design project

The goal of the whole project was to create *“Smart automated vent registers (Figure 5.4) for home HVAC systems to allow home owners control over temperature on a room-by-room basis.”* For the automated vent, the team used an SMA helical spring actuation device because it has *“the benefits of being simple, lightweight, compact, and inexpensive with silent operation.”* The project is summarized in this section with direct quotes from the team report [4] indicated using italic fonts.

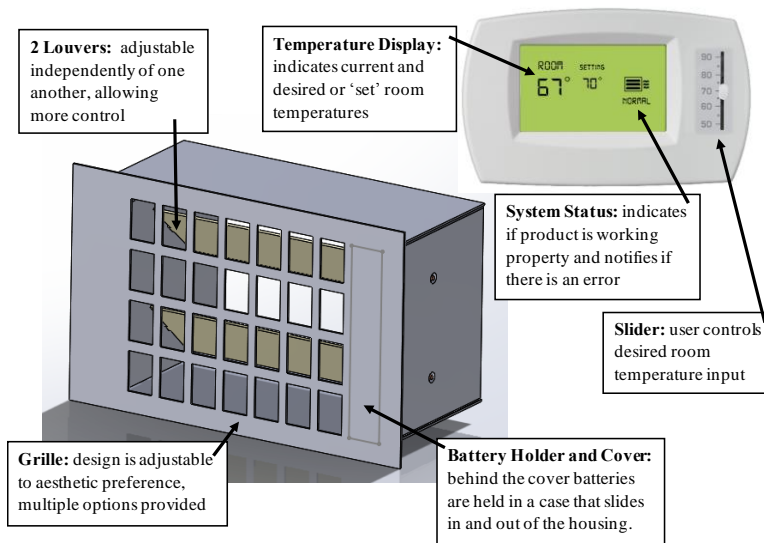


Figure 5.4. Concept of Smart Vent [4].

“The smart register design consists of two main components: the control panel interface and the automated vent installed into the wall or floor. The control panel interface is mounted in the room and houses a temperature sensor and Bluetooth transmitter. The user inputs a desired room temperature using a continuous slider and a screen displays the current and desired room temperatures, as well as, the system status that warns the user of any error or if the batteries need to be replaced. The automated vent opens or closes the louvers a certain amount based on instructions sent wirelessly through Bluetooth transmitters from the control panel.”

For the first step of the design process, the team selected a rotary ratchet mechanism (Figure 5.5) to actuate the vent louver. The operating concept of an SMA driven ratchet system is explained in depth in Appendix B.

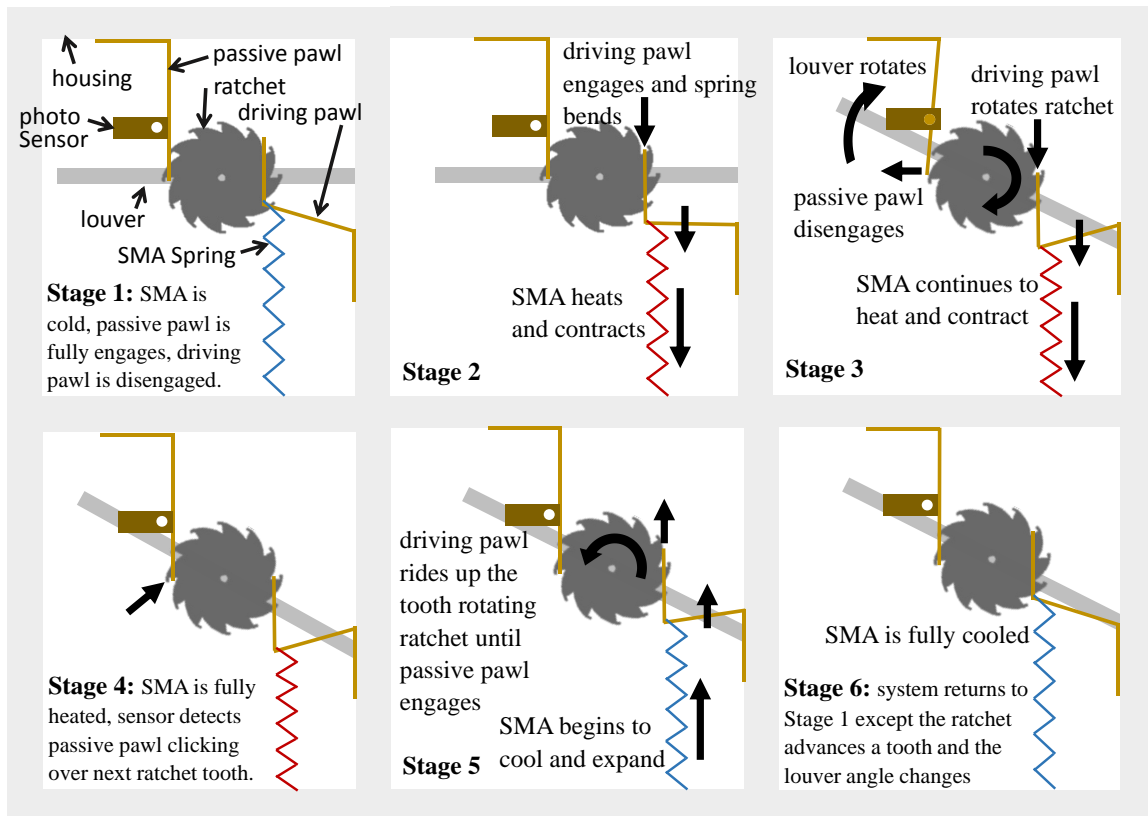


Figure 5.5. Operation of SMA helical spring driven ratchet and pawl mechanism [4].

While it was possible to design the entire ratchet mechanism following the design process in Section 4.4.3, the team simplified the design problem by setting a macro target element including the ratchet mechanism. Because the continuous rotary ratchet does not require the full ratchet mechanism design process accounting for a variable target element force during the overall actuation cycle, the design problem can be simplified to a single actuation stroke problem since each actuation step is identical. The team built a prototype of the automated vent except for the actuation device portion, and empirically characterized the target element behavior (Figure 5.6).

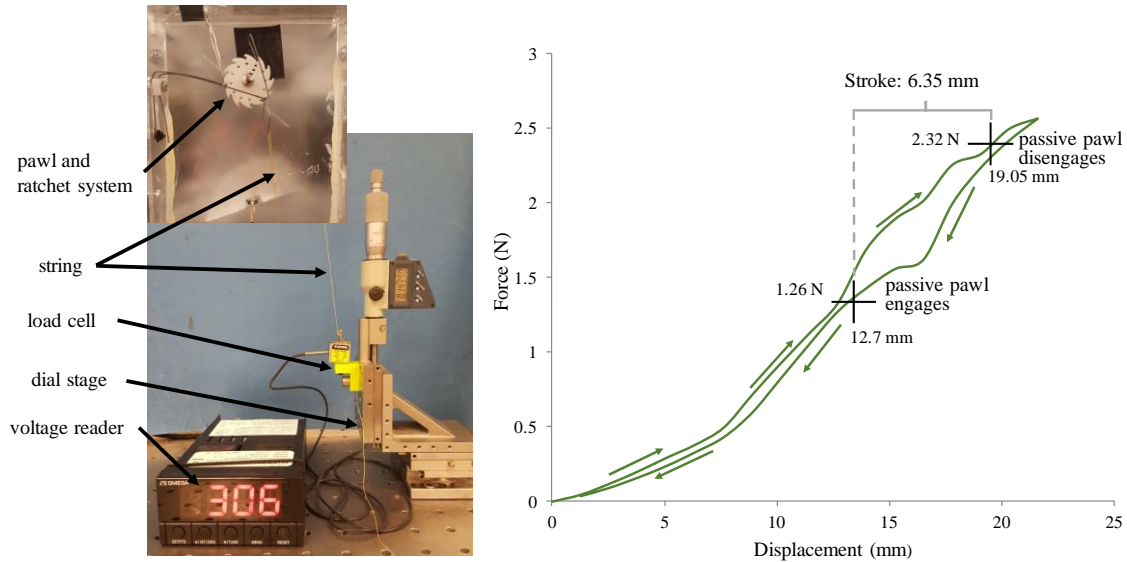


Figure 5.6. Target element behavior characterization setup and the result [4].

The team simplified the design problem by setting the macro target element including the ratchet mechanism. The team built the prototype of the automated vent except for the actuation device part, and empirically characterized the target element behavior.

While the non-expert engineer guiding tool was not implemented, the expert engineer supporting tool was provided with external in-person guidance equivalent to the three-step discrete equilibrium design procedure. The team created an initial design with the help of the expert engineer supporting design tool for performance prediction of the actuation device system (Figure 5.7). While the initial design barely produced the required stroke to actuate the louver of the automated vent, the team improved the design to ensure enough safety margin of the actuation stroke by adjusting the interface offset and the shape of the driving pawl, which works as a bias element as well. The design tool helped to find the target stiffness of the driving pawl to produce a larger stroke by replacing the actual target element behavior with a dummy linear stiffness target element. In Figure 5.7, the changed green target element curve shows the effect of the modified active pawl shape, and the change of the interface offset from 20 mm to 29 mm can be verified.

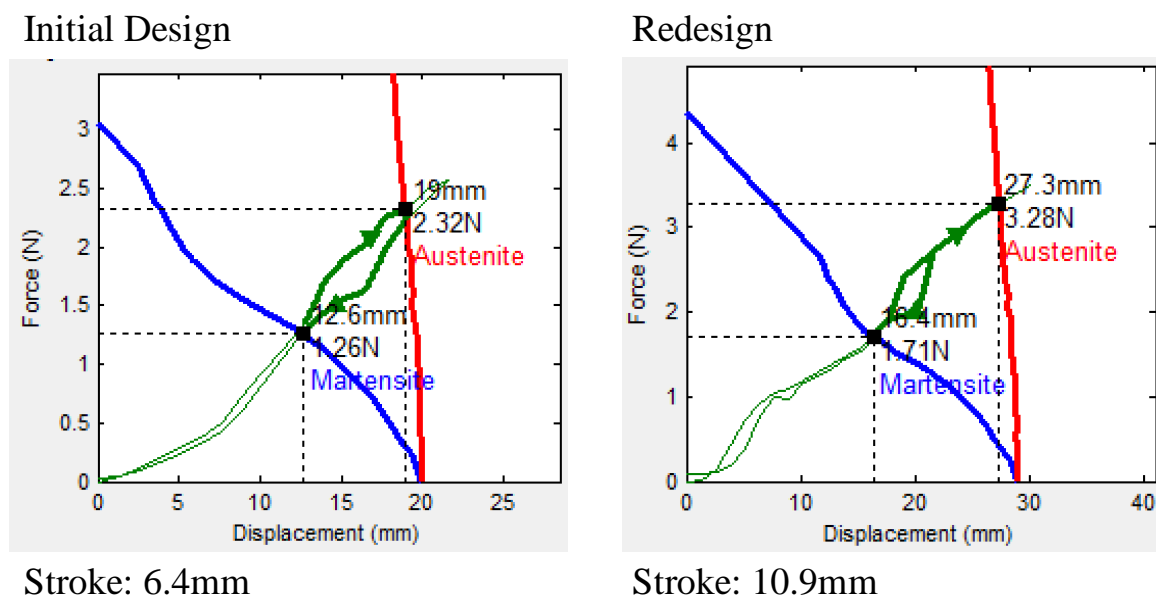


Figure 5.7. Smart vent design improvement using design tool [4].

“The SMA spring and ratchet system used were able to produce enough stroke for actuation. However, the lack of safety factor and robustness caused variability and inconsistency in the actuation and thus proving the initial design as invalid. The results of the experimentally measured actuation forces were compared with the SMA material curves to quantitatively determine more robust characteristics for the SMA spring and ratchet components.”

The redesigned SMA active element for the automated vent is implemented as shown in Figure 5.8, and the actual stroke matched the performance prediction by the design tool. This example demonstrates the usefulness of the design framework, which helped non-expert engineers to create a detailed design of SMA actuation device. Moreover, the team even improved the design with the help of the design framework by finding the desirable stiffness of the driving pawl by substituting the actual target element with a dummy linear stiffness target element. Because the expert engineer supporting design tool was used as an alternative to non-expert engineer guiding design tool with external help through the design process, a non-expert guiding tool is expected to provide better support for SMA actuation device design by non-expert engineers.

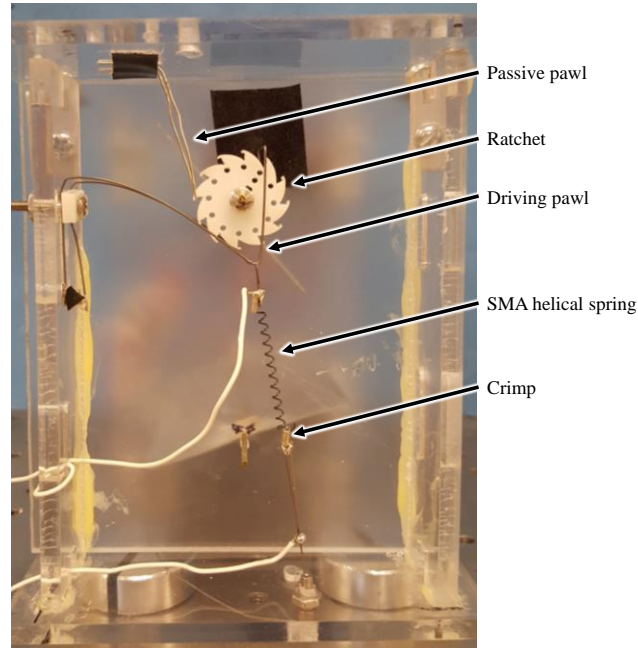
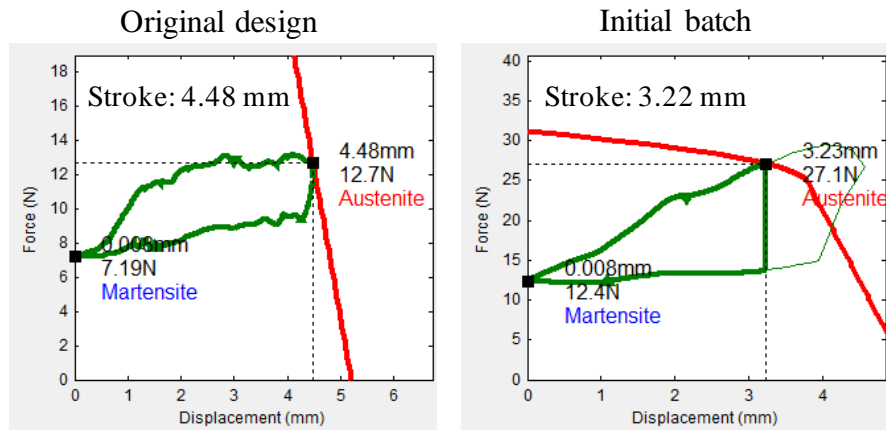


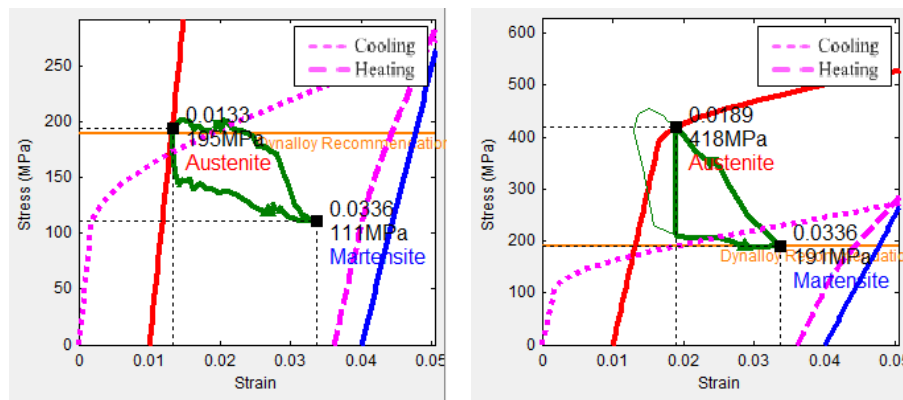
Figure 5.8. SMA helical spring driven ratchet mechanism of Smart Vent [4].
 The redesigned automated vent is implemented, and the actual stroke matched the performance prediction by the design tool.

5.6.2. Expert engineer use case: industrial prototype debugging

An SMA actuated air vent was designed for an automotive application. The initial design was completed by a group of skilled SMA engineers without the help of a design tool. However, when the first batch of devices were produced by a supplier, the flap of the vent did not fully open despite the fact that all the geometric specifications were met at that time. The design engineers measured the force-deflection behavior of both their working prototype and the first batch of products, and used the design tool (Figure 5.2) to investigate the issue (Figure 5.9). In this case, the first batch exhibited additional friction relative to the original design. The design tool predicted the reduced actuation stroke when the first batch force-deflection was imported as the target element, verifying that the larger force caused the issue. The visualization and performance prediction provided by the design tool helped the engineers to identify and communicate the issue with the supplier. Moreover, the additional visualization in the SMA material stress-strain coordinates exposed a potential issue with functional fatigue due to higher than recommended stress in the austenite phase (Figure 5.9b).



a) Actuation device system behavior in target element force-deflection coordinate



b) Actuation device system behavior in SMA material stress-strain coordinate

Figure 5.9. Design tool helped to identify manufacturing issue.

When the first batch of production did not produce the as-designed stroke, design tool helped to identify the manufacturing issue about internal friction between moving parts.

This use case example demonstrates that even an expert engineer group benefits from using the design framework for the evaluation and communication of a design. Moreover, non-expert engineers at the supplier could have used the design tool to identify the manufacturing issue before shipment of the first batch. This implies that diverse stakeholders of SMA actuation device design can benefit from the design framework and its implementation as a design tool.

5.7. Conclusions

The design framework consisting of the device grammar, design methods, and design process makes SMA related technologies more accessible to engineers with different levels of

expertise and roles in device development. A model-based design tool modular platform based on this framework enables the creation of computer-aided design tools to support a variety of design tasks. For example, a non-expert design tool guides engineers through the design process while an expert engineer can be supported by a design tool to more effectively explore the design space. Moreover, such tools support diverse visualization options tailored for individual stakeholder groups. The model-based modular design tool platform can be easily expanded not only to incorporate future material and architecture models for SMA actuation devices, but also to create design tools for different types of actuation devices other than SMAs because it is structured following the generalized actuation device structure.

5.8. References

- [1] Park, J.-K., and Washington, G., 2011, “Advanced Development of a Smart Material Design, Modeling, and Selection Tool,” ASME 2011 Conference on Smart Materials, Adaptive Structures and Intelligent Systems, ASME, Scottsdale, Arizona, USA, pp. 675–684.
- [2] Luntz, J., Barnes, B., Brei, D., Alexander, P., Browne, A., and Johnson, N., 2009, “SMA wire actuator modular design framework,” SPIE, San Diego, CA, USA, pp. 729008–12.
- [3] Meier, H., and Czechowicz, A., 2012, “Computer-Aided Development and Simulation Tools for Shape-Memory Actuators,” *Metall. Mater. Trans. A*, **43**(8), pp. 2882–2890.
- [4] Molepske, M., Braciszewski, V., Butler, J., Caputo, G., and Cheng, F.-N., 2015, *Smart Automated Vent Register Using an SMA Spring Actuated Rotary Ratchet*, University of Michigan, Ann Arbor.

Chapter 6.

Conclusions

The main goal of this research was to develop a systematic design framework for SMA wire device design that incorporates the grammar, design methods, and design process to enable engineers of different backgrounds to make efficient design decisions in different stages of the design process. Four key objectives were accomplished to realize this goal:

1. **Grammar:** Defined a reference SMA device hierarchical structure by establishing an actuation device grammar including basic and macro elements and connectivity rules to set up a common language and enlighten non-expert engineers about necessary elements and their structure.
2. **Methods:** Formalized design methods for modular modeling, model aggregation and performance prediction, and visualization to support design decisions to examine and evaluate the effect of device elements and design parameter variations to serve diverse groups of stakeholders.
3. **Process:** Formalized a design process over various stages of SMA device design to support appropriate decision making with necessary precision at each stage to ensure better design quality, expedite the design cycle, and enable design automation.
4. **Framework:** Created and demonstrated an expandable model-based design tool software platform and user interface that systematically organizes and presents device grammar, design methods, and design process for diverse expert and non-expert stakeholders.

The results from the grammar, methods, and process enabled the creation of the design framework and its implementation as a model-based design platform, which allows the creation of software design tools to support engineers to make design decisions to create a detailed design by organizing and presenting SMA design knowledge. In this chapter, the summarized research results and contributions are discussed. Future research directions to extend the design framework are also suggested.

6.1. Research summary and contributions

To achieve the goal stated, individual areas of research issues in device grammar, design methods, and design process were addressed, and the design framework consolidated these three areas. A device grammar was defined to describe actuation device structures, and a reference SMA actuation device hierarchical structure was created to describe most SMA actuation devices. Design methods for modeling, performance prediction, and visualization were formalized using the device grammar and the reference SMA actuation device structure to support design decisions. A design process was established to guide engineers to create a detailed design of an SMA actuation device. A design framework was created to systematically organize and present device grammar, design methods, and design process, and to be implemented as software design tools.

6.1.1. Device grammar

To set up a common language to discuss actuation device systems including SMA actuation device systems, a device grammar was defined which is useful for actuation device system design. While other modular system methods focused on system engineering or dynamic system modeling, the device grammar defined in this study focuses on device design. The device grammar helps the design of an actuation device system by providing a foundation to understand the system structure, identity the device elements and their design parameters, and discover possible design options. For this purpose, the emphasis was placed on the connection between the physical device elements and their representations.

Basic elements were defined as building blocks for actuation device structures. Active elements initiate actuation by changing their effort-position behavior upon an input signal change. Reactive elements respond to a stimulus following their effort-position behavior. Modifier elements transform an input effort-position behavior into a desired effort-position output behavior. Coupling elements provide mechanical connection between three or more elements providing

position behavior synchronization of multiple behavior flows initiating from active and/or reactive elements. Macro elements allow flexible grouping of meaningful conceptual sets of basic elements. These basic and macro elements are connected together following a set of connectivity rules to preserve the behavior flows. The actuation device structure expressed using the grammar defined captures the physical connections and interactions between the device elements.

A reference SMA actuation device modular structure is standardized using the actuation device grammar. The typical SMA actuation device has two macro elements: an SMA active element and a device modifier element. The SMA active element initiates actuation by changing material behavior upon its temperature dependent phase change. The SMA material stress-strain behavior is transformed into force-deflection output behavior through an SMA architecture. The force-deflection behavior of the SMA active element is further transformed to a desired force-deflection output behavior of the SMA actuation device by the device modifier element, which consists of a series of sub-elements such as bias elements, stroke limiters, mechanical leverage, and ratchet mechanisms. This reference SMA actuation device represents most SMA actuation device system structures.

The device grammar and diagrammatic representations defined in this study provide a simple but effective method to document, communicate, evaluate, assess, double check, and regulate actuation devices. The device grammar helps in understanding actuation device systems by categorizing the device elements in an actuation device system into the three types of basic elements, and helps to identify the design variables of each element. Moreover, the device grammar and the device structure capture the relationship between the physical device elements, and provide the means to check the integrity of an actuation device system by applying the connectivity rules. Furthermore, the modular nature of the device grammar enables the modular modeling of actuation devices, which can improve the reusability of the outcomes of the previous design research for future design projects. Engineers can apply the concept and models of macro and/or basic elements from previous research to their design projects using the modular structure.

The reference structure enables a framework to generate design concepts of SMA actuation devices by providing a starting point to modify the actuation device structure, and helps the education of non-expert engineers on typical SMA actuation device systems. A set of common SMA actuation device elements, which were defined with the reference system, provides a

common language for typical basic elements of SMA actuation devices. These formalized basic elements help engineers to understand the role and common usage of typical device elements, and enable exploration of design options by allowing engineers to check possible device elements. Moreover, the unified terminology for SMA actuation devices helps collaboration between design groups and/or stakeholders of SMA actuation device design.

6.1.2. Design methods

Design methods are formalized to support diverse sets of stakeholders to make design decisions by providing the means to model actuation device systems, predict the system performance, and visualize the system behavior. To overcome the limitations of previous performance prediction methods, the emphasis of the design methods in this study was placed on the evaluation and presentation of the effects of individual device elements and their design parameters on the actuation system behavior. By taking advantage of the modular SMA actuation device system hierarchical structure, the modular modeling approach exposes the effect of individual device elements and ensures reusability of the individual macro and/or basic device element models.

The modeling approach for each basic element type is formalized to provide guidelines for modeling. The active and reactive element models define the effort-position behavior(s). The modifier element models define the transformation of an input effort-position behavior to an output effort-position behavior. The coupling element models define the synchronization of the multiple behavior flows. The modeling approaches for commonly used SMA device elements and SMA architectures are suggested. The categorization and the corresponding modeling approaches for SMA architectures provide guidance to engineers for modeling and expose the limitations of applying the performance prediction method. Modeling approaches for commonly used device modifier elements educate engineers about the general effect of each device element on system behavior, and help to select appropriate device elements for an actuation device design project.

A solution coupling, where the force balance is found for performance prediction, is placed in an actuation device system as a special type of coupling element. The placement of the solution coupling determines the behavior flow grouping and the corresponding model aggregation for the force balance prediction. While both discrete equilibrium performance prediction and integrated transient behavior prediction approaches evaluate the actuation device system behavior at the

solution coupling, the placement of the solution coupling is more important for the integrated transient behavior approach because the evaluation results are bound to the coordinates of the solution coupling location.

However, with the discrete equilibrium performance prediction approach, grouping of the behavior flows enables visualization of the actuation device behavior that exposes the effect of individual macro or basic elements on the actuation performance. The behavior visualization can be further tailored to support diverse sets of stakeholders by projecting the performance prediction from the solution coupling to other coordinates in the actuation device system. These systematic design methods expose the effects of individual device elements on the actuation device system behavior, provide design metrics to select the design parameters of individual elements, and prevent potential design iteration by exposing the individual element effects. By applying these design methods, a diverse group of stakeholders including design engineers can make better design decisions using model-based design evaluation and visualization of actuation device behavior tailored for individual stakeholder groups and design tasks.

6.1.3. Design process

A multi-stage design process is formalized to guide engineers to create a detailed actuation device system design by addressing design tasks in the sequential stages of the SMA device design cycle. The first stage is the initial design decision stage where the feasibility of applying SMA wire actuation is evaluated, material usage decisions are made, and an appropriate SMA architecture is selected to produce the required force and stroke. The second stage is the discrete equilibrium design stage where a detailed SMA device design is generated using quasi-static equilibrium assumptions. A three-step design procedure of the discrete equilibrium design stage is formalized which can guide non-expert engineers to create a concrete detailed design of an SMA device. The third and last stage is the integrated transient behavior evaluation stage where the interactive transient behavior of the SMA device and the target element is evaluated. The formalized multi-stage design process helps engineers create a good detailed design by presenting necessary design decisions to make at each stage. The multi-stage design process allows engineers to work with models of different types and resolutions at both high and low levels of detail.

The design process for the discrete equilibrium design stage is further formalized as a three-step design procedure: the Kinematic Design step, the Kineto-static Design step, and the Thermo-

mechanical Design step. In the Kinematic Design step, the actuation stroke related design parameters are selected using the material usage decisions which were made during the initial design decision stage, and the free clearance is set for the desired actuation positions. Kinematic Actuation Maps are created as a design method for individual modifier elements to support the design decisions in this design step. In the Kineto-static Design step, the force related design parameters are selected such as the SMA wire total cross-sectional area under the set maximum allowable stress. During this Kineto-static design step, the device bias can be designed to meet the material usage decisions such as the martensite transformation temperature and stress. A Bias Design Map is devised as an additional design method to support the bias spring selection. In the Thermo-mechanical Design step, the number and diameter of SMA wires are decided based on the selected cross-sectional area considering the heating and cooling time, and device operation parameters such as power and cooling medium are determined and evaluated.

The three-step discrete equilibrium design procedure prevents potential iteration by decoupling the force and stroke of actuation output behavior, and hides the complexity of material and SMA architectural models from engineers while still exposing the impact of design parameters. For example, the non-linear leveraging of the web geometry makes the design of SMA web actuators difficult because accounting for stroke and force requirements often requires an iterative process. However, by following the discrete equilibrium design procedure, engineers can create a detailed design by designing for stroke and force in an order that addresses the coupling of design variables without requiring an iterative process. Moreover, this sequential design procedure helps engineers to overcome the complex non-intuitive relationship between design parameter variations and actuation performance changes by guiding engineers to select values for only the appropriate design variables at each step. Furthermore, the formalized systematic design process provides a foundation to automate the design process.

6.1.4. Design framework

To make SMA design knowledge accessible to engineers, a design framework is created as a systematic foundation to organize and present the device grammar, design methods, and design process. For implementation of the design framework as software design tools, a model-based design tool modular platform is created which is structured with four major functional modules: the actuation device system modular structure, the evaluation manager module, the

design decision manager module, and the user interface. The actuation device modular structure, the evaluation manager module, and the design decision module are implementations of the device grammar, the design methods, and the design process respectively. The device modular structure consists of instances of basic element objects which work as building blocks of the device structure. Individual elements are aggregated as a device structure by engineers and/or the design decision manager module through the evaluation manager module by setting the port connectivity of individual elements. The evaluation manager module predicts the performance of the actuation device system through the solution coupling in the device modular structure, evaluates design metrics for the design comparison, and generates behavior visualization using grouping and projection to support diverse design tasks and stakeholders. The design decision manager module guides non-expert engineers to create a detailed design by updating the user interface and actuation device system modular structure to present and manage the three-step discrete equilibrium design procedure. The user interface provides a software user interface to set the device structure, select the design parameters, and present the performance prediction results. The model-based design tool modular platform provides a framework to consolidate future material and architectural models, and is applicable to other types of actuation device systems.

Two types of implementations are designed: an expert engineer supporting design tool, and a non-expert engineer guiding design tool. The expert engineer supporting design tool makes design methods available to engineers to help make design decisions. The expert engineer supporting tool is highly related to the evaluation manager module, which manages performance prediction, design metric evaluation, and behavior visualization. The expert engineer supporting tool allows engineers to explore the design space interactively by trying design options with real-time design evaluation and visualization feedback. The non-expert engineer guiding design tool presents design decisions to make in each step of the discrete equilibrium design procedure, and proceeds to the next step by updating the user interface following the design process. This design procedure is managed by the design decision manager module, which updates the user interface and the actuation device system modular structure. The non-expert engineer design tool guides engineers to follow the design procedure to create a good detailed design without requiring in-depth knowledge on complex SMA actuation device design. An example design tool has been applied to both academic and industrial projects, and the tool helped non-expert engineers to create

a functioning detailed design, and expert engineers to identify a manufacturing issue for mass production.

6.2. Future research

The model-based design framework provides an expandable modular platform to accommodate a broad range of future research efforts on actuation device design. Several areas of future research directions are identified to provide guidance for utilizing the design framework.

6.2.1. Additional SMA design methods

Additional design methods for SMA wire actuation devices can be developed and consolidated with the design framework. While the modeling, performance prediction, and visualization methods in Chapter 3 provides general methods to address general design tasks, particular tasks can be addressed more effectively using additional design methods developed for specific tasks. The Kinematic Actuation Maps and the Bias Design Map in Chapter 4 are examples of such methods, but the additional design methods are not limited to these. For example, a conglomerate stabilization curve design method in Appendix C can be implemented into the design tool to present the design method accounting for functional fatigue (shakedown) to engineers. Cyclic shakedown is a well-known issue with SMA actuation devices, and the conglomerate curve design method provides a design method to account for the stroke and strain shakedown of the SMA material. The conglomerate stabilization curves can be implemented as a modifier element to modify the SMA material behavior, accompanying with a stroke limiter, to provide a proper design envelope to account for functional fatigue. Further research on other SMA design issues, such as uncertainties due to the material behavior variation, operation environment, and manufacturing uncertainties, can enhance the design framework.

6.2.2. Comprehensive design process

While a systematic design procedure to create a detailed SMA actuation device design using a given SMA architecture is formalized in this study, the selection of SMA architecture still relies on engineers' experience and/or an iterative process. As a first step of addressing this design task, an SMA architecture Suggestion Map (Figure 4.2) is created to provide a qualitative support on selecting among various SMA architectures to produce the desired force and stroke. However, it is far from a rigorous systematic design procedure. Further research can focus on the creation

of quantified methods and a procedure for SMA architecture selection, and it will enable the completion of the fully systematic multi-stage design process, which includes the feasibility assessment, material usage decision, and comparison with other actuation device options.

Another future research topic for the design process is a *constraint-driven* design process. The design process presented in this dissertation is a *performance-driven* design process, where the design process proceeds to meet the desired actuation performance such as stroke, force, and actuation time. However, design problems of real world applications are often constrained heavily by geometric packaging constraints to avoid interference between moving parts, and to be installed in a limited packaging space. Future research on constraint-driven design processes can help engineers to address these design problems systematically.

6.2.3. Expand to new smart materials and architectures

The design framework can be further expanded to support the design of actuation devices using other smart materials. Although the design tool platform can be directly applied for actuation device design using other smart materials, there are several modules requiring further research. The design process needs to be tailored for individual materials, and the design decision manager module needs to be updated following the tailored design process. The evaluation manager module needs to have evaluation methods specific to individual smart materials. Moreover, reference actuation device structures and typical basic elements for individual smart materials need to be defined along with the modeling for individual basic elements.

However, the modeling of basic elements for new materials does not have to be done at once. By applying the concept of macro elements for modeling, the macro element models can be first implemented using empirical behavior representations, and later replaced with detailed sub-elements models when such models become available. For example, a NEW actuator can be implemented as a macro active element using empirical representations to capture its behavior, before the full development of a NEW actuator model, which has all the geometric design variables as model parameters. The full model of a NEW actuator can be implemented when the model is completed to provide more design options. Meanwhile, engineers can design actuation device systems using NEW actuators by applying the macro element, although engineers do not have full flexibility of changing all design variables. For example, the current example design tool includes SMA helical springs (new SMA architecture), and dielectric elastomer (DE) tape actuators (new

smart material), and provides a limited scope of design methods for performance prediction and visualization. The current implementation of SMA helical springs and DE tape actuators use empirical behavior representations of the force-stretch ratio and force-deflection respectively. However, when detailed models including more design variables are developed, the design tool can provide more flexible design options by implementation of the detailed models.

6.3. Closing

This research was started to create a software design tool to accelerate the acceptance of SMA technology. One of the issues with the adoption of SMA technology is there are not many engineers who know how to design SMA actuation devices. The project was launched to address this issue using a software design tool to support non-expert engineers to create a detailed design. However, in the process of developing and distributing the software design tool, the need for a further formalized design framework was identified. Three areas of design research to support the design framework, device grammar, design methods, and design process, were identified while adding new features and new SMA architectures to the design tool.

The study of design has been formalized by structuring it into four major areas. While many previous research efforts claimed to be “Design Tool” studies, most of them focused on an analysis tool (a method) to finalize a detailed design. While it is important to create design methods to address design tasks, making these design methods to available to engineers is also important to support engineers to make design decisions. This study formalized the design framework, which consists of the device grammar, design methods, and design process. This formalization extended the scope of the design tool study from a method to address a certain design task to a holistic framework to systematically organize and present the design knowledge to engineers.

The model-based design framework, which was developed in this study, streamlines the acceptance of SMA actuation in the real world by helping engineers to create a detailed SMA actuation device system design. By providing a framework to organize and present the design knowledge of new smart materials and structures, the model-based design framework accelerates the transition of new actuation technology with a wide range of smart materials and structures from the research community to real world applications.

Appendix A.

Model-based design process for the shape memory alloy web actuator architecture

Designing Shape Memory Alloy (SMA) actuators to produce motion normal to a shallow packaging form factor is challenging because SMA wires produce motion along their length. One actuator architecture that exploits the wide space within a shallow package is the SMA wire web, which zigzags along the width between the two surfaces to generate stroke amplification normal to the surfaces. This paper presents a formalized design process and parameter studies which enable the synthesis of SMA web actuators using a discrete state quasi-static force-deflection model. The model-based design process consists of three steps: 1) a kinematic design step for feasibility evaluation and to select geometric parameters to obtain the required stroke using an actuation map, 2) a kineto-static design step to select wire cross-sectional area to produce a required force, and 3) a thermo-mechanical design step to select cycle time related parameters such as diameter and number of SMA wires, heating current, and environmental medium. Parameter studies are presented that expose the effects of web geometry (width/gap ratio), SMA material properties (initial two-way strain), and external system characteristics (stiffness). The discrete state quasi-static force-deflection model and parameter studies provide a basis to synthesize the web actuators for best actuation performance for constrained shallow form factor applications.

1. Introduction

There are many applications that require actuation motion in the direction normal to the longest packaging dimension. Unfortunately, for most actuators this is difficult to achieve because they generally generate motion along their longest package length. This is especially true with SMA wire actuators which contract lengthwise. A good example of this is aerospace

applications which employ adaptive wing camber for efficient air-flow control for different flight mission states [1,2]. The wide shallow span of the wing is useful for packaging actuators for camber change, however the required actuation is in the chord direction, perpendicular to the span (Figure A.1a). Thus, an additional mechanism is required, such as a scissor mechanism [3] or a linkage mechanism [4], to redirect the stroke of the actuator which resides in the span direction. Another example is an active automotive door seal that adjusts the height of the seal normal to its length to improve seal quality in one state while lowering closing effort in another state (Figure A.1b) [5,6]. Because of the nature of the seal geometry, there is a long package length along the perimeter of the door, but the required actuation direction is perpendicular to the available package length. Packaging issues also exist in medical applications such as a hand held tremor cancellation device which generates stabilization motion normal to the hand grip to aid patients with Essential Tremor (Figure A.1c) [7]. Due to the limited package space within the hand grip, it shares the same shallow packaging problem. These examples are just a few of many across fields where actuation is required normal to a shallow package footprint, with packaging length available in the other direction. A method for solving this difficult packaging issue without the additional weight and bulk of redirection and/or leveraging mechanisms is the Shape Memory Alloy (SMA) web actuator architecture. SMA is a class of materials which

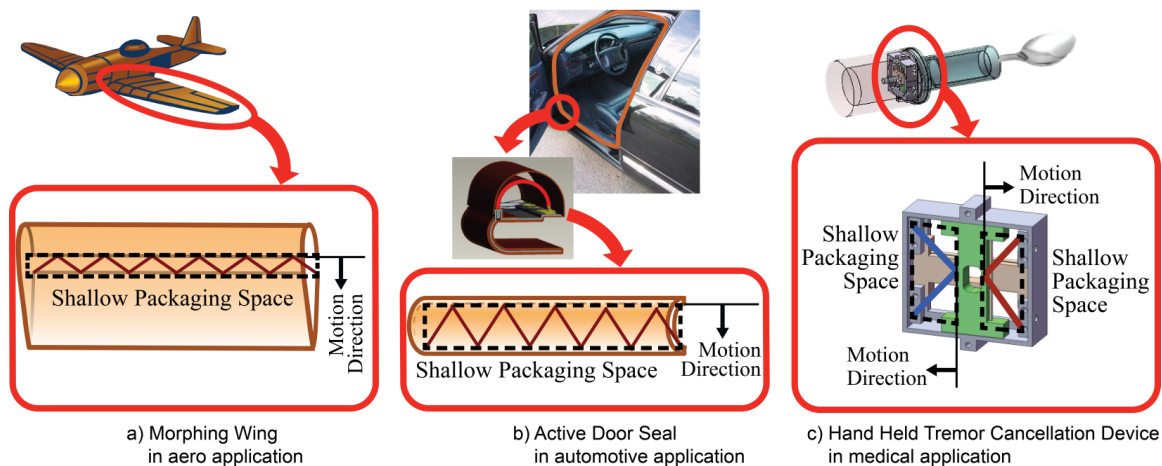


Figure A.1. Shallow packaging challenges.

a) One way to change the camber of a wing is to have a slit and pull the sides of the slit together, where the actuator must fit within this long narrow slit, b) active seals bring two sides together to change stiffness of structure during closing and sealing, which must fit within the long thin door seal, c) for hand held tremor cancellation devices, the antagonistic actuator needs to be packaged inside the handle.

transforms its crystal structure upon temperature and/or applied stress changes, leading to a change in material behavior useful for actuation against an external system. When cool, the SMA in its compliant martensite phase rests in equilibrium, in an elongated position, with the force provided by the external system. When heated, the SMA transforms to the stiff austenite phase, overcoming the force from the external system, contracting to a new equilibrium position. This change in equilibrium position produces linear actuation without the bulky volume and heavy mass of conventional actuators.

While the 2 ~ 4% useful actuation strain of an SMA wire actuator is large relative to many other smart materials, the length of SMA required to produce a certain stroke normal to the package is still an issue for shallow form factors. However, by using the leverage of the web architecture, an SMA wire web actuator can fit into a shallow package, as illustrated in Figure A.1, providing a long stroke perpendicular to its package length. The SMA web architecture arranges the SMA wire in a zigzag pattern between two surfaces. The web pulls the surfaces closer together against an external system force when heated to the austenite phase, amplifying the stroke produced by the SMA wire. The web returns to the extended position under the influence of the external system when cooled to the martensite phase. Thus, the motion generated by the SMA wire arranged along the length of the shallow package is redirected normal to its length through the web without the use of bulky and heavy redirection and/or leveraging mechanisms. There are several examples of applications where the SMA web architecture has been used to overcome the shallow packaging problem. One example is the active automotive door seal [5], shown in Figure A.1b, where an SMA web actuator pulls the free end of a cantilevered arch seal from a soft released state for reduced closing effort to a stiffer constrained state for improved sealing. Another example is the hand held tremor cancellation device [7], where the two opposing SMA web actuators are each arranged within the half of the square packaging space, generating the tremor cancellation motion in the direction normal to the longer package length. While these and others have been successful implementations of SMA web actuators [5,7–10], designs have been generally ad-hoc, and there exists no systematic approach to designing these actuators based on an understanding of packaging and performance tradeoffs.

This paper presents a generalized design process and parameter studies based on a discrete state quasi-static force-deflection model to provide the necessary foundation and insight for the

synthesis of SMA web actuators. The basic SMA web actuator configuration and three state operation mode are introduced along with the design parameters and drivers. A discrete state quasi-static force-deflection model of the SMA web actuator is derived relating the material stress-strain properties to the actuator output force-deflection performance through the geometric relations and external system forces, and validated with a set of experiments. Using this force-deflection model, a formalized three stage quasi-static design process is presented. First, a kinematic design step uses an SMA web architecture Kinematic Actuation Map, which relates actuator performance to packaging and material usage, for feasibility evaluation and the selection of web geometry parameters to produce a required stroke. Second, a kineto-static design step allows the selection of wire cross-section to provide sufficient actuation force through the leveraging of the architecture. Finally, a thermo-mechanical design step determines the cycle time related parameters such as diameter and number of SMA wires, heating current, and environmental medium, using a lumped heat transfer model. Design parameter studies on the SMA web architecture focus on three major aspects of device design to provide a basis for design decisions: web geometry (width/gap ratio), SMA material properties (initial two-way strain), and external system characteristics (stiffness). The design process and the design insight from the parametric studies form a foundation to enable synthesis of compact light weight SMA web actuators in a challenging shallow form factor.

2. Web Architecture

In the SMA web actuator architecture, SMA in wire form is connected between a stationary and a moving surface in a zigzag pattern. The SMA web actuator architecture operates in three states: reference strain-free state, austenite equilibrium state, and martensite equilibrium state (Figure A.2). Actuation is the movement between the austenite equilibrium state and the martensite equilibrium state. The first state, *reference strain-free state* (Figure A.2a), defines the reference width of the web segment (W), gap between the fixed base and the moving attachment point (G), length of the SMA wire (l), and the free clearance (C_0). The free clearance is defined as the relative position between the web and the origin of the external system (simplified here as a spring in Figure A.2), using the heated unloaded wire before they are attached. In the second state, the *austenite equilibrium state* (Figure A.2b), the external system is attached to the web in the austenite phase at an equilibrium position with an austenite

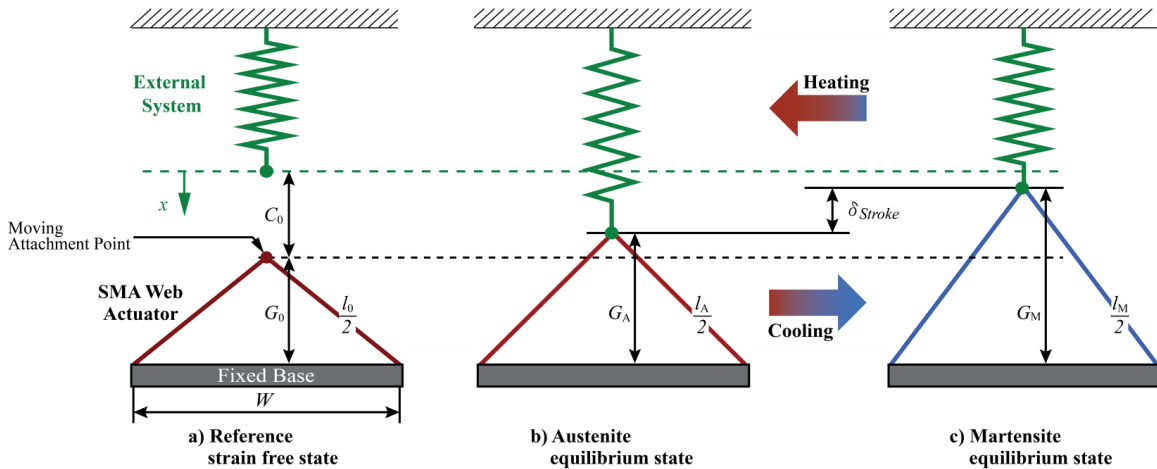


Figure A.2. Operation concept of SMA web architecture.

a) In the reference strain-free state, the initial geometric parameters are defined. b) In the austenite equilibrium state, the SMA wire in the hot austenite phase moves to an equilibrium position when the web actuator is connected to the external system. c) In martensite equilibrium state, the external system stretches the web to an elongated position when the SMA wire is cooled to the martensite phase. By changing the temperature of the SMA wire, the gap changes, producing stroke.

equilibrium gap G_A , where the force from the web balances the force from the external system. In the third state, the *martensite equilibrium state* (Figure A.2c), the SMA wire is cooled to the compliant martensite phase, and the external system force stretches the web to a new equilibrium position with a martensite equilibrium gap G_M . Actuation stroke is defined as the difference in the gaps ($\delta_{Stroke} = G_M - G_A$) when the wire is heated and cooled between the martensite and austenite equilibrium states. The primary benefit of using this architecture is that it exploits the wide length of the packaging space, and amplifies and redirects the stroke of the SMA wire perpendicular to its length without any additional mechanisms.

Designing the SMA web actuator requires the determination of wire geometry parameters (diameter, number, and length of the wire) and the web geometry parameters (width and gap). The SMA wire geometry parameters, *diameter* and *number* (cross-sectional area of the SMA wire) are related to the tension at a certain stress, while the *length* of the SMA wire determines the elongation at a certain strain. These wire geometric parameters must be determined based on the *material usage decisions* (SMA wire net strain and maximum allowable stress) which are made during the device design process considering the expected lifetime and the tolerable material shakedown (degradation over cycles) [11–13]. SMA wire net strain is the net actuation

strain produced by the SMA wire, which is the difference between the hot austenite wire strain and the cool martensite strain. Although the SMA wire net strain can be limited by using strain limiters such as a mechanical hard stop and/or a position-based heating current cutoff switch, it cannot exceed the maximum strain achieved by the SMA material stress-strain behavior without such strain limiters. Therefore, it is important to characterize the material stress-strain properties in the austenite and martensite phases which impose important constraints to make material usage decisions. Moreover, SMAs vary in their coupled stress-strain-temperature behavior depending on the chemistry and the processing of the material [14], and there exist multiple material constitutive models which can be used for the SMA actuator design [15–20]. For the quasi-static design of SMA wire actuators, these model can generate the required material stress-strain behavior in the austenite and martensite phases. It is also possible to experimentally measure the stress-strain behavior in both austenite and martensite phases to use for design.

The SMA wire geometry parameters are coupled together with the web geometry parameters: *width* and *gap* of the SMA web actuator which determines the mechanical leveraging rate through the *width/gap ratio*. These web geometry parameters are constrained by the available packaging footprint which is the main reason to use the SMA web actuator architecture. Because the width/gap ratio determines the stroke amplification rate, to increase the mechanical leveraging from the web geometry, it is desirable to use the entire available package width, and it is possible to make partial use of the available package gap for further leveraging. The coupled wire geometry parameter, wire length, is geometrically constrained by the width and gap of the web. Another wire geometry parameter, cross-sectional area of the wire, is also coupled to the mechanical leveraging determined by the width/gap ratio limiting the maximum allowable stress under applied external system force. This mechanical leveraging is non-linear because the angle between the SMA wire and the output motion direction changes during actuation. To address these complexities, a design model and corresponding design process are required to synthesize the SMA web actuator architecture.

3. Discrete state quasi-static Force – Deflection Model and Experimental Validation

To provide a foundation for an SMA wire actuator design process, a discrete state quasi-static force-deflection model is derived by first relating stress and strain in the SMA wire to force

and deflection at the output of the actuator and then finding the equilibrium between the SMA wire web and the external system force in each state. The actuation stroke is predicted as the distance between the two equilibrium states. Using this state-based force-deflection model, the material conditions during actuation and the actuation performance are predicted to make design decisions during the design process. The model is validated by a set of experiments measuring the actuation stroke of SMA web actuators under load.

3.1. Discrete state quasi-static Force-deflection Model Derivation

The performance of the actuator is characterized as the stroke it produces working against the external system. The discrete state quasi-static model is focused on the transformation of the material stress-strain behavior into the force-deflection coordinates of the actuator output performance, and finding its equilibrium with the external system force-deflection properties. The SMA stress-strain behavior is characterized by two functions: f_{SMA}^M and f_{SMA}^A which represent the constitutive laws for the martensite (M) and austenite (A) phases. The exact functions vary for different types of SMAs, and the form of the functions (analytical vs. numerical, *etc.*). The external system is a mechanical system which is subject to be actuated by the SMA web, assumed to produce a force $F(x)$ as a function of only its deflection x . Being connected to the SMA web actuator, the external system determines both the martensite and austenite equilibrium positions and provides a return force while the SMA wire cools.

Several simplifications have been applied to maintain model tractability appropriate for the device design process. First, friction in the moving parts of the actuator is modeled as part of the external system, which can be accomplished by separating $F(x)$ into two functions; one applied during heating and the other applied during cooling. Second, bending effects at the moving attachment point(s) are ignored, as they have a limited effect on the actuator output for widely packaged web actuators with a large angle. Third, the shape of the web is assumed to be symmetric; while asymmetric webs are possible, they are not desirable due to the uneven stress distribution between the two sides of the web introducing moments in the system.

The stroke of the SMA web actuator (δ_{stroke}) is predicted by finding the distance between the *martensite equilibrium gap* (G_M) and the *austenite equilibrium gap* (G_A), which are the equilibria between the external system and the SMA web actuator in the martensite and austenite equilibrium states,

$$\delta_{Stroke} = G_M - G_A. \quad (1)$$

The geometry of the web (Figure A.2) defines the relation between the gap and the length of the SMA wire, which are geometrically related as

$$G_\chi = \sqrt{\left(\frac{l_\chi}{2}\right)^2 - \left(\frac{W}{2}\right)^2}, \quad (2)$$

where l_χ is the length of the SMA wire, G_χ is the gap between the fixed base and the moving attachment point, and W is the width of the web segment. The subscript χ refers to the state of the actuator; 0 represents the reference strain-free state, M represents the martensite equilibrium state, and A represents the austenite equilibrium state. These gaps in each state are found by relating the SMA material stress-strain properties to the actuator force-deflection output through the web architecture geometry and the external system interaction.

3.1.1. Reference strain-free state

The reference to compute the gap must be set to relate the web geometry to the SMA material properties in both the martensite and austenite equilibria. The reference strain-free state is set to be the state of the SMA web actuator when it is not connected to the external system and the SMA wire is in the fully austenite phase (Figure A.2a). The reference strain-free gap (G_0) of the web geometry is related to the reference strain-free length (l_0) of the wire through the web geometry relation (Equation 2), and the lengths of the wires in the austenite and martensite states are defined as the strained wire lengths relative to the reference strain-free length.

For a typical position-dependent external system such as a linear or non-linear stiffness, the placement of the external system relative to the SMA web actuator is defined in terms of *free clearance* (C_0) which is the distance between the moving attachment point(s) of the SMA web actuator in the reference strain-free state and the zero deflection position of the external system. However, for the special case of a constant force dead weight, which is used for model validation, the external system force is not dependent on the deflection position which is the only variable directly affected by the free clearance C_0 . Thus, the output performance is unaffected by the free clearance for a constant external force.

3.1.2. Austenite equilibrium state

When the external system is attached, the SMA web actuator and the external system are in the austenite equilibrium state where the SMA wire has extended to a length,

$$l_A = l_0(1 + \varepsilon_A), \quad (3)$$

where ε_A is the applied strain in the austenite phase due to the external system force. The resulting austenite equilibrium gap (from Equation 2) is

$$G_A = \sqrt{\left(\frac{l_0}{2}\right)^2 (1 + \varepsilon_A)^2 - \left(\frac{W}{2}\right)^2}. \quad (4)$$

The wire strain in the austenite phase is a function $f_{SMA}^A(\sigma_A)$ of the stress on the wire σ_A . This function can be any constitutive relation between stress and strain representing it in the full austenite phase [15–20]. By substituting the austenite strain ε_A with the austenite constitutive law $f_{SMA}^A(\sigma_A)$, the austenite equilibrium gap (Equation 4) can be rewritten as

$$G_A = \sqrt{\left(\frac{l_0}{2}\right)^2 (1 + f_{SMA}^A(\sigma_A))^2 - \left(\frac{W}{2}\right)^2}. \quad (5)$$

The stress in the wire in the austenite phase is determined by the tension (T_A)

$$\sigma_A = \frac{T_A}{A_{SMA}}, \quad (6)$$

where A_{SMA} is the cross-sectional area of the SMA wire. The tension on the SMA wire is dependent on the leveraging of the web actuator geometry, such that

$$T_A = \frac{l_A F_A}{4G_A}, \quad (7)$$

where F_A is the force from the external system at the austenite equilibrium. Thus, the austenite equilibrium stress (Equation 6) is rewritten as

$$\sigma_A = \frac{l_A F_A}{4A_{SMA} G_A}. \quad (8)$$

The external force at the austenite equilibrium is defined as a function of the external system deflection at the austenite equilibrium x_A ,

$$F_A = F(x_A). \quad (9)$$

Because the system deflection x_A and the deflection of the moving connecting point relative to the reference strain-free state ($G_A - G_0$) must sum to the free clearance when the external system is connected to the web actuator,

$$x_A = C_0 - (G_A - G_0). \quad (10)$$

Thus, solving for the austenite wire length l_A from the geometric relation (Equation 2), the austenite equilibrium stress (Equation 8) can be rewritten solely in terms of the austenite equilibrium gap,

$$\sigma_A = \frac{\sqrt{4G_A^2 + W^2} F(C_0 - (G_A - G_0))}{4A_{SMA} G_A}. \quad (11)$$

Thus, the austenite equilibrium gap G_A can be solved for by substituting the austenite equilibrium stress (Equation 11) into the expression for the austenite equilibrium gap (Equation 5).

3.1.3. Martensite equilibrium state

When the SMA wire is cooled to the martensite phase, the SMA wire constitutive relation changes to f_{SMA}^M (Figure A.2c) resulting in the new equilibrium position (G_M), which is expressed in the same manner as the austenite equilibrium gap (Equation 5),

$$G_M = \sqrt{\left(\frac{l_0}{2}\right)^2 (1 + f_{SMA}^M(\sigma_M))^2 - \left(\frac{W}{2}\right)^2}, \quad (12)$$

where the σ_M is the stress in the SMA wire in the martensite phase under the tension on the wire. The martensite equilibrium gap is solved for in the same manner as the austenite equilibrium gap,

by solving for the martensite equilibrium stress solely in terms of the martensite equilibrium gap (similar to Equation 11),

$$\sigma_M = \frac{\sqrt{4G_M^2 + W^2}F(C_0 - (G_M - G_0))}{4A_{SMA}G_M}, \quad (13)$$

and then substituting the martensite equilibrium stress (Equation 13) into the martensite equilibrium gap (Equation 12).

3.1.4. Stroke evaluation

The stroke of the SMA web actuator is the difference between the austenite and martensite equilibrium gaps ($\delta_{Stroke} = G_M - G_A$). The evaluation of the stroke, however, is not trivial due to the coupling between the geometric variables and the material constitutive laws and the transcendental form of the equations. There are two strategies to solve the model. One is a bottom-up approach where the computation starts from the material constitutive laws, and the other is a top-down approach where the computation starts from the external system behavior. In the bottom-up approach, the material constitutive laws are transformed into SMA wire tension-elongation performance using the wire geometry (diameter and length), and then the wire performance is transformed into the web actuator force-deflection performance using the web geometry (width and gap). In the top-down approach, the external system force-deflection behavior is transformed into the tension-elongation on the wire, and then into the stress-strain of the wire.

The models in this section are formulated to support the bottom-up approach, where the force-deflection output performances of an SMA wire web actuator in both the austenite and martensite phases are pre-evaluated for given material properties and web geometry. For this pre-evaluation, a range of external loads is set and discretized for numerical computation. These external loads are transformed into applied stresses in the SMA wire using the expressions for the austenite and martensite equilibrium stresses (Equations 11 and 13). The gap which represents the web actuator deflection is predicted using these stresses relating the range of external forces to deflection of the actuator from the expressions for the austenite and martensite equilibrium gaps (Equations 5 and 12). The equilibria are found by intersecting the external system force-deflection performance curve with these pre-evaluated web actuator output

performance curves. If any of the design variables are changed, this procedure must be repeated to predict the new performance.

3.2. Experimental Validation

The discrete state quasi-static force-deflection model of the SMA wire web actuator was validated by comparing with experimental SMA web actuator stroke performance over a range of parameters. Experimental stroke performance was measured using the apparatus shown in Figure A.3. A 0.01 inch diameter 70°C Flexinol® wire was mounted with fixture crimps in the fixed base with a width (W) of 198 mm and a set of reference strain-free gaps (G_0) of 41.8 mm ($W/G_0 = 4.7$), 32.7 mm ($W/G_0 = 6.1$), and 17.7 mm ($W/G_0 = 11.2$) after being pre-heated to the austenite reference strain-free phase with 0.8 A current. These crimps function as heating power supply terminals connecting to an ELECTRO INDUSTRIES DIGI 360 power supply. Once the SMA wire was cooled to the martensite phase, a weight was connected to the sliding plate through a Kevlar thread over a pulley. The martensite equilibrium gap was measured by a MICRO-EPSILON optoNCDT 1300 laser optical displacement sensor mounted on the ground plate. To actuate the SMA web actuator, electric current was applied and slowly increased until the actuator reached a stable austenite equilibrium, and the austenite equilibrium gap was measured with the laser displacement sensor. The same procedure was repeated for a range of applied dead weights from 200 g to 1000 g for each reference strain-free gap case.

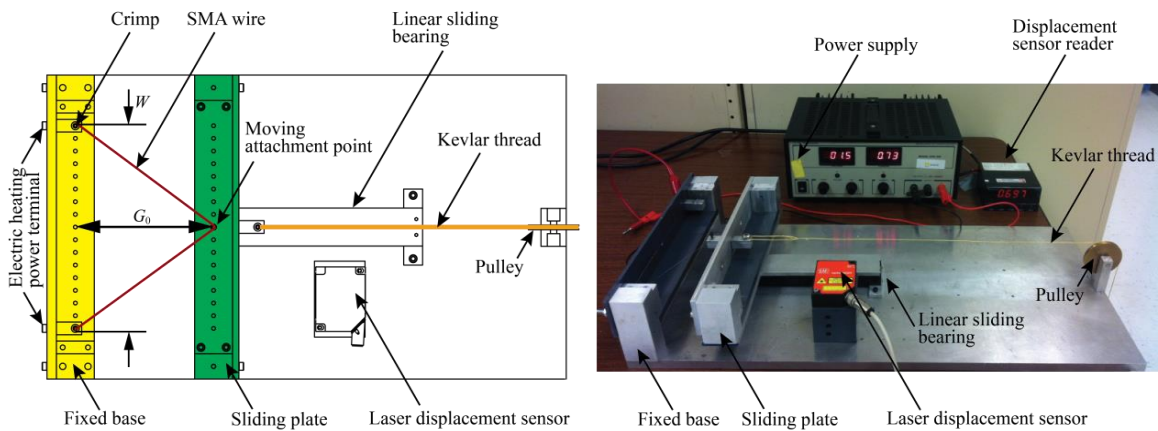


Figure A.3. Experimental setup for model validation.

The test rig is capable of adjusting the geometry of the SMA web actuator, applying dead weight as external system, and measuring deflection.

The experimental result was compared with the stroke prediction from the discrete state quasi-static force-deflection model. As a model input, the material stress-strain behavior of the SMA wire was directly measured in the martensite and austenite phases (Figure A.4). Single straight wires were subject to dead weight tensile loading tests in single heating/cooling cycles. A fresh wire was used for each applied load in a series of loads to prevent shakedown [13]. The geometric parameters of the experiments and experimentally characterized material constitutive laws were input to the model, and the predicted performance of the SMA web actuator is shown in Figure A.5 and plotted along with the experimental result.

The model predictions show a good correlation with the experimental validation result with an error in stroke prediction within 9.6%. Even without consideration of friction and bending at the moving attachment point(s), the simple geometry based model provides a good prediction of SMA web actuator performance. The model prediction curves show curvature due

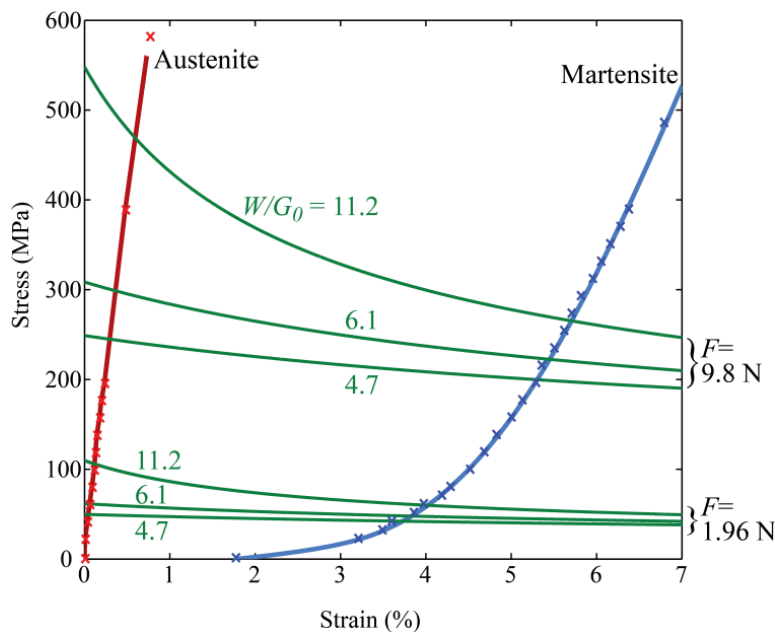


Figure A.4. SMA material constitutive relation for experimental validation (0.01 inch diameter 70°C Flexinol®) and Internal leveraging of external system.

The stress-strain curves in both martensite and austenite phases are generated by simple tensile test to be **used** for the performance prediction model. Applied stress on the SMA wire from a constant dead weight varies during heating and cooling due to the non-linear leveraging coupled to the geometry change. The higher width / gap ratio produces the bigger stress difference between the austenite equilibrium and the martensite equilibrium.

to the martensite material performance where the martensite stresses lie on the martensite plateau. Similar to straight wire SMA actuators, the SMA web actuator performance around this martensite plateau region is very sensitive to the external system force and build offsets. Because the angle between the SMA wire and the output motion direction changes during actuation, the mechanical leveraging through the web geometry is non-linear. This *non-linear leveraging* causes the changes in the stress on the SMA wire during actuation. The external system lines in Figure A.4 represent the stress on the SMA wire from the non-linearly leveraged dead weight external system. Due to the non-linear leveraging, higher width/gap ratios produce larger stress differences between the martensite and austenite equilibria, which are the intersections between the material curves and the external system lines. The gap of the web becomes smaller during actuation from the martensite equilibrium gap to the austenite equilibrium gap making the width/gap ratio higher, and a higher width/gap ratio produces a larger stroke amplification and a higher tension, and therefore higher stress, on the SMA wire. The stress difference is even larger under a larger external system force which enables larger

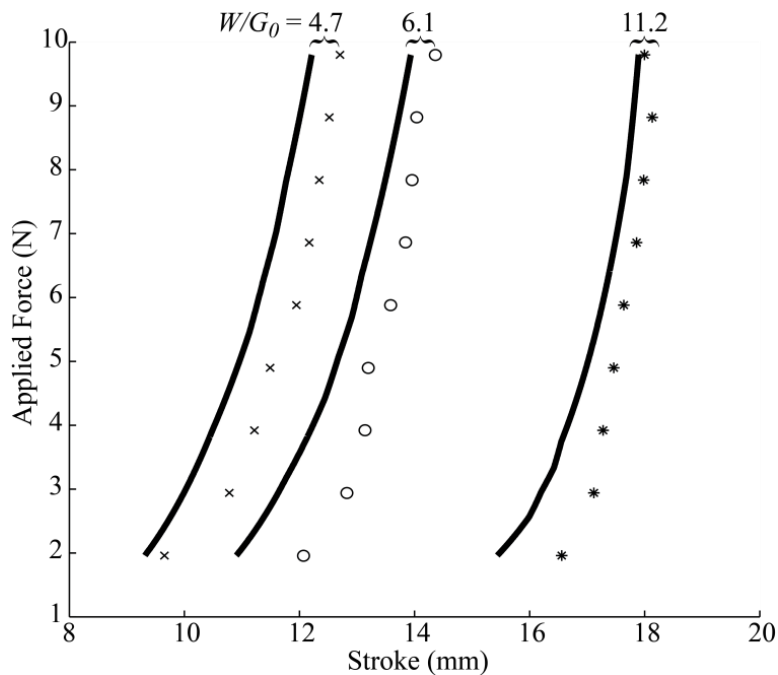


Figure A.5. Experimental validation result.

The behavioral model predicts the SMA web actuator actuation within 10% error (average error: 5%) over a range of applied stress and width / gap ratio.

actuation strains, producing larger stroke amplifications from the web geometry change. Designing under this complexity requires the use of parameter studies to build design insight.

4. Web actuator design Process

A design process for the SMA wire web actuator architecture is broken into three stages which proceed in increasing design complexity using the validated discrete state quasi-static force-deflection model. Step 1: The *Kinematic Design step* uses an SMA web architecture Kinematic Actuation Map created from the model to perform a feasibility check, where the possibility to create sufficient motion within a given packaging constraint is evaluated, and to select the actuation stroke related design parameters: *width/gap ratio (length of wire)*, *SMA wire net strain*, and *maximum allowable stress*. The material usage decisions (SMA wire net strain and maximum allowable stress) drive the structural fatigue (lifetime to failure) and the functional fatigue (shakedown resulting in degradation of stroke) [11–13]. The SMA wire net strain is constrained by the martensite and the austenite material behaviors because the SMA material cannot stretch further than its natural reaction to the applied stress. However, to increase lifetime, the strain can be further limited by design within these boundaries through techniques such as cutting off the heating current [21] before full transformation at the hot austenite end, and limiting the material strain using a mechanical hard stop at the cool martensite end [11,13]. Step 2: In the *Kineto-static Design step*, the *SMA wire cross-sectional area* is selected along with the *free clearance* to carry the required force under the set maximum allowable stress. Although the free clearance is not relevant to the position independent constant force external system which was used for model validation, for a typical position dependent external system, the free clearance is an important design variable which decides the applied stress on the wire. Step 3: In the *Thermo-mechanical Design step*, the *number and diameter of the SMA wires* are decided based on the selected cross-sectional area considering the heating and cooling time, and *device operation parameters* such as power and cooling medium are determined and evaluated.

4.1. Kinematic Design

For the first step of the SMA wire web actuator design process, feasibility of producing a required stroke out of a given packaging form factor is evaluated based on the web architecture kinematics, and design parameters to produce the required stroke are determined. To evaluate feasibility, an applicable width/gap ratio range is calculated for a given packaging constraint and

build tolerance. Because the foot print of the actuator commonly acts as a strong driver of the design, the width/gap ratio is defined in the cold martensite phase with the external system connected to represent the largest package size of the SMA wire web actuator for the design process and the design study. In general, a width/gap ratio larger than 10 is difficult to implement because small build offsets can change the width/gap ratio significantly leading to large changes in output performance. SMA material usage parameters such as the maximum allowable stress and the SMA net actuation strain are decided when evaluating feasibility. These material usage decisions are made considering the life cycle and operating conditions of the application. The SMA wire net strain and maximum allowable stress should be limited for long life cycle applications which necessarily reduces the output force and stroke [11–13,22]. By applying these design decisions to the design model, the stroke of the actuator can be predicted for evaluating feasibility.

A model-based **SMA Web Actuator Kinematic Actuation Map** was devised to help the designer to explore the design space and examine the effects of the diverse design options (Figure A.6). This map quantifies the non-linear leveraging of the web architecture which transforms the internal SMA wire actuation to the output actuation. The actuator output strain ($\varepsilon_{Act.} = \delta_{Stroke}/G_M$) is defined as the ratio of the actuator stroke to the initial martensite gap (G_M). By rearranging the force-deflection model, the internal SMA wire strain is related to the actuation strain as

$$\varepsilon_{Act.} = 1 - \sqrt{\left(1 + \left(\frac{W}{2G_M}\right)^2\right) (1 - \varepsilon_{SMA})^2 - \left(\frac{W}{2G_M}\right)^2}, \quad (14)$$

where ε_{SMA} is the internal SMA wire net strain, which is the difference between the martensite strain and the austenite strain. The map shows the actuator output strain for a range of packaging configurations and internal SMA wire strains. The actuation strain contours on the map indicate that higher width/gap ratios and larger SMA wire net strains produce larger actuator strains. Below a width/gap ratio of 2, the angle between the SMA wire and the output motion direction is less than 45°, each actuator output strain contour approaches a vertical line at its value on the SMA net strain axis because the actuator architecture no longer exploits the leveraging effect.

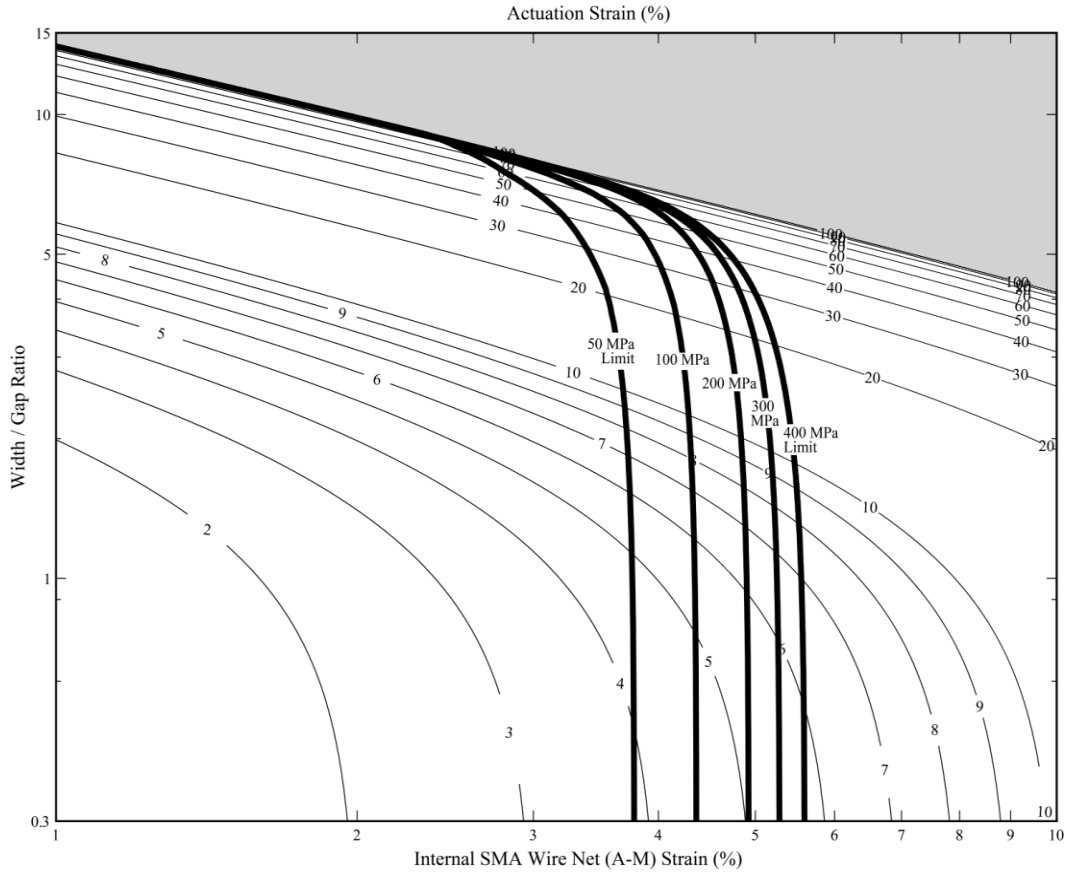


Figure A.6. SMA Web Actuator Kinematic Actuation Map.

The actuator output strain contours on the map indicate that higher width / gap ratios and larger SMA wire net strains provide larger amplification resulting in larger actuator strains. The gray triangular region on the top right side of the map shows geometric limitations of SMA web actuators, where the actuation strain contours approach 100 % and the shape of the web becomes completely flat. The thick vertical curved lines show material limitations due to the SMA properties when different maximum allowable stresses are applied. Only designs on left side of these limitation lines are feasible.

There are two types of infeasible areas on the map. The first, the shaded area on the top right of the map, is due to the geometry of the SMA web. Designs in this area are not feasible since the SMA web actuator becomes flat at the diagonal border line producing no more stroke. If a larger net strain is attempted beyond this line, the already flattened wire would simply produce additional internal stress. The second infeasible area, the right side of any one of the thick actuation limitation lines, is due to the material properties; each line delineates an infeasible design space where the SMA wire cannot provide the required internal strain difference between martensite and austenite at the given applied stress level as defined in the austenite state. This limitation is further affected by the geometric amplification at larger

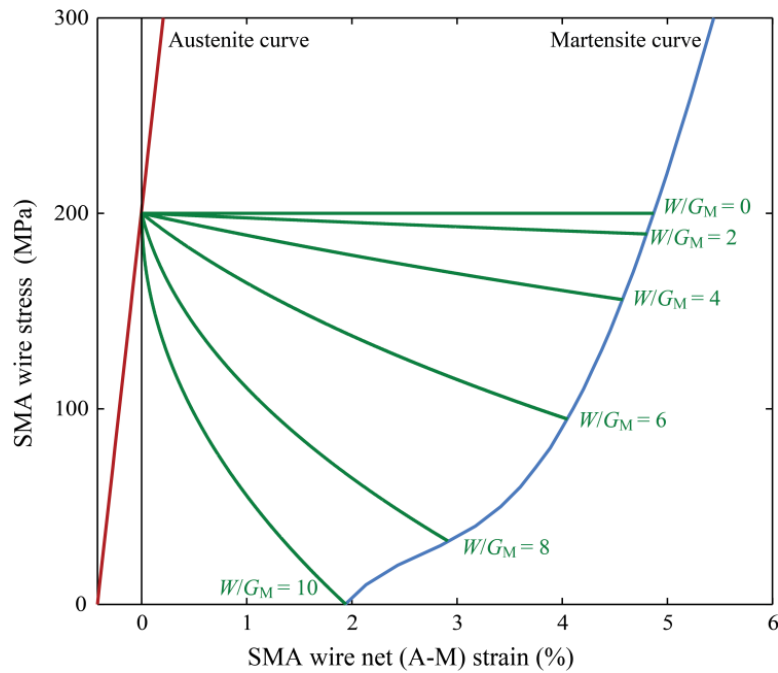


Figure A.7. Internal tension amplification (200 MPa maximum allowable stress)

The tensile stress on the wire varies during actuation, and the rate of this variation differs with different width / gap ratios. The intersections with the martensite curve impose limitations to the usable SMA wire net strain for each case.

width/gap ratios, where the amplification changes through the actuation stroke. Thus the equilibrium stress in the martensite state settles to a lower stress than in the austenite state, limiting internal SMA net strain by the strain response of the martensitic material at that reduced stress. Figure A.7 shows a set of constant force external system curves mapped into the material stress-strain space at a range of width/gap ratios. Larger values of width/gap ratio produce very large differences between the austenite and martensite stress, and the resulting strains limit the usable net strain. In Figure A.6, several example actuation limitation lines are plotted for a range of austenite stresses (50 MPa, 100 MPa, 200 MPa, 300 MPa, and 400 MPa) using the material constitutive laws characterized for model validation (Section 3.2).

The martensite stresses for each case (i.e. for each combination of width/gap ratio and internal SMA wire net strain) are calculated assuming a constant force external system. If the external system is not a constant force, the designer needs to verify the availability of the SMA wire net strain after finalizing the design by checking both the austenite equilibrium strain and the martensite equilibrium strain. The actuation strain for each case is then compared with the difference between the austenite strain and the corresponding martensite strain at the reduced stress. The limitation lines are vertical at low width/gap ratios since there is very little

leveraging in this region, and they asymptotically approach the geometric limitation boundary due to the drastic reduction in martensite stress. Despite these limitations, most of the reasonable designs lie in the feasible region in the actuation map. For example, even with a large value of 4% SMA wire net strain (limited as a design decision to mitigate functional and structural fatigue [11–13,22]), and the manufactures recommended stress of 200 MPa [23], width/gap ratios as large as 6 are feasible producing up to 55% actuation strain. This implies that the main driver is generally the packaging footprint and not material usage limitations. Thus, in this design step, the width/gap ratio and stroke are the primary concerns for feasibility and design selection.

4.2. Kineto-static Design

The second step of the design process is to determine the cross-sectional area of the SMA wires to carry the required external force based on the width/gap ratio and the maximum allowable stress. Because the width/gap ratio is defined in the martensite state and the stress in the wire increases to a maximum in the austenite state, it is required to relate external force to the tension (and resulting stress) on the wire in the martensite state, and also in the austenite state. The required cross-sectional area of the SMA wire to avoid exceeding a specified maximum stress ($\sigma_{max.}$) in the austenite state for a constant force ($F = F_A = F_M$) external system is calculated using the web kinematics (Equations 5 and 13) along with the stress developed in the wire due to the applied load (Equation 8) as

$$A_{SMA} = \frac{F}{\sigma_{max.}} \times \frac{1}{2} \frac{\sqrt{1 + R_M^2} - \varepsilon_{SMA}}{\sqrt{\left(\sqrt{1 + R_M^2} - \varepsilon_{SMA}\right)^2 - R_M^2}}, \quad (15)$$

where R_M is the half of the width/gap ratio at the martensite equilibrium ($R_M = W/2G_M$).

However, for a typical position dependent external system, due to the non-linear leveraging coupled to the web geometry, the cross-sectional area of the SMA wire and the free clearance need to be calculated numerically as mentioned in Section 3.1. The cross-sectional area of the SMA is expressed using the web leverage in the austenite state (Equation 8) and the force from the external system evaluated at the austenite position $F(x_A)$ as

$$A_{SMA} = \frac{F(x_A)}{\sigma_{max.}} \times \frac{1}{2} \sqrt{1 + R_A^2}. \quad (16)$$

This cross-sectional area needs to be determined through an iterative numerical process along with the free clearance (since $x_A = C_0 - (G_A - G_0)$), which affects both the maximum stress in the austenite state and the martensite stress during actuation.

4.3. Thermo-mechanical Design

As the last step of the design process, the number and diameter of the SMA wires can be selected from many combinations based on available wire diameters and required actuation cycle time. The diameter of the SMA wire is selected to meet the required cooling time, which is evaluated using a lumped heat transfer model accounting for the specific heat of the material (C_0) and the latent heat of the martensite to austenite phase transformation (Λ_{AM}), and convective heat transfer from the wire (film coefficient h). This model is described by the differential equation,

$$\begin{aligned} \rho V_{SMA} C_0 \frac{dT}{dt} \Big|_{T_0 > T > T_{Ms}} + \rho V_{SMA} (C_0 + \Lambda_{AM}) \frac{dT}{dt} \Big|_{T_{Ms} > T > T_{Mf}} \\ = -h A_{surface} (T(t) - T_\infty), \end{aligned} \quad (17)$$

where ρ is the density of the SMA, V_{SMA} is the volume of the SMA wire, T_0 is the temperature of the SMA wire when the cooling starts, T_{Ms} and T_{Mf} are the start and finish temperatures of the austenite to martensite transformation, $A_{surface}$ is the surface area of the SMA wire, and T_∞ is the ambient temperature. For a given heated temperature T_0 , this equation can be solved for the time to cool to the martensite finish temperature T_{Mf} , such that

$$t_{cooling} = \frac{\rho d_{SMA}}{4h} C_0 \ln \left(\frac{T_0 - T_\infty}{T_{Ms} - T_\infty} \right) + \frac{\rho d_{SMA}}{4h} \left(C_0 + \frac{\Lambda_{AM}}{T_{Ms} - T_{Mf}} \right) \ln \left(\frac{T_{Ms} - T_\infty}{T_{Mf} - T_\infty} \right), \quad (18)$$

where, d_{SMA} is the diameter of the SMA wire. The thermo-mechanical material properties (ρ , Λ_{AM} , C_0 , T_{Ms} , and T_{Mf}) can be characterized from the material [14], and the film heat transfer coefficient (h) can be empirically measured [24]. While smaller diameter wire is desirable for a fast cooling time, there are limitations for using smaller diameter wires due to an increased complexity related to making mechanical and electrical connections to larger numbers of wires. Moreover, using multiple smaller diameter wires requires more power than using a single larger diameter wire due to the increased heat transfer.

After setting the diameter of the wire, the heating power is determined to meet the required actuation time to heat the wire to the austenite state, along with other design metrics such as power/work efficiencies. The heating time is evaluated similar to the cooling time with an additional Joule heating term as

$$\begin{aligned}
 t_{Heating} = & \frac{\rho V_{SMA}}{I^2 R} (C_0 (T_{As} - T_{\infty})) - h A_{SMA} \left(\frac{T_{As} - T_{\infty}}{\ln \left(\frac{T_{As}}{T_{\infty}} \right) - T_{\infty}} \right) \\
 & + \frac{\rho V_{SMA}}{I^2 R} (C_0 (T_{Af} - T_{As}) + \Lambda_{MA}) - h A_{SMA} \left(\frac{T_{Af} - T_{As}}{\ln \left(\frac{T_{Af} - T_{\infty}}{T_{As} - T_{\infty}} \right)} \right),
 \end{aligned} \tag{19}$$

where I is the heating electric current, R is the resistance of the SMA wire, T_{As} and T_{Af} are the austenite transformation start and finish temperatures, and Λ_{MA} is the latent heat of the martensite to austenite transformation. The heating time can be reduced by increasing the heating electric current while accounting for limitations in available power. This thermo-mechanical design step is general to all SMA wire actuator architectures, not specifically to web actuators.

By following this three step design process, an SMA wire web actuator to meet packaging and stroke requirements can be designed while addressing lifetime related material usage considerations such as maximum allowable stress and net actuation strain. The SMA Web Actuator Kinematic Actuation Map was created for feasibility evaluation and kinematic web configuration design. However, there are still many decisions and tradeoffs available to the designer. In the following section, a broad parameter study is performed to build an understanding of the SMA web actuator design space to provide insight to aid design decisions.

5. Design Parameter Tradeoff Study

To explore various design tradeoffs and build design insight, a set of parameter studies have been performed numerically using the discrete state quasi-static force-deflection model with respect to three major aspects of the SMA actuator design: actuator geometry, SMA material properties, and external system characteristics. The effect of web geometry parameter (width/gap ratio) variation on the output performance is explored by providing useful

performance plots in different coordinate spaces. The effect of the material behavior (initial two-way strain) variation on the performance is studied by applying two additional material constitutive laws to the performance prediction model. The effect of the external system characteristics (system stiffness) on the feasible design boundaries is investigated using constant stiffness external systems. These numerical studies provide design insight to aid design decisions during the design process.

5.1. Architecture geometry: width/gap ratio

The width/gap ratio is one of the major drivers of the SMA wire web actuator design due to the packaging space constraint, which both forces and enables the use of the web architecture. The effect of architecture geometry (width/gap ratio) on actuator stroke amplification and output force loss are explored along with their design implications. These numerical studies use the material constitutive laws for Flexinol[®] wire which was characterized for the experimental validation of the discrete state quasi-static force-deflection model.

5.1.1. Effect of width/gap ratio on actuator stroke amplification

Higher width/gap ratio provides higher actuator output strain. Figure A.8, which is generated numerically using the actuation strain equation (Equation 14), shows the stroke amplification over a range of width/gap ratios; the x-axis shows the width to martensite gap ratio, and the y-axis shows the actuator output strain. Each thin line shows a different SMA net strain case. The actuator output strain is monotonically increasing with width/gap ratio for all SMA wire net strains. Thus, the largest width/gap ratio allowed by the packaging constraint produces the maximum actuator stroke amplification. This non-linear stroke amplification increases drastically with larger SMA net strain. For example, the 4% net strain case shows a much more sharply increasing stroke amplification with width/gap ratio than does the 1% net strain case; the gap can be completely closed using 4% net strain at a 7 width/gap ratio, but 1% net strain only allows a 14% closing of the gap at a 7 width/gap ratio. This drastic amplification imposes a usable width/gap ratio limit by making the shape of the web completely flat. Moreover, an actuation limit exists for a given maximum allowable stress, shown as the thick line in Figure A.8 for a 200 MPa austenite maximum allowable stress level (recommended by the manufacturer [23]), which is based on the strain response of the material at the resulting stress levels.

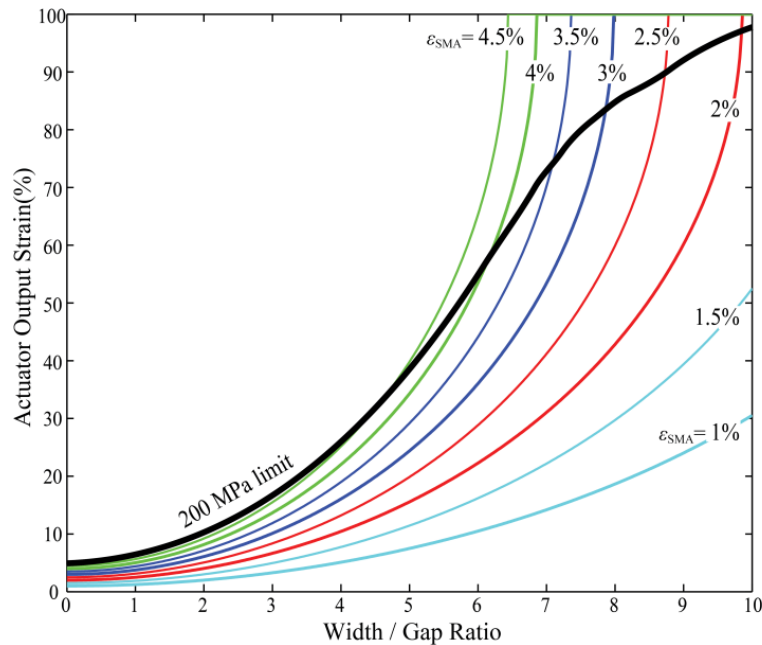


Figure A.8. Actuator output strain amplification.

Higher width / gap ratios allow larger actuator output stroke amplification for every SMA net strain case. This non-linear stroke amplification increases drastically with larger SMA net strains, imposing a usable width / gap ratio limit by making the shape of the web completely flat.

Another issue with using higher width/gap ratios is the sensitivity to build offsets, since the slopes of each net strain curve become stiffer at higher width/gap ratios, and even more so in the larger net strain cases. However, the web actuator design is not significantly limited by the SMA material properties for reasonable width/gap ratios. Most reasonable SMA wire net strain cases (below 4%) are within the material strain limitation under a width/gap ratio of 6, which is a reasonable upper limit due to build offset sensitivity. This implies that the design of SMA wire web actuators is driven mainly by the web kinematics.

5.1.2. Effect of width/gap ratio on output force

While the actuation amplification is higher for higher width/gap ratios, the force loss due to leveraging is also larger. Figure A.9 shows the actuator output strain and the relative output force on a log scale; the x-axis shows the width/gap ratio, and the upward diagonal lines show the actuator stroke for each different SMA net strain case. The spreading downward lines show the SMA wire web actuator output force loss relative to the characteristic force (F_C), which is defined as the force of 2 straight wires (unleveraged) at the same maximum allowable stress

($\sigma_{max.}$) because the 2 straight wires can be considered as an extreme case of an SMA web actuator which has the width of 0. The non-dimensionalized actuator output force ($\hat{F}_{Act.}$) is defined as the ratio between the SMA wire web actuator output force in the austenite state (F_A) and this characteristic force,

$$\hat{F}_{Act.} = \frac{F_A |_{\sigma_{max.}}}{F_C} \quad (20)$$

The non-dimensionalized force $\hat{F}_{Act.}$ characterizes the output force loss, where an $\hat{F}_{Act.}$ of 100% implies no force loss (but also no stroke amplification) while a small value of $\hat{F}_{Act.}$ indicates that only a small portion of F_C (larger force loss) is produced. To carry the same force at a higher width/gap ratio, a bigger diameter wire and/or a larger number of wires needs to be used. For a given width/gap ratio, smaller internal wire strains allow the actuator to carry a larger force, but the actuator output strain is less than that produced from a larger internal wire strain. Thus, there is a tradeoff between the stroke amplification and the output force loss.

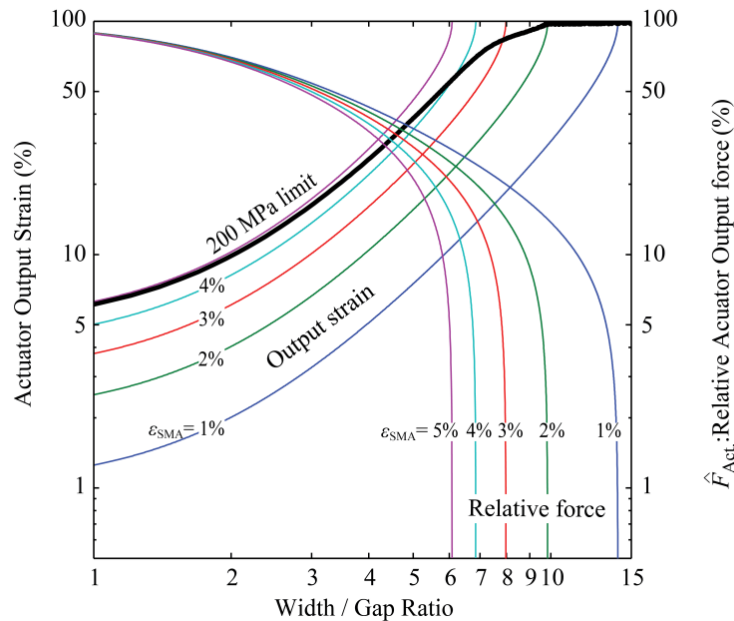


Figure A.9. Actuator Output Performance Plot.

There is tradeoff between the stroke amplification and the output force loss where higher width / gap ratios allow higher stroke amplification but also limit the output force. Moreover, when the shape of web becomes flat, the web cannot carry any more force, limiting the use of larger SMA net strain.

Higher width/gap ratios limit the use of larger SMA net strains. Figure A.9 shows that the relative output force approaches zero when the actuator output strain reaches 100% in every SMA net strain case. This occurs because at high width/gap ratios, the web cannot carry any output force when the web becomes flat. Even in the smaller SMA net strain cases, higher width/gap ratios still limit the output force due to this kinematic loss although the limit occurs at larger width/gap ratios. Another limitation of using high width/gap ratios is that the drastic stress decrease in the martensite phase at high width/gap ratios, shown in Figure A.7, lowers the martensite finish temperature, slowing cooling time and requiring a lower ambient temperature to fully cool the wire.

5.1.3. Effect of partial use of packaging

One method to exploit the benefit of the higher width/gap ratio within a given packaging constraint is limiting the size of the martensite equilibrium gap to not occupy the entire available packaging space. For a fixed package width, while the initial martensite gap is smaller when the web architecture only uses a portion of the package gap, the increased amplification due to the higher width/gap ratio produces a larger absolute output stroke. The Kinematic Actuation Map (Figure A.6) is redrawn in Figure A.10 showing contours of stroke as a fraction of package width instead of as a fraction of initial martensite gap. The stroke increases when width/gap ratio increases except for the width/gap ratios below 2, where the architecture no longer exploits the stroke amplification. Thus, using a smaller martensite gap to increase the width/gap ratio pays off in terms of a larger absolute stroke within a fixed width although with a corresponding increased output force loss (Figure A.11).

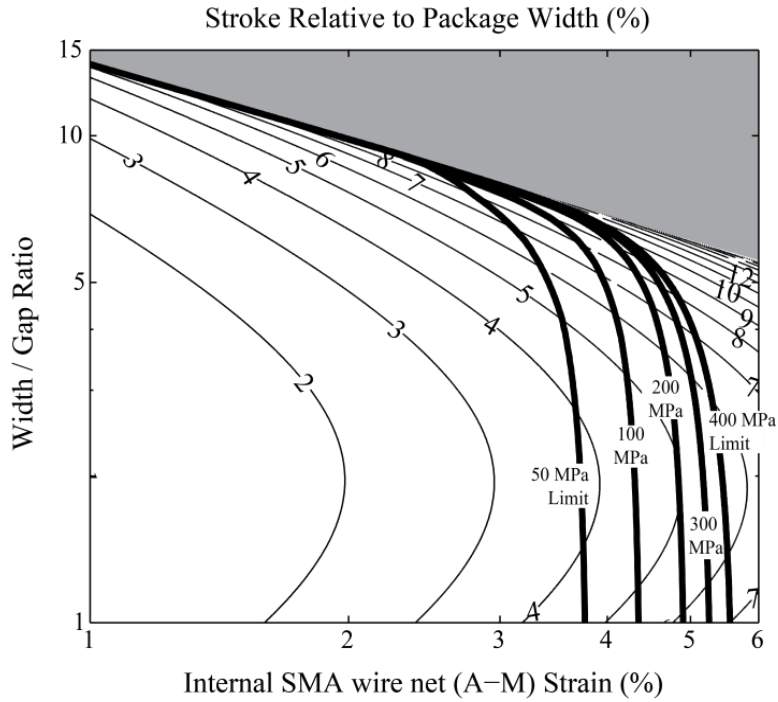


Figure A.10. Kinematic Actuation Map in stroke relative to package width.

For a fixed width, the higher width / gap ratio, i.e. the smaller martensite gap, produces the larger absolute stroke.

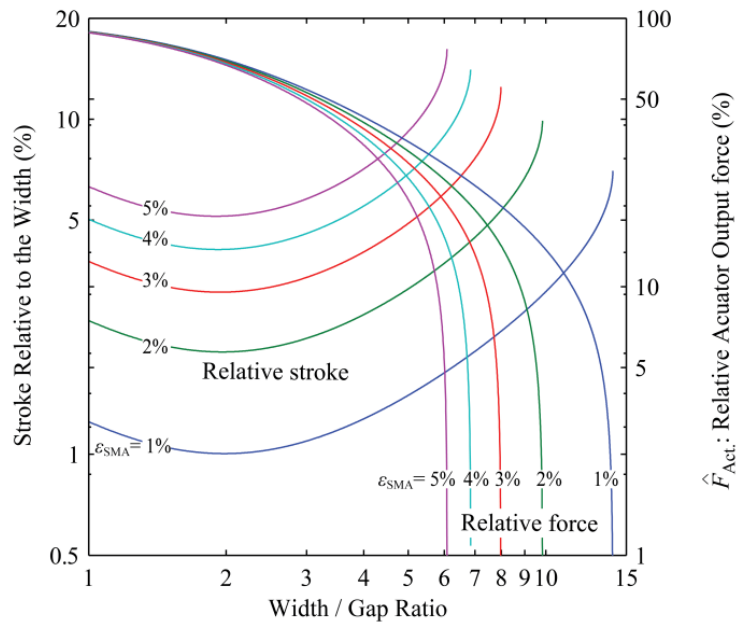


Figure A.11. Actuator Output Performance Plot in stroke relative to the width.

The stroke is increasing monotonically for each actuation strain case above the width / gap ratio of 2. Using partial packaging space to limit the martensite gap pays off in terms of the absolute stroke while the out force loss becomes bigger with the higher width / gap ratio.

5.2. Material properties: initial two-way strain

SMA wires show different material behavior depending on the composition of the material and the manufacturing process [14] often leading to changes in the actuator performance. Particularly, the presence of the initial martensite two-way strain and martensite plateau in the stress-strain curve affect the amount of usable actuation net strain. To investigate the effect of the SMA behavior, the web actuator stroke performance was evaluated numerically using two additional material constitutive laws with different SMA stress-strain properties (Figure A.12): one without an initial two-way effect strain (with a martensite plateau), and the other with a full initial two-way strain (without a martensite plateau). The material with a martensite plateau (*full martensite plateau wire*) is similar to unprocessed NiTiNOL, and the material without a martensite plateau (*no martensite plateau wire*) represents SMA wire after extensive cold work [25]. The actual wire characterized for the model validation exhibits behavior between these two extremes. A Kinematic Actuation Map (Figure A.13) and an Actuator Output Performance Plot (Figure A.14) show the material limitation deviations due to the different material characteristics. The full martensite plateau wire limit line and the no martensite plateau wire limit line deviate

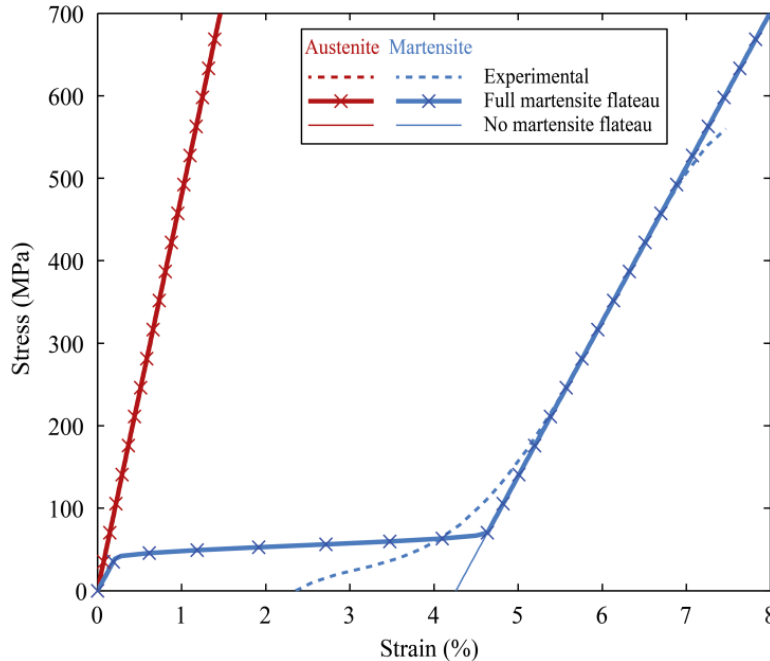


Figure A.12. SMA material constitutive relations for output performance comparison.

Three SMA material constitutive relations are applied to the actuator performance prediction model: one is experimentally characterized for the model validation, another is model based one without initial two-way effect strain which has the martensite plateau, and the other is also model based one with full initial two-way effect strain without the martensite plateau.

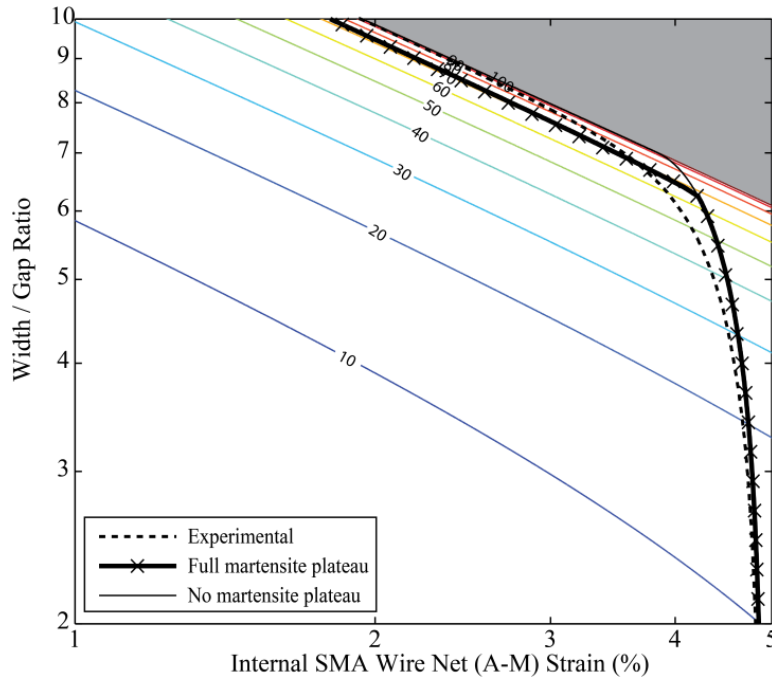


Figure A.13. Material limits for different SMA material properties (Kinematic Actuation Map).

Three different SMA material constitutive laws are applied to the actuator output performance prediction model. The material properties have very limited effect on the SMA wire web actuator design boundaries.

from each other above a width/gap ratio of 6.5 where the leveraged external force intersects to the martensite plateau. The experimentally characterized wire limit line deviates from both of these curves due to its different martensite plateau shape.

The use of different SMA material does not affect the actuator output strain because the actuator output strain is solely dependent on the web geometry (width/gap ratio) and the material usage (SMA wire net strain). It only affects the material net strain limit because different materials produce different austenite and martensite strains at the same austenite maximum allowable stress and reduced martensite stress. However, the effect of the martensite plateau is very limited. The martensite plateau reduces the material limitation lines by 30 – 35 % in actuator output strain at high width/gap ratio near the geometric feasibility boundary (Figure A.13). This is because the high width/gap ratio reduces the martensite stress to the martensite plateau limiting the available net strain. This shift is not significant to the design of the actuator, however, because the output forces at these width/gap ratios have become too small to be useful for application design (Figure A.14).

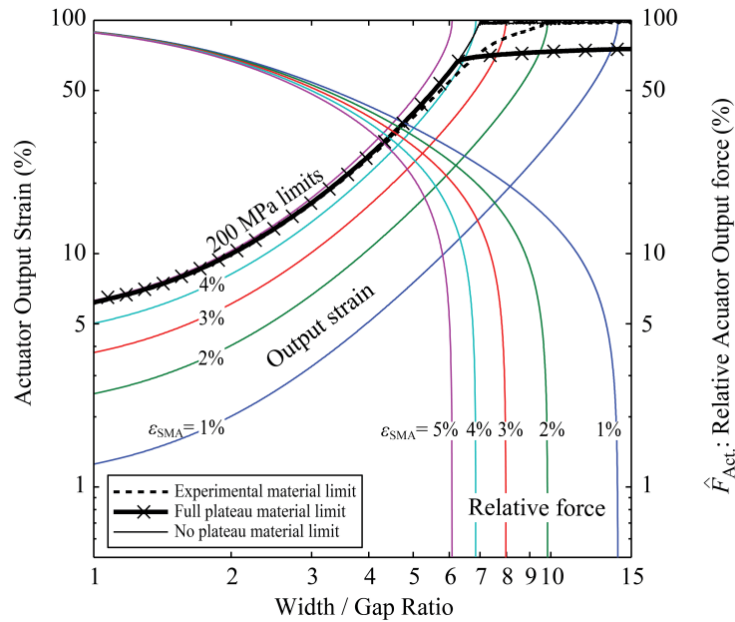


Figure A.14. Effect of different SMA material properties (Actuator Output Performance Plot).

The material limit changes due to the material properties difference are not significant to the actuator design because the output forces at the limit are already too small to be used for actuators.

5.3. External system characteristics: stiffness

While a constant force external system was used previously in this paper, a typical external system varies in force with position. The performance of the SMA actuator is coupled to the external system due to the stress-strain-temperature coupling of the SMA material. Depending on the stiffness of the external system, the stress change in the SMA wire during actuation differs leading to a change in actuation stroke. The effect of the external system stiffness on the web actuator performance is studied using constant stiffness external systems. Linear stiffness external systems further reduce the martensite stress due to the applied force difference between the austenite and martensite equilibria. The resulting martensite stress due to the external system stiffness k_S is

$$\sigma_M = \sigma_{max.} \times \left(\frac{1 - \varepsilon_{Act.}}{1 - \varepsilon_{SMA}} - \frac{k_S G_M \varepsilon_{Act.} \sqrt{1 + (W/2G_M)^2}}{2 A_{SMA} \sigma_{max.}} \right). \quad (21)$$

The external system stiffness is normalized relative to the characteristic force (F_C) and the martensite gap (G_M) which provides a characteristic length. The non-dimensionalized system stiffness \hat{k}_S is defined as

$$\hat{k}_S = \frac{k_S}{F_C/G_M} = \frac{k_S G_M}{2 A_{SMA} \sigma_{max.}}. \quad (22)$$

The leveraged stress reduction ratio between the martensite stress and the maximum allowable austenite stress is

$$\frac{\sigma_M}{\sigma_{max.}} = \left(\frac{1 - \varepsilon_{Act.}}{1 - \varepsilon_{SMA}} - \hat{k}_S \varepsilon_{Act.} \sqrt{1 + R^2} \right). \quad (23)$$

Again, the actuator output strain is solely dependent on the web geometry and the material usage, and the external system stiffness only affects the material limitation, which comes from the usable actuation net strain. A Kinematic Actuation Map (Figure A.15) and an Actuator Output Performance Plot (Figure A.16) show the material limit changes due to the external system stiffness changes. The cases of non-dimensionalized system stiffness 0 (constant force), 0.25 and 1 are plotted for both full martensite plateau wire and no martensite plateau wire. For a martensite gap (G_M) of 30 mm and maximum austenite allowable stress ($\sigma_{max.}$) of 200 MPa, the actual external system stiffness (k_S) is 0.16 N/mm for the non-dimensionalized system stiffness (\hat{k}_S) of 0.25, and 0.66 N/mm for $\hat{k}_S = 1$.

The effect of the external system stiffness is more significant than that of the SMA material property variation. For example, in the 3% net strain case, the no martensite plateau wire limits the width/gap ratio to a maximum of 8 where the output strain line corresponding to the 3% SMA net strain case reaches 100% actuator output strain, and the full martensite plateau wire limits the width/gap ratio to 7.6 under a constant force external system, where the output strain line corresponding to the 3% net strain case intersects the full plateau wire material limit at 72% actuation strain. However, the $\hat{k}_S = 0.25$ external system limits the width/gap ratio to 7 for

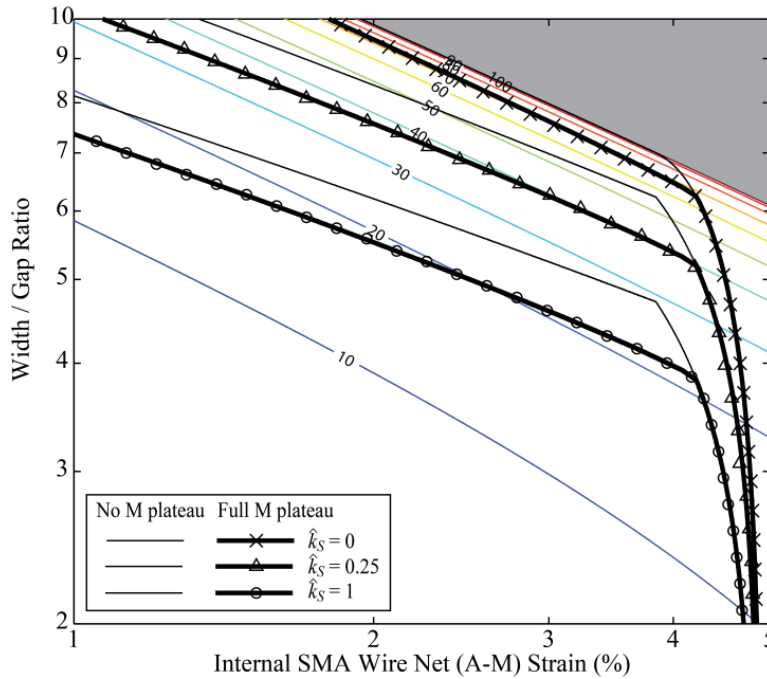


Figure A.15. Material limits for different external system stiffness (Kinematic Actuation Map).

The material limit lines of three different relative stiffness external systems are compared for both full two-way strain wire and no two-way strain wires.

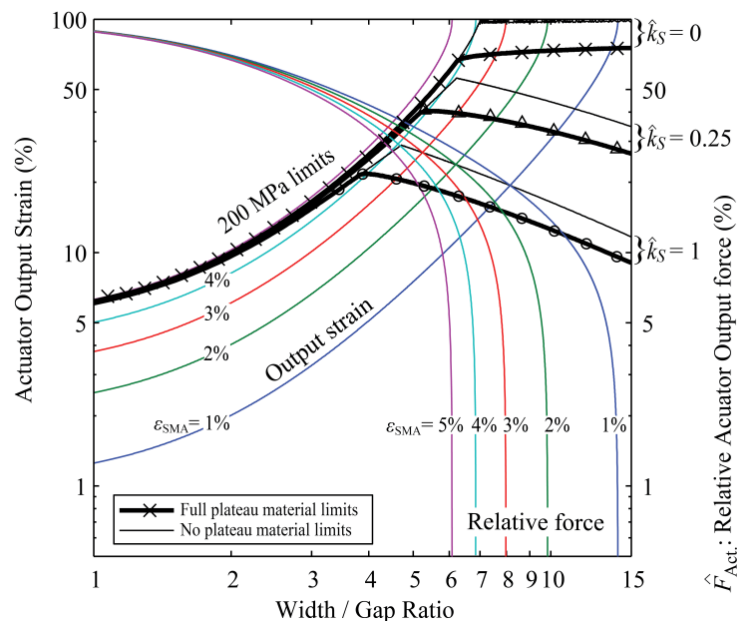


Figure A.16. Effect of external system stiffness (Actuator Output Performance Plot).

The material limit lines of three different relative stiffness external systems are compared for both full two-way strain wire and no two-way strain wires. The effect of the system stiffness is more significant than that of the different material properties.

the no plateau wire at 53% actuation strain, and 6.3 for the full plateau wire at 40% actuation strain. The $\hat{k}_S = 1$ external system further limits the width/gap ratio to 5.2 for the no plateau wire at 26% actuation strain, and 4.6 for the full plateau wire at 20% actuation strain. The stiffer external system limits the usable width/gap ratio due to a lower martensite stress causing a large reduction in actuator output strain.

5.4. Design insight

These design parametric studies indicate many design implications that must be considered when designing web actuators. These design implications apply to the kinematic design step, which decides the web geometry and the material usage. Higher width/gap ratios allow larger stroke amplification, and further stroke amplification and increased absolute output stroke can be obtained from a given package size by a web which only partially occupies the package gap. While the material response limits the possible actuation strain, most reasonable SMA wire net strain cases are within the material strain limitation, thus the design of SMA wire web actuators is driven mainly by the web kinematics. Higher width/gap ratios, however, limit the available output force such that pushing the material usage to the material limitation is not desirable. Higher width/gap ratios also require longer cooling times and/or low ambient temperatures due to the martensite stress being reduced by the drastic non-linear leveraging. In addition, the build tolerance needs to be considered for higher width/gap ratios.

While the effect of material property changes on web actuator design is limited, a stiffer external system limits the usable width/gap ratio. When the austenite maximum allowable stress is regulated to avoid functional and structural fatigue, stiffer external systems reduce the martensite stress drastically limiting actuation net strain with a more restrictive material limit line on the SMA web Kinematic Actuation Map,. Moreover, a system which is stiffer than the non-dimensionalized stiffness (\hat{k}_S) of 1 should be avoided because it limits both actuation output strain and force (both under 20%). If an SMA wire web actuator needs be designed for a high stiffness external system, the cross-sectional area of the SMA wire (A_{SMA}) can be increased to reduce \hat{k}_S . However, increasing A_{SMA} requires higher heating power and longer cooling time. Another method to decrease \hat{k}_S is to increase the maximum allowable stress (σ_{max}), although increasing σ_{max} also creates issues with functional fatigue (shakedown) and structural fatigue

(lifetime). These design implications can provide guidance to designers by exposing the various effects of the design parameters.

6. Conclusion

This paper presented a three step design process and design parameter tradeoff studies for SMA wire web actuators based on a discrete state quasi-static force-deflection model. The model was derived to predict the performance of SMA wire web actuators relating kinematic properties of the web to generic SMA constitutive laws, and validated with a set of experiments. Based on this model, a three step design process is presented. A kinematic design step evaluates the feasibility and designs the web geometry parameters to produce a required stroke using an SMA web Kinematic Actuation Map. The following kineto-static design step selects wire cross-sectional area along with the free clearance to produce a required force output. The final thermo-mechanical design step determines the number and diameter of wire using a lumped heat transfer model to meet the heating/cooling time requirements. To help decisions during the design process, model-based numerical parameter studies explored the design space exposing several important design tradeoffs and implications in terms of three major aspects of device design: web geometry, SMA material properties, and external system characteristics. Higher width/gap ratios produce larger actuation stroke, but with larger output force loss. Higher ratios also require tighter build tolerances and longer cooling times and/or lower ambient temperatures due to the low martensite transformation finish temperature caused by the drastic martensite stress reduction. While material property variations have limited effect on the SMA web actuator design, the external system stiffness imposes constraints on the design reducing the usable actuation net strain. The discrete state quasi-static force-deflection model and three step design process presented in this paper supported by the design insight generated by the numerical parametric studies provide a systematic approach to the design of SMA wire web actuators. These help to bring this SMA wire device architecture to bear to provide compact actuators with shallow form factor packaging useful for a wide range of applications.

7. References

- [1] Sofla, A. Y. N., Meguid, S. A., Tan, K. T., and Yeo, W. K., 2010, "Shape morphing of aircraft wing: Status and challenges," *Mater. Des.*, **31**(3), pp. 1284–1292.

- [2] Previtali, F., Bleischwitz, R., Hasse, A., Campanile, L., and Ermanni, P., 2011, “Compliant Morphing Wing,” ICAST2011: 22 nd International Conference on Adaptive Structures and Technologies, Corfu, Greece, p. #063.
- [3] Joo, J. J., Sanders, B., Johnson, T., and Frecker, M. I., 2006, “Optimal actuator location within a morphing wing scissor mechanism configuration,” pp. 616603–616603.
- [4] Bharti, S., Frecker, M., Lesieutre, G., and Browne, J., 2007, “Tendon actuated cellular mechanisms for morphing aircraft wing,” pp. 652307–652307.
- [5] Toma, M., Luntz, J., Brei, D., Alexander, P. W., Browne, A. L., and Johnson, N. L., 2012, “Design and Proof-of-Concept Validation of a Latched Arch Active Seal,” *J. Mech. Des.*, **134**(7), p. 075001.
- [6] Nagesh, S., Luntz, J. E., Brei, D., Alexander, P. W., Browne, A. L., and Johnson, N. L., 2010, “Customer Tailored Active Weatherstrip Design,” pp. 491–502.
- [7] Pathak, A., Brei, D., and Luntz, J., 2009, “Design and preliminary testing of a handheld antagonistic SMA actuator for cancellation of human tremor,” SPIE, San Diego, CA, USA, p. 72881B–13.
- [8] Dynalloy, Inc., 2006, “Comfort Seating,” *Dynalloy Newsl.*, p. 2.
- [9] Jiang, C., Uchida, K., and Sawada, H., 2011, “Development of vision based tactile display system using shape memory alloys,” *Advanced Mechatronic Systems (ICAMEchS)*, 2011 International Conference on, pp. 570–575.
- [10] Grant, D., and Hayward, V., 1997, “Variable structure control of shape memory alloy actuators,” *Control Syst. Mag. IEEE*, **17**(3), pp. 80–88.
- [11] Sun, H., Pathak, A., Luntz, J., Brei, D., Alexander, P. W., and Johnson, N. L., 2008, “Stabilizing shape memory alloy actuator performance through cyclic shakedown: an empirical study,” SPIE, San Diego, California, USA, p. 69300Q–11.
- [12] Bertacchini, O. W., Schick, J., and Lagoudas, D. C., 2009, “Parametric study and characterization of the isobaric thermomechanical transformation fatigue of nickel-rich NiTi SMA actuators,” SPIE, San Diego, CA, USA, p. 72890P–12.
- [13] Kim, W., Barnes, B. M., Luntz, J. E., and Brei, D. E., 2011, “Conglomerate Stabilization Curve Design Method for Shape Memory Alloy Wire Actuators With Cyclic Shakedown,” *J. Mech. Des.*, **133**(11), p. 111010.
- [14] Shaw, J. A., Churchill, C. B., and Iadicola, M. A., 2008, “Tips and Tricks for Characterizing Shape Memory Alloy Wire: Part 1; Differential Scanning Calorimetry and Basic Phenomena,” *Exp. Tech.*, **32**(5), pp. 55–62.
- [15] Tanaka, K., Kobayashi, S., and Sato, Y., 1986, “Thermomechanics of transformation pseudoelasticity and shape memory effect in alloys,” *Int. J. Plast.*, **2**(1), pp. 59–72.
- [16] Liang, C., and Rogers, C. A., 1990, “One-dimensional thermomechanical constitutive relations for shape memory materials,” *J. Intell. Mater. Syst. Struct.*, **1**(2), pp. 207–34.
- [17] Brinson, L. C., 1993, “One-Dimensional Constitutive Behavior of Shape Memory Alloys: Thermomechanical Derivation with Non-Constant Material Functions and Redefined Martensite Internal Variable,” *J. Intell. Mater. Syst. Struct.*, **4**(2), pp. 229–242.

- [18] Buravalla, V., and Khandelwal, A., 2008, “Phenomenological Modeling of Shape Memory Alloys,” AIP Conference Proceedings, S.M. Sivakumar, V. Buravalla, and A.R. Srinivasa, eds., IIT Madras, Chennai, India, pp. 104–123.
- [19] Boyd, J. G., and Lagoudas, D. C., 1996, “A thermodynamical constitutive model for shape memory materials. Part I. The monolithic shape memory alloy,” *Int. J. Plast.*, **12**(6), pp. 805–842.
- [20] Shaw, J. A., 2002, “A thermomechanical model for a 1-D shape memory alloy wire with propagating instabilities,” *Int. J. Solids Struct.*, **39**(5), pp. 1275–1305.
- [21] Mitteer, D. M., Ridge, L. D., and Brown, J., 2010, “A Shape Memory Alloy Actuator Suitable for Use in Automatic Transmission Shift Systems,” Proceedings ACTUATOR 2010, WFB Wirtschaftsfoerderung Bremen GmbH, Bremen, Germany.
- [22] Churchill, C. B., 2010, “Experimental Techniques for Characterizing the Thermo-Electro-Mechanical Shakedown Response of SMA Wires and Tubes,” University of Michigan.
- [23] Dynalloy, Inc., 2010, “Technical and Design Data for FLEXINOL Wire from Dynalloy, Inc.” [Online]. Available: <http://www.dynalloy.com/TechData.html>. [Accessed: 16-Feb-2010].
- [24] Pathak, A., Brei, D., and Luntz, J., 2010, “Transformation strain based method for characterization of convective heat transfer from shape memory alloy wires,” *Smart Mater. Struct.*, **19**(3).
- [25] Roy, D., Buravalla, V., Mangalgiri, P. D., Allegavi, S., and Ramamurty, U., 2008, “Mechanical characterization of NiTi SMA wires using a dynamic mechanical analyzer,” *Mater. Sci. Eng. A*, **494**(1-2), pp. 429–435.
- [26] Huber, J. E., Fleck, N. A., and Ashby, M. F., 1997, “The Selection of Mechanical Actuators Based on Performance Indices,” *Proc. Math. Phys. Eng. Sci.*, **453**(1965), pp. 2185–2205.
- [27] Kim, W., Thota, M., Luntz, J., and Brei, D., 2012, “Analytical Model and Design Study on Shape Memory Alloy Web Actuator,” ICAS2012, Nanjing, China, pp. 031–16.
- [28] Redmond, J. A., Brei, D., Luntz, J., Browne, A. L., and Johnson, N. L., 2012, “Spool-Packaging of Shape Memory Alloy Actuators: Performance Model and Experimental Validation,” *J. Intell. Mater. Syst. Struct.*, **23**(2), pp. 201–219.
- [29] Park, B., Shantz, M., and Prinz, F. B., 2001, “Scalable rotary actuators with embedded shape memory alloys,” *Smart Structures and Materials 2001: Smart Structures and Integrated Systems*, Newport Beach, CA, United states, pp. 79–87.
- [30] Barnes, B. M., Brei, D. E., Luntz, J. E., Strom, K., Browne, A. L., and Johnson, N., 2008, “Shape memory alloy resetable spring lift for pedestrian protection,” SPIE, San Diego, California, USA, pp. 693005–13.
- [31] Utter, B., Barnes, B., Luntz, J., Brei, D., Teitelbaum, D. H., Okawada, M., and Miyasaka, E., 2010, “Design of an SMA Actuated Mechanotransductive Implant for Correcting Short Bowel Syndrome,” Proceedings of the 2010 Smart Materials, Adaptive Structures, and Intelligent Systems, Philadelphia, Pennsylvania, USA, pp. 875–892.

- [32] Dittmer, D. K., Buchal, R. O., and MacArthur, D. E., 1993, "The SMART wrist-hand orthosis (WHO) for quadriplegic patients," *JPO J. Prosthet. Orthot.*, **5**(3), p. 73.
- [33] Sholl, M., Donakowski, W., Sirk, M. M., Clauss, T., Lampton, M. L., Edelstein, J., and Hurwitz, M., 2003, "Optomechanical design of the cosmic hot interstellar plasma spectrometer (CHIPS)," pp. 467–478.
- [34] Bertacchini, O. W., Lagoudas, D. C., Calkins, F. T., and Mabe, J. H., 2008, "Thermomechanical cyclic loading and fatigue life characterization of nickel rich NiTi shape-memory alloy actuators," SPIE, San Diego, California, USA, pp. 692916–11.

Appendix B.

Model-based shape memory alloy wire ratchet actuator design

Shape Memory Alloy (SMA) wire ratchet actuators overcome SMA wire strain limitations by accumulating actuation stroke over multiple cycles. The underlying architecture is effective for producing large strokes from a small package, creating continuous rotation or extended displacement, and precise. It also provides discrete positioning with zero-power hold. While there have been several successful implementations of SMA ratchet actuators, most are designed ad-hoc since limited models exist to predict the stroke and force interaction during actuation cycles. Since the SMA wire actuation is highly dependent on the forces experienced through the ratchet mechanism, a model requires the prediction of the force interaction between the rack and pawl teeth along with friction in the device, and of the external force variation over actuation cycles due to the relative position change between the external system and the SMA wire. This paper presents a model-based systematic design methodology for SMA ratchet actuator which actuates position-dependent external systems. A generalized ratchet mechanism and operation sequence is introduced along with a force balance model for both austenite and martensite equilibrium to address the mechanical coupling changes. Analytical kinematic and kineto-static rack and pawl interaction models are reviewed, which feed into the force balance models. The effective stroke is evaluated by subtracting backlash from the SMA wire stroke, found through equilibrium with the mechanism and external system. This effective stroke accumulates to produce the overall actuator motion. A design methodology is suggested along with visualization methods to aid design decisions. Parametric studies expose the effects of design parameters on the SMA ratchet actuator to gain further design insight. This model-based design foundation and parametric understanding enable the synthesis of SMA wire ratchet actuators.

1. Introduction

Shape memory alloy is a class of material which can produce actuation motions from temperature and/or applied stress induced transformations between a cold, compliant martensite phase and a hot, stiff austenite phase. While SMAs exhibit larger work density ($0.2 \sim 30 \times 10^6 W/m^3$ [1]) than most other smart materials, the usable strain of SMA wire is typically limited to 2 ~ 4 % for most applications. There are several techniques to overcome this stroke limitation including amplification architectures such as mechanical leveraging and the SMA wire web architecture (also known as a bow string actuator) [2–5], as well as packaging techniques such as spool packaging [6]. Another technique is a ratchet actuator which uses time leveraging of SMA wire as an actuator to advance a ratchet to accumulate steps, achieving large overall stroke of a long rack or continuous rotation of a gear [7–9]. While mechanical leveraging architectures trade off output force to achieve larger stroke, time leveraging architectures do not sacrifice the output force. In addition to producing large stroke or continuous rotation, the SMA ratchet architecture is capable of precisely controlling position in discrete steps, and holding intermediate and/or final positions without requiring power.

While there are several successful implementations of SMA ratchet actuators [7–11], limited design models exist. Barnes *et al.* [8] introduced a design method focusing on the final actuation step to ensure the maximum required output force when compressing a spring for an automotive pedestrian protection device. Although this method is useful to select the diameter and the number of the SMA wires, it does not guide the designer to select other device element parameters such as wire length and bias spring stiffness. Utter *et al.* [9] developed rack and pawl tooth interaction kinematic and kinetic models along with the Reset View design methodology to select reset spring stiffness for a mechanotransductive bowel extender implant device. While this method provides a useful visualization technique to select the reset spring, it does not address consecutive actuations against a position dependent external system where the load varies with each step.

This paper presents a model-based design methodology for SMA wire ratchet actuators which enables complete device design working against a general position dependent external system. The basic SMA wire ratchet actuator mechanism and operation states are introduced along with variations in configuration. To evaluate the effective stroke performance of the SMA wire ratchet actuator, force balance models for each state during actuation and a free clearance update

model accounting for partial steps and backlash are derived. A design methodology consisting of mechanism design and SMA actuation design is formalized supported by the SMA wire view design visualization method. The visualization method is extended to address the accumulation of multiple steps and mechanical coupling changes during the actuation cycle. Design insight is provided by parameter studies on three major design variables: the device bias stiffness, the bias free clearance, and the SMA wire length. The design methodology and the design insight from the parametric study provide a foundation to synthesize SMA wire ratchet actuators to overcome the actuation strain limitations of SMA.

Nomenclature

Ratchet device elements and actuation:

b_A	Austenite backlash
b_M	Martensite backlash
b_r	Effective distance between the active and passive pawls
C_0	System free clearance
C_0^{bias}	Device bias free clearance
$D_0^{ratchet}$	Offset between the active and passive pawl
F_{SMA}^A	SMA wire force in austenite phase
F_{SMA}^M	SMA wire force in martensite phase
F_{ext}	External system force
$F_{ratchet}^{active}$	Interaction force between the rack and the active pawl
$F_{ratchet}^{passive}$	Interaction force between the rack and the passive pawl
F_{bias}	Device bias force
$F_{friction}^{rack}$	Rack sliding friction force
$F_{friction}^{active}$	Active pawl sliding friction force
p	Rack tooth pitch
δ_A	SMA wire deflection in austenite phase
δ_M	SMA wire deflection in martensite phase
δ_{SMA}	SMA wire stroke for each step
δ_{eff}	Effective stroke for each step

Rack and pawl geometry and interaction:

F_0^{engage}	Initial pawl engagement force
----------------	-------------------------------

F_f	Pawl-rack friction force vector during disengagement
F_n	Normal force vector between pawl and rack
F_n	Scalar normal force
$F_{ratchet}$	Interaction force to disengage ratchet pawls
k_{engage}	Pawl engagement spring stiffness
L^*	Effective moment arm length of the pawl
l_y	Rack and pawl tooth depth
l_{xr}	Rack/pawl tooth length on reengagement surface
l_{xd}	Rack/pawl tooth length on disengagement surface
t_x	Horizontal pawl tip position relative to pivot
t_y	Vertical pawl tip position relative to pivot
μ	Static friction coefficient between rack and pawl teeth
τ	Engagement torque on pawl

2. Ratchet mechanism

The SMA ratchet actuator is a type of SMA architecture which uses the ratchet mechanism to accumulate the SMA actuation stroke over multiple cycles. It is a time leveraging architecture useful for overcoming SMA wire strain limitations. SMA wire ratchet actuators consist of a linear rack or rotating gear, an active pawl including an SMA actuator, and a passive pawl (Figure B.1). The linear rack or rotating gear provides the mechanical connection between the active pawl and the external system. The active pawl, which advances the linear rack or rotating gear, is connected to the SMA wire and accompanying device bias, which antagonistically actuates and restores the active pawl. The passive pawl holds the rack or gear during restoration of the active pawl. In this

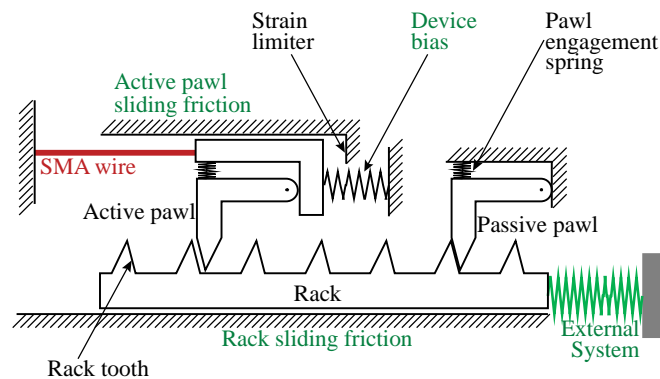


Figure B.1. Schematic of SMA wire ratchet actuator.

The typical ratchet device configuration is shown in the schematic.

paper, the SMA wire ratchet actuator with a linear rack is discussed; the rotating gear ratchet actuator can be designed using an equivalent approach.

The actuation sequence of a linear SMA wire ratchet actuator is illustrated in Figure B.2. The device elements depicted in Figure B.1 are simplified, and the initial arrangement of device elements is defined in Figure B.2a. In the martensite equilibrium state (Figure B.2b), the external system force is supported by the passive pawl, and the active pawl is in the equilibrium position between the cold compliant martensitic SMA wire and the device bias. This martensite equilibrium position is affected by the pre-tension from the device bias, which is determined by the stiffness of the device bias, k_{bias} , and the bias free clearance, C_0^{bias} . The bias free clearance is defined as the relative separation between the device bias and the SMA wire in the austenite strain-free state before they are connected.

When the SMA wire is heated, the active pawl first moves from the martensite equilibrium position, which may lie between rack teeth, to the nearest rack tooth position, engaging the rack. This free sliding distance, which is named as the *martensite backlash*, b_M , does not contribute to the output stroke because the rack is not moving during this lost portion of SMA wire stroke. Once the active pawl engages the rack, the SMA wire pulls the external system, F_{ext} , along with the rack while overcoming the device bias force, F_{bias} , the rack sliding friction, $F_{friction}^{rack}$, the active pawl sliding friction, $F_{friction}^{active}$, and the disengagement interaction force between the passive pawl and the rack tooth, $F_{ratchet}^{passive}$ (Figure B.2c). This disengagement interaction force occurs when the passive pawl is climbing the rack tooth to allow passage of the rack under the pawl. When the SMA wire is fully transformed to the hot stiff austenite state, the active pawl reaches the austenite equilibrium position (Figure B.2d). This austenite equilibrium position is affected by the external system force, F_{ext} , which is a function of its deflection, x . At this austenite equilibrium position, the external system deflection is the sum of the rack sliding distance and the system free clearance, C_0 , which increases after each actuation cycle.

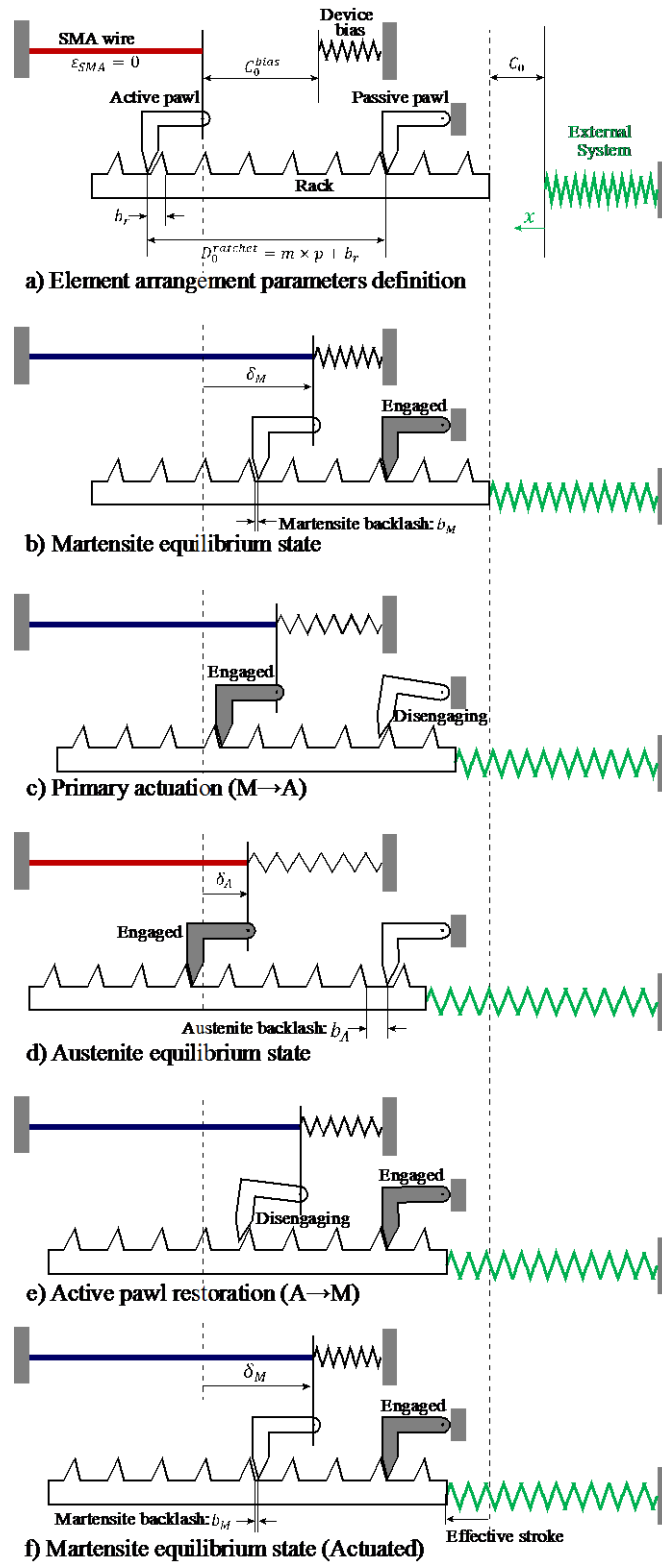


Figure B.2. SMA ratchet actuation cycle.

A single step actuation cycle of the SMA wire ratchet actuator is illustrated. By heating and cooling the SMA wire the rack advances by the effective stroke which is a portion of the SMA wire stroke subtracting the austenite and martensite backlashes.

Upon cooling of the SMA wire, the active pawl and rack retract until the passive pawl engages the rack and holds the external system at the actuated position. This sliding distance, which is named as the *austenite backlash*, b_A , is another loss from the SMA wire stroke because the rack is moving backward. At this point, the rack is shifted by the *effective stroke*, which is the stroke of the active pawl from the austenite equilibrium position to the martensite equilibrium position after subtracting the austenite and martensite backlashes. Because each actuation step starts and ends in the condition of the passive pawl engaging the rack tooth and holding the external system, the effective stroke advances a discrete distance, which is multiple of the tooth pitch length. Once the passive pawl holds the rack, the device bias moves the active pawl while overcoming the martensitic SMA wire force, F_{SMA}^M , the active pawl sliding friction force, $F_{friction}^{active}$, and the disengagement interaction between the active pawl and the rack tooth, $F_{ratchet}^{active}$ (Figure B.2e). When the SMA wire is fully transformed to the cold compliant martensite phase, the active pawl is restored to the martensite equilibrium position, and this process completes one *step* (Figure B.2f). By repeating the heating and cooling of the SMA wire, the SMA wire ratchet actuator accumulates steps, and the *overall stroke* of the actuator output is the sum of the effective strokes of each step.

Because the SMA wire directly pulls the rack while it is heating, this mode of ratchet actuation is called the *SMA pull* mode. An alternative mode of actuation is the *bias push* mode, where the SMA wire compresses the device bias spring and the device bias spring directly pushes the rack while the SMA wire cools. One of the benefits of the bias push mode is that the SMA wire is protected from external system disturbances because the SMA wire only interacts with the device bias. However, the bias push mode ratchet actuator requires a stiffer device bias to drive the external system requiring a higher force from the SMA wire to overcome the stiffer device bias. The proper actuation mode depends on the specific application. Another alternative configuration of the SMA ratchet actuator is the *friction hold* mode. The passive pawl of the SMA ratchet mechanism is not necessary when the sliding friction force of the rack is large enough to hold the rack against the external load during the active pawl restoration stage. While friction hold enables a simpler mechanism by eliminating the passive pawl, the large sliding friction force of the rack also requires a higher force from the SMA wire and/or device bias force.

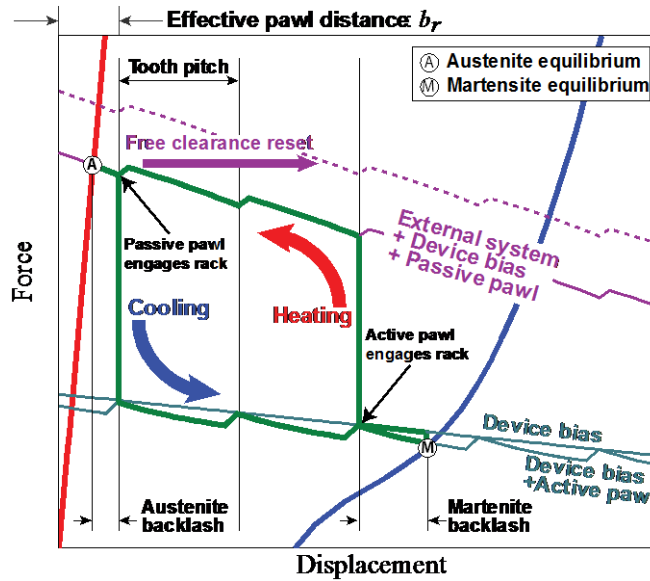


Figure B.3. Ratchet actuator loading / unloading path of a single actuation step in SMA wire coordinate system.

The loading and unloading path shows the mechanical coupling changes during the actuation cycle. Upon the active pawl engagement during the loading, the path jumps from the device bias to the combined force curve adding the external system force and the passive pawl interaction. During the cooling, the unloading path drops to the device bias and active pawl interaction curve after the passive pawl holds the external system.

This paper focuses on the SMA pull mode ratchet actuator with passive pawl hold mode; the model and the design approach for the bias push mode actuator and/or the friction hold mode actuator can be easily modified from the SMA pull mode ratchet actuator with passive pawl. A typical ratchet actuation loading and unloading path of a single actuation step is shown in Figure B.3. The red curve represents the SMA wire force-deflection behavior in the hot austenite phase, and the blue curve represents the cold martensite SMA wire force-deflection behavior. These force-deflection behaviors are characterized by two functions: F_{SMA}^A and F_{SMA}^M which represent the constitutive laws. The purple curve represents the combined force of the external system, device bias, and the passive pawl disengagement interaction. The cyan straight line represents the device bias force, and the cyan curve represents the combined force b_r of the device bias and the active pawl disengagement interaction.

When the SMA wire is in the cold compliant martensite phase, the system is in the martensite equilibrium position \textcircled{M} . Upon heating the SMA wire, the loading path follows the

device bias line until the active pawl engages the rack, overcoming the martensite backlash. At this point the external system force and the passive pawl interaction force are added to the device bias, the loading path jumps to the purple colored lumped force curve, and reaches the austenite equilibrium position \textcircled{A} . When the wire is cooling, the unloading path follows the lumped force curve of the external system and device bias until the passive pawl engages and holds the rack, overcoming the austenite backlash. After the passive pawl holds the rack, the SMA wire is working against the device bias and the active pawl interaction force dropping the unloading path to the cyan colored lumped force curve. At this point, the system free clearance, C_0 , is reset by the effective stroke which is an integer number of tooth pitch lengths. The lumped force curve of the external system, device bias, and passive pawl disengagement interaction force shifts to the right (dotted curve) by the distance of the effective stroke. This shift is the accumulated actuation portion of the SMA wire stroke.

Because the SMA wire and the external system are mechanically connected through the rack, the relative position between the SMA wire and the external system, which is defined as the free clearance, C_0 , resets for each step of actuation due to the accumulated advancement of the rack. Because of the increased system free clearance and resulting external system force change, the active pawl reaches a new austenite equilibrium position while the martensite equilibrium stays at the same position. Due to this austenite equilibrium position shift, the effective stroke size varies between actuation cycles. The ratchet mechanism can be understood as a *free clearance update mechanism* because of this unique update of the relative position between the SMA wire and the external system over accumulated actuation cycles.

3. Ratchet design model

To predict the effective stroke for each step of actuation, the austenite and martensite equilibria need to be found, and then an effective stroke is determined by subtracting the backlashes from the distance between the equilibria. Using this effective stroke, the relative position between the external system and the SMA wire, which is the device free clearance, C_0 , is updated, and the performance for the next step is predicted. There are three main aspects of the SMA wire ratchet actuator model: force balance model, rack and pawl interaction model, and the effective stroke evaluation and free clearance update. The force balance model addresses the mechanical coupling changes for each state during actuation. The interaction force model for the

rack and pawl tooth disengagement interaction is a unique ratchet actuator specific component in the force balance model. The effective stroke evaluation and free clearance update model tracks the effective stroke and the free clearance changes for accumulated steps.

3.1. Force balance model

The force balance model of the SMA wire ratchet actuator is complicated by the mechanical coupling of the device elements during actuation. In the martensite equilibrium state, the passive pawl holds the external system, and the device bias (F_{bias}) stretches the cold martensite SMA wire (F_{SMA}^M) moving the active pawl to the equilibrium position while working against the active pawl sliding friction force, $F_{friction}^{active}$ and the disengagement interaction force between the active pawl and the rack tooth, $F_{ratchet}^{active}$ (Figure B.2b),

$$F_{bias} = F_{SMA}^M + F_{friction}^{active} + F_{ratchet}^{active}. \quad (1)$$

Upon heating, the hot stiff austenite SMA wire (F_{SMA}^A) pulls the external system (F_{ext}) through the active pawl while overcoming the rack sliding friction force, $F_{friction}^{rack}$, the active pawl sliding friction forces, $F_{friction}^{active}$, the disengagement interaction force between the passive pawl and the rack tooth, $F_{ratchet}^{passive}$, and the device bias, F_{bias} (Figure B.2d),

$$F_{SMA}^A = F_{ext} + F_{friction}^{rack} + F_{friction}^{active} + F_{ratchet}^{passive} + F_{bias}, \quad (2)$$

where the external system force, F_{ext} is a function of the external system deflection, x

$$F_{ext} = F(x). \quad (3)$$

As the actuation stroke is accumulated over steps, the external system deflection, x increases. Thus the austenite equilibrium position changes for each step due to changes in the external system force, while the martensite equilibrium stays at the same position since the external force does not affect it (Equation 1).

3.2. Rack and pawl interaction kinematic and kinetic model review

The disengagement interaction force between the rack and pawl $F_{ratchet}$ is a unique component of the force balance models. Utter *et al.* [9] derived the rack and pawl interaction kinematic and kinetic model to evaluate the interaction force, and the model is reviewed here with

slight modification of the axis direction. The model is derived using the geometry parameters in Figure B.4. The interaction force between the rack and pawl, $F_{ratchet}$ is computed as the sum of the projections of the normal force, F_n and the corresponding friction force, F_f onto the x-axis,

$$F_{ratchet} = [1 \quad 0](\mathbf{F}_n + \mathbf{F}_f). \quad (4)$$

The normal force, \mathbf{F}_n on the pawl is a scalar force, F_n in the contact direction between the tip of the rack tooth and the surface of the pawl (unit normal, $\hat{\mathbf{n}}_0$) to the rack surface in the fully engaged position rotated by the pawl angle, θ_{pawl}

$$\mathbf{F}_n = \begin{bmatrix} \cos \theta_{pawl} & \sin \theta_{pawl} \\ -\sin \theta_{pawl} & \cos \theta_{pawl} \end{bmatrix} \hat{\mathbf{n}}_0 F_n, \quad (5)$$

where the initial unit normal, $\hat{\mathbf{n}}_0$ is a function of the pawl geometry expressed as

$$\hat{\mathbf{n}}_0 = \frac{1}{\sqrt{l_{xd}^2 + l_y^2}} \begin{bmatrix} l_{xd} \\ l_y \end{bmatrix}. \quad (6)$$

Solving the moment balance for the scalar normal force, F_n using the pawl disengagement kinematics for the pawl angle, θ_{pawl} in terms of the rack displacement, x_{rack} yields

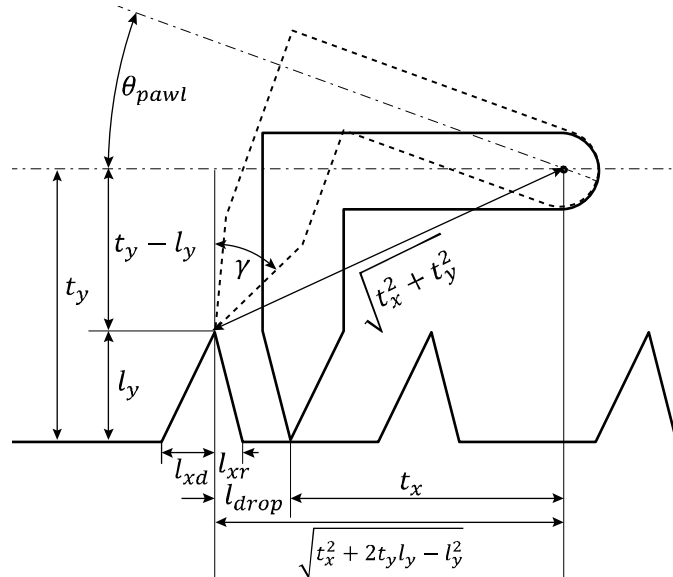


Figure B.4. Rack and pawl geometry parameters.

The rack and pawl geometric parameters are defined along with the pawl drop length.

$$F_n = \frac{-\tau}{L^*} \quad (7)$$

where L^* is the effective pawl moment arm

$$L^* = \sin \gamma (\mu(l_y - t_y) - x_{rack} - t_x + l_{xr}) + \cos \gamma (\mu(x_{rack} + t_x - l_{xr}) + l_y - t_y), \quad (8)$$

γ is the angle of the contact surface

$$\gamma = \theta_{pawl} + \tan^{-1} \left(\frac{l_{xd}}{l_y} \right), \quad (9)$$

and τ is the torque from the pawl engagement spring.

The corresponding friction force, \mathbf{F}_f is found by rotating the normal force, F_n by 90° and scaling by a Coulomb friction coefficient, μ ,

$$\begin{aligned} \mathbf{F}_f &= \begin{bmatrix} 0 & -1 \\ 1 & 0 \end{bmatrix} F_n \mu \\ &= \begin{bmatrix} 0 & -1 \\ 1 & 0 \end{bmatrix} \begin{bmatrix} \cos \theta_{pawl} & \sin \theta_{pawl} \\ -\sin \theta_{pawl} & \cos \theta_{pawl} \end{bmatrix} \hat{\mathbf{n}}_0 F_n \mu. \end{aligned} \quad (10)$$

By completing the combined interaction force equation (Equation 4) using the equations for the normal and friction forces (Equations 5-10), the rack and pawl interaction force can be evaluated. In some cases, the active pawl and passive pawl may have different geometries and/or engagement torque, such that the disengagement interaction forces, $F_{ratchet}^{active}$ and $F_{ratchet}^{passive}$ must be evaluated separately.

3.3. Effective stroke evaluation and free clearance update

The stroke for each step is evaluated by finding the austenite and martensite equilibria using the force balance models (Equations 1 and 2), although only a portion of the distance between the equilibria is accumulated due to the stroke loss from the austenite and martensite backlashes. The effective stroke needs to be evaluated to predict the actuator output performance, which also affects the performance of the next step through the free clearance update.

In the martensite equilibrium state (Figure B.2b), the system satisfies the martensite force balance model (Equation 1), and the deflection of the SMA wire in the martensite phase, δ_M can be found from the martensitic SMA wire force, F_{SMA}^M using the constitutive relation. From this martensite deflection, δ_M , the martensite pitch number, n_M , which is the integer number of pitch lengths from the zero deflection point of the SMA wire, and the martensite backlash, b_M are evaluated using the known pitch length, p and the effective distance between the active pawl and the passive pawl, b_r

$$n_M \times p + b_M = \delta_M - b_r. \quad (11)$$

Because the SMA wire actuates by contracting from the martensite equilibrium position to the austenite equilibrium position, the martensite pitch number, n_M represents the maximum pitch length which can contribute to the effective stroke. However, the tip of the pawl is not moving only in the x-axis direction, thus there needs to be a check that the rack tooth completely passes under the pawl to ensure the full disengagement. For this check, the drop length is defined, which is the horizontal distance between the peak of the rack tooth and the position of the pawl tip when it drops down from the tip immediately after passing over the rack tooth tip (Figure B.4). The drop length, l_{drop} is calculated using the geometric parameters as

$$l_{drop} = \sqrt{t_x^2 + 2t_y l_y - l_y^2} - t_x, \quad (12)$$

which can be larger or smaller than the rack tooth length on the disengaging surface, l_{xd} depending on the geometry. When the martensite backlash is smaller than the difference between the active pawl drop length and the rack tooth length on the reengagement surface

$$b_M < l_{drop}^{active} - l_{xr}, \quad (13)$$

additional motion is necessary to drop the pawl and complete the disengagement. Under this condition, the backlash must be measured from the previous tooth on the rack, reducing the martensite pitch number, n_M by one.

For the initial martensite equilibrium state, the actuator output stroke, x , which is the deflection of the external system, is the same as the initial system free clearance, C_0 because the rack is held by the passive pawl and the external system is extended to the rack

$$x = C_0. \quad (14)$$

When the SMA wire is heated, the system satisfies the austenite force balance model (Equation 2) in the austenite equilibrium state (Figure B.2d), and the austenite deflection, δ_A is found from the austenite SMA wire force, F_{SMA}^A . Similarly, the austenite pitch number, n_A and the austenite backlash, b_A is assessed

$$n_A \times p - b_A = \delta_A - b_r. \quad (15)$$

If the austenite backlash is smaller than the difference between the passive pawl drop length and the rack tooth length on reengagement surface is

$$b_A < l_{drop}^{passive} - l_{xr}. \quad (16)$$

The backlash must be measured from the previous tooth on the rack, increasing the austenite pitch number, n_A by one.

At the point of austenite equilibrium, the external system deflection, x is the sum of the system free clearance, C_0 and the rack advancement distance, which is the SMA wire stroke minus the martensite backlash. The SMA wire stroke is the distance between the austenite equilibrium and the martensite equilibrium,

$$\begin{aligned} \delta_{SMA} &= \delta_M - \delta_A \\ &= (n_M - n_A) \times p + b_M + b_A. \end{aligned} \quad (17)$$

The external system deflection, x is

$$x = C_0 + (n_M - n_A) \times p + b_A, \quad (18)$$

thus the external force in the austenite equilibrium is

$$F_{ext} = F(C_0 + (n_M - n_A) \times p + b_A). \quad (19)$$

When the SMA wire is again cooled (Figure B.2f), the active pawl restores to the martensite equilibrium position while the rack retracts only until it engages the passive pawl and then stays at the actuated position. The effective stroke after this retraction, which is the net advancement distance of the rack, is

$$\delta_{eff} = (n_M - n_A) \times p, \quad (20)$$

which is an integer multiple of the tooth pitch length, including zero if the SMA wire stroke is completely wasted by the martensite and austenite backlashes.

For the next actuation step, the external system free clearance is updated by adding the effective stroke from the previous step:

$$C_0^{next} = C_0 + \delta_{eff}. \quad (21)$$

Because of the increased system free clearance, the austenite force balance model creates a new austenite equilibrium position while the martensite stroke stays at the same position. Due to the austenite equilibrium position shift, the effective stroke size of the SMA wire ratchet actuator may vary over the accumulated actuation.

By solving the force balance models repeatedly using the rack and pawl interaction kinematics and kinetics model and the effective stroke evaluation model, the overall performance of the SMA wire ratchet actuator is predicted. While the SMA wire ratchet mechanism can step indefinitely, there are other constraints limiting the overall output stroke such as the maximum stress on the wire and the length of the rack. Moreover, there are many design parameters that affect the overall performance such as the device bias stiffness, bias free clearance, initial system free clearance, SMA wire parameters, and pawl and rack tooth geometry. To address this complexity, a design study is helpful to provide design insight.

4. Design study

The design process for SMA wire ratchet actuators consists of two main steps: the mechanism design and the SMA actuation design. The mechanism design selects the rack and pawl geometry parameters to carry the external system load while satisfying geometric constraints. Utter *et al.* [9] discussed design considerations for the rack tooth and pawl geometry parameters: a *packaging constraint* to avoid geometric interferences between moving parts and the package boundary, the *load bearing capacity* to carry the external system force, and a *self-locking condition* to ensure the engaged state between the rack tooth and the pawl during actuation. Given the tooth geometry, the SMA actuation design has two parts: force parameter design and stroke parameter design. A design visualization method for SMA wire ratchet actuators using an SMA wire view is modified to aid these design decisions.

4.1. SMA actuation design

The first step of the SMA actuation design is the force parameter design: the number and the diameter of the SMA wire are selected to meet the maximum actuation force requirement. The maximum austenite SMA wire force, F_{SMA}^A can be calculated from the force balance equation for the austenite equilibrium (Equation 1) using the maximum external system force, F_{ext} required by the application. The number and diameter of SMA wires acting in parallel must be selected to produce the required SMA wire force, F_{SMA}^A at a set maximum austenite stress. The specification of maximum stress is a design decision to protect the SMA material from functional and/or structural fatigue [12–14], while the wire diameter and resulting number of wires to maintain this stress is selected considering power consumption and actuation cycle time.

The second step of the SMA actuation design is the stroke parameter design: the SMA wire length, and ratchet device elements parameters such as device bias stiffness and bias and system free clearance. For the device element parameter design, the effective stroke evaluation model can be solved interactively using the SMA wire view, which is commonly used for graphical SMA wire device design [12]. In a typical SMA wire view (Figure B.5), the austenite and martensite SMA wire force-deflection curves are plotted in red and blue, and all other device elements of the actuator and the external system are lumped together as a green F-d curve. However, due to the changing mechanical coupling during the actuation stages which is unique to ratchet actuators, the lumped loading curve is plotted in green, and the lumped unloading curve is plotted in cyan. The loading curve represents the lumped force of the external system, device bias, and passive pawl disengagement interaction, while the unloading curve represents the lumped force of the device bias and active pawl disengagement interaction only. The black vertical solid lines represent the locations of the rack teeth, which start at the effective pawl distance b_r from the active pawl zero deflection position. By finding the austenite and the martensite equilibrium positions (*i.e.* intersections between the austenite curve and the loading curve, and the martensite curve and the unloading curve) on the SMA wire view plot and counting the rack tooth lines between the equilibria, the effective stroke for each step can be easily evaluated, and the loading curve can be

shifted by the effective stroke distance after each step. To check for partial disengagement of the pawls, the supplemental black dotted lines are marked to indicate the pawl drop positions. If the equilibrium point does not pass a pawl drop position, the effective stroke loses one pitch length.

An example SMA wire ratchet actuator performance prediction is plotted in the SMA wire view (Figure B.5). Given a tooth geometry (Table B.1), a 100 mm long 15 mil (15/1000 in) diameter SMA wire is connected to a 0.5 N/mm stiffness device bias with 14 mm device free clearance to actuate a 0.75 N/mm stiffness external system, which is connected to the rack, which

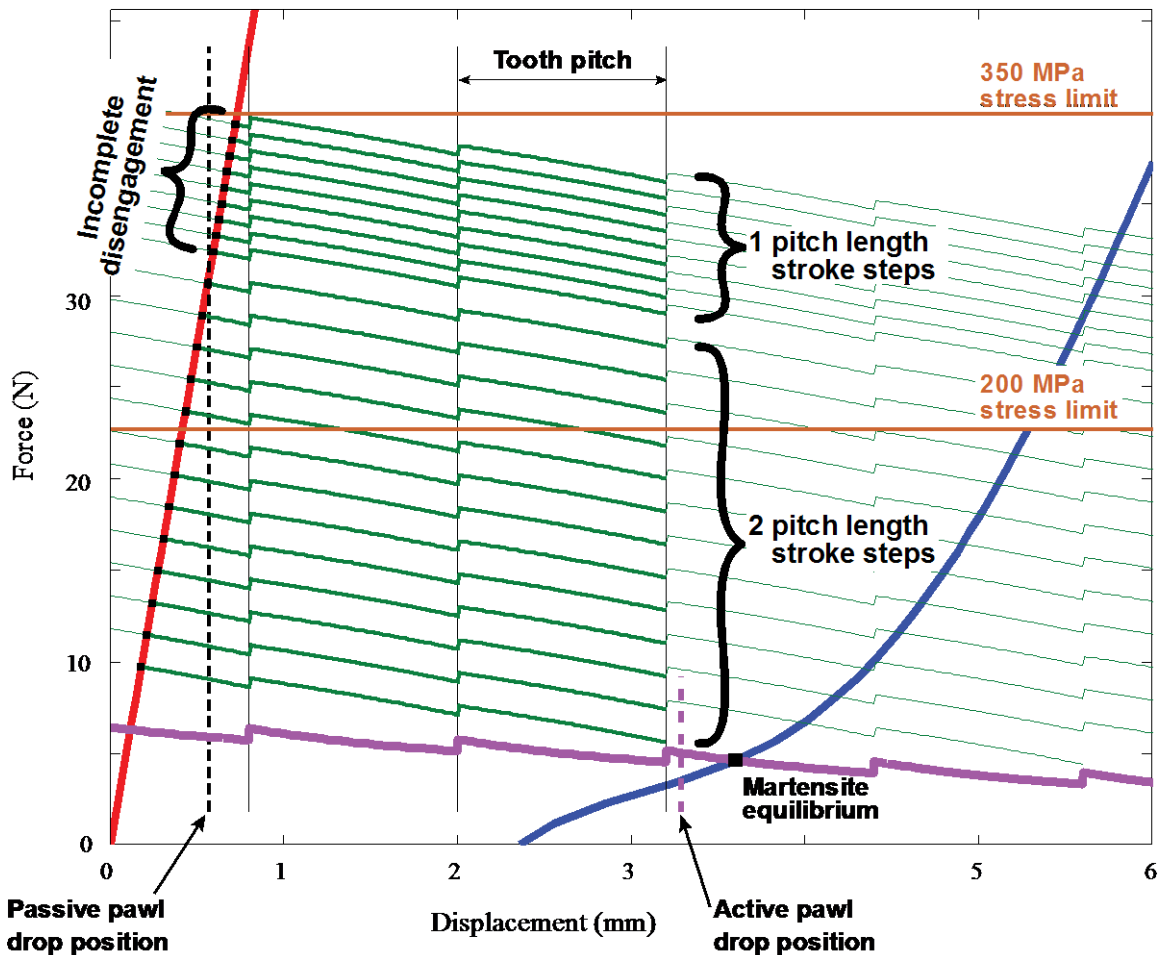


Figure B.5. An example SMA wire ratchet actuator performance prediction in SMA wire view.

A 100 mm length the SMA wire is connected to the 0.5 N/mm stiffness device bias with the 14 mm device free clearance to actuate 0.75 N/mm stiffness external system, which is connected to the rack, which has the 1.2 mm pitch tooth, with 0 mm system free clearance. While a 100 mm length SMA wire can only produce 2 ~ 4 mm stroke, the example SMA wire ratchet actuator can produce 45.2 mm stroke until the SMA wire reaches the 350 MPa stress limit.

has a 1.2 mm tooth pitch, with 0 mm system free clearance. Without the ratchet actuator mechanism, a 100 mm length SMA wire can only produce 2 ~ 4 mm stroke, however, the example SMA wire ratchet actuator can produce a 45.2 mm stroke until the SMA wire reaches the 350 MPa stress limit. Even with a more conservative 200 MPa stress limit, a 19.2 mm stroke can be produced. The choice of 200 and 350 MPa stress limits is a material usage decision effecting the functional and structural fatigue (shakedown and lifetime) [12–14].

Table B.1. Rack and pawl geometric parameters

Rack tooth geometry			Pawl geometry		
			Active pawl		Passive pawl
l_{xd}	0.6	mm	t_x	2.6	mm
l_{xr}	0.6	mm	t_y	3.12	mm
l_y	0.66	mm	k_{engage}	2	N/mm
p	1.2	mm	F_0^{engage}	0.3	N
b_r	8	mm	μ	0.1	

This plot presents a great deal of decision making related information to designers. For performance evaluation, the effective stroke is found by counting the number of pitch lengths between the austenite and martensite equilibria. The effective stroke also indicates the overall actuation cycle time because the heating / cooling cycle takes almost the same time for a 1 pitch length stroke actuation and a 2 pitch length actuation. The plot also shows the quantitative and qualitative actuation characteristics at the same time such as the number of steps to reach the maximum stress limit and the effective stroke variation during overall actuation. For example, the actuator stroke changes after 13 steps from 2 pitch length strokes to 1 pitch length stroke when the passive pawl fails to fully disengage the rack tooth. This incomplete disengagement is visualized using the vertical black dotted passive pawl drop position line, which also shows the safety margin of the actuation. The effects of key design parameters can be evaluated with this plot. For example, by changing the bias free clearance, the martensite equilibrium position is changed, and if the equilibrium position moves to the left of the active pawl drop position, the actuator loses 1 pitch length of effective stroke. The plot also shows the zero effective stroke condition, where the SMA wire stroke is completely lost to backlash, along with the design parameter changes to avoid this condition. This interactive evaluation using SMA wire view design method enables designers to make better design decisions.

4.2. Design parameter studies

A set of numerical parameter studies helps the designer to understand the effect of the design parameters and the usage of the design plot, and provide design insight with respect to three major example design parameters: the device bias stiffness, k_{bias} , the bias free clearance, C_0^{bias} , and the SMA wire length, l_{SMA} . The effects of these design parameters on the actuator performance (overall stroke and speed) are evaluated using the SMA wire view design plots. These studies provide design insight to aid design decisions during the design process.

4.2.1. Effect of the device bias stiffness

The device bias stiffness, k_{bias} (combined with the bias free clearance, C_0^{bias}) affects the device bias force, F_{bias} . To explore the effect of the device bias stiffness, all other design parameters are fixed as the example in the previous section, and only the device bias stiffness is changed from 0.1 N/mm to 2 N/mm (Figure B.6). The maximum austenite stress is set to 350 MPa and the overall stroke and the step count (speed) are used as comparison metrics. While the actuator with the 0.1 N/mm bias advances with 1 pitch length strokes during the entire 38.4 mm overall actuation stroke, the actuator with the stiffer 0.5 N/mm bias advances with 2 pitch length strokes for the first 13 steps, then advances with 1 pitch length strokes for a total of 22 steps, creating a longer 42 mm overall stroke with fewer actuation steps thereby moving faster. The 1 N/mm device bias stiffness actuator produces a smaller 33.6 mm overall stroke in 9 steps of 2 pitch length stroke and 10 steps of 1 pitch length stroke, while the 2 N/mm actuator creates a much shorter 15.6 mm stroke in one step of 3 pitch length stroke and 6 steps of 2 pitch length stroke, decreasing the overall stroke due to the increased device bias force.

Because the hot austenite SMA wire works against the device bias as well as the external system, a stiffer device bias increases the austenite equilibrium stress, causing the SMA wire to reach the maximum austenite stress limit in fewer steps. The examples of 0.5 N/mm, 1 N/mm, and 2 N/mm device bias stiffness actuators show this trend. Although a soft device bias is effective to reduce the device bias force, as shown in Figure B.6a, the soft device bias may not stretch the SMA wire sufficiently in the martensite equilibrium state, thus limiting the SMA wire stroke to 1 tooth pitch lowering the action speed. Moreover, the 0.1 N/mm device bias stiffness case shows that the actuator fails to produce an effective stroke after 32 steps even before the SMA wire

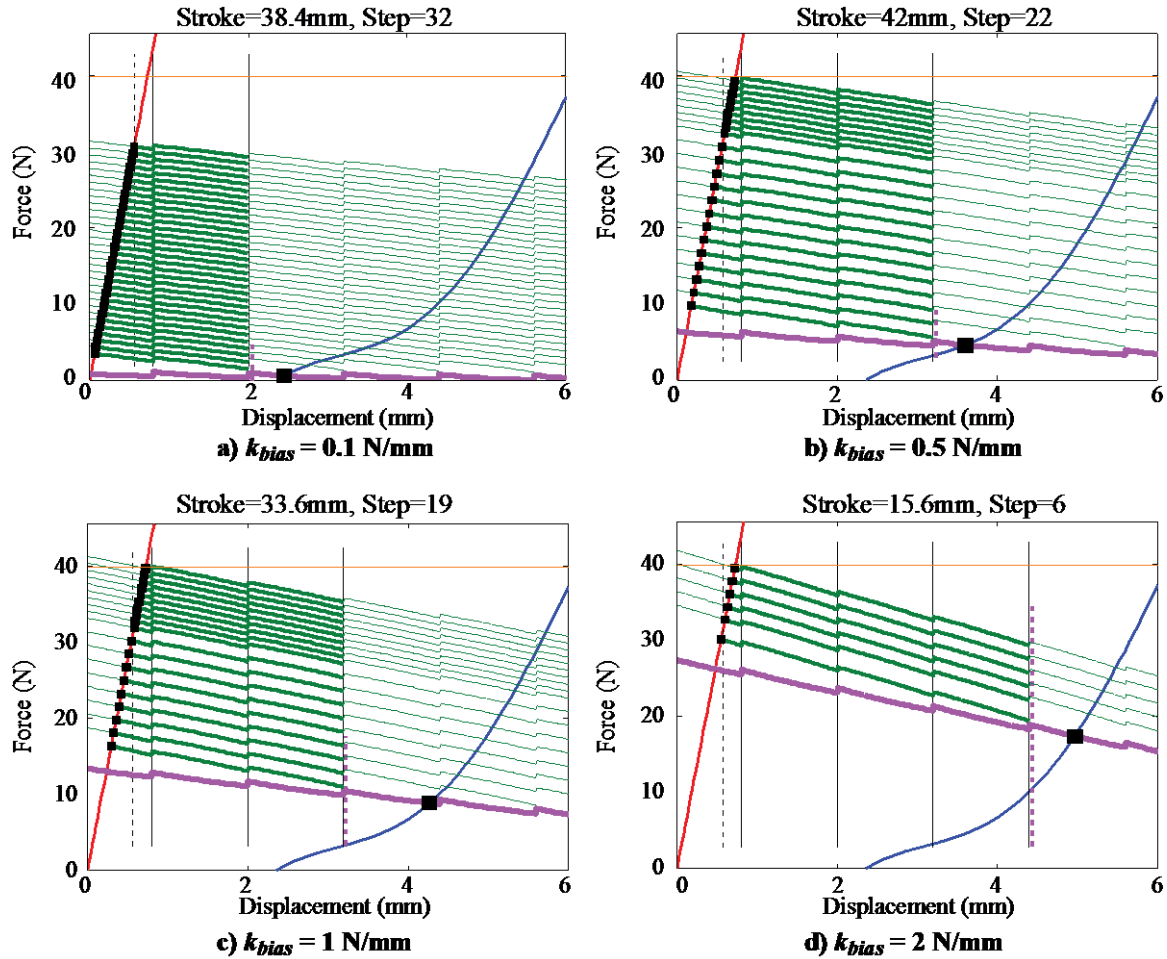


Figure B.6. Effect of device bias stiffness on the SMA wire ratchet actuator performance. Because the hot austenite SMA wire works against the device bias as well as the external system, a stiffer device bias increases the austenite equilibrium stress, causing the SMA wire to reach the maximum austenite stress limit in fewer steps. However, a soft device bias may not stretch the SMA wire sufficiently in the martensite equilibrium state, thus limiting the SMA wire stroke to 1 tooth pitch lowering the action speed.

reaches the maximum stress due to incomplete passive pawl disengagement limiting the overall stroke to 38.4 mm. The softer device bias stiffness is useful to limit the maximum austenite stress, but the martensite equilibrium position needs to be checked to ensure sufficient SMA wire stroke. The martensite equilibrium stress also affects the material transformation temperatures, which limits the minimum ambient operation temperature, and the heating and cooling time during actuation cycles. Thus the tradeoff between these metrics needs to be considered during the design process.

4.2.2. Effect of the bias free clearance

Like the bias stiffness, k_{bias} , the bias free clearance, C_0^{bias} also affects the device bias force. To explore the effect of the bias free clearance, the device free clearance is changed from 3 mm to 30 mm, while all other parameters are fixed as the example case in section 0 (Figure B.7). The 3 mm bias free clearance actuator fails to create any effective stroke since the SMA wire stroke is completely wasted by the martensite and austenite backlashes. The 4 mm bias free clearance actuator creates a 38.4 mm stroke with 32 steps of 1 pitch length stroke. The 14 mm and 30 mm bias free clearance actuators create 42 mm and 30 mm strokes with 22 and 10 steps respectively.

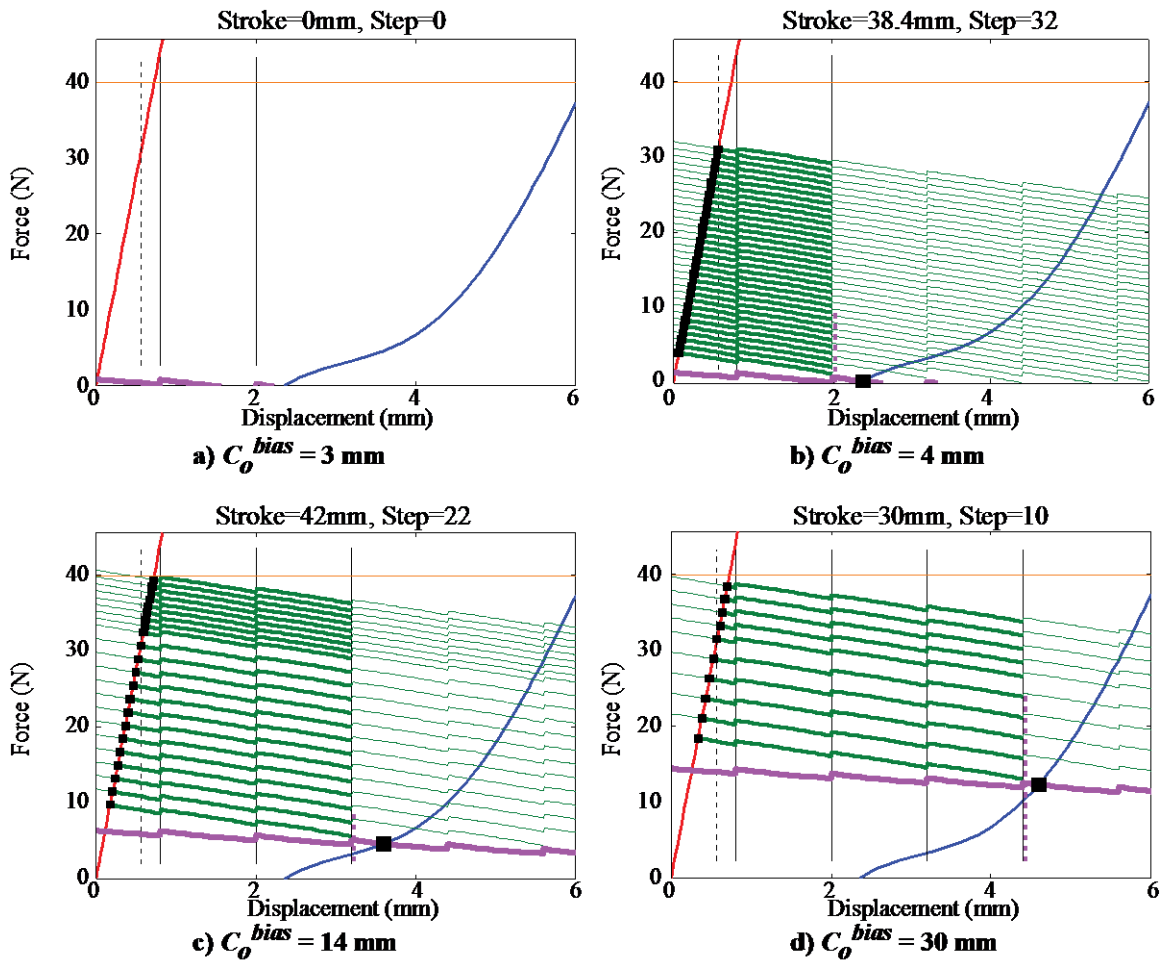


Figure B.7. Effect of bias free clearance on the SMA wire ratchet actuator performance.

Increasing the bias free clearance reduces the overall stroke by increasing the austenite equilibrium stress due to the increased device bias force. However, at smaller bias free clearance, the overall stroke is reduced due to a reduced martensite deflection. Increasing the bias free clearance makes the actuation speed faster by increasing the effective stroke length per step.

Increasing the bias free clearance reduces the overall stroke by increasing the austenite equilibrium stress due to the increased device bias force. However, at smaller bias free clearance, the overall stroke is reduced due to a reduced martensite deflection. A *feasibility boundary* exists where very small bias free clearances no longer produce any stroke, and only a 1 mm difference in the bias free clearance changes the actuation performance drastically. This implies that the manufacturing tolerance needs to be carefully considered for bias free clearance selection near this boundary, although setting a safety margin can ensure device operation.

Increasing the bias free clearance makes the actuation speed faster by increasing the effective stroke length per step. But, there is a limitation in certain conditions to increasing the step stroke length by increasing the bias free clearance. Because the austenite modulus is higher than the martensite modulus, if the martensite equilibrium position is moved further from the origin by increasing the bias free clearance, the austenite equilibrium position may move inside the passive pawl drop position losing a tooth pitch of effective stroke length. Furthermore, increasing the bias free clearance reduces the overall stroke because the increased device bias force limits the number of steps before reaching the maximum stress.

Combined with the device bias stiffness, the proper location of the martensite equilibrium position has to be set to ensure enough SMA wire stroke and minimize the martensite backlash, while limiting the device bias force to limit the maximum austenite equilibrium stress.

4.2.3. Effect of the SMA wire length

The SMA wire length, l_{SMA} scales the SMA wire actuation stroke. While this actuation stroke scaling does not affect the force balance models, it affects the effective stroke. To explore the effect of the SMA wire length on the overall performance, the SMA wire length is varied from 50 mm to 200 mm, while all other parameters are fixed as the example in section 0 (Figure B.8). The 50 mm SMA wire actuator failed to create any effective stroke, while the 60 mm SMA wire actuator creates a 42 mm stroke in 36 steps. While all three feasible actuators create similar overall stroke, the 100 mm SMA wire actuator produces a 42 mm stroke in 13 steps of 2 pitch length stroke and then 9 steps of 1 pitch length stroke, making the actuation faster. The 200 mm SMA wire actuator produces 2 steps of 4 pitch length stroke and 9 steps of 3 pitch length stroke, making the action even faster. Although the 60 mm SMA wire actuator uses the least amount of SMA wire (and therefore the lowest activation power) among the example cases, the 200 mm SMA wire actuator produces the overall stroke within shortest total actuation time exposing the design

tradeoff between the actuation time and the SMA wire and power use. Depending on the particular application constraints the designer can select the proper SMA wire length while avoiding the feasibility boundary.

These example studies demonstrate the usefulness of the SMA wire view design visualization method for SMA wire ratchet actuators by exposing important design tradeoffs. The method enables the designer to see the effects of design changes and build an intuitive understanding of the design space.

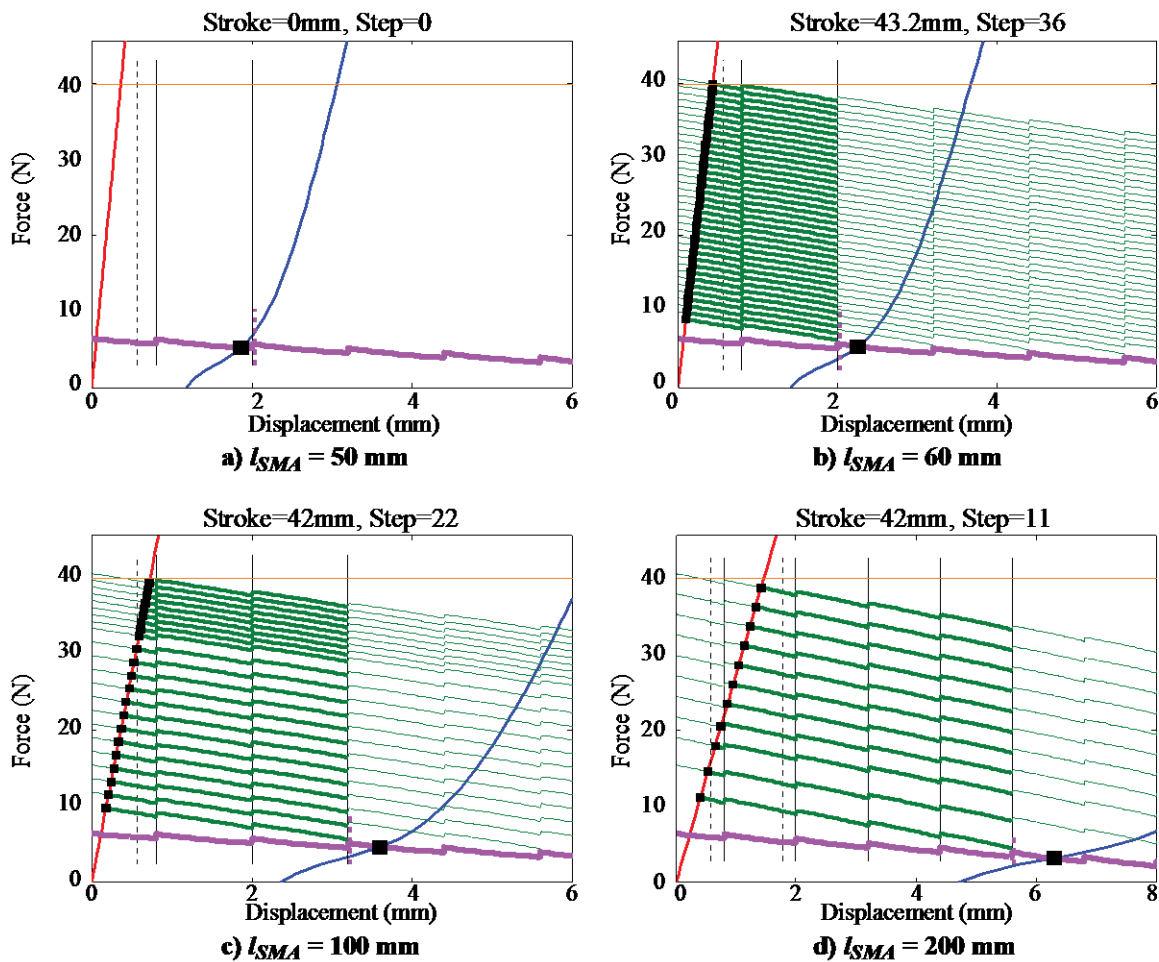


Figure B.8. Effect of SMA wire length on the SMA wire ratchet actuator performance. While all three feasible actuators create similar overall stroke, the longest SMA wire produces the overall stroke within shortest total actuation time exposing the design tradeoff between the actuation time and the SMA wire and power use.

5. Conclusions

This paper presented a model-based design approach for SMA wire ratchet actuators. A force balance model and effective free clearance evaluation model were derived to predict the ratchet actuator performance. Using these models, a design approach was introduced using the SMA wire view design plot to interactively select the actuator stroke related parameters. The parametric design studies demonstrated the SMA wire view design method and exposed design insights. A softer device bias stiffness is useful to reduce the stresses experienced by the SMA wire, although too soft a device bias might fail to restore the active pawl in the martensite equilibrium state. A smaller bias free clearance enables longer overall stroke by reducing the austenite equilibrium stress, while there is a feasibility boundary to create an effective stroke. The SMA wire length allows a design tradeoff between the actuation speed and the SMA material and power use. The SMA wire view design method helps designer make better decisions by presenting the performance evaluation and parameter sensitivities in a manner which allows the effects of the design parameters and interactions among the various components of the ratchet mechanism to be easily understood. The systematic design approach presented in this paper along with the design plot and insight generated by the parametric study helps designers take advantage of SMA wire ratchet actuators to overcome the SMA wire actuation stroke limitation, enabling large stroke applications.

6. References

- [1] Huber, J. E., Fleck, N. A., and Ashby, M. F., 1997, "The Selection of Mechanical Actuators Based on Performance Indices," *Proc. Math. Phys. Eng. Sci.*, **453**(1965), pp. 2185–2205.
- [2] Grant, D., and Hayward, V., 1997, "Variable structure control of shape memory alloy actuators," *Control Syst. Mag. IEEE*, **17**(3), pp. 80–88.
- [3] Jiang, C., Uchida, K., and Sawada, H., 2011, "Development of vision based tactile display system using shape memory alloys," *Advanced Mechatronic Systems (ICAMechS)*, 2011 International Conference on, pp. 570–575.
- [4] Toma, M., Luntz, J., Brei, D., Alexander, P. W., Browne, A. L., and Johnson, N. L., 2012, "Design and Proof-of-Concept Validation of a Latched Arch Active Seal," *J. Mech. Des.*, **134**(7), p. 075001.
- [5] Kim, W., Thota, M., Luntz, J., and Brei, D., 2012, "Analytical Model and Design Study on Shape Memory Alloy Web Actuator," *ICAST2012*, Nanjing, China, pp. 031–16.

- [6] Redmond, J. A., Brei, D., Luntz, J., Browne, A. L., and Johnson, N. L., 2012, "Spool-Packaging of Shape Memory Alloy Actuators: Performance Model and Experimental Validation," *J. Intell. Mater. Syst. Struct.*, **23**(2), pp. 201–219.
- [7] Park, B., Shantz, M., and Prinz, F. B., 2001, "Scalable rotary actuators with embedded shape memory alloys," *Smart Structures and Materials 2001: Smart Structures and Integrated Systems*, Newport Beach, CA, United states, pp. 79–87.
- [8] Barnes, B. M., Brei, D. E., Luntz, J. E., Strom, K., Browne, A. L., and Johnson, N., 2008, "Shape memory alloy resetable spring lift for pedestrian protection," *SPIE*, San Diego, California, USA, pp. 693005–13.
- [9] Utter, B., Barnes, B., Luntz, J., Brei, D., Teitelbaum, D. H., Okawada, M., and Miyasaka, E., 2010, "Design of an SMA Actuated Mechanotransductive Implant for Correcting Short Bowel Syndrome," *Proceedings of the 2010 Smart Materials, Adaptive Structures, and Intelligent Systems*, Philadelphia, Pennsylvania, USA, pp. 875–892.
- [10] Dittmer, D. K., Buchal, R. O., and MacArthur, D. E., 1993, "The SMART wrist-hand orthosis (WHO) for quadriplegic patients," *JPO J. Prosthet. Orthot.*, **5**(3), p. 73.
- [11] Sholl, M., Donakowski, W., Sirk, M. M., Clauss, T., Lampton, M. L., Edelstein, J., and Hurwitz, M., 2003, "Optomechanical design of the cosmic hot interstellar plasma spectrometer (CHIPS)," pp. 467–478.
- [12] Kim, W., Barnes, B. M., Luntz, J. E., and Brei, D. E., 2011, "Conglomerate Stabilization Curve Design Method for Shape Memory Alloy Wire Actuators With Cyclic Shakedown," *J. Mech. Des.*, **133**(11), p. 111010.
- [13] Sun, H., Pathak, A., Luntz, J., Brei, D., Alexander, P. W., and Johnson, N. L., 2008, "Stabilizing shape memory alloy actuator performance through cyclic shakedown: an empirical study," *SPIE*, San Diego, California, USA, p. 69300Q–11.
- [14] Bertacchini, O. W., Lagoudas, D. C., Calkins, F. T., and Mabe, J. H., 2008, "Thermomechanical cyclic loading and fatigue life characterization of nickel rich NiTi shape-memory alloy actuators," *SPIE*, San Diego, California, USA, pp. 692916–11.

Appendix C.

Conglomerate stabilization curve design method for shape memory alloy wire actuators with cyclic shakedown

The high energy density actuation potential of SMA wire is tempered by conservative design guidelines set to mitigate complex factors such as functional fatigue (shakedown). In addition to stroke loss, shakedown causes practical problems of interface position drift between the system and the SMA wire under higher stress levels if the wire does not undergo a pre-installation shakedown procedure. Constraining actuation strain eliminates interface position drift, and has been reported to reduce shakedown as well as increase fatigue life. One approach to limit actuation strain is using a mechanical strain limiter which sets a fixed Martensite strain position - useful for the development of in-device shakedown procedures which eliminates time consuming pre-installation shakedown procedures. This paper presents a novel conglomerate stabilization curve design method for SMA wire actuators which accounts for shakedown with and without the use of mechanical strain limiters to enable higher stress designs to maximize actuator performance. Shakedown experimental data including the effect of strain limiters along with stroke and work density contours form the basis for this new design method. For each independent mechanical strain limiter, the maximum of the individual post-shakedown Austenite curves at a range of applied stress are combined into a conglomerate stabilization design curve. These curves over a set of mechanical strain limiters including the zero set provide steady state performance prediction for SMA actuation, effectively decoupling the shakedown material performance from design variables that affect the shakedown. The use and benefits of the conglomerate stabilization curve design method are demonstrated with a common constant force actuator design example which was validated in hardware on a heavy duty latch device. This new design method, which accounts for shakedown, supports design of SMA actuators at higher stresses with more economical use of

material/power, and enables the utilization of strain limiters for cost saving in-device shakedown procedures.

1. Introduction

Because of their exceptional actuation characteristics such as high energy density, silent operation, and flexible packaging, the use of Shape Memory Alloys (SMAs) has been increasing in aerospace, automotive, robotics and medical applications [1-9]. In particular, NiTiNOL wire has become a popular subject of study due to its mass-producability, low cost, and relatively consistent material properties [7, 10-12]. Commercial and industrial SMA applications, however, are limited because of issues related to the complexity of SMA such as behavioral models, actuation speed and frequency, and mechanical connections. Many of these issues are being addressed by recent research [13-20], although the additional issue of unstable performance due to shakedown still hinders the design of SMAs for commercial applications [21-23].

Shakedown is the degradation of actuation performance of SMAs both in stroke and strain. During thermomechanical cycles, SMA wire changes its crystal structure between the Austenite and Martensite phases creating actuation stroke, which is the difference between these strains. Over consecutive actuation cycles, the Austenite and Martensite strains change resulting in a decrease in actuation stroke due to the different rates of change of the Martensite and Austenite strain (Figure C.1). Shakedown negatively impacts the stability of actuator performance because of the stroke reduction during product life. Moreover, strain shakedown which is the increase of Austenite and Martensite strain during actuation cycles, can shift the relative interface position between the system and the SMA wire. For the example, in the latch system shown in Figure C.2, in normal operation (Figure C.2a) the actuator locks the system in the cool Martensite phase, and unlocks the system in the hot Austenite phase. However, due to strain increase during shakedown of both Austenite and Martensite, the relative position between the system and the actuator drifts. This position drift causes the actuation system to malfunction because the shaken down wire is offset and does not lift the key the extra distance to unlock the system even with the same stabilized stroke (Figure C.2b). For reliable actuator design, providing a stable interface position between the system and SMA wire is important as well as the stabilization of actuation stroke.

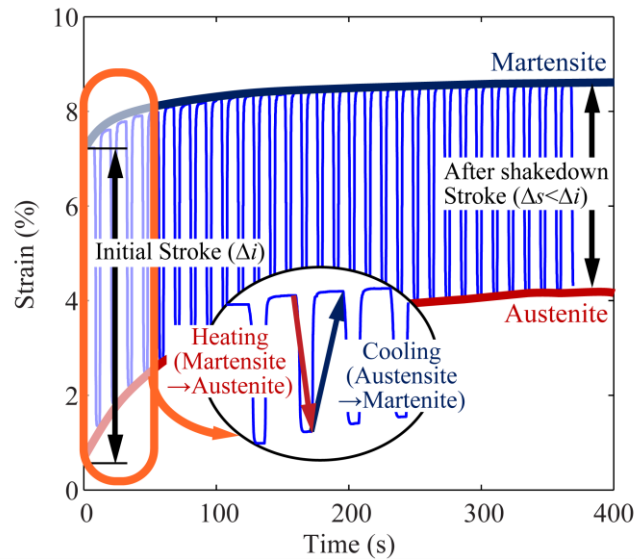


Figure C.1. Shakedown of Shape Memory Alloy.

During the thermo-mechanical cycles, SMA wire changes its crystal structural phase between Austenite and Martensite. Both Martensite and Austenite strain generally increase while the thermomechanical cycles repeat. However, because of the different increase rate of Martensite and Austenite strain, the actuation stroke decreases. (70°C Flexinol® 10 mil wire, 500MPa)

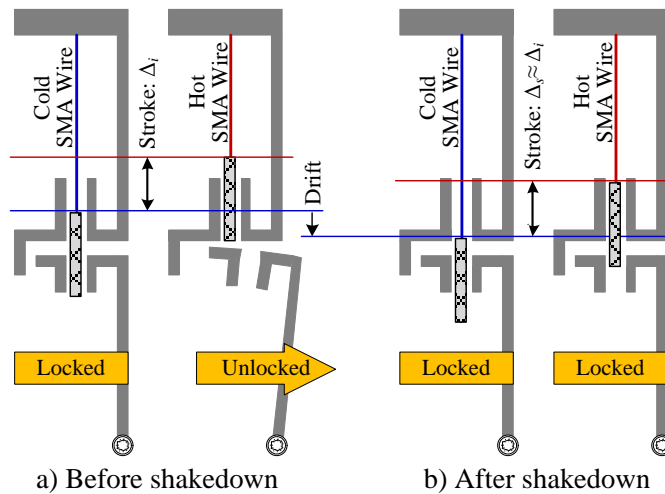


Figure C.2. Negative Effect of Strain Shakedown.

Strain increase during shakedown can cause malfunction of actuators. Here is an example of lock actuator. At cool Martensite phase, the actuator locks the system, and unlocks the system at hot Austenite phase (a). Because of strain increase during shakedown, even with the same amount of stroke ($\Delta i \approx \Delta s$), this actuator drifts thereby remaining locked (b).

There have been many efforts to describe and/or explain the mechanisms of shakedown [22-35]. Several factors that affect shakedown have been suggested such as maximum stress [23, 29, 31, 33, 36], strain rate [37, 38], partial transformation [39, 40], temperature [26, 29], pre-conditioning [22, 26, 27], and maximum allowed strain [23, 40]. However, the actual mechanisms of shakedown are still unknown and limited models exist. Because of this lack of knowledge about shakedown, designers of SMA wire actuators rely on the manufacturer's conservative guideline which limits the maximum stress on the wire, for example 180-190 MPa for commercially available Flexinol[®] wires [41]. This conservative design approach sacrifices some of the high energy density actuation potential of SMA, which would be otherwise available with SMA applications which actuate at high stress [12, 23]. To address the problem of stroke degradation, a pre-installation shakedown procedure has been demonstrated where the wire was shaken down for at least 1000 cycles under 1.5 times the designed load prior to installation in the device [29, 42]. However, this approach can increase the manufacturing cost of SMA devices due to the additional time-consuming pre-installation shakedown procedure. It would be beneficial to the development of economical SMA devices in terms of both manufacturing cost and material use to develop an in-device shakedown procedure where shakedown occurs post installation during the regular actuation operation of the device maintaining desired performance. For the development of an in-device shakedown procedure, a method to fix the position of at least one end of the actuation stroke during shakedown is required as well as to stabilize the stroke.

Recent research has indicated that limiting actuation strain, through various methods such as partial transformation and mechanical strain limiters, can reduce shakedown as well as increase the fatigue life in both pseudoelastic [43-47] and shape memory modes [23, 40]. For example, improved fatigue life by an order of magnitude and reduced shakedown has been demonstrated using constrained shape memory actuation strain with partial transformation (transformation between a point above the Martensite finish temperature and a point below the Austenite finish temperature) with temperature monitoring for the control of Joule heating [40]. This approach, however, increases the complexity of SMA actuators because of the additional temperature monitoring and electrical current control. Another approach to reduce shakedown is to constrain the actuation strain using a mechanical strain limiter such as a hard stop [23]. Strain limiters can protect the compliant Martensite SMA wire from the full actuation stress as shown in Fig 3 as well as fix the Martensite strain during actuation, thus preventing position drift due to shakedown.

Using these types of methods, it is possible to shake down the wire, and thus utilize it at higher loads, often with an economic improvement (such as less wire, less power, more work, *etc.*); however, the traditional design methods do not accommodate high stress/post-shakedown design. While there are several approaches to designing SMA wire, such as those based on material models, stress-strain curves, and experimental methods [7, 48-50], most engineers employ a quasi-static graphical stress-strain curve design approach based on the assumption of actuation between the fully transformed Austenite and Martensite phases. Graphical approaches are useful because of their simplicity and physical intuitiveness, although stress-strain curve based methods can also be implemented numerically or analytically for higher precision and automation. As illustrated in Figure C.3, in this standard graphical method the SMA stress-strain curves at the Austenite and Martensite phases (red and blue curves in Figure C.3) and the system curve (green line in Figure C.3) are used to predict the motion by finding the intersections between the material curves and the system curve (points \textcircled{A} and \textcircled{M}); thereby, defining the equilibrium at each phase. The

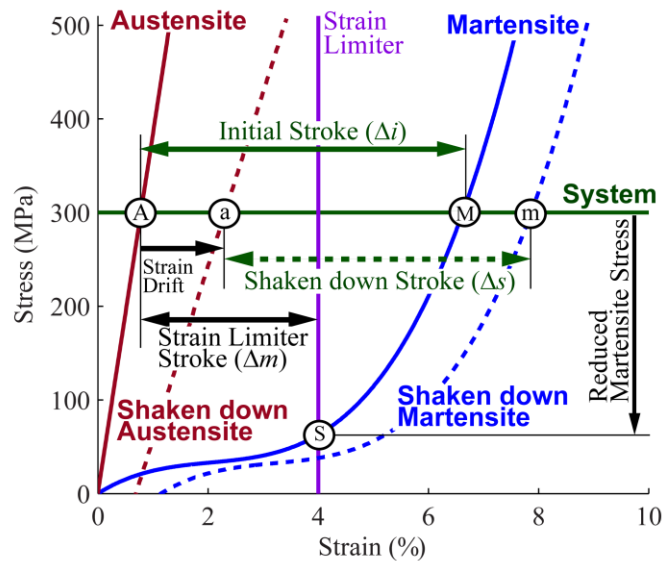


Figure C.3. Traditional stress-strain curve SMA actuator design method and the effect of shakedown.

The solid red and blue curves are stress-strain curves at the Austenite and Martensite before the shakedown, and the green line is the system curve which the SMA wire actuates against. The wire actuates between the intersection points \textcircled{A} and \textcircled{M} at first cycle, however, after shakedown, the actuation strain increases to the points \textcircled{a} and \textcircled{m} . A strain limiter such as a hard stop can limit the actuation strain protecting the compliant Martensite SMA wire; with a strain limiter, SMA wire actuates between the points \textcircled{A} and \textcircled{S} .

difference between them determines the actuation stroke [49]. When the mechanical strain limiter is used, it limits the actuation of wire to points Ⓐ and Ⓢ reducing the stress on the compliant Martensite wire.

This design approach, however, does not address shakedown. The dashed curves in Figure C.3 represent the fully shaken down Austenite and Martensite stress-strain curves at a particular stress level. For this example, the Austenite and Martensite actuation strains increase from points Ⓐ and Ⓜ to points Ⓐ and Ⓜ after shakedown. These Austenite and Martensite strain increases cause stroke reduction from Δi to Δs as well as strain drifts. It is cumbersome to use the traditional stress-strain curve design method in the presence of shakedown, because these shaken down stress-strain curves must be regenerated and replaced every time any design variables (wire diameter, length, *etc.*) are changed since the change in the curves are directly coupled to the design itself. Moreover, even if the shaken down stroke and strain drift can be predicted with this iterative method, the interface problem in Figure C.2 cannot be avoided. By using a mechanical strain limiter, the interface problem can be addressed with a fixed Martensite strain, and stroke shakedown can be reduced. However, introducing a strain limiter does not address the limitation of the traditional stress-strain curve method for shakedown since the strain limiter position change also requires the regeneration of shaken down stress-strain curves.

This paper presents a new conglomerate stabilization curve design method for SMA wire actuators which accounts for shakedown to enable higher stress designs to maximize actuator performance. The method is described with the case of a constant load with a mechanical strain limiter, although it also can be utilized for other loading cases or without a strain limiter. In this study the SMA wire without an initial two way shape memory effect was used. While cyclic actuation can induce a two way shape memory effect [22-24, 28], potentially larger than the strain limiter, the actuation stroke is still limited by the strain limiter position maintaining a stable interface while the wire may become slack. As a first step, a set of shakedown process data was collected and analyzed to derive empirical knowledge regarding the shakedown process with a mechanical strain limiter. The effects of strain limiter position and applied stress level are discussed including the tradeoff in work produced by the SMA wire. This empirical knowledge formed the basis for the new design method accounting for the shakedown effect through the use of conglomerate stabilization design curves which provide steady state performance predictions

for SMA actuation. Each of these curves was created from a set of post-shakedown Austenite curves at a given strain limiter position to decouple the shaken down wire performance from the design variables which themselves affect the material performance. The conglomerate stabilization curve design method is demonstrated with a common constant load actuator design example in which the SMA wire was subjected to the higher stress than the manufacturer's guideline stress generating savings in the wire length and the heating power. A benchtop validation was performed on a heavy duty dead-weight industrial latch. This new design method enables development of higher stress, economical SMA actuators utilizing the benefits of strain limiters for cost saving in-device shakedown procedures.

2. Empirical study of the effect of strain limiters on shakedown

The conglomerate stabilization curve design method for stably performing SMA wire actuators builds upon a set of data for a given SMA wire type shaken down at different mechanical strain limiter positions and applied stresses. This section describes a simple systematic experimental process for gathering this broad set of data along with a discussion of the effect of the strain limiter position and applied stress.

2.1. Experimental parameter set

The matrix of experimental tests conducted around the two main variables, placement of the strain limiter and the applied stress on the wire, is outlined in Table C.1. The strain limiter positions, which are defined relative to the Austenite free length of the specimen (reference point for 0 strain), varied from 2% to 8%, where 2% was chosen as the lower limit as it is quoted as providing longer fatigue life [44, 51], and 8% was chosen as the upper limit to avoid immediate damage to the wire inducing unrecoverable deformation. As a baseline case, additional cases without strain limiters were also tested. The applied stress on the wire was varied from 80 to 620 MPa, where 180 MPa is the SMA wire manufacturer's guideline stress level, and higher values in the range, 255 to 620 MPa were tested to understand the effect of strain limiter position on the shakedown process with stresses higher than the standard design guideline to produce more work from the wire. Lower values of 80 and 128 MPa were selected to verify the reverse shakedown effect which was reported by Churchill, *et al.* [31, 33]. The particular stress levels were selected based on commercially available constant force spring loads. Cases marked with X in the upper right of Table 1 could not be tested because the stress levels were insufficient to reach the strain

limiter, thus producing the same results as the cases without a strain limiter. The case marked with X in the lower left of Table 1 could not be tested because the strain limiter position is too close to the Austenite strain at that stress, thus producing no actuation stroke.

Table C.1. Experimental Parameter Matrix.

The strain limiter position varied from 2% to 8%, and applied stress level varied from 80 to 620 MPa. The cases without strain limiter were tested to be compared with strain limiter cases. Cases marked with X could not be tested because they are same as no strain limiter cases (upper right), or there is no actuation (lower left).

Stress (MPa)	No Strain Limiter	2 % Strain Limiter	4 % Strain Limiter	5 % Strain Limiter	6 % Strain Limiter	7 % Strain Limiter	8 % Strain Limiter
80	A0	A2	A4	X	X	X	X
128	B0	B2	B4	B5	X	X	X
180	C0	C2	C4	C5	X	X	X
255	D0	D2	D4	D5	D6	X	X
350	E0	E2	E4	E5	E6	E7	X
420	F0	F2	F4	F5	F6	F7	F8
500	G0	G2	G4	G5	G6	G7	G8
620	H0	X	H4	H5	H6	H7	H8

2.2. Experimental setup and procedure

The same experimental set up and procedure was used for each of the test cases. A custom built test apparatus was utilized for the high cycle rate (5 cycles per minute) collection of shakedown process data which is capable of controlling the current through an SMA wire, applying a desired tensile load profile such as from a dead weight or spring, limiting the maximum strain, and measuring the tensile load and displacement (Figure C.4). Commercially available preconditioned Flexinol[®] 70°C 10 mil (0.254 mm) diameter wire was utilized for this study which was cut into 500 mm lengths, and installed using custom made crimps between one end block and a sliding block which was attached to the guide rods. The test rig has six parallel stainless steel guide rods held by two end blocks. To measure the Austenite free length of a specimen (reference point for 0 strain), the wire was heated without stress, and the length was measured with a MICRO-EPSILON optoNCDT 1300 laser optical displacement sensor. Constant loads were the focus of previous shakedown studies because of their simplicity of analysis and implementation using dead weights [23, 31, 33, 40]. Inertia, however, causes oscillation problems when using high heating and cooling rates [52]. Interchangeable constant force springs, which were attached to the SMA

wire through a hook on the sliding block, were used for this study to mitigate this oscillation problem. Tensile load was monitored by a FUTEK LSB200 S beam load cell during actuation. Shakedown process data were collected with Joule heating which is commonly used in SMA actuators for actuation control [4, 5, 7, 9, 17] and data recording through a National Instruments PCI-6052E multifunction data acquisition board using LabView and a Sorensen SGI 100-150 DC power supply. The wire was heated with 24 V, taking 3 seconds for full transformation, and cooled for 9 seconds in machining oil coolant (with a flash point above 150°C), which was temperature controlled from 20 to 30°C using a heat exchanger and forced circulation. The wire was subjected to a sequence of heating and cooling cycles after which accumulated plastic strain on the wire was measured with the laser displacement sensor in the hot Austenite phase after disconnecting the constant force spring from the sliding block.

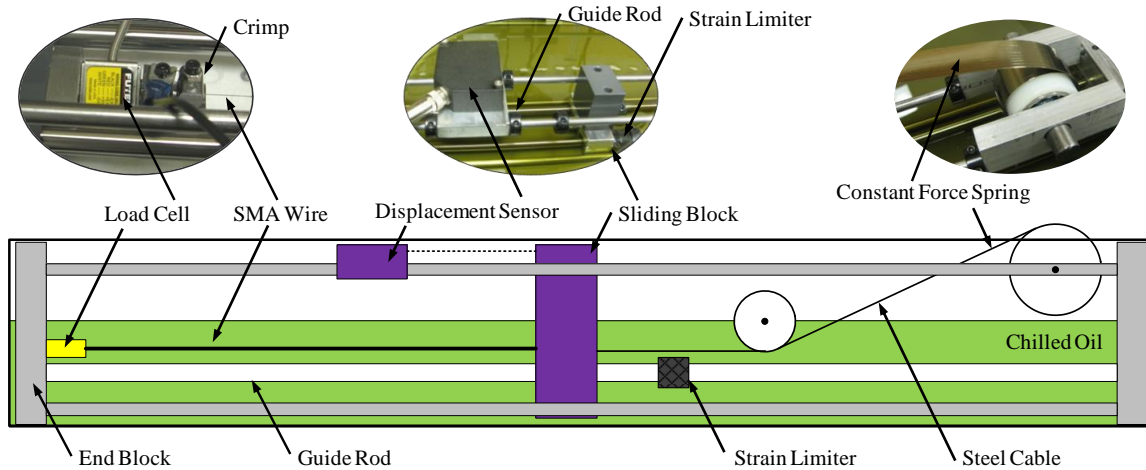


Figure C.4. Schematic of shakedown Experimental Setup.

Shakedown test apparatus is capable of controlling the heating and cooling of SMA wire, applying desired force, limiting the maximum strain, and measuring the tensile load and displacement.

2.3. Experimental Results

All of the strain shakedown curves resulting from the experimental shakedown study have the same decaying exponential form as shown in the example in Figure C.5. To verify that the shakedown process stabilizes in each case, the convergence criterion

$$\frac{\varepsilon^n - \varepsilon^{3n/4}}{\varepsilon^n - \varepsilon^1} \text{ or } \frac{\delta^n - \delta^{3n/4}}{\delta^n - \delta^1} < 0.03 \quad (1)$$

was set where ε and δ are strain and stroke respectively, and n is the number of cycles for the convergence test. In this study, stroke δ is defined as the difference in strain between the Martensite and Austenite:

$$\delta = \varepsilon_M - \varepsilon_A. \quad (2)$$

This convergence criterion was set based on the assumption of an exponential shakedown model [23, 33] where 95% of decay occurs after 3 time constants and 98% of decay occurs after 4 time constants, such that this criterion ensures that less than 2% of shakedown remains after n cycles. In most cases, both the strain and stroke shakedown process converged within 4000 cycles (Table C.2). From these converged test results, the effects of strain limiter position and applied stress level were studied including tradeoff in work generation.

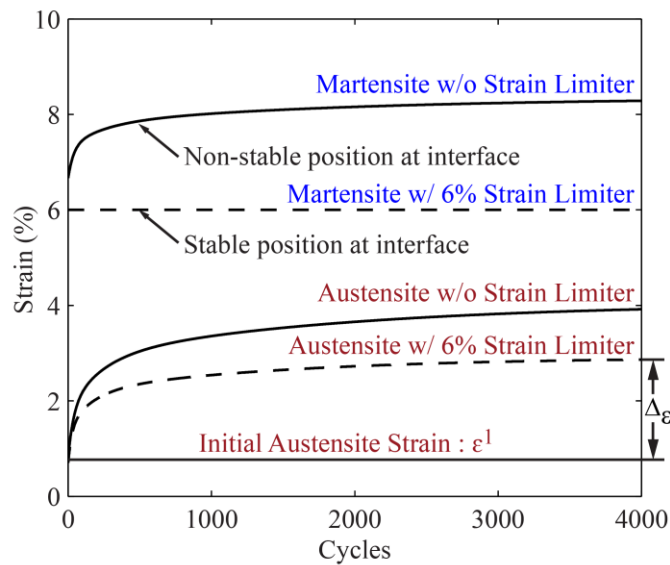


Figure C.5. Shakedown Processes With and Without Strain Limiter.

Without strain limiters, both Austenite and Martensite strain increase over cycles which can cause a position drift interface problem in a device if the SMA wire does not undergo a separate shakedown process prior to installation. With a strain limiter, the Martensite strain is constrained, providing a stable interface position enabling a more cost effective in-device, or even in-operation shakedown process.

Table C.2. Convergence Test Results (4000 cycles).

Table gives the convergence test results (Eq. 1) for each experiment, with any result less than 0.03 indicating convergence. The convergence test verifies that in most cases the shakedown process converged within 4000 cycles. ‘No’ represents cases with no strain limiter, in which both Austenite and Martensite strain increase. 2, 4, 6, and 8 % strain limiter cases represent the Austenite strain convergence which is the same as the stroke shakedown since the Martensite strain is fixed to the strain limiter position.

Strain Limiter		Applied Stress			
		255 MPa	350 MPa	420 MPa	500 MPa
2% (Austenite)		0.030	0.006	0.024	0.011
4% (Austenite)		0.021	0.013	0.013	0.028
6% (Austenite)		0.013	0.006	0.003	0.009
8% (Austenite)		0.013	0.006	0.012	0.016
No	Austenite	0.036	0.030	0.009	0.017
	Martensite	0.030	0.006	0.011	0.008
	Stroke	0.014	0.015	0.016	0.010

2.3.1. Effect of strain limiter position

Shakedown processes with a range of strain limiter positions under the same applied stress (350 MPa) were compared to understand the effect of the strain limiter position. Strain shakedown, Δ_ε is defined as

$$\Delta_\varepsilon = \varepsilon^1 - \varepsilon^n \quad (3)$$

for either Austenite or Martensite strain, where n is the number of cycles for convergence (Figure C.5). Using a strain limiter reduces the Austenite strain shakedown where the shorter strain limiters produce increased reduction (Figure C.6). For example, the 6% strain limiter reduced the Austenite strain shakedown by 43% from 3.30% strain without a strain limiter (Test case E0) to 1.89% strain (Test case E6). The shorter 4% strain limiter reduced the Austenite strain shakedown even more, by 74% from 3.30% strain to 0.85% strain (Test case E4). However, this reduced Austenite strain shakedown does not result in a longer stroke than those resulting from longer strain limiters since the shorter strain limiter holds the Martensite strain at its low level resulting in a shorter net stroke (Figure C.7). For example, the 4% strain limiter test (Test case E4) produces 55% smaller Austenite strain shakedown than the 6% strain limiter test (Test case E6). This Austenite strain shakedown reduction (1.04% strain) is, however, smaller than the stroke loss from

the shorter Martensite strain limiter position (2% strain). Resulting stabilized stroke of 4% strain limiter test (2.74% strain) is 0.96% strain shorter than the stabilized stroke of 6% strain limiter test (3.70% strain).

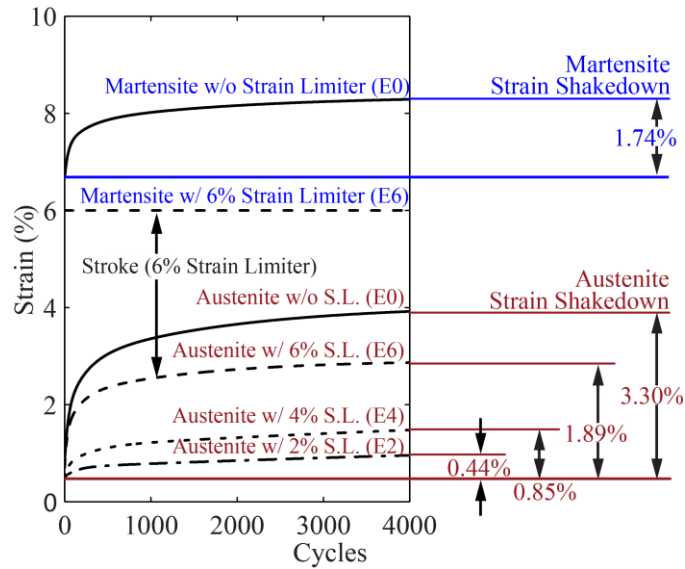


Figure C.6. Strain Limiter Position Effects on Strain Shakedown.

Shakedown processes with different strain limiters under 350 MPa stress show that shorter strain limiters reduce strain shakedown.

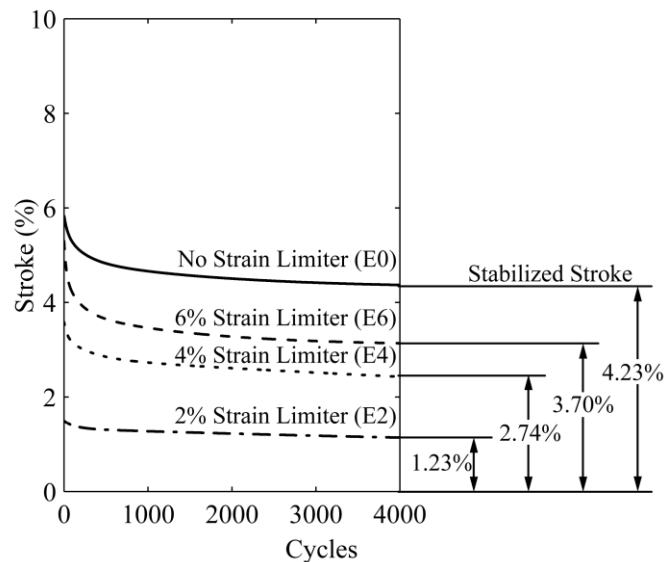


Figure C.7. Strain Limiter Position Effects on Stabilized Stroke.

Even though shorter strain limiters allow smaller strain shakedown, the resulting stabilized stroke is larger with longer strain limiters. (350 MPa)

This result implies that longer strain limiters, or even no strain limiter, allow better performance in terms of actuation stroke (Figure C.7). It should be noted that while longer strain limiters provide better performance, increased strain may have a negative effect on fatigue life although the exact relation is not clear [44]. Stroke stabilization without a strain limiter results both in Austenite and Martensite strain increase causing the interface to drift requiring a separate pre-installation shakedown procedure. Strain limiters provide a stable Martensite strain position as a fixed reference position for SMA actuators allowing in-device shakedown.

2.3.2. Effect of applied stress

To understand the effect of applied stress level on the shakedown process, multiple shakedown test results under a range of applied stresses with a fixed strain limiter position (4% strain limiter) were compared (Figure C.8). Higher stress increases the Austenite strain shakedown. For example, 500 MPa applied stress increases the Austenite strain shakedown by 1.36% strain from almost zero (0.03%) at 180 MPa (Test case C4) to 1.39% strain (Test case E4), resulting, as expected, in shorter stabilized stroke at higher stress.

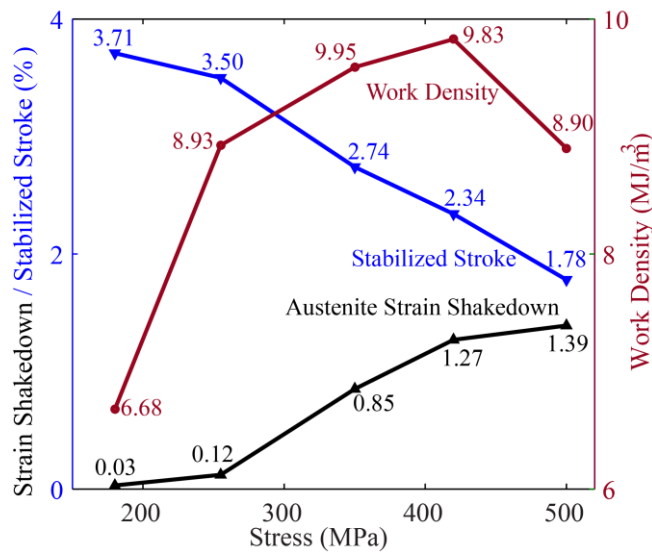


Figure C.8. Effect of Stress on Strain Loss, Stabilized Stroke, and Work Density (4 % Strain Limiter).

Austenite strain loss was increased with higher applied stress resulting smaller stabilized stroke. While stroke loss and stabilized stroke show monotonic relation with applied stress, work density, which is the multiplication of stabilized stroke and applied stress, shows non-monotonic relation with applied stroke allowing design tradeoffs.

While higher stress increases the strain shakedown in the stress range above the guideline stress of 180-190 MPa provided by the manufacturer [41], at lower stress levels, 80 and 128 MPa, a ‘reverse shakedown process’ was observed as previously reported by Churchill, *et al.* [31, 33]. The Austenite and Martensite strain shakedown curves for the 80 MPa case without a strain limiter (Figure C.9) are qualitatively different from those at the higher stress levels. The Austenite strain stays nearly constant, decreasing only a small amount (rather than increasing) by 0.18% strain from 0.08% to -0.10%, becoming shorter than its original Austenite free length even under load. The Martensite strain also decreases rather than increases, but by a large amount, by 45% from 4.75% strain at the first cycle to 2.62% strain after shakedown. Thus, even though very small stresses are applied, the net stroke is significantly reduced by 40% through this reverse shakedown process as a result of the difference between the Austenite and Martensite strain decrease.

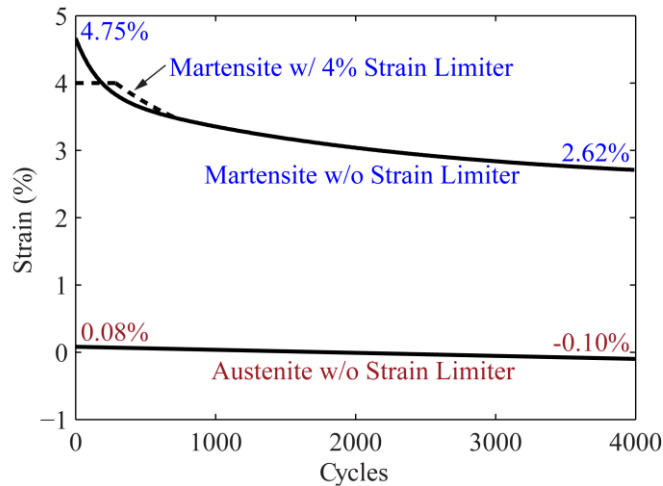


Figure C.9. Reverse Shakedown (80 MPa).

Shakedown processes with low applied stress (80 MPa and 126 MPa) show reverse shakedown. The Austenite strain decreases under zero strain and the Martensite strain decreases significantly, while both Austenite and Martensite strain increase during normal shakedown. The dotted line shows the 4% strain limiter test result.

In addition to reducing stroke, reverse shakedown can change the interaction between the wire and the strain limiter. With a 4% strain limiter at 80 MPa, the Martensite wire initially rested against the strain limiter, but as reverse shakedown occurred, the Martensite strain decreased and the wire no longer reached the strain limiter after 300 cycles. While the Martensite shakedown curve (shown by the dashed line) differs from that without a strain limiter initially, once the strain

limiter was no longer engaged, the curve quickly converges to the curve without a strain limiter, after which they are coincident indicating that load history does not affect the steady-state performance. Because the reverse shakedown process can cause the wire to no longer engage the strain limiter, there are reduced benefits to strain limiters at low levels of stress.

Thus, an appropriate level of stress needs to be applied to the wire. Even though the strain shakedown is increased, there are benefits to operating at higher stresses because more overall work can be generated. For example, in Figure C.8, a maximum in work density occurs at a stress of 420 MPa (Test case F4) which is 47% higher than the work density at the guideline stress of 180 MPa even though the stroke is 37% shorter. To further illustrate this tradeoff in work and stroke, performance contours were created using experimental data. The stabilized stroke at each data point in Figure C.10 was taken from the stabilized stroke of each test case, and the work density at those points was calculated by multiplying the stabilized stroke and applied stress. The stabilized stroke contours plotted over a range of strain limiter positions and applied stress in Figure 10 indicate that the maximum actuation stroke (about 4.7 cm out of 1 m length wire) is obtained in the stress range of 150 to 250 MPa which is in the neighborhood of the manufacturer’s guideline stress.

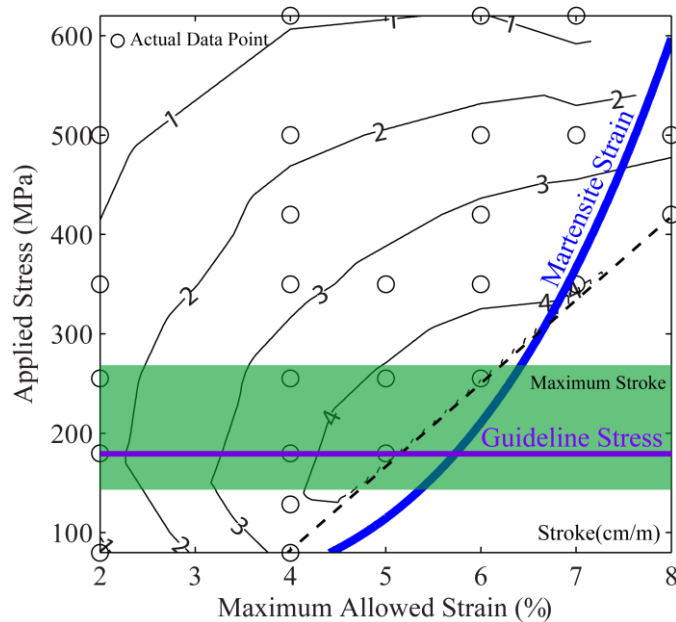


Figure C.10. Optimal Stroke Contour.

The maximum stroke can be obtained around 220 MPa stress, which is close to the manufacturer’s recommendation stress (180 MPa to 190MPa). Stroke is normalized as stroke in centimeter unit from 1 meter SMA wire.

While the maximum actuation stroke occurs around the guideline stress, the maximum work density occurs at higher stresses in the range of 370 to 450 MPa (Figure C.11). The maximum work density from this contour (15.6 MJ/m³ at 420 MPa stress with 8% strain limiter) is about twice the work density at the guideline stress (7.5 MJ/m³ at 180 MPa stress with 5% strain limiter).

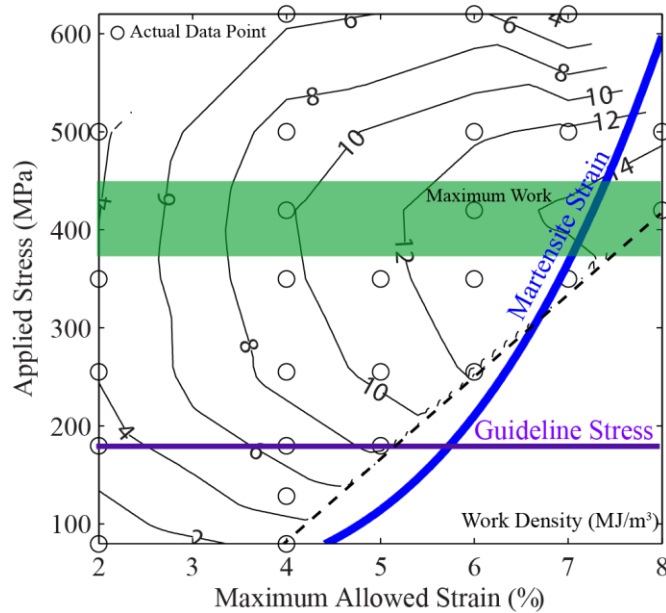


Figure C.11. Optimal Work Density Contour.

The maximum work density occurs at 400 MPa which is higher than recommendation stress. This maximum work density is about two times larger than the guideline design work density.

Based on the particular objectives of an actuator design problem, the designer can choose either a longer stabilized stroke or a larger work output from the shaken down wire. In general, strain limiters reduce the strain shakedown, but longer strain limiter positions result in longer stabilized stroke. Higher applied stress levels result in larger strain shakedown leading to shorter stabilized stroke. However, maximum work from the wire occurs at intermediate stress levels leading to a design tradeoff in work. Without strain limiters, both Austenite and Martensite strain increase over cycles which can cause a position drift interface problem in a device if the SMA wire does not undergo a separate pre-installation shakedown procedure prior to installation. With a strain limiter, the Austenite strain still increases, but the Martensite strain is constrained providing

a stable interface position enabling a more cost effective in-device, or even in-operation shakedown procedure.

3. Conglomerate stabilization curve design method accounting for shakedown

The empirical knowledge from the experimental study forms the foundation for the new design process accounting for shakedown. In this process depicted graphically, post-shakedown Austenite curves are generated for a set mechanical strain limiter and the maximum limit on these curves form a *conglomerate* stabilization curve. A family of conglomerate stabilization curves over a set of mechanical strain limiters can be utilized for a given system to select a higher stress actuation solution. This is demonstrated with a common constant load example and compared to the design result from the traditional stress-strain curve design method.

3.1. Conglomerate stabilization design curves

A set of conglomerate stabilization design curves was created to replace the Austenite stress-strain curve from the traditional graphical stress-strain curve design method providing stabilized stroke prediction together with the corresponding strain limiter lines which replace the Martensite curve. To form each conglomerate stabilization design curve, an Austenite stress-strain curve is generated for each test case *after* shakedown which is typically significantly different from the first cycle Austenite curve used in the traditional design process. Austenite post-shakedown curves with the same strain limiter position under a range of applied “shakedown” stresses are plotted on one graph (Figure C.12). These Austenite curves are only effective up to the stress level applied during shakedown. For example, the 350 MPa stress-strain curve is not valid at 500 MPa since further shakedown would occur once higher stress is applied resulting in a different stabilized stroke. A conglomerate stabilization design curve for a particular strain limiter position is formed by connecting the end points of the individual stabilized Austenite stress-strain curves ϵ^n which are related to the Austenite strain shakedown values $\Delta\epsilon$, in Fig. 8 as defined in Eq. 3. Using only the end points ensures that wires at intermediate stress levels are not shaken down more than necessary. A set of conglomerate stabilization design curves is created for a set of mechanical strain limiter positions (Figure C.13).

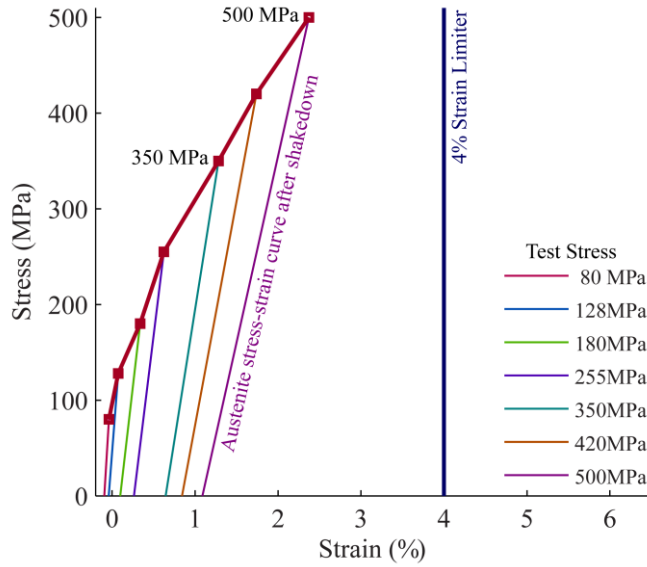


Figure C.12. Conglomerate Stabilization Design Curve (4 % Strain Limiter Curve).

To create 4 % strain limiter stabilization curve, Austenite stress-strain curves were created after Test case A4—G4. The interpolation curve, which is thick red line, provides stabilized stroke prediction after shakedown.

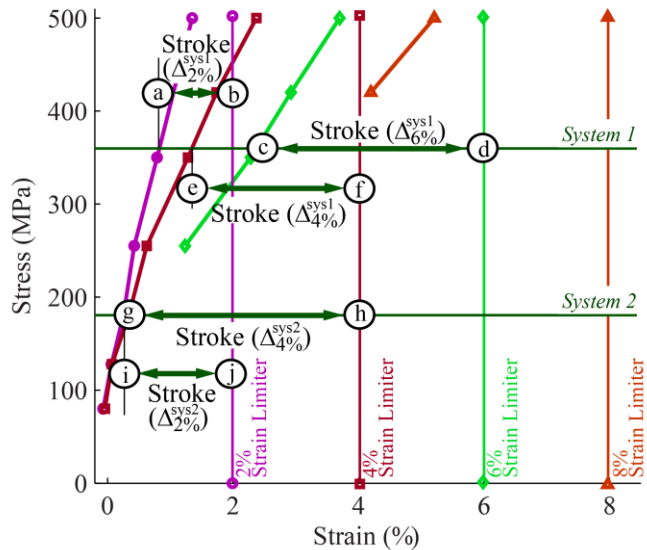


Figure C.13. A Set of Conglomerate Stabilization Design Curves.

For different strain limiter positions, a family of conglomerate stabilization curves was created. These curves are used with corresponding strain limiter lines.

In this new design process, these conglomerate stabilization curves replace the Austenite stress-strain curve and the corresponding vertical strain limiter lines replace the Martensite stress-strain curve in the traditional design method; thus, accounting for shakedown. Based on the applied stress on the wire, a set of conglomerate stabilization curves predicts the stabilized stroke for each strain limiter position. For an example actuator shown in Figure C.13, for the system curve with a single wire, the wire provides the longest stroke with a 6% strain limiter (points between © and Ⓓ) compared to the strokes with a 2% strain limiter (points between Ⓐ and Ⓑ), and with a 4% strain limiter (points between © and Ⓕ). The applied stress on SMA wire can be changed by changing some design variables such as wire diameter or number of wires. If the example actuator doubles the wire number, the stress on wire would be half shifting the system line to that for the double wire. At this applied stress level, the 6% strain limiter cannot be used since the wire does not reach the strain limiter position during and after the shakedown process. In this case for the double wire, a 4% strain limiter case provides the longest stroke (points between © and Ⓑ). While the single-wire stroke with a 6% strain limiter and the double-wire stroke with a 4% strain limiter are about the same, the work produced from the wire would be doubled with the longer strain limiter position at higher stress. Thus, changes in design parameters can be readily accounted for and visualized without having to regenerate the design curves.

3.2. Shakedown design example

To demonstrate the use and benefits of the conglomerate stabilization curve design method, a common design problem of a dead weight SMA wire actuator was designed. To illustrate this, performance specifications for this example were set for the actuator to lift a 1.8 kg weight with 1 cm stroke using 10 mil Flexinol[®] 70°C wire. Using the traditional SMA wire actuator design method with the Austenite and Martensite stress-strain curves (solid red and blue curves in Figure C.14), the actuator requires either a single wire with 360 MPa stress or a double wire with 180 MPa stress in each wire. A single wire would actuate between points Ⓐ and Ⓑ with 5.95% stroke requiring 16.8 cm of wire, and a double wire would actuate between points © and Ⓓ with 5.33% stroke requiring 18.8 cm of double wire (for total of 37.6 cm). Based on these evaluations, a single wire actuator requires less total SMA wire. However, because of shakedown, the single wire

actuator stroke would stabilize to 4.36% stroke between points ③ and ④ after 4,000 actuation cycles (Test case E0) resulting in 0.733 cm stroke which fails to meet the stroke requirement. A double wire actuator stroke remains at 5.30% stroke between points ③ and ④ (Test case C0) resulting in a 0.996 cm stroke which might be within the tolerance range. An additional issue is strain shakedown which can cause an interface alignment problem between the wire and the system; the Austenite end of the actuation stroke for a single wire actuator drifts by 0.51 cm from 0.88% strain (point ①) to 3.94% strain (point ③) after shakedown which is likely to cause an interface problem. In contrast, the conservatively designed double wire actuator drifts by 0.07 cm from 0.28% strain (point ③) to 0.65% strain (point ④) which is unlikely to cause a problem. Therefore, when using the traditional method, both strain and stroke shakedown require that the conservative guideline be followed.

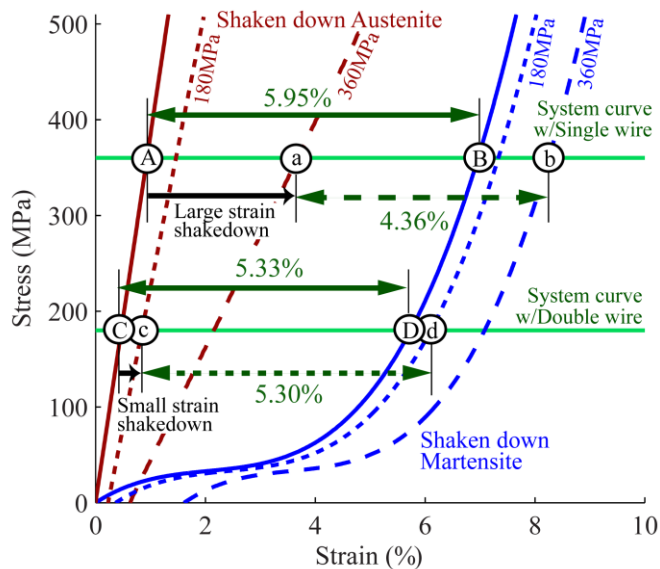


Figure C.14. SMA Wire Actuator Design Example with Traditional Design Method.

With the traditional stress-strain curve design method, a single wire actuator would actuate between points ① and ② at 360 MPa stress with 5.95% stroke, and a double wire actuator would actuate between points ⑤ and ⑥ with 5.33% stroke at 180 MPa stress in each. Before shakedown, single wire design can provide longer stroke at first cycle, but double wire design with manufacturer's guideline stress (180–190 MPa) can provide longer stabilized stroke after shakedown. Moreover, higher stress design also increases the strain shakedown which causes alignment problems between system and SMA wire.

With the new design method, conglomerate stabilization design curves are used with corresponding strain limiter lines instead of the Austenite and Martensite curves. In this example, a 6% strain limiter was chosen since it is the longest strain limiter providing the largest stroke which is reachable in Martensite at 360 MPa stress for a single wire design. With the same requirements, the stroke of an actuator with a single wire and a 6% strain limiter is predicted to be 3.55% stroke after stabilization (Figure C.15), requiring 28.2 cm of SMA wire. While this is longer than the unsuccessful single wire design in the traditional stress-strain curve design method, this is a stable design that saves 25% of SMA wire length relative to the double wire design (from 37.6 cm to 28.2 cm), leading to a corresponding 25% reduction in Joule heating power (from 8.4 W to 6.2 W) as well 25% savings in the cost of the wire. Moreover, this design provides a fixed end point of the actuation stroke allowing in-device shakedown, while the design resulting from the traditional method has problems with strain and stroke shakedown if it does not undergo a pre-installation shakedown procedure.

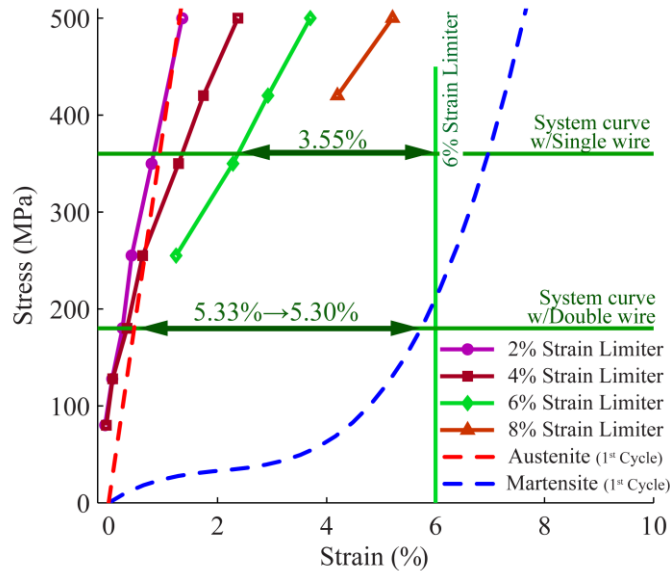


Figure C.15. Conglomerate Stabilization Curve Design Method.

A new conglomerate stabilization curve design method enables the use of SMA wire under higher stress leading economic use of material (shorter length of wire, and corresponding savings in cost and actuation power).

3.3. Experimental validation of design example

To provide physical validation of the design example, a heavy duty latch release SMA actuator was designed for use in applications such as canal door or moving bridge locks in civil structures, cargo doors on naval vehicles, oven gate/doors in manufacturing systems, or heavy duty cranes on construction structures [53-55]. A custom made latch release device was used for this experimental validation study where an SMA wire actuator lifts a 1.8 kg steel latch plate out of an aluminum slot to disengage the latch. This device has the same lift weight requirement as the design example, and the required stroke to release the latch was modified to 8.6 mm for fabrication and moving parts tolerance. The SMA wire actuator in the experimental setup (Figure C.16) was built to allow variations in length and number of wires, and included an adjustable strain limiter inserted beneath the latch plate. The three different actuator designs from the design example were tested: 1) the single wire actuator without a strain limiter, designed using the traditional method not accounting for shakedown which requires a 16.8 cm length of 10 mil SMA wire, 2) the double wire design without a strain limiter designed using the traditional method according to the manufacturers recommended stress which requires a pair of 18.8 cm long 10 mil Flexinol[®] 70°C SMA wires (for a total of 37.6 cm), and 3) the single wire actuator using a 6% strain limiter designed using the conglomerate stabilization curve design method accounting for shakedown which requires a 28.2 cm wire length. Each actuator design was tested for 4000 cycles, applying 1 A of current to each wire for 4 seconds to fully transform the SMA to Austenite, and allowing the wires to cool for 8 seconds at each cycle, while measuring the displacement of the latch plate with a laser displacement sensor.

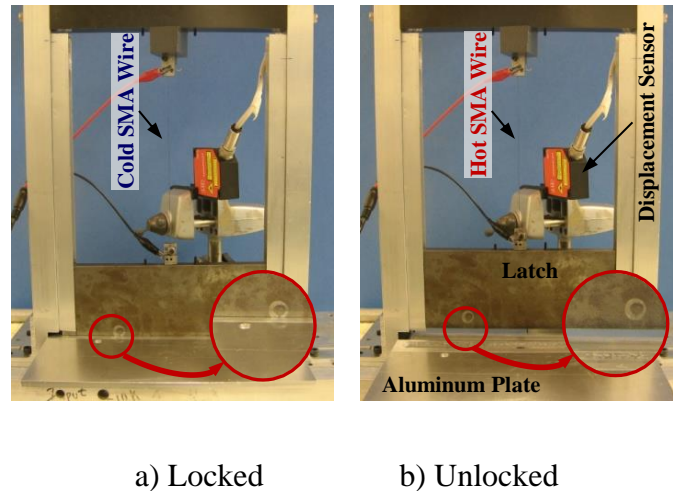


Figure C.16. A Latch Release SMA Actuator.

For the physical validation of design example, a dead weight latch release SMA actuator was built based on the section 3.2 design example. This structure designed to lock the aluminum plate in the cool Martensite phase, and unlock the plate in the hot Austenite phase

The evolution of the actuator displacements for the three actuator design are compared in Figure C.17 where the green line represents the minimum latch plate lift position to fully unlock the latch. The single wire traditional design (without considering shakedown) released the latch at the first cycle, but the vertical position latch both in Austenite and Martensite decreased quickly due to shakedown such that after only three cycles, the actuator failed to disengage the latch, and the lift height after 4000 cycles was reduced by 7 mm. The double wire traditional design observing the conservative guideline experienced little shakedown, losing only 0.5 mm of lift height in the Austenite state, and still released the latch after 4000 cycles. However, compared to this design, the single wire actuator with a 6% strain limiter designed using the new conglomerate stabilization curve design method used 33% less total wire length. On the first cycle, the conglomerate stabilization curve design started with 7.5 mm of excess lift height, which after 4000 cycles maintained 0.5 mm of excess lift height and fully disengaged the latch, demonstrating the ability of the new design method to meet a specified stroke and strain after shakedown. This in-operation shakedown process allowed for shakedown to occur during the regular operation of the device allowing a high performance design while avoiding a costly separate shakedown process. While both the traditional, conservative double wire design and the conglomerate stabilization curve, single wire design successfully disengaged the latch after shakedown, the conglomerate stabilization curve design method produced a design using 33% less material and actuation power

in a mechanically simpler design requiring attachments for only a single wire rather than two. These savings can enable SMA applications where cost and/or actuation power consumption are critical.

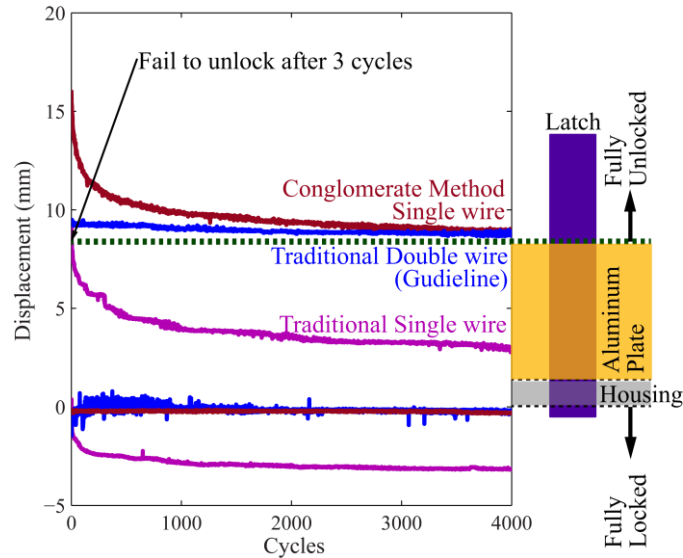


Figure C.17. A Latch Release actuation test result.

While single wire design without strain limiter failed to unlock after 3cycles, both double wire with conservative guideline and single wire with a new design method using strain limiter unlocked the plate after 4000 cycles.

This example demonstrates the benefit of the new design method using conglomerate stabilization design curves. With this method, designers can use SMA wire at higher stresses than the manufacturer’s guideline stress with possible tradeoff with fatigue life. Moreover, this method enables in-device shakedown eliminating a costly and time consuming out-of-device shakedown procedure while maintaining stable predictable performance leading to net savings in energy, wire, and manufacturing cost.

4. Conclusions

This paper presented a new conglomerate stabilization curve design method which maximizes the performance (stroke, work density) of SMA wire actuators accounting for shakedown with the use of strain limiters allowing for cost-saving in-device shakedown. To

support this, empirical knowledge was generated about the effect of different strain limiter positions on the shakedown process and the resulting stabilized performance under diverse applied stress levels. By using strain limiters, Austenite strain shakedown is reduced with a fixed Martensite strain limiter position providing a stable interface for device design. Shorter strain limiters reduce Austenite strain loss, although the resulting stabilized stroke is shorter because the Martensite strain is held by the strain limiter position. Higher stresses cause larger strain shakedown, resulting in shorter stabilized stroke, but a maximum in work density occurs at intermediate stress levels creating a design tradeoff.

A set of conglomerate stabilization design curves was created based on this empirical study to provide the basis for the new design method. These curves are used instead of the traditional Austenite stress-strain curve along with the corresponding strain limiter position lines which are used instead of the traditional Martensite stress-strain curve. These curves effectively decouple the shaken down material performance from the design variables eliminating the need for replacing the shaken down stress-strain curves for each design case. Since the conglomerate design curves are presented in terms of stress-strain, theoretically they apply to any wire length and diameter; although care must be taken as different diameter wires may have slightly different properties due to the different manufacturing process. While the conglomerate stabilization design method was demonstrated for constant load profiles with a mechanical strain limiter, this general approach can be applied without a strain limiter or to other load profiles, such as spring loads.

This new design method enables the design of SMA wire actuators with stable predictable stroke allowing for higher performance and a more economic use of material. This method also addresses the problem of interface position drift for those systems which do not undergo a pre-installation shakedown process, by providing a fixed Martensite strain allowing for an in-device or even in-operation shakedown procedure, saving time and expense over a separate out-of-device shakedown procedure.

5. References

- [1] Kudva, J. N., 2004, "Overview of the DARPA Smart Wing Project," *Journal of Intelligent Material Systems and Structures*, 15(4) pp. 261-267.
- [2] Mabe, J. H., Calkins, F. T., and Ruggeri, R. T., 2007, "Full-scale flight tests of aircraft morphing structures using SMA actuators," Y. Matsuzaki, M. Ahmadian and D. J. Leo, eds. SPIE, San Diego, California, USA, 6525, pp. 65251C-12-65251C-12.
- [3] Pollard, E. L., and Jenkins, C. H. M., 2007, "Shape Memory Alloy Deployment of Membrane Mirrors for Spaceborne Telescopes," *Journal of Spacecraft and Rockets*, 44(1) pp. 109-120.

- [4] Williams, E. A., and Elahinia, M. H., 2006, "Design of a two degree of freedom shape memory alloy actuator for mirror positioning," Y. Matsuzaki, ed. SPIE, San Diego, CA, USA, **6173**, pp. 617304-8.
- [5] Bellini, A., Colli, M., and Dragoni, E., 2009, "Mechatronic Design of a Shape Memory Alloy Actuator for Automotive Tumble Flaps: A Case Study," *Industrial Electronics, IEEE Transactions on*, **56**(7) pp. 2644-2656.
- [6] Kuribayashi, K., Tsuchiya, K., You, Z., 2006, "Self-Deployable Origami Stent Grafts as a Biomedical Application of Ni-Rich TiNi Shape Memory Alloy Foil," *Materials Science and Engineering: A*, **419**(1-2) pp. 131-137.
- [7] Lan, C., and Yang, Y., 2009, "A Computational Design Method for a Shape Memory Alloy Wire Actuated Compliant Finger," *Journal of Mechanical Design*, **131**(2) pp. 021009-9.
- [8] Sugawara, T., Hirota, K., Watanabe, M., 2006, "Shape Memory Thin Film Actuator for Holding a Fine Blood Vessel," *Sensors and Actuators A: Physical*, **130-131**pp. 461-467.
- [9] Utter, B., Luntz, J., Brei, D., 2009, "Design and operation of a fully implantable SMA actuated implant for correcting short bowel syndrome," M. Ahmadian and M. N. Ghasemi-Nejhad, eds. SPIE, San Diego, CA, USA, **7288**, pp. 72881A-13-72881A-13.
- [10] Chopra, I., 2002, "Review of State of Art of Smart Structures and Integrated Systems," *AIAA Journal*, **40**(11) pp. 2145-2187.
- [11] Kyu-Jin Cho, and Asada, H., 2005, "Multi-Axis SMA Actuator Array for Driving Anthropomorphic Robot Hand," *ICRA* pp. 1356-1361.
- [12] Barnes, B. M., Brei, D. E., Luntz, J. E., 2008, "Shape memory alloy resetable spring lift for pedestrian protection," L. P. Davis, B. K. Henderson and M. B. McMickell, eds. SPIE, San Diego, California, USA, **6930**, pp. 693005-13.
- [13] Brinson, L. C., 1993, "One-Dimensional Constitutive Behavior of Shape Memory Alloys: Thermomechanical Derivation with Non-Constant Material Functions and Redefined Martensite Internal Variable," *Journal of Intelligent Material Systems and Structures*, **4**(2) pp. 229-242.
- [14] Shaw, J. A., 2002, "A Thermomechanical Model for a 1-D Shape Memory Alloy Wire with Propagating Instabilities," *International Journal of Solids and Structures*, **39**(5) pp. 1275-1305.
- [15] Webb, G. V., Wilson, L. N., Lagoudas, D. C., 1999, "Control of SMA actuators in dynamic environments," V. V. Varadan, ed. SPIE, Newport Beach, CA, USA, **3667**, pp. 278-289.
- [16] Fu, Y., Du, H., Huang, W., 2004, "TiNi-Based Thin Films in MEMS Applications: A Review," *Sensors and Actuators A: Physical*, **112**(2-3) pp. 395-408.
- [17] Barnes, B., Brei, D., Luntz, J., 2006, "Panel Deployment Using Ultrafast SMA Latches," *ASME IMECE Chicago, Illinois, USA*, pp. 273-280.
- [18] Pathak, A., Aubuchon, J., Brei, D., 2008, "Carbon Nanotube (CNT) fins for the enhanced cooling of shape memory alloy wire," SPIE, San Diego, CA, United states, **6929**, pp.69291K .
- [19] Grummon, D. S., Shaw, J. A., and Foltz, J., 2006, "Fabrication of Cellular Shape Memory Alloy Materials by Reactive Eutectic Brazing using Niobium," *Materials Science and Engineering: A*, **438-440**pp. 1113-1118.
- [20] Redmond, J. A., Brei, D., Luntz, J., 2008, "Behavioral model and experimental validation for a spool-packaged shape memory alloy actuator," L. P. Davis, B. K. Henderson and M. B. McMickell, eds. SPIE, San Diego, California, USA, **6930**, pp. 693004-13.
- [21] Boyd, J. G., and Lagoudas, D. C., 1994, "Thermodynamical constitutive model for the shape memory effect due to transformation and reorientation," V. K. Varadan, ed. SPIE, Orlando, FL, USA, **2189**, pp. 276-288.
- [22] Erbstoesz, B., Armstrong, B., Taya, M., 2000, "Stabilization of the Shape Memory Effect in NiTi: An Experimental Investigation," *Scripta Materialia*, **42**(12) pp. 1145-1150.
- [23] Sun, H., Pathak, A., Luntz, J., 2008, "Stabilizing shape memory alloy actuator performance through cyclic shakedown: an empirical study," L. P. Davis, B. K. Henderson and M. B. McMickell, eds. SPIE, San Diego, California, USA, **6930**, pp. 69300Q-11-69300Q-11.

- [24] Liu, Y., and McCormick, P. G., 1990, "Factors Influencing the Development of Two-Way Shape Memory in NiTi," *Acta Metallurgica Et Materialia*, **38**(7) pp. 1321-1326.
- [25] Tanaka, K., Nishimura, F., Hayashi, T., 1995, "Phenomenological Analysis on Subloops and Cyclic Behavior in Shape Memory Alloys Under Mechanical and/or Thermal Loads," *Mechanics of Materials*, **19**(4) pp. 281-292.
- [26] Otsuka, K., and Wayman, C.M., 1999, "Shape Memory Materials," Cambridge University Press, .
- [27] Clark, C. R., and Marcelli, D. P., 1999, "Shape memory alloy actuator fatigue properties," M. R. Wuttig, ed. SPIE, Newport Beach, CA, USA, **3675**, pp. 311-320.
- [28] Lagoudas, D. C., and Bo, Z., 1999, "Thermomechanical Modeling of Polycrystalline SMAs Under Cyclic Loading, Part II: Material Characterization and Experimental Results for a Stable Transformation Cycle," *International Journal of Engineering Science*, **37**(9) pp. 1141-1173.
- [29] Mabe, J. H., Ruggeri, R. T., Rosenzweig, E., 2004, "NiTiNol Performance Characterization and Rotary Actuator Design," *Smart Structures and Materials 2004: Industrial and Commercial Applications of Smart Structures Technologies*, **5388**, pp. 95-109.
- [30] Feng, X., and Sun, Q., 2007, "Shakedown Analysis of Shape Memory Alloy Structures," *International Journal of Plasticity*, **23**(2) pp. 183-206.
- [31] Churchill, C. B., and Shaw, J. A., 2008, "Shakedown response of conditioned shape memory alloy wire," M. J. Dapino and Z. Ounaies, eds. SPIE, San Diego, California, USA, **6929**, pp. 69291F-12-69291F-12.
- [32] Bertacchini, O. W., Lagoudas, D. C., Calkins, F. T., 2008, "Thermomechanical cyclic loading and fatigue life characterization of nickel rich NiTi shape-memory alloy actuators," M. J. Dapino and Z. Ounaies, eds. SPIE, San Diego, California, USA, **6929**, pp. 692916-11.
- [33] Churchill, C. B., and Shaw, J. A., 2009, "Thermo-Electro-Mechanical Shakedown Response of Conditioned Shape Memory Alloy Wires," ASME SMASIS Oxnard, California, USA, pp. 137-148.
- [34] Bertacchini, O. W., Lagoudas, D. C., and Patoor, E., 2009, "Thermomechanical Transformation Fatigue of TiNiCu SMA Actuators Under a Corrosive Environment - Part I: Experimental Results," *International Journal of Fatigue*, **31**(10) pp. 1571-1578.
- [35] Nayan, N., Buravalla, V., and Ramamurty, U., 2009, "Effect of Mechanical Cycling on the Stress-Strain Response of a Martensitic Nitinol Shape Memory Alloy," *Materials Science and Engineering: A*, **525**(1-2) pp. 60-67.
- [36] Bo, Z., and Lagoudas, D. C., 1999, "Thermomechanical Modeling of Polycrystalline SMAs Under Cyclic Loading, Part III: Evolution of Plastic Strains and Two-Way Shape Memory Effect," *International Journal of Engineering Science*, **37**(9) pp. 1175-1203.
- [37] Tobushi, H., Okumura, K., Endo, M., 2002, "Deformation behavior of TiNi shape memory alloy under strain- or stress-controlled conditions," C. S. Lynch, ed. SPIE, San Diego, CA, USA, **4699**, pp. 374-385.
- [38] Sung Ho Yoon, , and Dong Jin Yeo, , 2008, "Experimental Investigation of Thermo-Mechanical Behaviors in Ni-Ti Shape Memory Alloy," *Journal of Intelligent Material Systems and Structures*, **19**(3) pp. 283-289.
- [39] Lagoudas, D. C., Li, C., Miller, D. A., 2000, "Thermomechanical transformation fatigue of SMA actuators," C. S. Lynch, ed. SPIE, Newport Beach, CA, USA, **3992**, pp. 420-429.
- [40] Bertacchini, O. W., Schick, J., and Lagoudas, D. C., 2009, "Parametric study and characterization of the isobaric thermomechanical transformation fatigue of nickel-rich NiTi SMA actuators," Z. Ounaies and J. Li, eds. SPIE, San Diego, CA, USA, **7289**, pp. 72890P-12-72890P-12.
- [41] Dynalloy Inc., "Technical and Design Data for FLEXINOL Wire," <http://www.dynalloy.com/TechData.html>.
- [42] Pathak, A., Brei, D., Luntz, J., 2008, "Dynamic characterization and single-frequency cancellation performance of SMASH (SMA actuated stabilizing handgrip)," D. K. Lindner, ed. SPIE, San Diego, California, USA, **6926**, pp. 692602-12.
- [43] Miyazaki, S., Mizukoshi, K., Ueki, T., 1999, "Fatigue Life of Ti-50 at.% Ni and Ti-40Ni-10Cu (at.%) Shape Memory Alloy Wires," *Materials Science and Engineering A*, **273-275**pp. 658-663.

- [44] Wilkes, K., Liaw, P., and Wilkes, K., 2000, "The Fatigue Behavior of Shape-Memory Alloys," *JOM Journal of the Minerals, Metals and Materials Society*, **52**(10) pp. 45-51.
- [45] Tobushi, H., Nakahara, T., Shimeno, Y., 2000, "Low-Cycle Fatigue of TiNi Shape Memory Alloy and Formulation of Fatigue Life," *Journal of Engineering Materials and Technology*, **122**(2) pp. 186-191.
- [46] Furuichi, Y., Tobushi, H., Ikawa, T., 2003, "Fatigue Properties of a TiNi Shape-Memory Alloy Wire Subjected to Bending with various Strain Ratios," *Proceedings of the Institution of Mechanical Engineers, Part L: Journal of Materials: Design and Applications*, **217**(2) pp. 93-99.
- [47] Cheung, G. S. P., and Darvell, B. W., 2007, "Fatigue Testing of a NiTi Rotary Instrument. Part 1: Strain-life Relationship," *International Endodontic Journal*, **40**(8) pp. 612-618.
- [48] Shaw, J. A., and Churchill, C. B., 2009, "A Reduced-Order Thermomechanical Model and Analytical Solution for Uniaxial Shape Memory Alloy Wire Actuators," *Smart Materials and Structures*, **18**(6) pp. 065001-065001.
- [49] Liang, C., and Rogers, C. A., 1997, "Design of Shape Memory Alloy Actuators," *Journal of Intelligent Material Systems and Structures*, **8**(4) pp. 303-13.
- [50] Duerig, T. W., and Melton, K. N., 1989, "Designing with the Shape Memory Effect," **9**pp. 581-597.
- [51] Churchill, C. B., 2010, "Experimental Techniques for Characterizing the Thermo-Electro-Mechanical Shakedown Response of SMA Wires and Tubes." Ph.D Thesis, University of Michigan Ann Arbor.
- [52] Pathak, A., 2010, "The Development of an Antagonistic SMA Actuation Technology for the Active Cancellation of Human Tremor." Ph.D Thesis, University of Michigan Ann Arbor.
- [53] Arabia, J., Frank Joseph, Bellew, C. L., Martin, I., 1998, "United States Patent: 5803515 - Vehicle Door Latch."
- [54] Aubry, M. E., Rogers, J., Lloyd Walker, Hlavaty, D. G., 1998, "United States Patent: 5715713 - Door Latch Locking Actuator Assembly."
- [55] Wittman, L. L., and Jensen, L. B., 1984, "United States Patent: 4483448 - Heavy Duty Crane.

Appendix D.

Design Tool User Scenario

1. Initial design decisions

1.1. Problem definition

Engineer	User interface	Decision manager	Evaluation manager
Set target element			
	present options to define target element behavior - Empirical data set - Analytical model - CAE model connector		
Select target element definition option			
	create instance of target element		
	present target element definition parameters - E : import / definition window - A : model parameters (w/range) - CAE : connector window (w/range)		
Set target element behavior			
	update target element parameters		

		generate target element behavior plot	
	present target element behavior plot		
Set actuation starting point and ending point on target element behavior plot and adjust the data range			
	update target element		
		evaluate maximum force and actuation stroke requirement	

1.2. Feasibility check and SMA architecture selection

Engineer	User interface	Decision manager	Evaluation manager
Select SMA architecture			
	present options to define SMA material behavior - Empirical data set - Constitutive model		
Select SMA material definition option			
	create instance of SMA material element		
	present SMA material behavior definition parameters - E : import/definition window - C : model selection & temperature selection (w/range)		
Set SMA material behavior parameters			
	update SMA material element		
	present SMA architecture options		
Select an SMA architecture			
	create instance of SMA architecture modifier element(s)		
		generate SMA architecture design space visualization	
	present SMA architecture design space visualization		
repeat the process until find a proper architecture			

1.3. Material usage decision

Engineer	User interface	Decision manager	Evaluation manager
Material usage decision			
	present material usage decision parameters		
Make material usage decision			
		store material usage decision	

2. Non-expert engineer design process

2.1. Kinematic design: select design parameters related to actuation stroke

Engineer	User interface	Decision manager	Evaluation manager
	present SMA architecture design parameters related to actuation stroke	set x-sectional area to match the maximum stress usage decision	
Select SMA architecture design parameters			
	update SMA architecture modifier elements		
		create a stroke limiter element and set parameter to reflect material usage decision	
			evaluate SMA active element behavior with stroke limiter
		create a dummy target element with constant max. force required	
		create interface element with arbitrary parameter	
		place solution coupling between interface element and dummy target element	
		assign ports connectivity	
			find force balance for martensite and austenite
			evaluate the actuation stroke
	present actuation stroke evaluation result		

2.2. Kineto-static design step: select design parameters related to force

Engineer	User interface	Decision manager	Evaluation manager
	present design parameters (e.g. x-sectional area) related to force including interface parameter		
Select design parameters			
	update SMA architecture modifier elements		
	update interface modifier		
			evaluate SMA actuation device system behavior using actual target element
		delete the dummy target element	
		reassign ports connectivity	
			find force balance for martensite and austenite
			evaluate the actuation stroke
			generate actuation device behavior visualization
	present actuation device behavior visualization		
		generate bias design map	
	present bias design map		
Select bias			
	create instance of bias elements		
			evaluate SMA actuation device system behavior
			generate actuation device behavior visualization
	present actuation device behavior visualization		

2.3. Thermo-mechanical design: select design parameters to actuation time

Engineer	User interface	Decision manager	Evaluation manager
		generate a set of number and diameter of SMA wires to meet the x-sectional area of SMA	
		compute cooling time for each possible diameter	
	present #, ϕ combination with cooling time		
Select a combination			
		compute current & voltage to reach set heated temperature	
		compute heating time	
	present current & voltage, and heating time		
Select heating current & voltage			

3. Expert engineer design process

3.1. Set actuation device system structure

Engineer	User interface	Decision manager	Evaluation manager
	present basic elements		
Select basic elements			
	create instance of basic elements		
	present design parameters for individual basic elements		
Set device system structure			
			aggregate device system
			store default port connectivity
			assign port connectivity
Set design parameters			
	update basic elements		

3.2. Plan actuation state sequence

Engineer	User interface	Decision manager	Evaluation manager
Set actuation state sequence			
	present state order		
	present device structure for each state		
Update device structure if needed			
			store port connectivity
	present directional element list and default direction		
Set directional elements			
			store directional elements
			evaluate potential solution coupling locations
	present potential solution coupling locations		
Select solution coupling location			
			store solution coupling location
	create solution coupling and assign port connectivity		
Select projection coordinate			
			store projection coordinate locations
			integrity check
			no loop
			dimension match for connected ports
			solution coupling connectivity for system
Repeat for each state			

3.3. Design evaluation

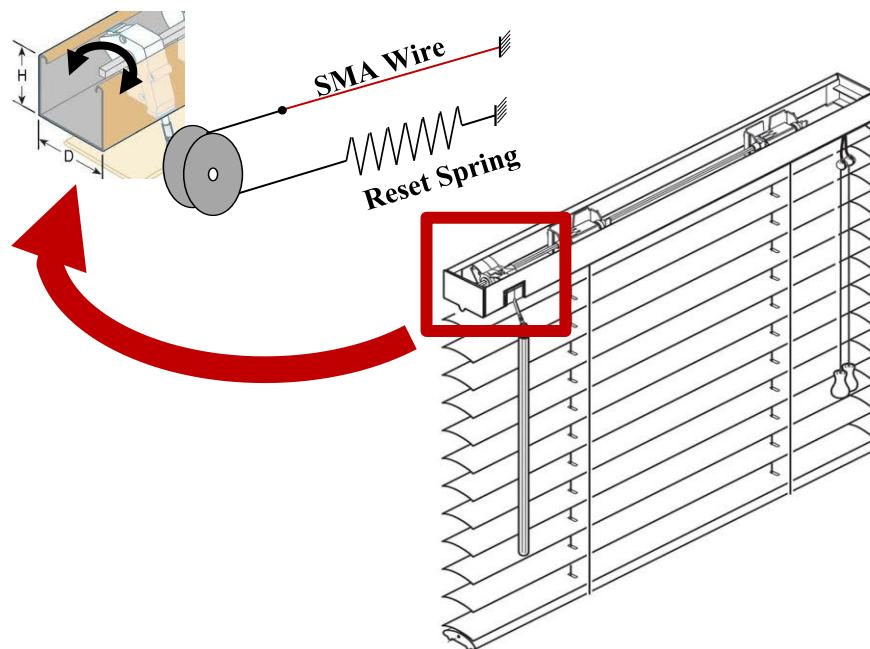
Engineer	User interface	Decision manager	Evaluation manager
			find the 1st state force balance
			set state handle as 1st state
			reassign port connectivity
			find force balance
			generate force balance visualizations
			find the 2nd state force balance
			set state handle as 1st state
			reassign port connectivity
			find force balance
			generate force balance visualizations
			evaluate actuation stroke
			update internal variables of individual basic elements if necessary
			repeat the states
			evaluate actuation stroke
			update internal variables of individual basic elements if necessary
			compare the actuation stroke and internal variables with previous step
			generate overlapping visualizations for each projection coordinate
	present behavior visualization		
	present metrics		evaluate metrics

3.4. Design modification

Engineer	User interface	Decision manager	Evaluation manager
Update design parameters			
	update basic elements		
			repeat evaluation
Update visualization			
	update solution coupling location		store solution coupling location
	reassign port connectivity		
	update projection coordinate locations		store projection coordinate locations
			repeat evaluation
	present behavior visualization		

Appendix E.

SMA Wire Design Tool Tutorial



In this tutorial, we are going to design an SMA wire device which rotates window blinds. The rotating mechanism was designed separately, and the mechanism converts the linear actuation of the SMA actuator into the rotation of the blinds. To fully open the blinds, the SMA actuator needs to provide the 4.4 mm stroke, and the force at the fully open position is predicted as 4.5 N. Because the device is exposed to the direct sun light, the ambient temperature is expected to be 55 °C during the summer. To increase the transition temperature, the maximum stress on the wire will be limited as ~ 350 MPa. For the robustness of the device, we are going to apply 1 % safety margin on the Austenite strain, and to ensure the life cycle we will limit the actuation strain as 2% using cold stop strain limiter.

This tutorial consists of three major tasks and these three tasks shows a design flow, where the Martensite finish temperature to ensure the operation at higher ambient temperature is the main design driver of the device. Each task is also designed to teach different functions of the design tool.

Task	Design Tool Function
<ol style="list-style-type: none"> 1. Initial design with estimated external systems <ol style="list-style-type: none"> 1.1. Setting external system 1.2. Setting material parameters 1.3. Select actuator architecture 1.4. Diameter / number of wires selection 1.5. Set the cold stop position and the wire length 1.6. Set the free clearance 	<ul style="list-style-type: none"> • Setting estimated external system with analytical model • Selecting material properties and setting the safety margin • Selecting actuator architecture type • Setting the wire and device design parameters
<ol style="list-style-type: none"> 2. Design reset element to increase the Martensite finish temperature (M_f) <ol style="list-style-type: none"> 2.1. Increase the cross-sectional area of the SMA wire 2.2. Find the available reset load increase 2.3. Find the softest reset spring which can provide the available reset force 2.4. Set the reset free clearance to provide the available reset force 2.5. Repeat the procedure until reach the target M_f 	<ul style="list-style-type: none"> • Setting and using reset view • Using data cursor • Setting reset element design parameters
<ol style="list-style-type: none"> 3. Verify the design with the prototyped data and set the actuation current <ol style="list-style-type: none"> 3.1. Import empirical external system data 3.2. Find the current to actuate the wire in 1 sec. 	<ul style="list-style-type: none"> • Setting the external system with empirical data using Excel file • Using operation temperature control window

TUTORIAL CONVENTIONS

Times New Roman font type is used to explain the general information about the design tool and the SMA device design procedure.

Using “External System” window, we can set the external system force-deflection profile as one of below or combination of them.

Calibri font type is used to explain the action items to use the design tool.

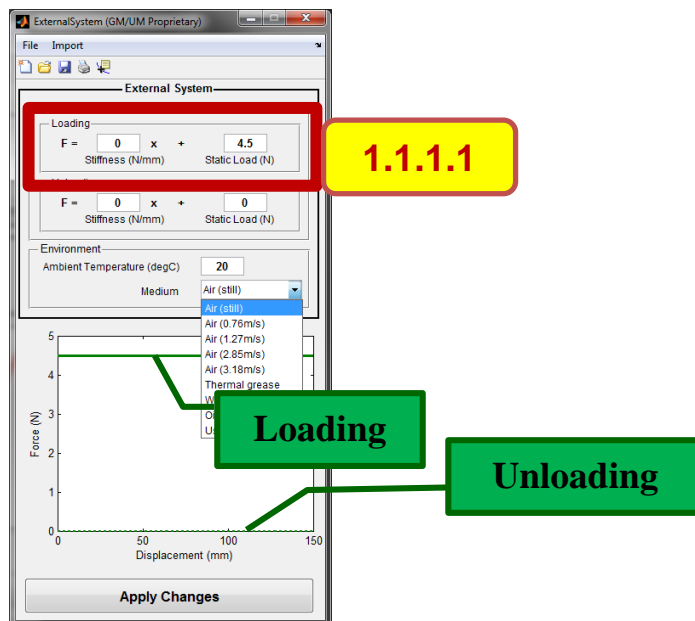
1.1.1.1. Set loading parameters

1.1.1.1.1. Type “0” N/mm in the “Stiffness” box

1.1.1.1.2. Type “4.5” N in the “Static Load” box

Red colored lines on the screen shot show the place you type in numbers or select items from the pull down menu. These items are labeled with yellow box with numbering for each action item

Green colored box explains additional information on the screen shot, such as how to interpret the plots.



1. INITIAL DESIGN WITH ESTIMATED EXTERNAL SYSTEM

We are designing an SMA actuator to meet the required force and stroke with given material use specifications. At this task, we will not constrain our design to the transition temperature.

External system

- Starting: 0 N @ 0 mm
- Target: 4.5 N @ 4.4 mm

SMA wire use specifications

- 90 degC Flexinol wire
- 1% Austenite strain safety margin
- ~ 350 MPa Austenite stress
- 2 % Actuation strain

1.1. Setting External System

Using “External System” window, we can set the external system force-deflection profile as one of below or combination of them.

- Analytical asymmetric external system model for loading and/or unloading
 - Linear stiffness system
 - Constant force load
- Arbitrary load data set as an Excel file,
- Pre-simulated data using ADAMS model.

For this task, we will use the asymmetric constant force load.

1.1.1. Open External System Window

1.1.1.1. If it appears on the screen, click any part of the External System Window.

1.1.1.2. If you can't find the window, use the main window menu bar. (“Window” > “External System”)

Integrated Model-Based SMA Wire DesignTool v.5 (GM/UM Proprietary)

File Window **External System** Actuator Architecture View Help **1.1.1.2.**

Material View: 350, 300

User Views: SMA Wire View: 40

ExternalSystem (GM/UM Proprietary)

File Import

External System

Analytical System Model

Loading

$$F = 0 \times + 4.5$$

Stiffness (N/mm) Static Load (N)

Unloading

$$F = 0 \times + 0$$

Stiffness (N/mm) Static Load (N)

Environment

Ambient Temperature (degC) 20

Medium Air (still)

Force (N)

Displacement (mm)

Apply Changes

Internal Architecture

SMA Wire Parameters

Wire Diameter (mil) Use Arbitrary Diameter

Number of Wires 04

Wire Length (mm) 300

Interface

Free Clearance (mm)	20	Free Clearance for Spooled Wire (mm)	8
Input / Output Ratio	1	Pre-Stress (MPa)	90.9
<input type="radio"/> Cold Stop Strain	0.04	Loading friction (N)	0
<input type="radio"/> Hot Stop Strain	0.01	Unloading friction (N)	0

Reset Element

Stiffness (N/mm)	0	Free Clearance for Spooled Wire (mm)	22
Leverage Ratio	1		
Free Clearance (mm)	10		
Pre Load (N)	0		

1.1.2. Set loading / unloading parameters

For this task, we are using the estimated external system for the initial design; the loading force is estimated at 4.5 N which includes the weight of the blades and friction of the rotating mechanism.

1.1.2.1. Set loading parameters

1.1.2.1.1. Type "0" N/mm in the "Stiffness" box

1.1.2.1.2. Type "4.5" N in the "Static Load" box

1.1.2.2. Set unloading parameters

1.1.2.2.1. Type "0" N/mm in the "Stiffness" box

1.1.2.2.2. Type "0" N in the "Static Load" box

1.1.3. Set Environment parameters

With the "Environment" box, you can set a) the ambient temperature and b) select the surrounding medium.

To calculate the heating and cooling time, the ambient temperature of the wire needs to be set.

You can select the environment medium from the pull-down menu. This will affect the heating and cooling time of the SMA wire by changing the film heat transfer coefficient which you can check on the main window.

For this task, we assume the average ambient temperature as 20 °C although the worst extreme case is 55 °C. We will check this case in task 2.

1.1.3.1. Set ambient temperature as "20" degC

1.1.3.2. Select "Air (still)" from the "Medium" pull down menu

1.1.4. Transfer the External System parameters to the Main Window

1.1.4.1. Click "Apply Changes" button

ExternalSystem (GM/UM Proprietary)

File Import

External System

Analytical System Model

Loading

$F = 0 \times + 4.5$

Stiffness (N/mm) Static Load (N)

1.1.2.1

Unloading

$F = 0 \times + 0$

Stiffness (N/mm) Static Load (N)

1.1.2.2

Environment

Ambient Temperature (degC) 20

1.1.3.2

Medium

Air (still)

1.1.3.2

Air (0.76m/s)

Air (1.27m/s)

Air (2.85m/s)

Air (3.18m/s)

Thermal grease

Water

Oil

User Defined

Force (N)

5

4

3

2

1

0

0

50

100

150

Displacement (mm)

Loading

Unloading

Apply Changes

The screenshot shows the 'External System' configuration window. It is divided into three main sections: 'Analytical System Model', 'Environment', and a graph. The 'Analytical System Model' section contains two sub-sections: 'Loading' and 'Unloading'. The 'Loading' section has a stiffness of 0 N/mm and a static load of 4.5 N. The 'Unloading' section has a stiffness of 0 N/mm and a static load of 0 N. The 'Environment' section has an ambient temperature of 20 degC and a medium dropdown menu currently set to 'Air (still)'. A graph at the bottom shows Force (N) on the y-axis (0 to 5) and Displacement (mm) on the x-axis (0 to 150). The graph shows a loading curve starting at 0 displacement and 4.5 N, and an unloading curve starting at 50 mm displacement and 0 N. A green box labeled 'Loading' is placed on the loading curve, and another green box labeled 'Unloading' is placed on the unloading curve. A red box highlights the 'Air (still)' dropdown menu, and a yellow callout box with the number '1.1.3.2' points to it. Another yellow callout box with '1.1.3.2' points to the 'Air (still)' option in the dropdown menu. A yellow callout box with '1.1.2.1' points to the 'Loading' section, and another yellow callout box with '1.1.2.2' points to the 'Unloading' section. At the bottom of the window is an 'Apply Changes' button.

1.2. Setting Material parameters

“Material” window is used for

- Select 70 degC or 90 degC material model
- Import the austenite and martensite stress-strain curve of the SMA wire and the phase transition temperatures
- Select imported stress-strain curve

We can use the GM India Science Lab (ISL) material model to generate the stress-strain curve at the ambient temperature and the heated temperature, by selecting “70 degC Flexinol” or “90 degC Flexinol”, and setting the heated temperature. The ambient temperature was already set when you set the environment on the “External System” window, but you can still change the ambient temperature on the “Material” window. The heated temperature is set to “90” degC for the 70 degC Flexinol, and “110” degC for the 90 degC Flexinol, but you can change it either on the “Material” window or the main window.

1.2.1. Open Material Window

- 1.2.1.1. If it appears on the screen, click any part of the Material Window.
- 1.2.1.2. If you can't find the window, use the main window menu bar. (“Window” > “Material”)

1.2.2. Select the wire type

We are going to use “90 °C Flexinol” as the driver for this design case is the high transition temperature.

- 1.2.2.1. Select the “90 degC Flexinol” from the “Material” sub-window.

1.2.3. Set the safety margin

- 1.2.3.1. Type “0.01” in the “Austenite Strain Safety Margin” box.
- 1.2.3.2. Type “0” in the “Martensite Strain Safety Margin” box.
- 1.2.3.3. Check the “Apply Safety Margin” button.

1.2.4. Transfer material parameters to the main window

- 1.2.4.1. Push the “Apply Changes” button.

Integrated Model-Based SMA Wire DesignTool v.5 (GM/UM Proprietary)

File Window Actuator Architecture View Help

Material **1.2.1.2.**

Material (GM/UM Proprietary)

Material

70 degC Flexinol (degC) 20

90 degC Flexinol **1.2.2.1.** (degC) 110

User Material

15_mil_90degC.xls **1.2.3.**

Safety Margin

Apply Safety Margin

Austenite Strain Safety Margin 0.01

Martensite Strain Safety Margin 0.000

Stress (MPa)

Strain

Original Austenite

Shifted Martensite

Martensite

1.2.4.

Apply Changes

Austenite safety margin

1.3. Select actuator architecture

There are three available actuator architectures at this time; 1) straight wires, 2) spool packaging using single spool, and 3) web actuators (bow string actuators). By using the main window tool menu bar, we can select the actuator architecture and the “Device Architecture” > “Internal Architecture” window shows the current actuator architecture schematic and corresponding design parameters for each architecture type.

For this example, we will use straight wires. The schematics and design parameter control window for the spool packaging architecture and the web actuator architecture are shown below the main window.

1.3.1. Select the SMA Actuator architecture type

- 1.3.1.1. Select “Straight Wire” from the main window menu bar.
 (“Actuator Architecture” > “Straight Wire”)

Integrated Model-Based SMA Wire DesignTool v.5 (GM/UM Proprietary)

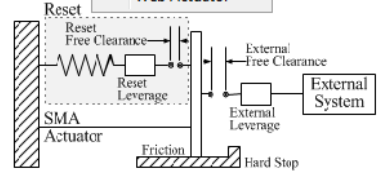
File Window **Actuator Architecture** View Help

Straight Wire

1.3.1.1.


Spool Packaging

Web Actuator



Reset
Reset Free Clearance
Reset Leverage
SMA Actuator
External Free Clearance
External Leverage
External System
Friction
Hard Stop

Internal Architecture



SMA Wire Parameter

Wire Diameter (mil) 15 mil Use Arbitrary Diameter

Number of Wires 1 Spooled Strain 0.04

Wire Length (mm) 300 As Spooled Length (mm) 312

Free Clearance (mm) 20 Free Clearance for Spooled Wire (mm) 8

Input / Output Ratio 1 Pre-Stress (MPa) 0

Cold Stop Strain 0.04 Loading friction (N) 0

Hot Stop Strain 0.01 Unloading friction (N) 0

Reset Element

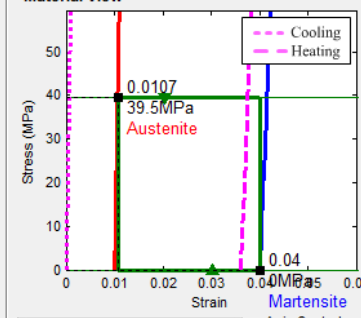
Stiffness (N/mm) 0

Leverage Ratio 1

Free Clearance (mm) 10 Free Clearance for Spooled Wire (mm) 22

Pre Load (N) 0

Material View



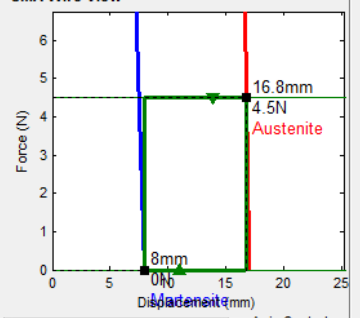
Stress (MPa)

Strain

0.0107
39.5 MPa
Austenite

0.04
Martensite

Material View



SMA Wire View

Force (N)

Displacement (mm)

8mm
16.8mm
4.5N
Austenite

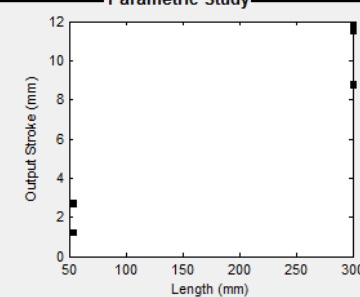
Axis Control

xMin 0 xMax 20 yMin 0 yMax 400

Design Metrics

Output Stroke	8.8 mm	SMA Stroke	2.93 %
Max Force	4.5 N	Cross Sectional Area	0.114 mm ²
Max Stress	39.5 MPa	Work Efficiency	1.52 %
Work	19.8 mJ	Power Efficiency	1.52 %
Specific Work	0.58 MJ/m ³	SMA Cost	0.35 \$
Total Material	34.2 mm ³	Weight of SMA	0.22 g

Parametric Study



Output Stroke (mm)

Length (mm)

Y Axis Output Stroke X Axis Length

Family Curve Diameter Auto Curve

Operation Temperature Control

Temp. Control (degC) Trans. Temp. (degC)

Amb. Temp. 20 Mf 28 Ms 55

Heated Temp. 110 As 72 Af 82

Ref. Temp. 70

h = 81 W/m²-K

Joule Heating Control

Input Volts (V) 3.57 Heating Time(s) (Amb. ~ Af) 2.28

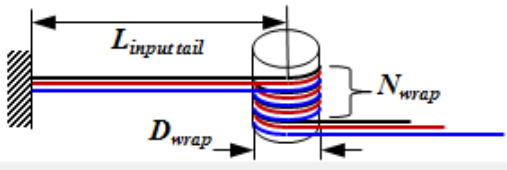
Input Current (A) 1.6 Cooling Time(s) (Heated ~ Mf) 25.6

Input Power (W) 5.71 Cycle Time(s) 27.9

Cooling time for cold stop

Spool Packaging Architecture

Internal Architecture



$L_{input\ tail}$

N_{wrap}

D_{wrap}

SMA Wire Parameter

Wire Diameter (mil) 15 mil Use Arbitrary Diameter

Number of Wires 1 Spooled Strain 0.04

Wire Length (mm) 300 As Spooled Length (mm) 312

Spool Packaging Parameter

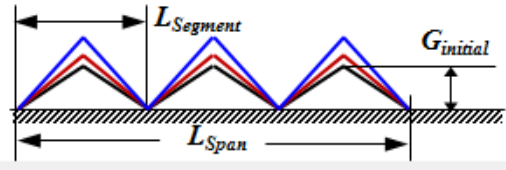
Input Tail Length (mm) 50

Spool Diameter (mm) 25.4

Number of Wraps 1

Web Actuator Architecture

Internal Architecture



$L_{Segment}$

$G_{initial}$

L_{Span}

SMA Wire Parameter

Wire Diameter (mil) 15 mil Use Arbitrary Diameter

Number of Wires 1 Spooled Strain 0.04

Wire Length (mm) 53.9 As Spooled Length (mm) 56

Web Parameter

Segment Length (mm) 50 Span Length (mm) 50

Initial Gap Length (mm) 10 Number of Segment 1

1.4. Diameter / Number of wires selection

At this step, we are setting the diameter and the number of wires to meet the maximum stress on the wire which we set as the material use specifications. In this example, we set the maximum stress as 350 MPa, as we want to increase the transition temperatures. As the force at the opening position is 4.5 N, we can meet the ~ 350 MPa maximum stress material use specification using single 5 mil wire.

$$\text{Wire Diameter} = \sqrt{\frac{4 \times \text{Required force}}{\pi \times \text{Max. Stress}}} = \sqrt{\frac{4 \times 4.5 \text{ N}}{\pi \times 350 \text{ MPa}}} \approx 5 \text{ mil}$$

For this example, we are using commercially available Flexinol wires from the pull down menu. However, it is possible to select custom diameter wire using type-in edit box.

1.4.1. Find the diameter and number of wire combination to get the proper austenite stress.

1.4.1.1. Select “5 mil” from the “Wire Diameter” pull down menu.

⇒ The austenite stress is 355 MPa, which is close to the target austenite stress.

Integrated Model-Based SMA Wire DesignTool v.5 (GM/UM Proprietary)

File Window Actuator Architecture View Help

Device Schematic

Device Architecture

Internal Architecture

SMA Wire Parameters

- Wire Diameter (mil): 5 mil (highlighted)
- Number of Wires: 1
- Wire Length (mm): 312
- Spooled Length (mm): 312

Interface

- Free Clearance (mm): 10
- Input / Output Ratio: 1
- Free Clearance for Spooled Wire (mm): 8
- Pre-Stress (MPa): 0
- Hot Stop Strain: 0.01
- Loading friction (N): 0
- Unloading friction (N): 0

Reset Element

- Stiffness (N/mm): 0
- Leverage Ratio: 1
- Free Clearance for Spooled Wire (mm): 22
- Pre Load (N): 0

User Views

Material View

SMA Wire View

Design Metrics

Output Stroke	7.22 mm	SMA Stroke	2.41 %
Max Force	4.5 N	Cross Sectional Area	0.013 mm ²
Max Stress	355 MPa	Work Efficiency	8.07 %
Work	16.3 mJ	Power Efficiency	8.07 %
Specific Work	4.28 MJ/m ³	SMA Cost	0.34 \$
Total Material	3.8 mm ³	Weight of SMA	0.02 g

Operation Temperature Control

Temp. Control (degC):

- Amb. Temp: 20
- Heated Temp: 110
- Ref. Temp: 70

Trans. Temp. (degC):

- Mf: 28 Ms: 55
- As: 107 Af: 117
- h = 163 W/m²-K

Joule Heating Control:

- Input Volts (V): 6.5
- Input Current (A): 0.32
- Input Power (W): 2.1
- Heating Time(s): 0.959
- Cooling Time(s): 4.18
- Cycle Time(s): 5.14
- Cooling time for cold stop:

Parametric Study

Y Axis: Output Stroke
X Axis: Length
Family Curve: Diameter

1.5. Set the cold stop position and the wire length

Purpose of using hard stops is to limit the SMA actuation. There are two types of hard stops; one is the cold stop which limits the Martensite actuation end, and the other is the hot stop which limits the Austenite actuation end.

There are two ways to set the cold stop position. One is to limit the Martensite strain with fixed value. In this case, the cold stop position is set to be the fixed Martensite strain value. The other is to limit the actuation strain. In this case, we need to find the Austenite strain value first, and then add the actuation strain value to the Austenite strain value to calculate the cold stop position value. In this example, we will use the actuation strain value as 2 % strain as we want to ensure longer life cycle. There is no golden model for setting the actuation strain or the Martensite strain for life cycle. This value (2 %) is a rule of thumb decision.

Using this actuation strain, we can calculate the required length to meet the stroke.

1.5.1. Set the cold stop position.

1.5.1.1. Find the austenite strain from the “Material View”

⇒ “0.0159”

1.5.1.2. Set the “Cold Stop Strain” as 0.0359 (austenite strain @ 355MPa) + 0.02 (2 % actuation strain) = “0.0359”.

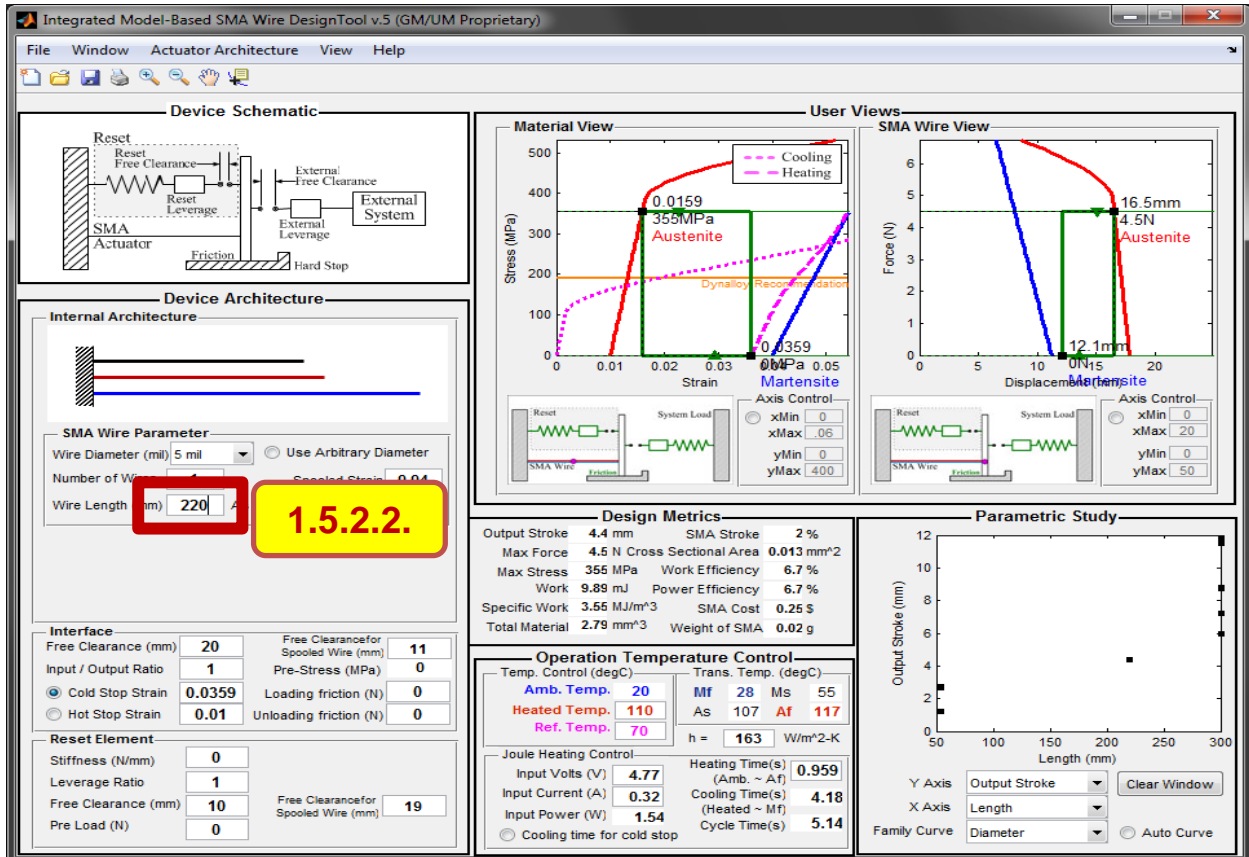
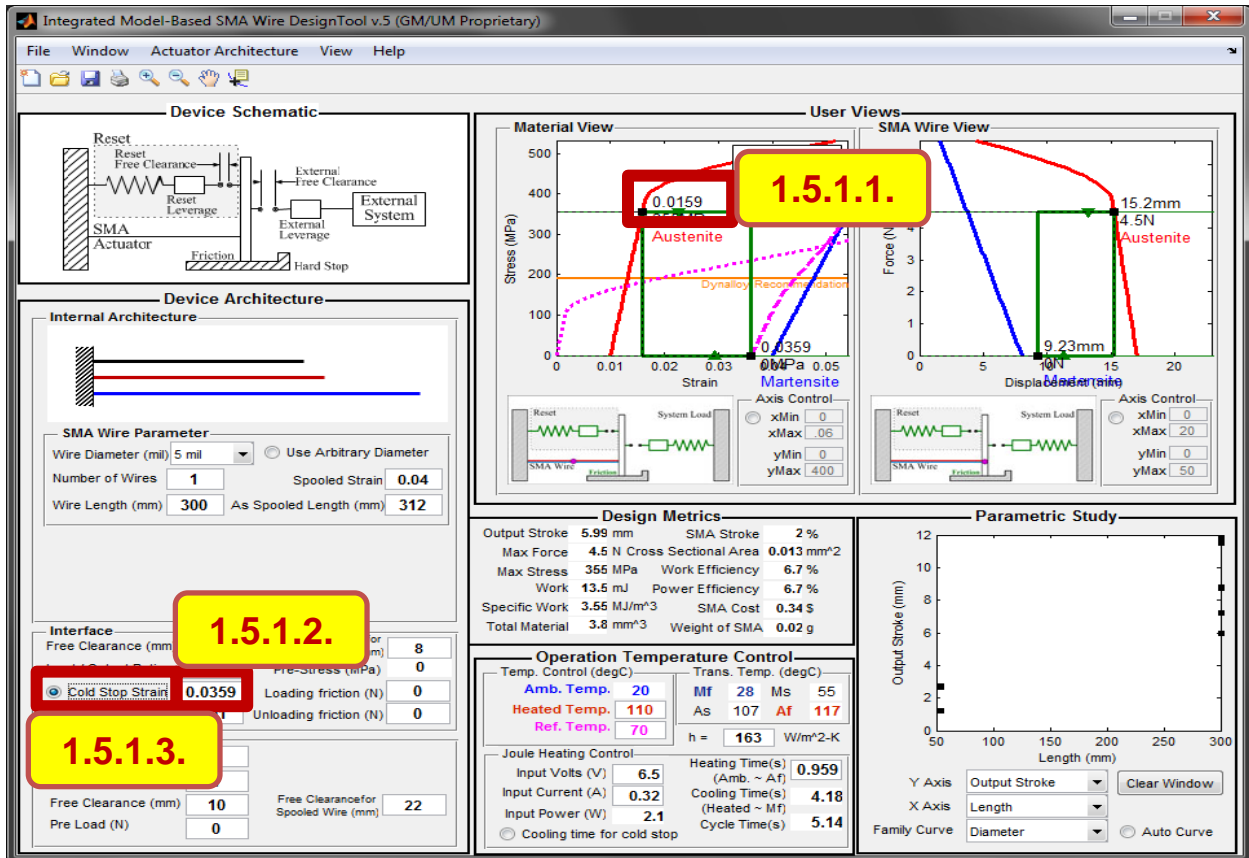
1.5.1.3. Check the “Cold Stop Strain” button.

1.5.2. Set the wire length

1.5.2.1. Calculate the wire length to get the required stroke.

$$\text{wire length} = \frac{\text{required stroke}}{\text{actuation strain}} = \frac{4.4 \text{ mm}}{0.02} = 220 \text{ mm}$$

1.5.2.2. Type “220” in the “Wire Length” box.



1.6. Set the free clearance

Now, we have an SMA actuator which has the 4.4 mm stroke and 4.5 N force at the actuation point. However, the stroke and force do not guarantee the successful opening of the blinds. To make the window blinds open, we need to match the initial position of SMA actuation to the initial position of the device operation, for this example the initial position of the blind opening. Right now, we have an SMA actuator which starts its motion arbitrarily at 12.1 mm from the device origin (yours might be different if you have different free clearance value than the 20 mm default). To use the full SMA actuation to open the window blinds open, we need to set the initial position as zero. Physically, this means we place the cold stop position at the zero position.

1.6.1. Calculate the free clearance.

1.6.1.1. Find the required shift from the “System View” window.

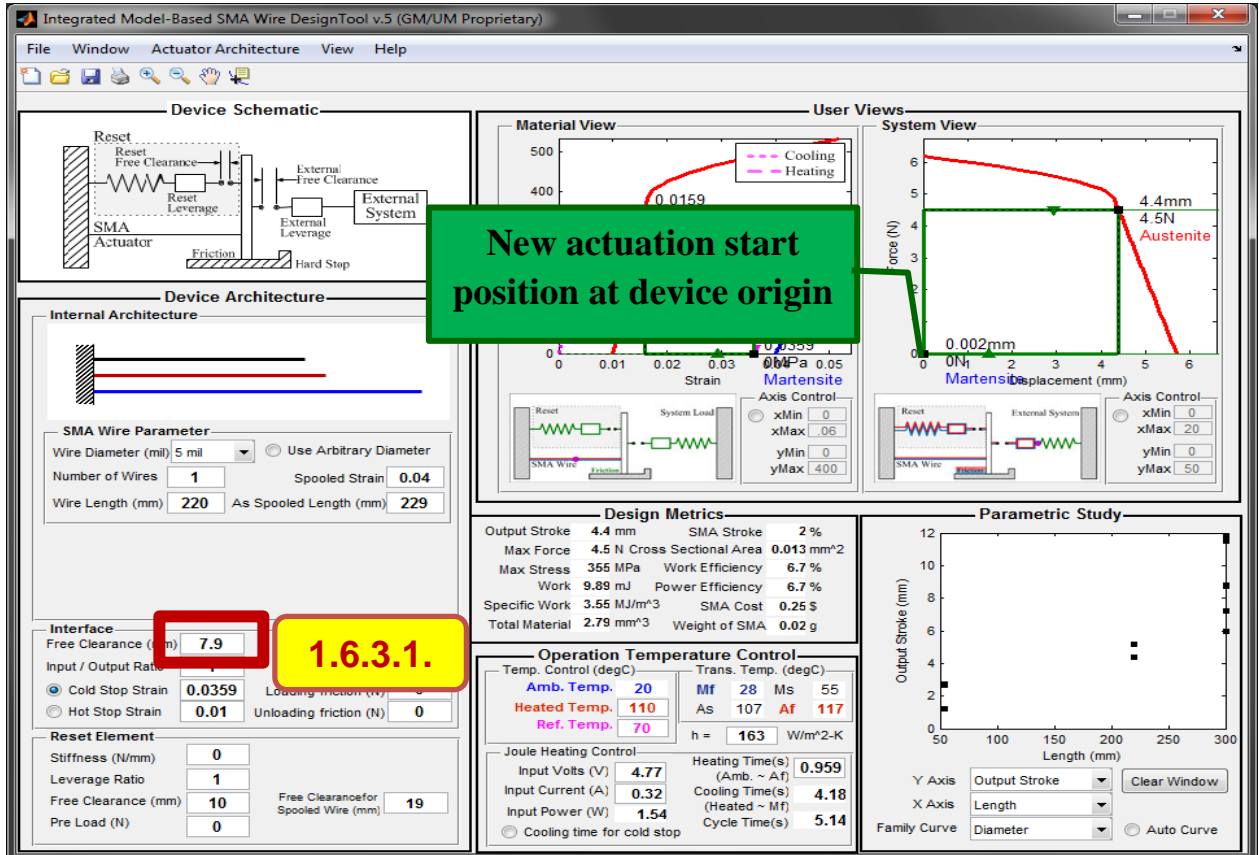
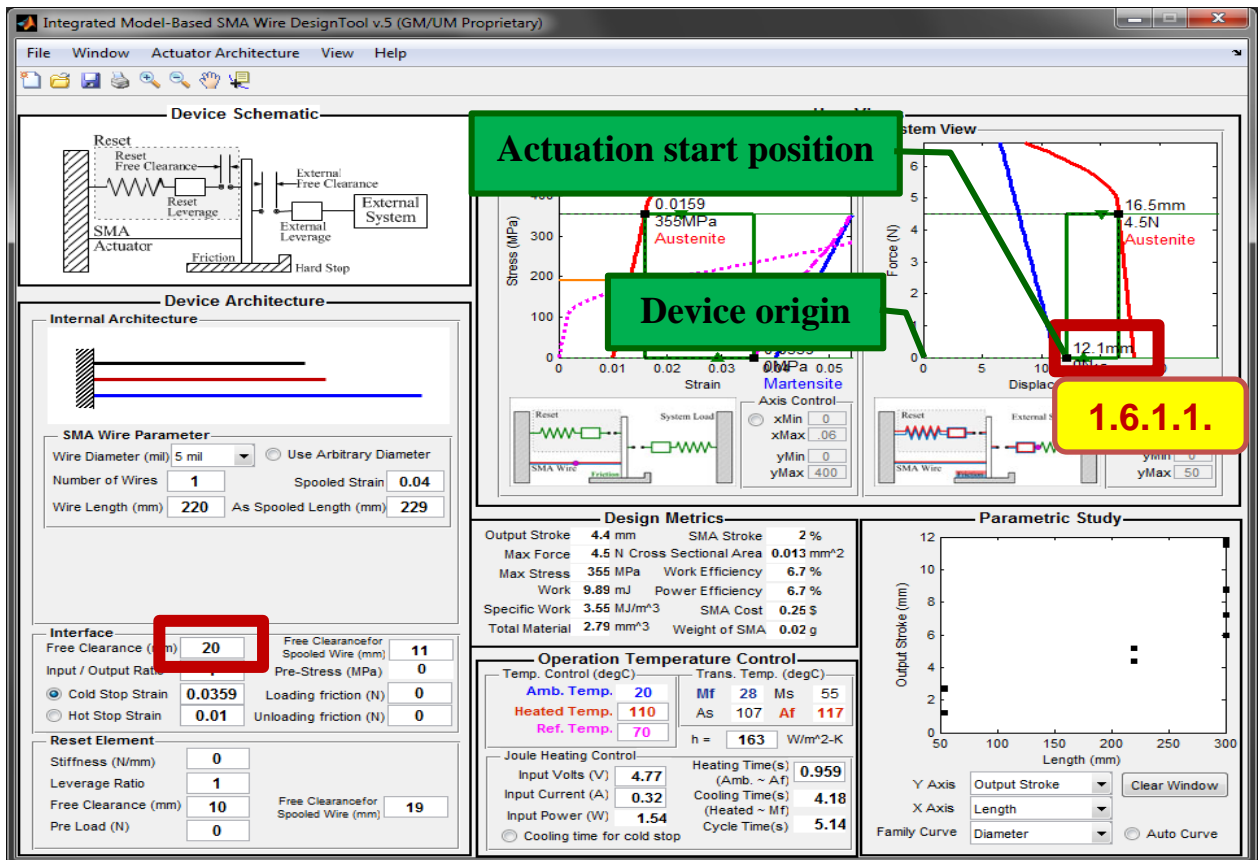
⇒ “12.1 mm”

1.6.2. Calculate the new free clearance value.

⇒ $\text{New free clearance} = \text{default free clearance} - \text{required shift}$
 $= 20 \text{ mm} - 12.1 \text{ mm} = 7.9 \text{ mm}$

1.6.3. Set the new free clearance

1.6.3.1. Type “7.9” in the “Free Clearance” box.

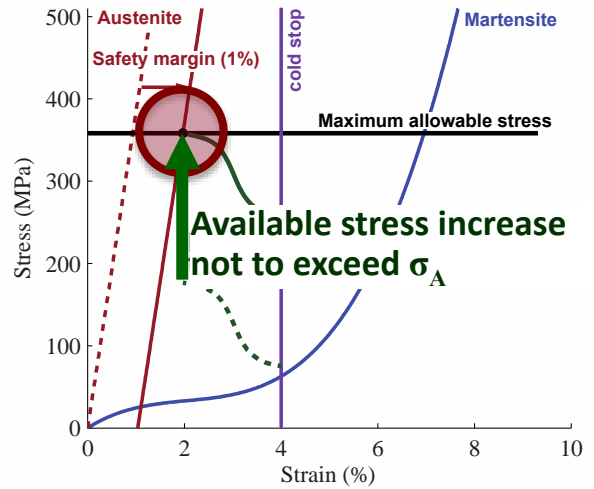
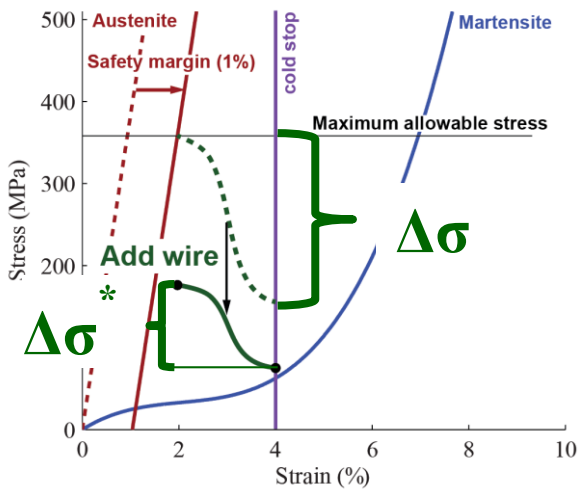
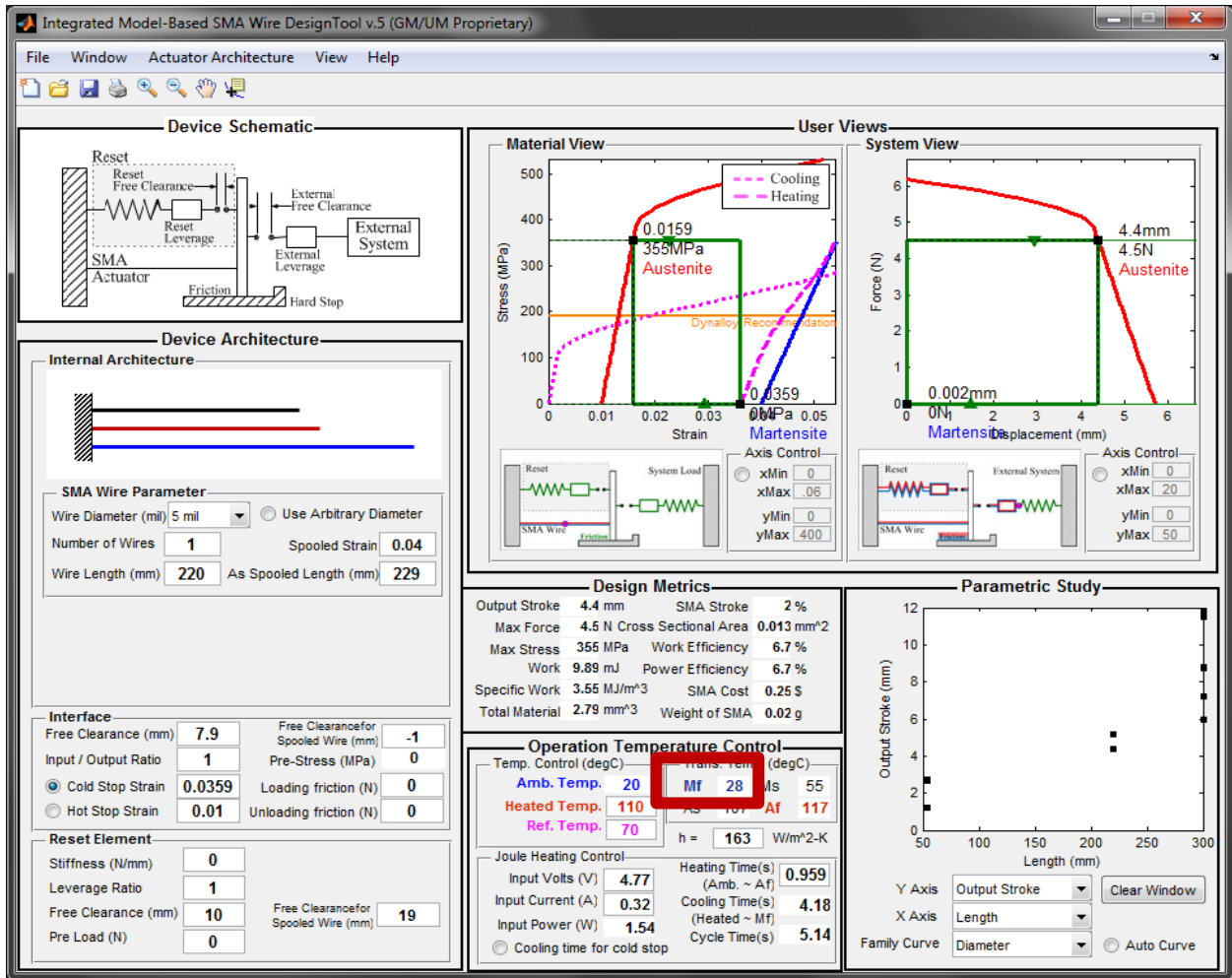


2. DESIGN RESET ELEMENT TO INCREASE THE M_F

Now, we have an SMA actuator, which can open the window blinds when we heat the wire. However, as the device is exposed to direct sun light, the ambient temperature of the device is expected to be 55 °C during the summer. Thus the Martensite finish temperature should be higher than 55 °C to ensure the window blinds close during the hot summer day. From the “Operation Temperature Control” window, we can check the Martensite finish temperature, which is 28 °C for the initial design. In this task 2, we will design a reset element to increase the Martensite finish temperature.

Required $M_f > 55$ °C

To increase the Martensite finish temperature and/or Martensite stress, the stress difference between the Austenite stress and the Martensite stress needs to be reduced. As the Austenite stress is set to meet the material use specification at the required force, reducing the stress difference will allow us room to increase the Martensite stress which is one criteria, and is also the dominate factor needed to set the Martensite finish temperature.



2.1. Increase the cross-sectional area of the SMA wire.

To decrease the stress difference, there are two options; one is to increase the diameter of the wire which sacrifices the cooling time, and the other is to add another wire which increases the manufacturing complexity.

In this example, we will increase the wire diameter from 5 mil to 8 mil to make the stress difference smaller.

2.1.1. Increase the wire diameter to “8 mil”.

Integrated Model-Based SMA Wire DesignTool v.5 (GM/UM Proprietary)

File Window Actuator Architecture View Help

Device Schematic

User Views

Material View

System View

Device Architecture

Internal Architecture

SMA Wire Parameters

Wire Diameter (mm) **2.1.1.** 8 mil

Number of Wires: 1 mil

Wire Length (mm): 2 mil

Spooled Length (mm): 229

Interface

Free Clearance (mm): 12 mil

Input / Output Ratio: 15 mil

Cold Stop Strain: 0.01

Hot Stop Strain: 0.01

Free Clearance for Spooled Wire (mm): -1

Pre-Stress (MPa): 0

Loading friction (N): 0

Unloading friction (N): 0

Reset Element

Stiffness (N/mm): 0

Leverage Ratio: 1

Free Clearance (mm): 10

Pre Load (N): 0

Free Clearance for Spooled Wire (mm): 19

Design Metrics

Output Stroke	5.19 mm	SMA Stroke	2.36 %
Max Force	4.5 N	Cross Sectional Area	0.032 mm ²
Max Stress	139 MPa	Work Efficiency	3.76 %
Work	11.7 mJ	Power Efficiency	3.76 %
Specific Work	1.64 MJ/m ³	SMA Cost	0.26 \$
Total Material	7.13 mm ³	Weight of SMA	0.05 g

Operation Temperature Control

Temp. Control (degC):

Amb. Temp. 20

Heated Temp. 110

Ref. Temp. 70

Trans. Temp. (degC):

Mf 28 Ms 55

As 83 Af 93

h = 121 W/m²-K

Joule Heating Control

Input Volts (V): 3.54

Input Current (A): 0.61

Input Power (W): 2.17

Heating Time(s) (Amb. ~ Af): 1.43

Cooling Time(s) (Heated ~ Mf): 9.1

Cycle Time(s) (Heated ~ Mf): 10.5

Cooling time for cold stop

Parametric Study

Y Axis: Output Stroke

X Axis: Length

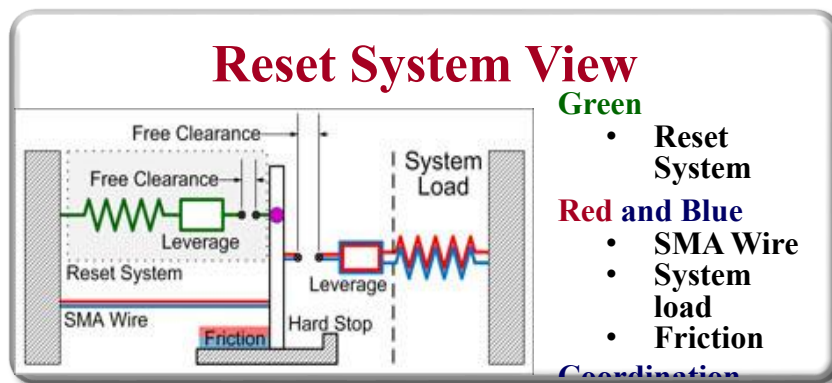
Family Curve: Diameter

Clear Window

Auto Curve

2.2. Find the available reset load increase.

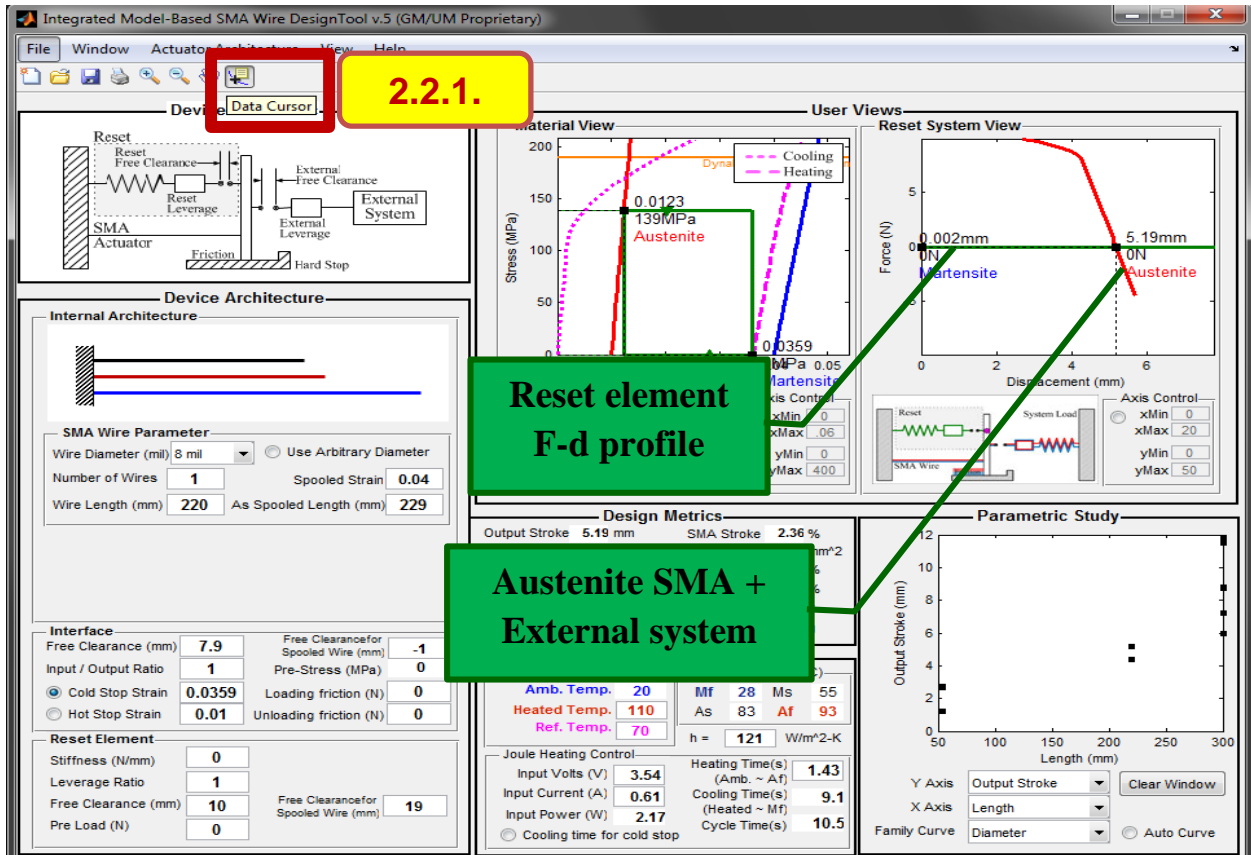
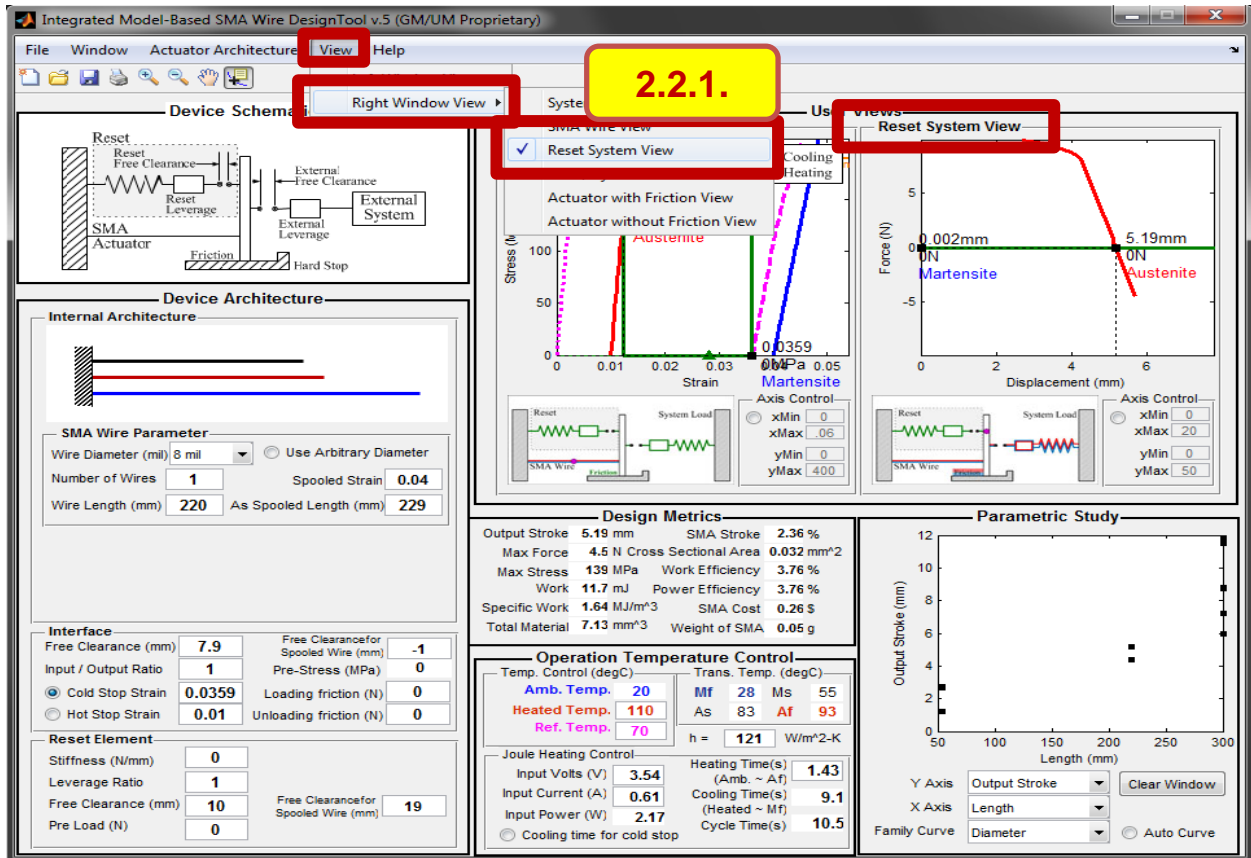
We now have smaller stress difference, thus the Austenite stress value is smaller than the maximum allowable stress. We can increase both the Austenite stress and the Martensite stress using a reset element. However, to design the reset element, we first need to figure out by how much we can increase the stress. Here, we can easily find out the value using the “Reset System View” and the “data cursor” of the design tool. “Reset System View” is very useful when you design the reset system. The green line represents the reset element, and all other parts (SMA wire, External system) lump together with the red and blue line.



2.2.1. Change the right window of the “User Views” to “Reset System View” using the menu bar. (“View” > “Right Window View” > “Reset System View”)

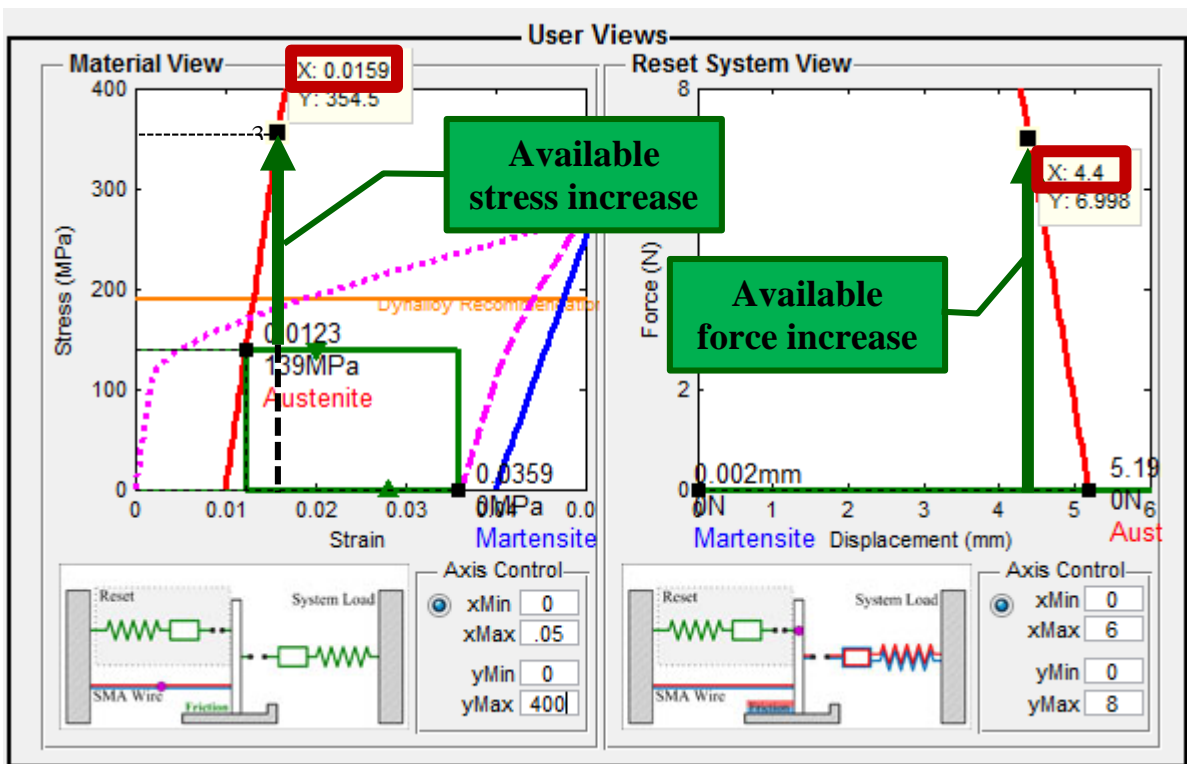
Initially the green line is horizontal of zero force since we have not yet specified a reset element.

2.2.2. Select the “Data Cursor” from the tool bar.



There are two ways to find the available force increase; one is to convert the available stress increase into the available force numerically, and the other is to use the Reset view. In this example, we will use the Reset view method.

On the main window, we have a slightly longer stroke than what we designed because the Austenite stress level is smaller than the design value (355 MPa) thus the Austenite strain is smaller than the design value. As we designed the stroke to be 4.4 mm, if we find the force on the reset view corresponding to the designed stroke (4.4 mm), that corresponding force is the available force increase from the reset element.



2.2.3. Select one point on the austenite curve on the “Reset System View” window.

2.2.4. Move the cursor to the target displacement (4.4 mm) to find the available reset force.

⇒ “7 N”

Integrated Model-Based SMA Wire DesignTool v.5 (GM/UM Proprietary)

File Window Actuator Architecture View Help

Device Schematic

Device Architecture

Internal Architecture

SMA Wire Parameter

Wire Diameter (mil) 8 mil Use Arbitrary Diameter

Number of Wires 1 Spooled Strain 0.04

Wire Length (mm) 220 As Spooled Length (mm) 229

Interface

Free Clearance (mm) 7.9 Free Clearance for Spooled Wire (mm) -1

Input / Output Ratio 1 Pre-Stress (MPa) 0

Cold Stop Strain 0.0359 Loading friction (N) 0

Hot Stop Strain 0.01 Unloading friction (N) 0

Reset Element

Stiffness (N/mm) 0

Leverage Ratio 1

Free Clearance (mm) 10 Free Clearance for Spooled Wire (mm) 19

Pre Load (N) 0

Material View

Reset System View

Design Metrics

Output Stroke 5.19 mm SMA Stroke 2.36 %

Max Force 4.5 N Cross Sectional Area 0.032 mm²

Max Stress 139 MPa Work Efficiency 3.76 %

Work 11.7 mJ Power Efficiency 3.76 %

Specific Work 1.84 MJ/m³ SMA Cost 0.26 \$

Total Material 7.13 mm³ Weight of SMA 0.05 g

Operation Temperature Control

Temp. Control (degC) Trans. Temp. (degC)

Amb. Temp. 20 Mf 28 Ms 55

Heated Temp. 110 As 83 Af 93

Ref. Temp. 70

h = 121 W/m²-K

Joule Heating Control

Input Volts (V) 3.54 Heating Time(s) 1.43 (Amb. ~ Af)

Input Current (A) 0.61 Cooling Time(s) 9.1 (Heated ~ Mf)

Input Power (W) 2.17 Cycle Time(s) 10.5

Cooling time for cold stop

Parametric Study

Y Axis Output Stroke

X Axis Length

Family Curve Diameter Auto Curve

2.2.4.

Available force increase

2.3. Find the softest reset spring which can provide the available reset force

Ideally, if we can shift the Austenite and the Martensite stress with the same amount, that is the best reset element design. However, applying constant force using dead weight is not efficient in terms of the implementation. So, the reset spring is the usual approach to implement the reset element. As the Austenite stress increase is limited by the available reset load, not to lose the stress shift at the Martensite end, the softest spring which can provide the available reset force is the best choice for the reset spring design.

2.3.1. Find the softest reset spring which can provide the required reset force from a spring catalog (An example web site is shown below).

⇒ 0.33 N/mm for 7N

The screenshot shows the Lee Spring website catalog for extension springs. The table below is a representation of the data shown in the image:

Part Number	Outside Diameter	Wire Diameter	Max Load	Free Length	Rate	Max Length	Initial Tension	Material
MS24586-C7	3.047 mm	0.457 mm	8.153 N	28.575 mm	0.42 N/mm	45.974 mm	0.742 N	SS
MS24586-1008	3.047 mm	0.457 mm	9.785 N	31.750 mm	0.44 N/mm	51.561 mm	0.889 N	MW
MS24586-508	3.047 mm	0.457 mm	9.785 N	31.750 mm	0.44 N/mm	51.561 mm	0.889 N	MW
MS24586-8	3.047 mm	0.457 mm	9.785 N	31.750 mm	0.44 N/mm	51.561 mm	0.889 N	MW
MS24586-C8	3.047 mm	0.457 mm	8.153 N	31.750 mm	0.37 N/mm	51.561 mm	0.742 N	SS
MS24586-1009	3.047 mm	0.457 mm	9.785 N	34.925 mm	0.39 N/mm	57.150 mm	0.889 N	MW
MS24586-509	3.047 mm	0.457 mm	9.785 N	34.925 mm	0.39 N/mm	57.150 mm	0.889 N	MW
MS24586-9	3.047 mm	0.457 mm	9.785 N	34.925 mm	0.39 N/mm	57.150 mm	0.889 N	MW
MS24586-C9	3.047 mm	0.457 mm	8.153 N	34.925 mm	0.33 N/mm	57.150 mm	0.742 N	SS
MS24586-10	3.047 mm	0.457 mm	9.785 N	38.099 mm	0.36 N/mm	62.738 mm	0.889 N	MW
MS24586-1010	3.047 mm	0.457 mm	9.785 N	38.099 mm	0.36 N/mm	62.738 mm	0.889 N	MW
MS24586-510	3.047 mm	0.457 mm	9.785 N	38.099 mm	0.36 N/mm	62.738 mm	0.889 N	MW
MS24586-C16	3.047 mm	0.508 mm	11.115 N	28.575 mm	0.61 N/mm	41.655 mm	1.112 N	SS
MS24586-C17	3.047 mm	0.508 mm	11.115 N	31.750 mm	0.66 N/mm	46.736 mm	1.112 N	SS
MS24586-C18	3.047 mm	0.508 mm	11.115 N	34.925 mm	0.59 N/mm	51.815 mm	1.112 N	SS
MS24586-19	3.047 mm	0.508 mm	13.344 N	38.099 mm	0.64 N/mm	56.641 mm	1.334 N	MW
MS24586-519	3.047 mm	0.508 mm	13.344 N	38.099 mm	0.64 N/mm	56.641 mm	1.334 N	MW
MS24586-C19	3.047 mm	0.508 mm	11.115 N	38.099 mm	0.53 N/mm	56.641 mm	1.112 N	SS
MS24586-20	3.047 mm	0.508 mm	13.344 N	41.275 mm	0.58 N/mm	61.722 mm	1.334 N	MW
MS24586-520	3.047 mm	0.508 mm	13.344 N	41.275 mm	0.58 N/mm	61.722 mm	1.334 N	MW

2.3.2. Set the reset spring stiffness

2.3.2.1. Type "0.33" in the "Reset Stiffness" box

Integrated Model-Based SMA Wire DesignTool v.5 (GM/UM Proprietary)

File Window Actuator Architecture View Help

Device Schematic

Device Architecture

SMA Wire Parameter

Wire Diameter (mil) 8 mil Use Arbitrary Diameter

Number of Wires 1 Spooled Strain 0.04

Wire Length (mm) 220 As Spooled Length (mm) 229

Interface

Free Clearance (mm) 7.9 Free Clearance for Spooled Wire (mm) -1

Input / Output Ratio 1 Pre-Stress (MPa) 21.4

Cold Stop Strain 0.0359 Loading friction (N) 0

Hot Stop Strain 0.01 Unloading friction (N) 0

Reset Element

Stiffness (N/mm) 2.3.1.

Leverage Ratio

Free Clearance (mm) 10 Free Clearance for Spooled Wire (mm) 19

Pre Load (N) 0

User Views

Material View

Reset System View

Design Metrics

Output Stroke 4.93 mm SMA Stroke 2.24 %

Max Force 6.82 N Cross Sectional Area 0.032 mm²

Max Stress 210 MPa Work Efficiency 4.13 %

Work 18.5 mJ Power Efficiency 4.13 %

Specific Work 2.59 MJ/m³ SMA Cost 0.26 \$

Total Material 7.13 mm³ Weight of SMA 0.05 g

Operation Temperature Control

Temp. Control (degC) Trans. Temp. (degC)

Amb. Temp. 20 Mf 31 Ms 58

Heated Temp. 110 As 91 Af 101

Ref. Temp. 70 h = 121 W/m²-K

Joule Heating Control

Input Volts (V) 3.54 Heating Time(s) 2.06 (Amb. ~ Af)

Input Current (A) 0.61 Cooling Time(s) 7.61 (Heated ~ Mf)

Input Power (W) 2.17 Cycle Time(s) 9.67

Cooling time for cold stop

Parametric Study

Y Axis Output Stroke X Axis Length

Family Curve Diameter Auto Curve

2.4. Find reset free clearance to provide the available reset force

To provide the reset force as found before, the reset free clearance needs to be set, which is different than the device free clearance which we set before. The reset free clearance is relative position of the reset spring free end to the Austenite zero length SMA wire connecting point. The reset free clearance calculation formula is stated below.

2.4.1. Calculate the reset free clearance

The reset free clearance needs to be set such that the force from the reset spring is equal to the available force at the actuated position. The reset spring extension of the spring at this point is determined by subtracting the reset free clearance by the device free clearance and adding required stroke.

$$\text{Available force} = \text{Reset spring stiffness} \times \text{Reset spring extension}$$

$$= \text{Reset spring stiffness} \times (\text{Reset free clearance} - \text{Device free clearance} + \text{required stroke})$$

$$\text{Reset free clearance}$$

$$= \frac{\text{Available force}}{\text{Reset spring stiffness}} + (\text{Device free clearance} - \text{required stroke})$$

$$= \frac{7 \text{ N}}{0.33 \text{ N/mm}} + (7.9 \text{ mm} - 4.4 \text{ mm}) = 24.7 \text{ mm}$$

2.4.2. Increase the reset spring free clearance to provide the required reset force

2.4.2.1. Type “24.7” in the “Reset Free Clearance”

2.4.3. Check the Martensite finish temperature

$$\Rightarrow M_f : 49 \text{ }^\circ\text{C} < 55 \text{ }^\circ\text{C} \text{ (target } M_f)$$

With the first design using reset element, we did not meet the transition temperature requirement to ensure the operation at the higher ambient temperature. We will iterate this procedure until we meet the requirement.

Integrated Model-Based SMA Wire DesignTool v.5 (GM/UM Proprietary)

File Window Actuator Architecture View Help

Device Schematic

Device Architecture

Internal Architecture

SMA Wire Parameter

Wire Diameter (mil) 8 mil Use Arbitrary Diameter

Number of Wires 1 Spooled Strain 0.04

Wire Length (mm) 220 As Spooled Length (mm) 229

Interface

Free Clearance (mm) 7.9

Reset Element

Stiffness (N/mm) 0.33

Leverage Ratio 4

Free Clearance (mm) 24.7

Pre Load (N) 0

User Views

Material View

Reset System View

Design Metrics

Output Stroke	4.4 mm	SMA Stroke	2 %
Max Force	11.5 N	Cross Sectional Area	0.032 mm ²
Max Stress	355 MPa	Work Efficiency	13.8 %
Work	37.5 mJ	Power Efficiency	13.8 %
Specific Work	5.25 MJ/m ³	SMA Cost	0.26 \$
Total Material	7.13 mm ³	Weight of SMA	0.05 g

Operation Temperature Control

Temp. Control (degC)

Amb. Temp. 20 **Mf 49**

Heated Temp. 110

Ref. Temp. 70

h = 121 W/m²-K

Joule Heating Control

Input Volts (V)	3.54	Heating Time(s)	1.25
Input Current (A)	0.61	(Amb. ~ Af)	
Input Power (W)	2.17	Cooling Time(s)	4.03
		(Heated ~ Mf)	
		Cycle Time(s)	5.28

Cooling time for cold stop

Parametric Study

Y Axis: Output Stroke

X Axis: Length

Family Curve: Diameter

Auto Curve

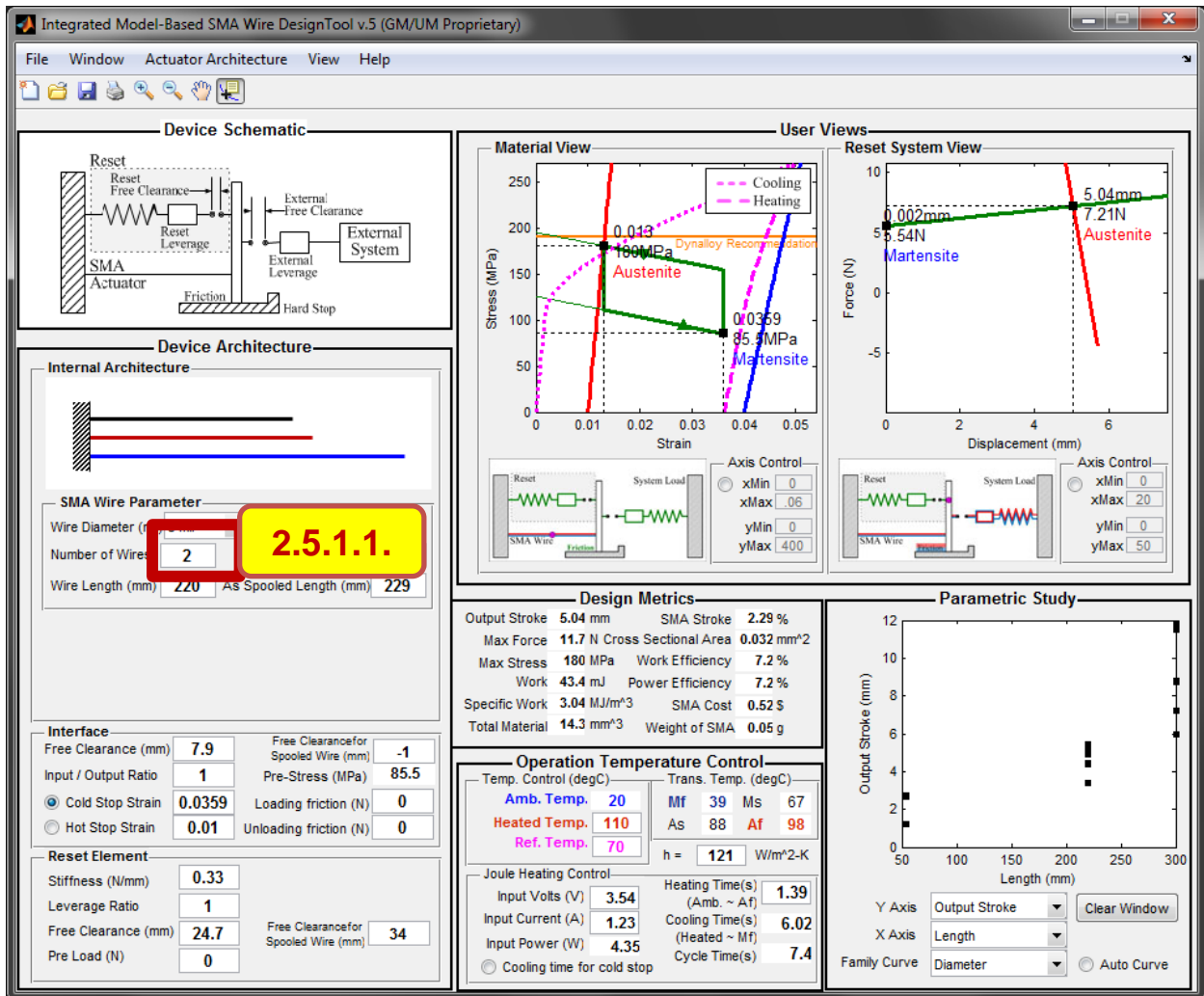
2.5. Repeat the procedure until reach the target M_f

Even after we applied the reset spring, the Martensite finish temperature of the device is still lower than required. The iteration of the previous procedure is required until reach the target Martensite finish temperature. For this time, we will add another 8 mil wire instead of further increasing the wire diameter.

2.5.1. Increase the cross-sectional area of the SMA wire. (Same as 2.1)

2.5.1.1. Add another wire

2.5.1.1.1. Type "2" in the "Number of Wires" box



2.5.2. Find the available reset load increase. (Same as 2.2)

This is the exactly the same process as before, but this time the 4.4 mm stroke point is out of the visible range of the plot. Here, we go through the manual axis setting procedure before we find the available reset force.

2.5.2.1. Initialize the reset element

2.5.2.1.1. Type "0" in the "Reset Element Stiffness" box.

2.5.2.2. Set the "Reset System View" window axis

2.5.2.2.1. Type "6" in the "xMax" box in the "Axis Control" window

2.5.2.2.2. Type "30" in the yMax" box

2.5.2.2.3. Check the radio button in the "Axis Control" window

2.5.2.3. Select one point on the austenite curve on the "Reset System View" window.

2.5.2.4. Move the cursor to the target displacement (4.4 mm) to find the required reset force.

⇒ "18.5 N"

Integrated Model-Based SMA Wire DesignTool v.5 (GM/UM Proprietary)

File Window Actuator Architecture View Help

Device Schematic

Device Architecture

Internal Architecture

SMA Wire Parameter

Wire Diameter (mil) 8 mil Use Arbitrary Diameter

Number of Wires 2 Spooled Strain 0.04

Wire Length (mm) 220 As Spooled Length (mm) 229

Interface

Free Clearance (mm) 7.9 Free Clearance for Spooled Wire (mm) -1

Input / Output Ratio 1 Pre-Stress (MPa) 0

Cold Stop Strain 0.0359 Loading friction (N) 0

Hot Stop Strain 0.01 Unloading friction (N) 0

Reset Element

Stiffness (N/mm) **2.5.2.1.**

Leverage Ratio 1

Free Clearance (mm) 24.7 Free Clearance for Spooled Wire (mm) 34

Pre Load (N) 0

Material View

Reset System View

Axis Control

xMin 0 xMax 6 yMin 0 yMax 30

Design Metrics

Output Stroke 5.44 mm SMA Stroke 2.47 %

Max Force 4.5 N Cross Sectional Area 0.032 mm²

Max Stress 69.4 MPa Work Efficiency 1.97 %

Work 12.3 mJ Power Efficiency 1.97 %

Specific Work 0.86 MJ/m³ SMA Cost 0.52 \$

Total Material 14.3 mm³ Weight of SMA 0.05 g

Operation Temperature Control

Temp. Control (degC) Trans. Temp. (degC)

Amb. Temp. 20 Mf 28 Ms 55

Heated Temp. 110 As 76 Af 86

Ref. Temp. 70 h = 121 W/m²-K

Joule Heating Control

Input Volts (V) 3.54 Heating Time(s) (Amb. ~ Af) 1.43

Input Current (A) 1.23 Cooling Time(s) (Heated ~ Mf) 9.1

Input Power (W) 4.35 Cycle Time(s) 10.5

Cooling time for cold stop

Parameter

Y Axis Output Stroke X Axis Length

Family Curve Diameter Auto Curve

2.5.3. Find the softest reset spring which can provide the required reset force (Same as 2.3)

2.5.3.1. Find the softest reset spring which can provide the required reset force from the spring catalog

⇒ 0.6 N/mm for 18.5 N

2.5.3.2. Set the reset spring stiffness

2.5.3.2.1. Type “0.6” in the “Reset Stiffness” box

Integrated Model-Based SMA Wire DesignTool v.5 (GM/UM Proprietary)

File Window Actuator Architecture View Help

Device Schematic

Device Architecture

SMA Wire Parameter

Wire Diameter (mil) 8 mil Use Arbitrary Diameter

Number of Wires 2 Spooled Strain 0.04

Wire Length (mm) 220 As Spooled Length (mm) 229

Interface

Free Clearance (mm) 7.9 Free Clearance for Spooled Wire (mm) -1

Input / Output Ratio 1 Pre-Stress (MPa) 155

Cold Stop Strain 0.0359 Loading friction (N) 0

Hot Stop Strain 0.01 Unloading friction (N) 0

Reset Element

Stiffness (N/mm) **0.6**

Leverage Ratio 1

Free Clearance (mm) 24.7 Free Clearance for Spooled Wire (mm) 34

Pre Load (N) 0

Material View

Reset System View

Design Metrics

Output Stroke	4.71 mm	SMA Stroke	2.14 %
Max Force	17.4 N	Cross Sectional Area	0.032 mm ²
Max Stress	268 MPa	Work Efficiency	8.44 %
Work	64.8 mJ	Power Efficiency	8.44 %
Specific Work	4.54 MJ/m ³	SMA Cost	0.52 \$
Total Material	14.3 mm ³	Weight of SMA	0.05 g

Operation Temperature Control

Temp. Control (degC) Trans. Temp. (degC)

Amb. Temp. 20 Mf 47 Ms 77

Heated Temp. 140 As 98 Af 108

Ref. Temp. 70

h = 121 W/m²-K

Joule Heating Control

Input Volts (V) 4.27 Heating Time(s) 1.21 (Amb. ~ Af)

Input Current (A) 1.48 Cooling Time(s) 5.05 (Heated ~ Mf)

Input Power (W) 6.33 Cycle Time(s) 6.26

Cooling time for cold stop

Parametric Study

Y Axis: Output Stroke

X Axis: Length

Family Curve: Diameter

Auto Curve

2.5.3.2.

2.5.4. Find reset free clearance to provide the required reset force (Same as 2.4)

2.5.4.1. Calculate the reset free clearance

$$\begin{aligned} \text{reset free clearance} &= \frac{\text{Available force}}{\text{Reset spring stiffness}} \\ &+ (\text{Device free clearance} - \text{required stroke}) \\ &= \frac{18.5 \text{ N}}{0.6 \text{ N/mm}} + (7.9 \text{ mm} - 4.4 \text{ mm}) = 34.4 \text{ mm} \end{aligned}$$

2.5.4.2. Increase the reset spring free clearance to provide the required reset force

2.5.4.2.1. Type "34.4" in the "Reset Free Clearance"

2.5.4.3. Check the Martensite finish temperature

$$\Rightarrow M_f : 59 \text{ }^\circ\text{C} > 55 \text{ }^\circ\text{C} \text{ (target } M_f)$$

Integrated Model-Based SMA Wire DesignTool v.5 (GM/UM Proprietary)

File Window Actuator Architecture View Help

Device Schematic

Device Architecture

SMA Wire Parameter

Wire Diameter (mil) 8 mil Use Arbitrary Diameter

Number of Wires 2 Spooled Strain 0.04

Wire Length (mm) 220 As Spooled Length (mm) 229

Interface

Free Clearance (mm)	7.9	Free Clearance for Spooled Wire (mm)	-1
Input / Output Ratio	1	Pre-Stress (MPa)	245
<input checked="" type="radio"/> Cold Stop Strain	0.0359	Loading friction (N)	0
<input type="radio"/> Hot Stop Strain	0.01	Unloading friction (N)	0

Reset Element

Stiffness (N/mm)	0.6
Leverage Ratio	1
Free Clearance (mm)	34.4
Pre Load (N)	0

User Views

Material View

Reset System View

Design Metrics

Output Stroke	4.4 mm	SMA Stroke	2%
Max Force	23 N	Cross Sectional Area	0.032 mm ²
Max Stress	355 MPa	Work Efficiency	16.9%
Work	85.6 mJ	Power Efficiency	16.9%
Specific Work	6 MJ/m ³	SMA Cost	0.52 \$
Total Material	14.3 mm ³	Weight of SMA	0.05 g

Operation Temperature Control

Amb. Temp.	20	Mf	59
Heated Temp.	110	h	121 W/m ² -K
Ref. Temp.	70	Heating Time(s)	1.16
Input Volts (V)	3.54	(Amb. ~ Af)	
Input Current (A)	1.23	Cooling Time(s)	3.29
Input Power (W)	4.35	(Heated ~ Mf)	
		Cycle Time(s)	4.46

Parametric Study

Y Axis: Output Stroke
X Axis: Length
Family Curve: Diameter

2.5.4.2.

34.4

2.5.4.3.

Mf 59

3. VERIFY THE DESIGN WITH THE EMPIRICALLY MEASURED EXTERNAL SYSTEM DATA FROM THE PROTOTYPE AND FIND THE CURRENT TO ACTUATE IN 1 SEC.

Once the design is finished with the estimated external system, we can verify the design by importing the empirically measured external system data from the prototype. Here we will practice how to import the external data with the Excel form. This function is not only used with the physical prototype but also used with any kind of force-deflection format data such as the simulation result from non-compatible tool.

3.1. Import the experimental data

- 3.1.1. Change the right window of the “User Views” to “System View” using the menu bar. (“View” > “Right Window View” > “System View”)

Integrated Model-Based SMA Wire DesignTool v.5 (GM/UM Proprietary)

File Window Actuator Architecture **View** Help

3.1.1

Left Window View Right Window View System View User Views

Device Schema

Device Architecture

SMA Wire Parameter

Wire Diameter (mil) 8 mil Use Arbitrary Diameter

Number of Wires 2 Spooled Strain 0.04

Wire Length (mm) 220 As Spooled Length (mm) 229

Interface

Free Clearance (mm) 7.9 Free Clearance for Spooled Wire (mm) -1

Input / Output Ratio 1 Pre-Stress (MPa) 245

Cold Stop Strain 0.0359 Loading friction (N) 0

Hot Stop Strain 0.01 Unloading friction (N) 0

Reset Element

Stiffness (N/mm) .6

Leverage Ratio 1

Free Clearance (mm) 34.4 Free Clearance for Spooled Wire (mm) 43

Pre Load (N) 0

SMA Wire View

Reset System View

Wire / System View

Actuator with Friction View

Actuator without Friction View

Stress (MPa)

Strain

0.0359

245MPa

185.9N

Martensite

Austenite

Axis Control

xMin 0 xMax .06

yMin 0 yMax 400

Reset System View

Force (N)

Displacement (mm)

18.5N

4.4mm

Martensite

Austenite

Axis Control

xMin 0 xMax 20

yMin 0 yMax 50

Design Metrics

Output Stroke	4.4 mm	SMA Stroke	2 %
Max Force	23 N	Cross Sectional Area	0.032 mm ²
Max Stress	355 MPa	Work Efficiency	16.9 %
Work	85.6 mJ	Power Efficiency	16.9 %
Specific Work	6 MJ/m ³	SMA Cost	0.52 \$
Total Material	14.3 mm ³	Weight of SMA	0.05 g

Parametric Study

Output Stroke (mm)

Length (mm)

Y Axis Output Stroke

X Axis Length

Family Curve Diameter

Clear Window

Auto Curve

Operation Temperature Control

Temp. Control (degC) Trans. Temp. (degC)

Amb. Temp. 20 Mf 59 Ms 90

Heated Temp. 110 As 107 Af 117

Ref. Temp. 70

h = 121 W/m²-K

Joule Heating Control

Input Volts (V) 3.54 Heating Time(s) 1.16 (Amb. ~ Af)

Input Current (A) 1.23 Cooling Time(s) 3.29 (Heated ~ Mf)

Input Power (W) 4.35 Cycle Time(s) 4.46

Cooling time for cold stop

3.1.2. Open External System Window

3.1.2.1. If it appears on the screen, click any part of the External System Window.

3.1.2.2. If you can't find the window, use the main window menu bar. ("Window" > "External System")

External System (GM/UM Proprietary)

3.1.2.2.

External System

Material View

User Views

SMA Wire View

ExternalSystem (GM/UM Proprietary)

File Import

External System

Analytical System Model

Loading

$F = 0 \times + 4.5$

Stiffness (N/mm) Static Load (N)

Unloading

$F = 0 \times + 0$

Stiffness (N/mm) Static Load (N)

Environment

Ambient Temperature (degC) 20

Medium Air (still)

Force (N)

Displacement (mm)

Apply Changes

Internal Architecture

SMA Wire Parameters

Wire Diameter (mm) Use Arbitrary Diameter

Number of Wires

Wire Length (mm)

Interface

Free Clearance (mm)	<input type="text" value="20"/>	Free Clearance for Spooled Wire (mm)	<input type="text" value="8"/>
Input / Output Ratio	<input type="text" value="1"/>	Pre-Stress (MPa)	<input type="text" value="90.9"/>
<input type="radio"/> Cold Stop Strain	<input type="text" value="0.04"/>	Loading friction (N)	<input type="text" value="0"/>
<input type="radio"/> Hot Stop Strain	<input type="text" value="0.01"/>	Unloading friction (N)	<input type="text" value="0"/>

Reset Element

Stiffness (N/mm)	<input type="text" value="0"/>
Leverage Ratio	<input type="text" value="1"/>
Free Clearance (mm)	<input type="text" value="10"/>
Pre Load (N)	<input type="text" value="0"/>
	Free Clearance for Spooled Wire (mm) <input type="text" value="22"/>

3.1.3. Import the experimental data

3.1.3.1. Import the loading profile

3.1.3.1.1. Open the file import dialog box. (“Import” > “Import from Excel” > “Loading Profile”)

3.1.3.1.2. Select the file using the dialog box.

3.1.3.1.3. The Force-deflection profile is imported

3.1.3.1.1.

3.1.3.1.2.

Name	Date modified	Size
AHV_Force_Profiles 3-15-2012	5/1/2012 2:49 PM	
AHV loading (2)	9/22/2011 10:27 AM	26 KB
AHV loading	9/22/2011 9:18 PM	32 KB
AHV Pass 10-4_4 Load	3/15/2012 1:36 PM	70 KB
AHV Pass 10-4_4 UnLoad	3/15/2012 2:28 PM	73 KB
AHV unloading	9/22/2011 10:27 AM	24 KB
AHV_new	9/22/2011 2:08 PM	32 KB
AHV_new2	9/22/2011 11:44 AM	55 KB

3.1.3.1.3.

Apply Changes

3.1.3.2. Import the unloading profile

3.1.3.2.1. Open the file import dialog box. (“Import” > “Import from Excel” > “Unloading Profile”)

3.1.3.2.2. Select the file using the dialog box.

3.1.3.2.3. The unloading Force-deflection profile is imported.

ExternalSystem (GM/UM Proprietary)

File > Import

- Import from Excel
- Import from ADAMS
- Import from ABAQUS

3.1.3.2.1.

Select File to Open

Look in: AHV Data

Name	Date modified	Size
AHV_Force_Profiles 3-15-2012	5/1/2012 2:49 PM	
AHV loading (2)	9/22/2011 10:27	26 KB
AHV loading	9/22/2011 9:18 PM	Microsoft Excel 97... 32 KB
AHV Pass 10-4_4 Load	3/15/2012 1:36 PM	Microsoft Excel 97... 70 KB
AHV Pass 10-4_4 UnLoad	3/15/2012 2:28 PM	Microsoft Excel 97... 73 KB
AHV unloading	9/22/2011 10:27 AM	Microsoft Excel 97... 24 KB
AHV_new	9/22/2011 2:08 PM	Microsoft Excel 97... 32 KB
AHV_new2	9/22/2011 11:44 AM	Microsoft Excel 97... 55 KB

File name: AHV loading
Files of type: (*.xls)

3.1.3.2.2.

Force (N)

Displacement (mm)

Loading

Unloading

3.1.3.2.3.

Apply Changes

3.1.4. Push “Apply Changes” button to transfer to the main window.

The performance of the device does not change much as we designed the device based on the estimated external system condition which matches very well with the real system. Because the stroke is set by the actuation strain and the cold stop position, the actuation performance does not vary. The interesting point with the real external system data is that the device goes through the higher force than the actuation point. Without the reset element, it is possible to have higher stress on the wire during the actuation (during the heating), but the reset spring mitigates this effect. The other interesting point is that the Martensite finish temperature is slightly higher than the initial design with the estimated system because the unloading path ends up at the non-zero force.

ExternalSystem (GM/UM Proprietary)

File Import

External System

Analytical System Model

Loading

F = x +

Stiffness (N/mm) Static Load (N)

Unloading

F = x +

Stiffness (N/mm) Static Load (N)

Environment

Ambient Temperature (degC)

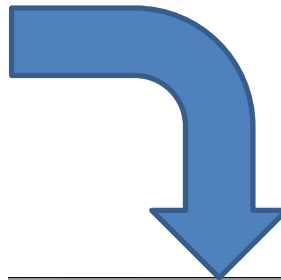
Medium

Force (N)

Displacement (mm)

3.1.4.

Apply Changes



Reset Leverage External System

SMA Actuator Friction Hard Stop

Device Architecture

Internal Architecture

SMA Wire Parameter

Wire Diameter (mil) Use Arbitrary Diameter

Number of Wires Spooled Strain

Wire Length (mm) As Spooled Length (mm)

Interface

Free Clearance (mm) Free Clearance for Spooled Wire (mm)

Input / Output Ratio Pre-Stress (MPa)

Cold Stop Strain Loading friction (N)

Hot Stop Strain Unloading friction (N)

Reset Element

Stiffness (N/mm)

Leverage Ratio Free Clearance for Spooled Wire (mm)

Free Clearance (mm)

Pre Load (N)

ExternalSystem (GM/UM Proprietary)

User Views

Material View

Stress (MPa)

Strain

0.0159 355MPa Austenite 0.0359 256MPa Martensite 0.04mm 0.687N

--- Cooling --- Heating

System View

Force (N)

Displacement (mm)

0.04mm 0.687N 4.4mm 4.5N Austenite

Design Metrics

Output Stroke	4.4 mm	SMA Stroke	2 %
Max Force	23 N	Cross Sectional Area	0.032 mm ²
Max Stress	355 MPa	Work Efficiency	18 %
Work	87.1 mJ	Power Efficiency	18 %
Specific Work	6.1 MJ/m ³	SMA Cost	0.52 \$
Total Material	14.3 mm ³	Weight of SMA	0.05 g

Parametric Study

Output Stroke (mm)

Length (mm)

Y Axis: Output Stroke

X Axis: Length

Family Curve: Diameter

Auto Curve

Operation Temperature Control

Temp. Control (degC)	Trans. Temp. (degC)
Amb. Temp. <input type="text" value="20"/>	Mf 60 Ms 92
Heated Temp. <input type="text" value="110"/>	As 107 Af 117
Ref. Temp. <input type="text" value="70"/>	
h = <input type="text" value="121"/> W/m ² -K	

Joule Heating Control

Input Volts (V)	<input type="text" value="3.54"/>	Heating Time(s)	<input type="text" value="1.12"/>
Input Current (A)	<input type="text" value="1.23"/>	Cooling Time(s)	<input type="text" value="3.05"/>
Input Power (W)	<input type="text" value="4.35"/>	Cycle Time(s)	<input type="text" value="4.17"/>

Cooling time for cold stop

3.2. Find the current to actuate the wire in 1 sec.

In the “Operation Temperature Control” box, the design tool recommends the smallest currents to heat the wire to the heated temperature, and shows the estimated heating and cooling time based on the temperature evolution simulations.

If you want to change the applied currents or volts, you can type-in the currents or volts value in the text box, and then the design tool will simulate the temperature evolution again.

In case of you want to calculate the required currents to heat the wire within a specified time, you can type in the required heating time.

3.2.1. Type “1” in the “Heating Time” box in the “Operation Temperature Control” window

3.2.2. It will take some time to finish the computation, and then the current and voltage to actuate the wire in 1 sec will show up.

